# The development of phenolic resin-based carbons with improved high temperature oxidation resistance

Bashir, Khalid Mohammed

*Award date:*
1988

*Awarding institution:*
University of Bath

# THE DEVELOPMENT OF PHENOLIC RESIN-BASED CARBONS WITH IMPROVED HIGH TEMPERATURE OXIDATION RESISTANCE

submitted by

Khalid Mohammed Bashir

for the degree of Doctor of Philosophy

at the University of Bath

September 1988







ProQuest LLC
789 East Eisenhower Parkway
P.O. Box 1346
Ann Arbor, MI 48106-1346

In the name of Allah, most Gracious, most Merciful

The ink of the Scholar is equal to the blood of the Martyr
Seek knowledge even if you have to travel (by foot) to China
(sayings of the Holy Prophet, Mohammed, peace be upon him)

I dedicate this work to my Mother, Father and Uncle and Aunt

## ACKNOWLEDGEMENTS

I wish to express my sincere gratitude to the following people for their help during the course of this work:

Dr. B. McEnaney for his help, advice and humour as supervisor of the project; Mr. P. Lemon and Mr. J. Ireland of Borden (U.K.) Limited, for further supervision, useful discussion and for the Industrial Research Grant; Dr. H. Perrot for help with EDAX and SEM work; Dr. T. Mays for help with QIA; Dr. A. Linares-Solano and other members of the Inorganic Chemistry Department, University of Alicante, for work on gas adsorption; Prof. H. Marsh, University of Newcastle-Upon-Tyne, for his gifts of pitch; Mr. P. Wakeford, Chief Technician, Bath University, school of Materials Science, Mr. P. Taylor and Mr. I. Trussler for their invaluable assistance throughout my research and to all my relatives and friends for their support and encouragement.

## ABBREVIATIONS

PF-Phenol Formaldehyde

HMTA-Hexa Methylene Tetra Amine

TG-Thermogravimetric

TGA-Thermogravimetric Analysis

DSC-Differential Scanning Calorimetry

SEM-Scanning Electron Microscopy

QIA-Quantitative Image Analysis

EDAX-Energy Dispersive Analysis of X-rays

HTT-Heat Treatment Temperature

std-standard

BC-Bulk Carbonisation

wt-weight

a.m.u.-atomic mass unit

3D-3-dimensional

dia-diameter

ASA-Active Surface Area

TSA-Total Surface Area

BET-Brunauer Emmett and Teller

# ABSTRACT

This thesis reports studies of several methods for improving the resistance to air-oxidation of phenol-formaldehyde resin-based carbons which are used as binders in oxide carbon refractories. Initial studies using thermogravimetric analysis concerned the effects of resin cure schedule on the performance of the resultant carbons, using more oxidation resistant coal tar pitch and petroleum pitch based carbons for comparison. Carbons with oxidation resistances approaching, and in some cases exceeding those of pitch-based carbons could be produced from a resole subjected to extended, high temperature cure and also from a resole/novolak co-polymer. The oxidation resistance of the co-polymer carbon was further improved compared to the pitch carbon by heat-treatment at 1700°C.

Resin based carbons of high oxidation resistance, exceeding those of pitch-based carbons in some cases, were obtained when organophosphorus compounds, which are used as fire retardants, were incorporated into a resole and resole/novolak co-ploymer prior to curing. Carbons with high oxidation resistance were also obtained from a boron-modified ortho-novolak resin and a silicone resin. The enhanced oxidation resistance of the additive modified resin carbons was further shown by the high amount of carbon residue remaining after oxidation at 1000°C. Progressive oxidation of carbons prepared from resins with organophosphorus additions resulted in the formation of globular glassy surface layers containing phosphorus (as the oxide), revealed by scanning electron microscopy and energy dispersive x-ray analysis. It is postulated that these layers act as barriers for the diffusion of

oxygen, so inhibiting the oxidation process. Total surface areas and micropore volumes of the pitch-based and resin-based carbons were measured by adsorption of nitrogen using volumetric and gravimetric techniques. Macropore volumes and macropore size distribution for the carbons were obtained by mercury porosimetry and image analysis.

TABLE OF CONTENTS


| | | Page |
|---|---|---|
| CHAPTER 1 | INTRODUCTION | 1 |
| 1.1 | The Structure of the Thesis | 3 |
| CHAPTER 2 | THE LITERATURE SURVEY | 4-68 |
| 2.1 | Phenol Formaldehyde (PF) Resins | 4-27 |
| 2.1.1 | The Synthesis and Applications of PF Resins | 4 |
| 2.1.2 | The Mechanism of Carbonisation | 10 |
| 2.1.3 | The Structure of Polymeric/PF carbon | 21 |
| 2.2 | The Structure and Applications of Pitches | 28-41 |
| 2.2.1 | The Materials and Applications | 28 |
| 2.2.2 | Formation of Mesophase | 33 |
| 2.2.3 | Growth of Mesophase | 38 |
| 2.2.4 | Graphitisation | 40 |
| 2.3 | FIRE RETARDANTS | 42-68 |
| 2.3.1 | Combustion Inhibition of Polymeric Materials by Fire Retardants | 42 |
| 2.3.2 | Flammability Evaluation | 47 |
| 2.3.3 | Pyrolytic Decomposition Temperature Profile | 49 |
| 2.4 | Combustion Inhibition of Phenolic Resins | 52-68 |
| 2.4.1 | Introduction | 52 |
| 2.4.2 | Halogen Based Additives | 54 |
| 2.4.3 | Boron Based Additives | 55 |
| 2.4.4 | Phosphorus Based Additives | 57 |
| 2.4.5 | Nitrogen Based Additives | 61 |
| 2.4.6 | Sulphur Based Additives | 62 |

CONTENTS (cont.) Page


| | | |
|---|---|---|
| 2.4.7 | Silicon Based Additives | 62 |
| 2.4.8 | Miscellaneous Additives | 64-65 |
| 2.4.8.1 | Oxide Based | 64 |
| 2.4.8.2 | Carbonate and Bicarbonate Based | 65 |
| CHAPTER 3 | EXPERIMENTAL | 69-93 |
| 3.1 | MATERIALS | 69-70 |
| 3.1.1 | The Phenolic Resins and Model Compounds | 69 |
| 3.1.2 | The Pitches | 69 |
| 3.1.3 | The Fire Retardants | 70 |
| 3.2 | Curing of the PF Resins and Additive Modified Resins | 70 |
| 3.3 | Bulk Carbonisation | 71 |
| 3.4 | High Temperature Heat Treatment | 73 |
| 3.5 | THERMAL ANALYSIS | 75-78 |
| 3.5.1 | Thermogravimetric Analysis (TGA) | 75 |
| 3.5.2 | Differential Scanning Calorimetry (DSC) | 78 |
| 3.6 | CHEMICAL ANALYSIS | 79-80 |
| 3.6.1 | Energy Dispersive Analysis of X-rays (EDAX) | 79 |
| 3.6.2 | Elemental Analysis | 80 |

CONTENTS (cont.) Page


| | | |
|---|---|---|
| 3.7 | TEXTURAL CHARACTERISATION | 80-91 |
| 3.7.1 | Scanning Electron Microscopy (SEM) | 80 |
| 3.7.2 | Determination of the Total Surface Area (TSA) from Gas Adsorption Isotherms at $77^{o}K$ | 81-91 |
| 3.7.2.1 | Gravimetric Techniques: Spring and Microbalance | 82 |
| 3.7.2.2 | Volumetric Technique | 86 |
| 3.7.3 | Mercury Porosimetry | 89 |
| 3.7.4 | Quantitative Image Analysis (QIA) | 89-91 |
| 3.7.4.1 | The System | 89 |
| 3.7.4.2 | Sample Preparation | 90 |

CONTENTS (cont.) Page

RESULTS AND DISCUSSION


| | | |
|---|---|---|
| CHAPTER 4 | CURING, CARBONISATION AND OXIDATION RESISTANCE OF THE RESINS AND RESIN AND PITCH CARBONS | 94-138 |
| 4.1 | Introduction | 94 |
| 4.2 | Curing of the Resins | 94-95 |
| 4.2.1 | Curing Weight Loss of the Resins | 94 |
| 4.2.2 | Differential Scanning Calorimetry, (DSC) | 95 |
| 4.3 | Carbonisation of Pitches and Resins | 96 |
| 4.4 | Oxidation of Resin and Pitch Carbons | 98 |
| 4.5 | Effects of Cure Schedule on Carbonisation of Resins and Oxidation of the Resin Carbons | 100 |
| 4.6 | Effect of Resole/Novolak Co-polymerisation on Carbonisation and Oxidation Resistance | 102 |
| 4.7 | Discussion of Results | 105 |

| | | |
|---|---|---|
| CHAPTER 5 | EFFECTS OF FIRE RETARDANT ADDITION ON RESINS: CURING, CARBONISATION AND OXIDATION RESISTANCE | 139-165 |
| 5.1 | Introduction | 139 |
| 5.2 | The Silicone Resin, Z6018 | 139 |
| 5.3 | The Boronated Resin, MT59 | 140 |
| 5.4 | The Organophosphorus Modified Phenolic Resins | 141 |
| 5.5 | Discussion | 143 |

CONTENTS (cont.) Page


| | | |
|---|---|---|
| CHAPTER 6 | EFFECT OF HEAT TREATMENT TEMPERATURE, (HTT), ISOTHERMAL OXIDATION STUDIES, EDAX AND CHEMICAL ANALYSIS | 166-198 |
| 6.1 | Effect of HEAT TREATMENT TEMPERATURE on Carbon Yield and Oxidation Resistance of the Resin and Pitch Carbons | 166-174 |
| 6.1.1 | Results | 166 |
| 6.1.2 | Discussion | 168 |
| 6.2 | Isothermal Oxidation Studies: Results and Discussion | 175 |
| 6.3 | Energy Dispersive Analysis of X-rays: Results and Discussion | 186 |
| 6.4 | Chemical Analysis | 195 |
| CHAPTER 7 | TEXTURAL CHARACTERISATION OF THE MATERIALS | 199-256 |
| 7.1 | Scanning Electron Microscopy, (SEM) | 199 |
| 7.2 | Adsorption Studies | 218-232 |
| 7.2.1 | Introduction | 218 |
| 7.2.2 | A Brief Review on the Development of the Adsorption Theory | 219 |
| 7.2.3 | Results and Discussion | 223 |
| 7.3 | Mercury Porosimetry: Results and Discussion | 233-236 |
| 7.3.1 | Introduction | 233 |
| 7.3.2 | Results and Discussion | 235 |
| 7.4 | Quantitative Image Analysis, QIA | 239-254 |
| 7.4.1 | Introduction | 239 |

CONTENTS (cont.) Page


7.4.2 Results and Discussion 240

7.5 Overall Summary of Chapter 7 255

CHAPTER 8 GENERAL DISCUSSION 257

CHAPTER 9 CONCLUSION AND SUGGESTIONS FOR FURTHER WORK 268

APPENDIX 272

REFERENCES 281

# INTRODUCTION

Composite oxide carbon refractories are being increasingly used in the metallurgical industry as converter linings of basic oxygen furnaces and electric arc furnaces and for the production of shapes, crucibles and ladles for steel making processes (1-3). These composites are manufactured from either silicon carbide, zirconia, magnesia, alumina or other ceramics and natural graphite flakes, as a carbon source, which are bound together by a carbon binder derived either from coal tar or petroleum pitch (5-8wt%) or from a polymeric resin (5-25wt%). Binders derived from phenolic resins confer several advantages to the resulting composite. These include increased specific adhesion to both oxide and graphite, low permeability to gases and high chemical resistance, hardness and thermal conductivity (4-7). Furthermore, the ability to control the chemistry of the phenolic resin allows production of materials with optimum properties. For example, unfired resin-based magnesia bricks, possessing adequate strength in the green state can be used directly in converter linings (8). Resin polymerisation is then achieved during heating up of the furnace. The resultant saving in energy costs, together with improvements in overall product performance, serve to counteract the higher cost of resin-based raw materials. Phenolic resins, i.e. resoles and novolaks, as binders are also used for the manufacture of brake and clutch linings, abrasive materials, and as ablative coatings and in the foundry industry (9). A major disadvantage of resin-based binders is their inferior resistance to oxidation at high temperature, which has

been linked to the carbon structure. Thermal decomposition of phenolic resin yields a carbon of high surface area and with a disordered, non-graphitic structure. Conversely, decomposition of pitches yield a carbon of lower surface area and with a more graphitic structure (10). These structural differences are considered in more detail in Chapter 2.

In view of the numerous advantages reported for phenolic resin-based carbons when used as binders for oxide-carbon refractories, it is potentially worthwhile to investigate the possibility of improving the cited inferior oxidation resistance of resin carbons. The general objective of the work reported in this thesis was:

1) to investigate the carbonisation of phenolic resins; 2) to investigate the influence of resin structure on the properties of the resultant carbon; 3) to study the oxidation of the resin carbon in air; and 4) to explore methods for improving the oxidation resistance of the resin carbons by variation of the cure schedule, high temperature heat treatment or by incorporation, at the resin stage, of fire-retardant compounds based on boron, silicon, phosphorus and halogens.

The phenolic resins studied include a series of novolaks of different initial molecular weight, one resole, various resole/novolak compositions, additive-modified novolaks and two model compounds.

## 1.1 The Structure of the Thesis

A literature survey, divided into four sections is presented in Chapter 2. The first and second sections cover characteristics, applications and carbonisation of phenolic resins and pitch, respectively. Relevant parts of the literature on additives including their method of incorporation into materials and mechanism of combustion inhibition is presented in sections three and four. In Chapter 3 materials and material properties are presented along with the experimental procedure and relevant diagrams of the apparatus used. The results and discussion are presented in Chapters 4 to 7 followed by a general discussion in Chapter 8. In Chapter 9 a summary, conclusion, and suggestions for further work are presented.

# CHAPTER 2 THE LITERATURE SURVEY

The subject of this thesis requires several aspects of the scientific and technical literature to be reviewed. The principal subject of the thesis is phenol formaldehyde (PF) resin-based carbons. Thus, PF resin synthesis, the mechanism of carbonisation and the structure of the resultant carbon are discussed. Pitch carbons are included for comparative purposes and the structure of pitches and their conversion to carbon are similarly reviewed. The potentiality of fire retardant compounds for improving the oxidation resistance of resin-based carbons is explored in this work. Hence the relevant literature on fire retardants is also reviewed and a list of candidate materials was compiled from consideration of the properties and requirements of oxidation inhibition of resin carbons.

## 2.1 Phenol Formaldehyde (PF) Resins

### 2.1.1 The Synthesis and Applications of PF Resins

The reaction between phenol and formaldehyde was first described by Bayer in 1872 (11) and further investigated by Baekeland (12). Since Baekeland's findings, phenolic resins have become some of the most prominent and widely used polymers and represent the first true engineering plastic. Moulded phenolic resins are employed as parts for automotive, radio, television and other electrical appliances. They are also used in laminates

of paper and wood (major application), foams and electrical insulatives, as adhesives, varnishes, abrasives and abrasive coating, foundry castings and as binders between graphite and refractory oxides (2-9). The biocompatibility of phenolic resin carbons with body tissue represents another area of application e.g. replacement of tendons and ligaments and manufacture of aorta valves (13). The major source of phenol is the cumene peroxidation process. In this process, benzene and propylene are used to produce the intermediate cumene from which phenol is derived, along with the co-product acetone. Coal tar distillation is also used to produce (about 3%) phenol. Formaldehyde is obtained by dehydrogenation of methanol.

In the refractory industry, economic considerations indicate that the cost of phenolics as a source of carbon binder, is greater than other available raw materials. Thus, with pitch, the price ratio is 1:3.5 in favour of the pitch. However, various factors serve to justify the future use of phenolics e.g. superior quality and strength of the products, good chemical resistance, low permeability, and significant reduction in energy costs (7,8).

In simplistic terms, phenol reacts with an aldehyde (formaldehyde is used almost exclusively) to give a range of condensation products. The reaction is catalysed by acids or bases . and the nature of the product formed depends on catalyst type, temperature, time and ratio of reactants (9). Two main categories of condensation products are formed, namely, resoles

and novolaks, fig.2.1a-e. A novolak is formed under acidic conditions with P/F ratio >1. In industry, the molar P/F ratio is 1:0.75 to 1:0.85. The novolaks are linear, condensation products (molecular weight ~2000) which are soluble and permanently fusible i.e. thermo-plastic. They can be converted into insoluble and infusible products by addition of a hardener e.g. hexamethylene tetraamine (HMTA), and heating to above 100°C.

Resoles are obtained under alkaline conditions and excess formaldehyde; the P/F ratio is 1:1 to 1:3. The resulting methylol phenols condense further to form methylene (major) or ether (minor) linkages upon further heating, to yield three-dimensionally (3-D) cross-linked, insoluble and infusible polymers (resits). Intermediate or partially cured resols (which are soluble in alkaline solutions) and resitols (long chain linear polymers, soluble in organic solvents) are thermoplastic in nature. These intermediates can be separated but possess limited storage stability at ambient temperature. Thus, ammonia catalysed solid resols are used for production of moulding compounds, brake lining mixtures, abrasive materials and as resin coatings. Conversely, ammonia catalysed resol solutions are used as impregnating resins for electrical laminates and as coatings.

The PF reaction proceeds via a resonance stabilised phenoxide ion, fig.2.1a, and involves electrophilic aromatic substitution in both acidic and alkaline media. The catalysts used for resole

synthesis include sodium hydroxide, ammonia, HMTA, sodium carbonate, tertiary amines (e.g. triethyl amine) and hydroxides of calcium, barium and magnesium. The kinetics of the reaction have been well documented and involve a first order mechanism (14-16). Theoretically, 1.5 mole of formaldehyde is necessary for complete cross-linking of 1 mole of phenol, i.e. substitution at two ortho and one para positions. Usually 1.6 mole formaldehyde are used to ensure resin efficiency, free phenol content and to meet other technical requirements.

The inductive electron-withdrawing and conjugatively electron releasing nature of the hydroxyl group and steric considerations, favour para-substitution compared to ortho while meta substitution is negligible, Fig.2.1b. Polar solvents and acidic media also favour para attack. Ortho attack is enhanced by non-polar solvents, alkaline conditions and group 11 oxide, hydroxide and acetate catalysts. High "ortho novolaks" have been prepared using boric acid or a combination of zinc acetate followed by magnesium oxide and triethyl amine as catalysts. These novolaks have high curing rates with HMTA because of the free reactive para position. Despite the higher reactivity of the para position towards formaldehyde, o-hydroxymethyl phenol is formed at a faster rate due to the availability of two ortho positions. Under alkaline conditions, the most important reaction is the formation of diphenylmethane, fig.2.1c, reaction 2. The dihydroxybenzylether, fig.2.1c, reaction 1, is thought to be prevalent under neutral or weakly acidic conditions and at temperatures upto 130$^{o}$C (17). Methylene bridge formation, which

is thermodynamically the most stable, becomes dominant in the range 130-150°C and at still higher temperatures, a number of ill-defined reactions prevail (18). Resole cross-linking is performed by application of heat between 130-200°C. Resoles can also be acid cured using strong organic and inorganic acids at ambient temperature e.g. p-toluene sulphonic acid, phenol sulphonic acid, phosphoric acid, oxalic acid and hydrochloric acid. The novolaks are formed under acidic conditions and are fully cross-linked by application of a hardener, HMTA (9-15 wt%) and heating to above 100°C, fig.2.1e. The final cross-linked material is postulated to have a structure similar to the fully cured resole, fig.2.1d. Curing with HMTA involves gas evolution (of which 95% is ammonia) with the hardened resin containing 6% chemically bound nitrogen as a benzyl amine. The yellow colouration of the oligmers observed indicates the presence of azomethine groups, -CH=N- .

FIG.2.1a Formation of a resonance stabilised phenoxide ion

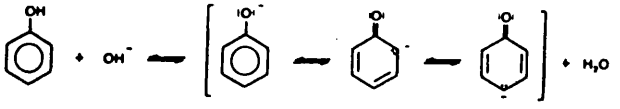

FIG.2.1b Reaction of phenol and formaldehyde under basic conditions to form hydroxymethylol phenols

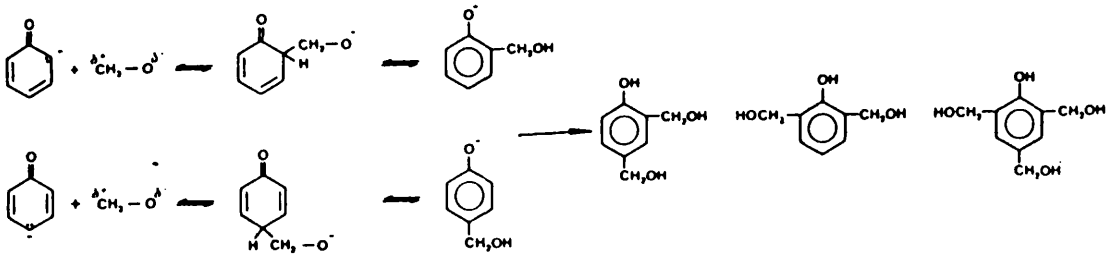

FIG.2.1c Reactions of hydroxymethylol phenols

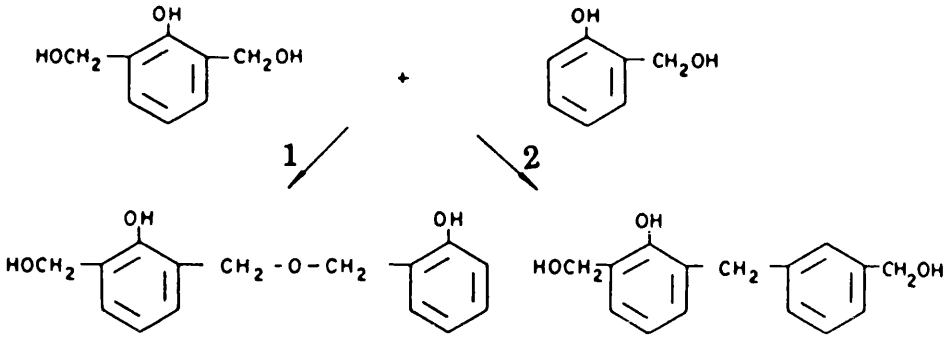

FIG.2.1d Partially cured resole showing the presence of three types of aromatic rings differing in the degree of substitution. A fully cured resole (or novolak) would contain mainly trisubstituted rings (type c).

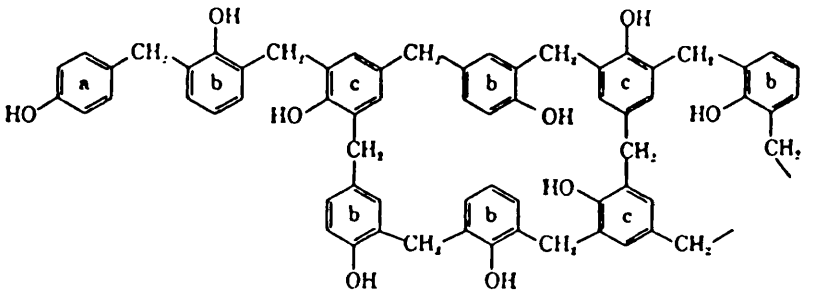

FIG.2.1e Acid catalysed reaction of phenol and formaldehyde to form a novolak

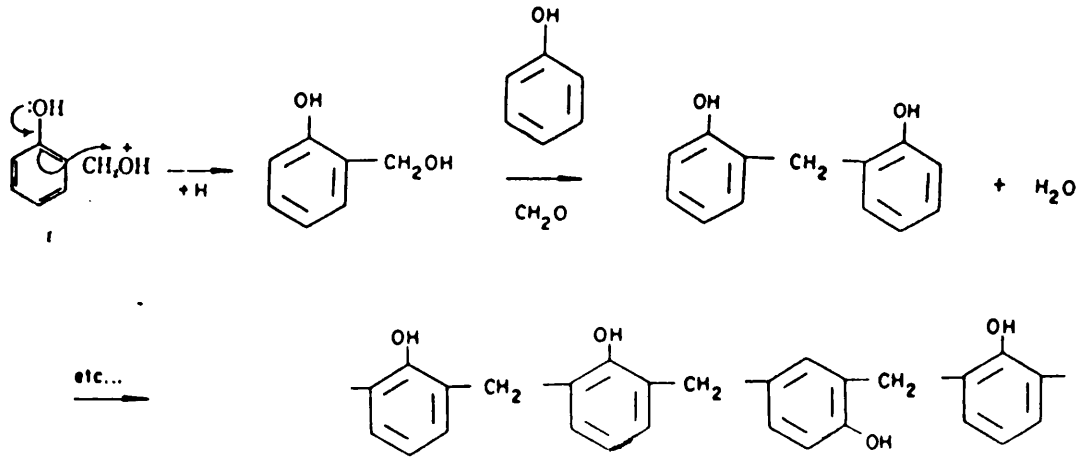

SUMMARY

Resoles are prepared under alkaline conditions with a P/F ratio less than 1. The reaction proceeds via intermediate stages of resol, resitol and resit. The resit is obtained by the application of heat in the temperature range 170-200°C. Novolaks are linear condensation products prepared under acidic, low temperature conditions with a P/F ratio greater than 1. The dihydroxybenzylether linkage initially present is converted to the more stable diphenylmethane bond by heating. Complete cross-linking of the novolak is achieved by application of a hardener (HMTA) and heating to above 100°C. The range of resoles and novolaks which can be prepared depend on the ratio of reactants, catalyst type, time and temperature of reaction.

## 2.1.2 The Mechanism of Carbonisation

Conley and others (19-33) have extensively investigated phenolic resin degradation by using a combination of experimental techniques. Table 2.1a shows the changes in the infrared absorption bands observed upon heating the resin to 200°C in air. The first new band to appear in the infrared spectrum was the carbonyl band formed via a peroxide intermediate. Conley verified the existence of the latter by chemical analysis and predicted the initial stage of resin oxidation as shown in fig.2.2.

FIG.2.2 Primary oxidation route of phenolic resins: the diphenylmethane unit is converted to a benzophenone linkage via a peroxide intermediate.

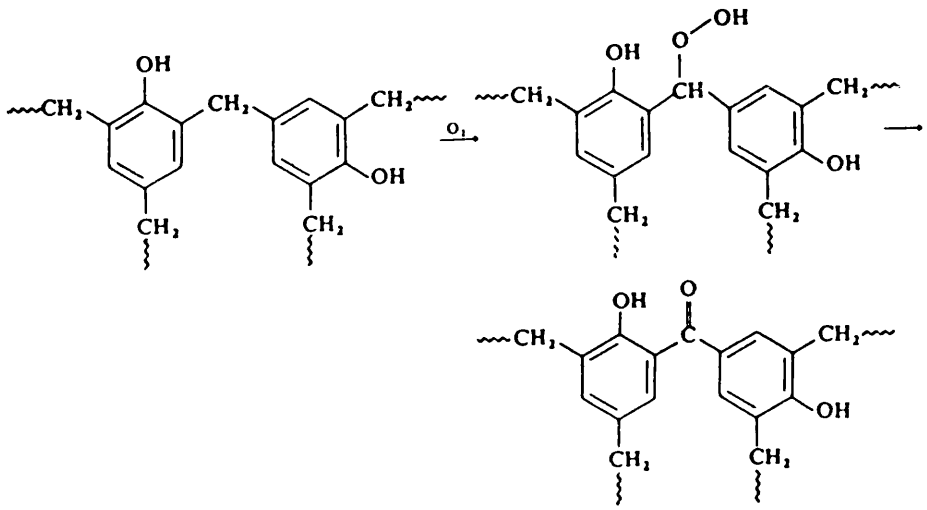

A benzophenone linkage is generated from the diphenylmethane via a dewatering reaction. Further oxidation results in a quinoid type structure and finally a break-up to acid and quinone groupings, fig.2.3. The reaction scheme depicted in fig.2.2 is confirmed by the appearance of a carbonyl band in the infrared spectra at a frequency of 1650cm$^{-1}$. Only two chemical processes can yield such carbonyl groups; 1) cleavage to acid fragments and 2) rearrangement to quinoid-type structures. The 1650cm$^{-1}$ band is too low for an acid moiety and therefore was postulated to arise from quinone-type structures which are known to exhibit bands in the 1650-1690cm$^{-1}$ wave number region (34). It has been reported that sterically hindered phenols are oxidised to quinone-type structures and that the latter are unable to form in the presence of alpha-hydrogens, located alpha to the aromatic ring (35).

Once the carbonyl structure is formed from the methylene group, the conditions of steric hindrance and absence of alpha-hydrogen are fulfilled, thereby lending support to quinoid intermediate formation in the secondary oxidative process (36). The rate of quinoid species formation increases as the temperature is increased. The primary degradation route for the phenolic resin system, regardless of whether the resin was exposed to elevated temperatures in an inert atmosphere or air, is oxidation. This has been linked to the high oxygen content of the resins. At very high temperatures (>700°C) products are also observed from thermal pyrolysis.

FIG.2.3 Second stage of the primary oxidation route

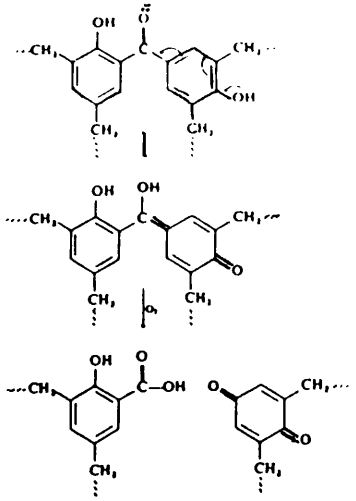

After the early weight loss (<300°C), the resins exhibit very similar high temperature degradation regardless of the P/F ratio. Weight loss rate is affected by the heating rate, particle size and by the atmosphere surrounding the sample (37). Weight losses

for materials cured below 300°C were found to be greater than the post-cured samples. This is consistent with the loss of entrapped solvent, water from methylol condensation and low molecular weight components arising from volatilisation as the temperature is increased. In the 300-400°C region, all samples show similar weight losses as the material is almost fully cured, thus explaining the similarity between the cured and post-cured systems. Indeed the weight loss is postulated to be similar for resoles and novolaks, provided the initial curing process is complete. Major weight losses occur between 400-700°C and are similar regardless of the starting resin or its degree of cure. This is supported by the similarity in type and absorption intensity of infrared bands arising from the newly formed functional groups. The products formed during pyrolysis can be separated on a chromatographic column and identified on the basis of their retention time, table 2.1b. Of the observed weight losses, 50% percent is due to loss of phenol, o-cresol, p-cresol, CO, $CH_4$, $CO_2$, benzene, toluene and benzaldehyde. The remaining 50% is due to loss of water and formaldehyde and formation of a high molecular weight non-volatile char or residue.

It is known that the methylol species and the dibenzylether linkage (minor) play a role in phenolic resin chemistry. The former is a primary reaction product formed during base catalysed synthesis, while the latter arises upon heating methylol species to aboye 120°C or from resin synthesised under acidic conditions (novolaks). Methylol groups participate in three reactions: 1) reversal of condensation to form formaldehyde; 2) upon heating,

a methylene group is formed with evolution of water; and 3) oxidation to acid groups.

The amount of water produced from unchanged methylol groups is reported to be as high as 50% of the total water generated below 340°C. Water is evolved over the temperature range extending to 900°C, although maxima are observed at 200°C and 400°C.

Table 2.1a Infrared absorption bands of phenolic resins heated at 200°C (ref:30)

| FREQUENCY ($cm^{-1}$) | ASSIGNMENT | CHANGE |
|---|---|---|
| 3300 | -OH | decrease |
| 3200 | -COOH (OH) | increase |
| 1650 | -C=O | increase |
| 1720 | -COOH | increase |
| 1480 | -CH | decrease |
| 875, 820 | 1,2,4-trisubstituted aromatic ring | decrease |

The de-watering reactions are shown in fig.2.4. Methylene groups not involved in dehydration reactions become bonded to the benzene nuclei, thus remaining in the resultant carbon char, while about 29% are evolved as methane. The oxygen in the resin participates mainly in reaction 2, fig.2.4, while a small percentage plays a role in the curing reaction, reaction 1 and reaction 3. Reaction 1 occurs between 100-300°C while reactions 2 and 3 are dominant above 300°C. Above 340°C, 95-97% of the water

evolved is due to reaction 2.

2.1b Detection of phenolic resin degradation products by Gas Chromatography (ref. 26)

| PEAK No. | DEGRADED COMPOUND |
|---|---|
| 1 | non-condensable product gases: CO, $CO_2$, $CH_4$ |
| 2 | benzene |
| 3 | toluene |
| 4 | water, formaldehyde, 2,4-dimethylol phenol, o-cresol, phenol and p-cresol |

FIG.2.4 Dewatering reactions of PF resins

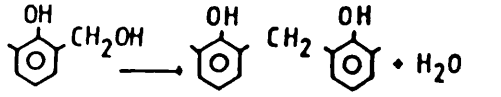


(1)

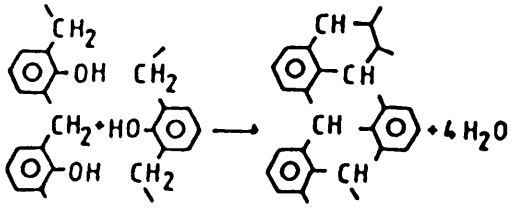


(2)

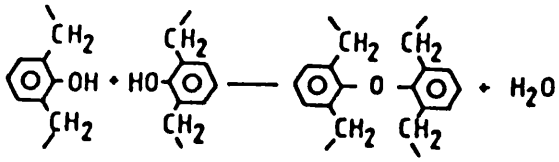


(3)

## 2.1.3 Mechanism for Weight Loss

Weight losses at lower heating rates are expected to be greater if diffusion of material of high volatility is the

controlling mechanism. At higher heating rates, the volatile species would undergo thermally-induced post-curing reactions as they would not have time to diffuse out of the solid matrix. Thermal decomposition of entrapped solvent may account for propanol, propylene, ethane and ethylene reported by various authors working on PF degradation (38,39). Water and formaldehyde are detected upon heating to 400°C, but below this temperature occur in trace amounts. This confirms that they arise from high temperature resin reactions and are not present as mere impurities. The initial cured resin contains methylene linkages, residual methylol groups and dihydroxybenzophenone linkages (arising from partial oxidation during resin curing). Variations in the amounts of these species from methylene oxidation and salicyclic acid moities, from methylol oxidation, account for the variation of CO and $CO_2$. Methane formation increases above 400°C while cresol and xylenol species are formed in constant amounts as the temperature increases. Benzene, toluene and benzaldehyde are formed via loss of the phenolic hydroxyl group. The hydroxyl radical is a source of oxygen for further oxidation and is a source of water through hydrogen atom extraction from methylene linkages. Phenols, cresols and higher phenolic species are produced at lower temperatures. They are postulated to arise from dihydroxydiphenylmethane and other slightly higher homologues, entrapped in the cured resin, rather than from non-oxidised post-cured resins. The reaction scheme shown in fig.2.5a-e takes into account all observations in the high temperature degradation of PF resins. The scheme is idealised since experimental verification for differences in reactivity of

2,2'- ; 2,4'- and 4,4'- isomeric units has not been possible.

TABLE 2.2 Gaseous products of PF resin degradation (ref.40)

| COMPOUND | MOLE % |
|---|---|
| hydrogen | 54 |
| phenol | 2.5 |
| cresols | 2.5 |
| carbon monoxide | 12 |
| methane | 12 |
| water | 12 |
| miscellaneous | 5 |

However high temperature degradation studies coupled with gas phase product distribution, spectral examination of the residual material and other physical data (19-33) do give an almost complete degradation scheme. Thermo-oxidative degradation and fragmentation reactions are presented in fig.2.5a while fig.2.5b shows the route for benzene and toluene formation. Methane formation occurs in increasing amounts above 400°C, fig.2.5c. The splitting of phenols to aromatic hydrocarbons is a difficult process and leads to benzenoid species formation, fig.2.5d involving splitting-off of the hydroxyl group. Formation of the aromatic hydrocarbons is observed in metal casting having phenolic resin bonded sand moulds. Various other polymeric materials formed during degradation are depicted in fig.2.5e. The overall mechanism of carbonisation is presented in fig.2.6 along with the predicted temperature.

FIG.2.5a High temperature degradation of phenolic resins: Route 1; oxidative degradation process; Route 11; fragmentation reactions

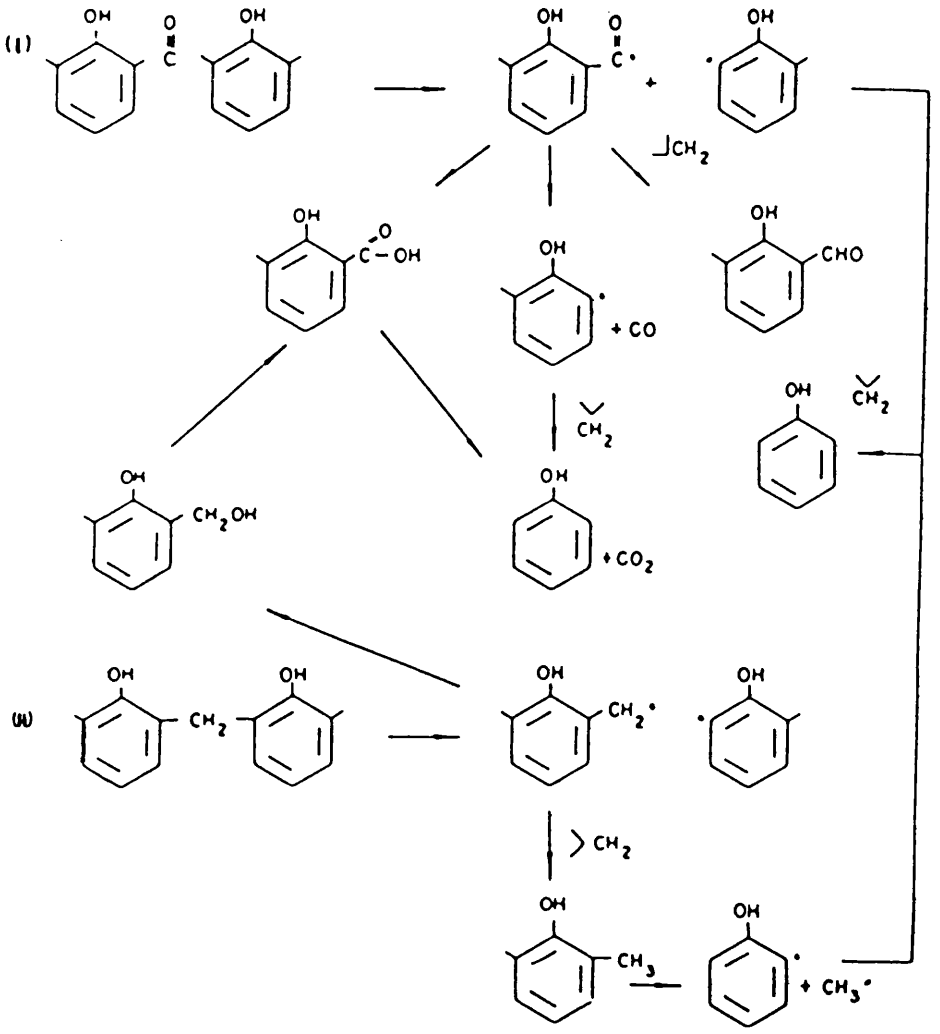


FIG.2.5b High temperature degradation of phenolic resins showing formation of benzene and toluene

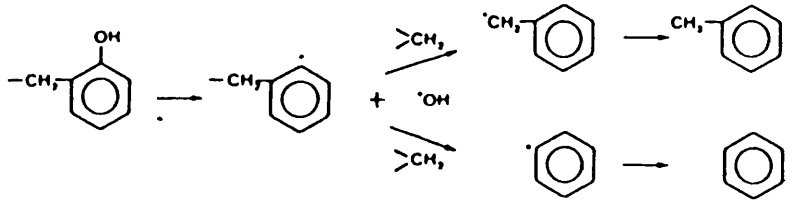

FIG.2.5c Formation of methane

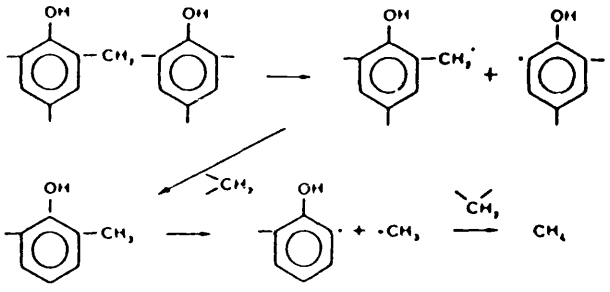

FIG.2.5d Benzenoid species formation from degradation of phenolic resins

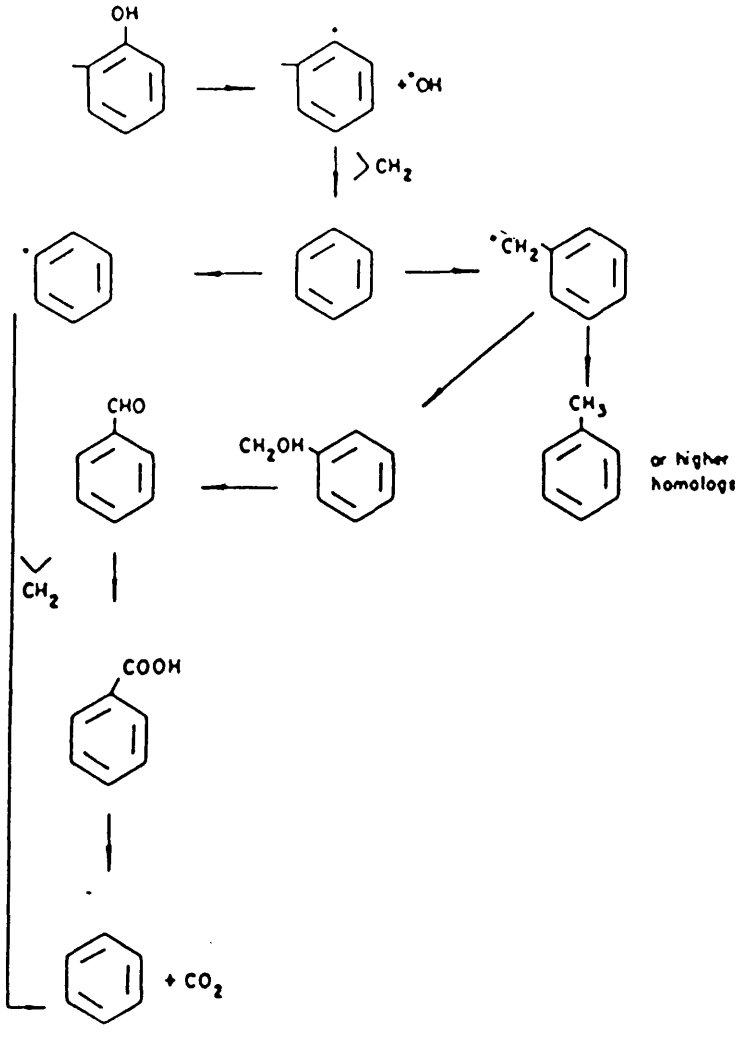

FIG.2.5e Formation of di-phenoquinones and other polymeric materials.

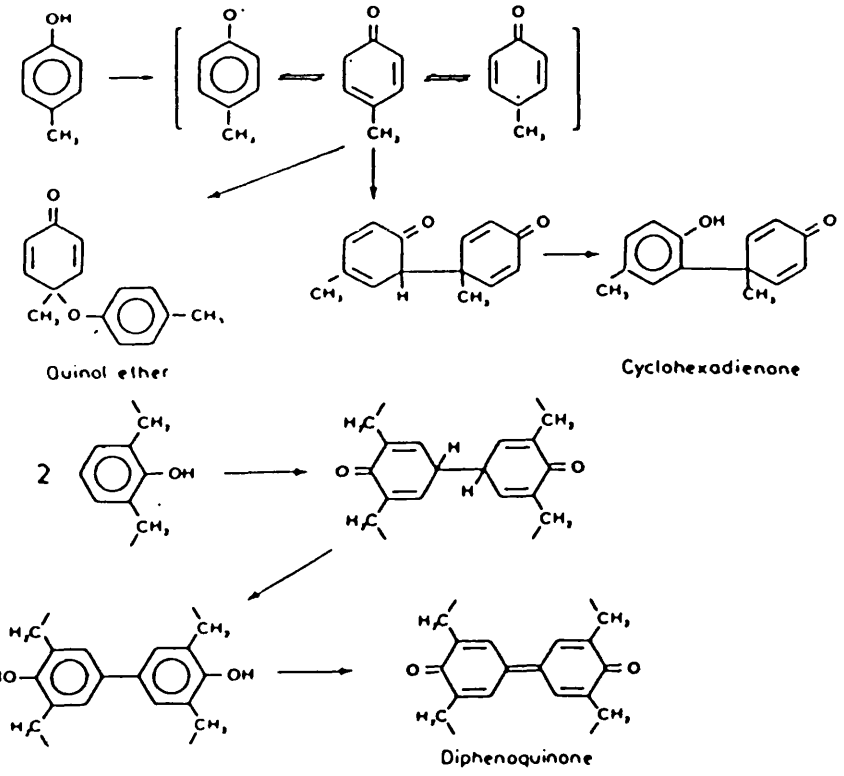


FIG.2.6 Schematic presentation of the mechanism of carbonisation of PF resin showing the approximate temperature range of the pyrolysis reactions

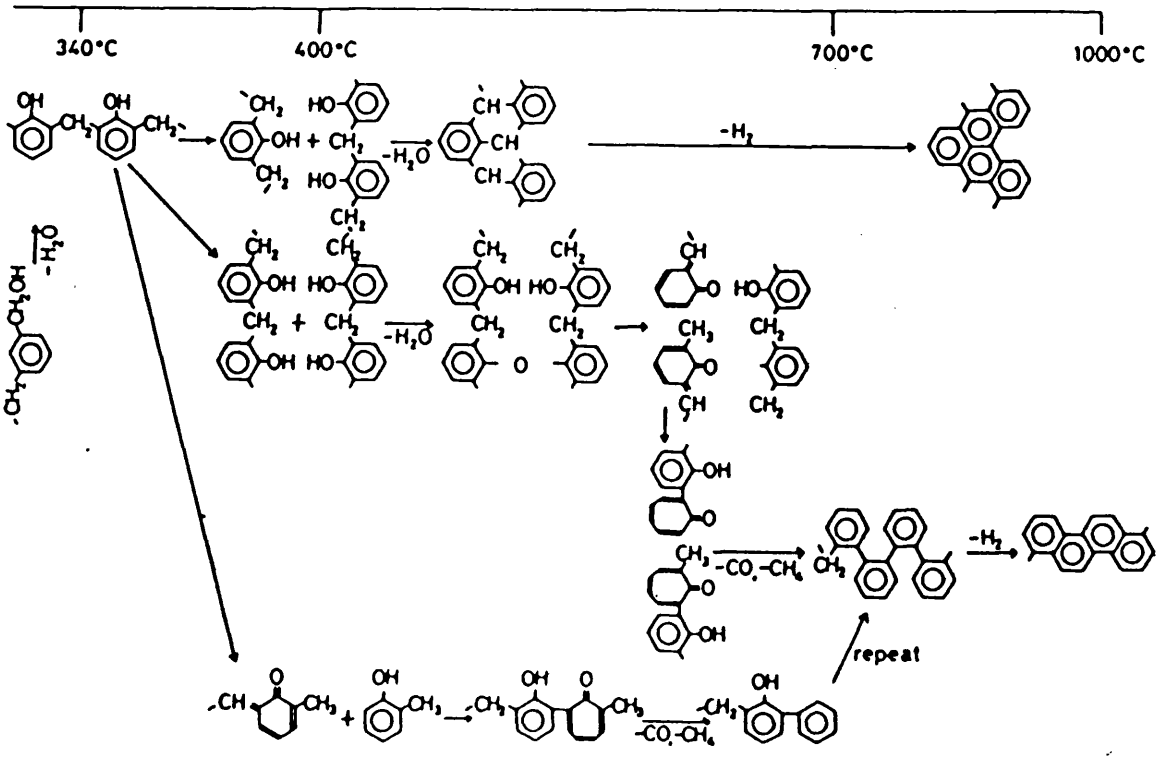

SUMMARY

In summary, collected data concerning PF resin degradation, suggests that regardless of the particular species present before curing i.e. resole or novolak, the degradation processes ocurring at elevated temperatures are dependent upon the concentration and thermal and oxidative stability of the diphenylmethane unit. Hence, once curing is complete, these resins follow the same high temperature degradation route. In the temperature range 300-500$^{o}$C, oxygen and nitrogen are removed and cross-linking between the polymer chains increases with an increase in strain energy. Between 500-1200$^{o}$C, hydrogen is gradually eliminated and the separate, conjugated, aromatic network becomes inter-connected to form a conducting system. This is manifested by an increase in electrical conductivity, density, hardness and stiffness.

## 2.1.3 The Structure of Polymeric/PF Carbons

The carbonisation of PF resins does not involve a fused state due to the high degree of cross-linking inherent to the system. Thus, the absence of an intermediate liquid phase results in an isotropic carbon char, which is non-graphitisable and exhibits properties different from the pitch-based graphitic (coke) carbon, see section 2.2. Primary evidence for char formation rests on the

fact that quinoid species are readily formed from dihydroxybenzophenone moities as the temperature is increased above 600°C, fig.2.7 (41,42). Formation of carbon char closely parallels CO evolution. The latter arises via a ring scission reaction (see section 2.1.2). Char formation can be detected visually or by the presence of a graphite-like line in the x-ray spectrum of the residue i.e. the La, Lc and $d_{002}$ crystalline parameters, where La is the mean layer diameter, Lc is the microfibril thickness and the $d_{002}$ line represents the spacing between graphitic layers, fig.2.8 (43). The non-graphitic character of polymeric carbons is further indicated by the absence of the 101 peak representative of an extensive ABA register of graphitic sheets.

FIG.2.7 Reaction scheme showing the mechanism of char formation.

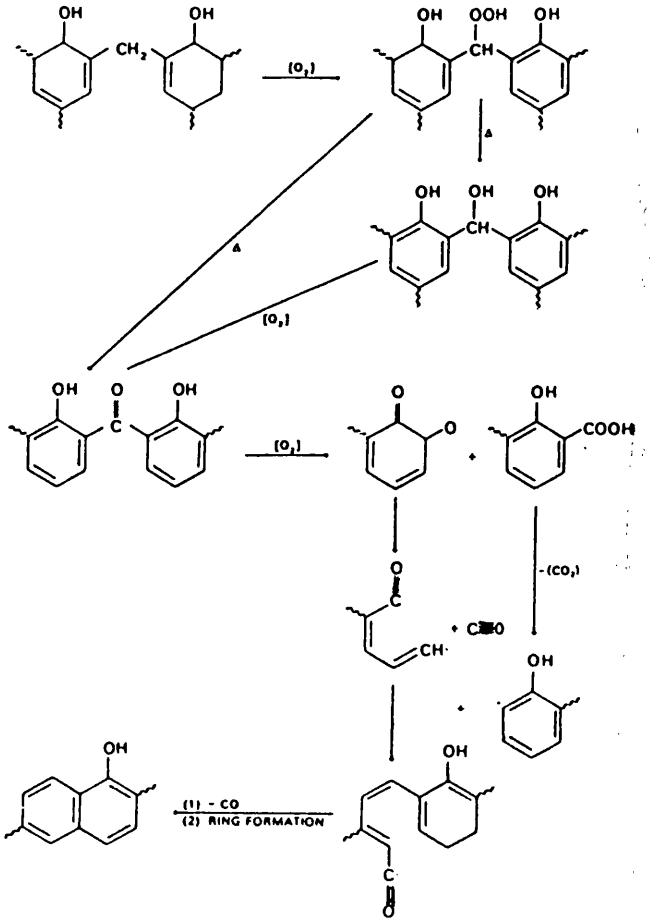

During carbonisation, the inter-molecular bonds of the phenolic network as a whole remain intact. The structure of the final carbon, after further heat treatments, is essentially only a minor modification of the structure of the material produced at 500°C. The polymeric carbon network is arranged to form layer planes similar to the graphitic planes, but they are limited in extent and are highly disordered. The resulting amorphous structure, interspersed with limited areas of ordered structure, affords a high degree of bonding and a high surface area (41,44). These factors are useful for the production of formed, or unformed, refractory materials such as bricks, shapes e.g. shrouds, ladle and slide gates, and crucibles. The phenolic resin being used as a binder together with magnesite, dolomite, bauxite, corrundum and other materials. By correlation of experimental data it was concluded that carbonisation of PF resulted in a progressive coalescence of the polymeric chains (45-48). These chains were stabilised by inter-chain methylene cross-links. Essentially, as carbonisation proceeds, the polymer chain is converted into a narrow ribbon of condensed aromatic molecules which are randomly oriented. Above 500°C, inter-ribbon cross-links (edge-to-edge-bonds) are formed both perpendicular and parallel to the plane of each ribbon, with a resulting increase in carbon hardness. These strong, covalent carbon-carbon bonds act as a constraint to the formation of a three-dimensional graphitic structure. As the temperature is raised (1400-1500°C) infrared spectroscopy shows the gradual loss

of inter-ribbon cross-links. Other internal defects and distortions are also removed, allowing the gradual release of internal strain energy and a decrease in hardness. The final defect-free ribbons stack above each other to form microfibrils with about 10 ribbons in each stack. The microfibrils are bonded to each other at the edges of the ribbons with strong covalent bonds. THe latter prevent the narrow graphite ribbons from developing parallel stacked, extensive graphite sheets and thus moving into 3-D graphitic ABA order. The microfibrils twist, bend and intertwine and are randomly arranged in space. These distortions are easily accommodated by the ribbon structure but not by the graphitic sheet structure. Fig.2.8 is a highly simplified model for glassy carbon. In reality, the fibrils should pack close together to form a tighter structure. Strong confluences arise where ribbons merge into each other and weak confluences exist at regions of ribbon overlap (13, 47).

The highly strained 'curly carbon' structure shows a continuous arrangement of microfibrils and the apparent absence of 'loose ends'. This explains the chemical inertness of the polymeric carbon. Since the ribbons cannot be drawn straight and parallel in one direction (due to random inter-ribbon cross-links) but remain tangled, a large number of internal slot-shaped, fine pores are generated, reflecting inefficient space filling (47).

FIG.2.8 Hypothetical model for a polymeric carbon (ref. 47)

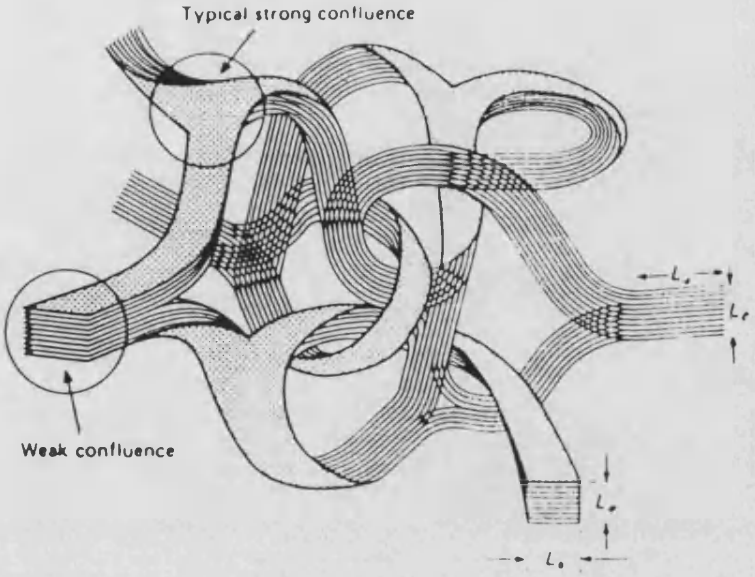


It has been reported for phenolic resins that heat treatment to 2700°C results in a network having carbon atoms in $sp^2$ hybridisation. Furthermore, the high temperature treatment promotes a continuous transition from random to oriented fibrils, tightening of the ribbon clusters, release of internal strain energy and removal of the closed or internal porosity. Although full graphitic character is never achieved, changes in the x-ray diffraction pattern e.g. emergence of new lines superimposed on the $d_{002}$ band, after heat treatment between 2000-3000°C have been detected. These were linked to the formation of isolated, perfect, graphitic crystallites embedded in the bulk isotropic matrix. Franklin (45, 46) referred to this compositional arrangement as a two phase and three phase graphitisation and attributed the localised appearance of the crystalites as a consequence of stress-induced transformation. Full graphitisation

was not achieved due to the presence of strong edge-to-edge bonding and non-perfect alignment of the crystallites so that ordered stacking does not occur. The resulting structure reflects the absence of extensive AB stacking. The isolated graphitisation introduces internal strain within the vicinity of the graphitic crystallite, thereby leading to a drastic decrease in strength. Thus glassy carbon is hard but brittle, as reflected by its poor mechanical shock resistance. Evolution of a high percentage of volatiles during pyrolysis (40-50% by mass), accompanied by a 25% linear shrinkage, is reflected by the increased density and high internal stresses. These factors control porosity, cracks and adhesive properties of the carbon and are obviously important when the resin is used as a binder in carbon-oxide composites. If heat treatment at high temperatures is accompanied by a partial oxidation, a large increase in surface area is observed, reflecting the high internal porosity which is opened up (43).

In summary, the ribbon model of isotropic glassy carbon is confirmed by the following reported observations: 1) Thermal properties are very similar to those of normal polycrystalline graphite with small crystal size. 2) Resistivity is similar to polycrystalline graphite since electron movement is easy along perfect ribbons. 3) Superior stiffness and resistance to deformation is attributed to the strong boundary restraint at the edges of the component ribbons and strong inter-lammellar bonding prevalent at high heat treatment temperatures (>2000$^{o}$C). 4) Increase in hardness after 350$^{o}$C heat treatment is due to formation of inter-molecular cross-links between the polymer

chains. Heat treatment above 500°C produces a rapid increase in hardness due to formation of inter-ribbon cross-links. 5) Inter-ribbon cross-links are broken between 1500-2000°C thereby allowing release of internal strain energy, decrease in the inter-molecular forces and hence, hardness. 6) Non-graphitisable carbons have a high surface area at 700°C. Above this temperature, the ribbon clusters tighten and the intrinsic fine porosity is sealed off, as reflected by a decrease in the surface area.

## 2.2 The Structure and Applications of Pitches

### 2.2.1 The Materials and Applications

Pitches form a class of materials containing a diverse range of organic compounds. Petroleum pitch, PP, is obtained by the thermal cracking of crude oil or heavy residues in the gas phase, at temperatures of 600-700$^{o}$C. Coal tar pitch, CTP, is obtained by distillation of coal tars. Steam cracking of naphtha or the gas oils, yield a by-product called 'steam cracker tar, SCT, (49). SCT is composed of low molecular weight fractions of asphaltenes which are soluble in benzene but insoluble in paraffins. By polycondensation of aromatic rings via either a thermal process or catalytic oxidation, SCT pitch of high aromaticity and coke yield is obtained. Further pitch-forming materials include PVC, PVDC, anthracene, naphthalene and phenanthrene.

Depending on the source and thermal history, CTP and PP contain hundreds of aromatic and aliphatic hydrocarbon compounds. Generally, CTP is more aromatic in nature than PP. As it is difficult to characterise the pitch chemically, i.e. by analysis of individual compounds, physical data are usually reported. These include: 1) Thermal parameters viz. boiling range, glass transition temperature, Tg, softening temperature, Ts, and decomposition temperature, Td.; 2) Coke yield; 3) Density; and 4) Solubility in various solvents, table 2.4. Pitch is an organic glass at room temperature exhibiting a characteristic Tg.

Similarly the liquid crystal mesophase (see below) existing in the pitch melt is also reported to behave as a glass at low temperature with its own specific Tg which is higher than pitch Tg (50-51) Determination of Ts allows prediction of pitch decomposition temperature, Td. A linear relationship between Tg and Ts has been reported for several pitches (52).

The numerous constituents of pitch can be isolated by solvation in a range of solvents. A typical solvent fraction scheme will involve several stages as shown in fig.2.9. The individual fractions can be isolated by vacuum evaporation of the solvent and their molecular weight distribution and size determined by high pressure liquid and gas chromatography or vapour pressure osmometry (53-55).

FIG.2.9 Fractionation scheme for a CTP

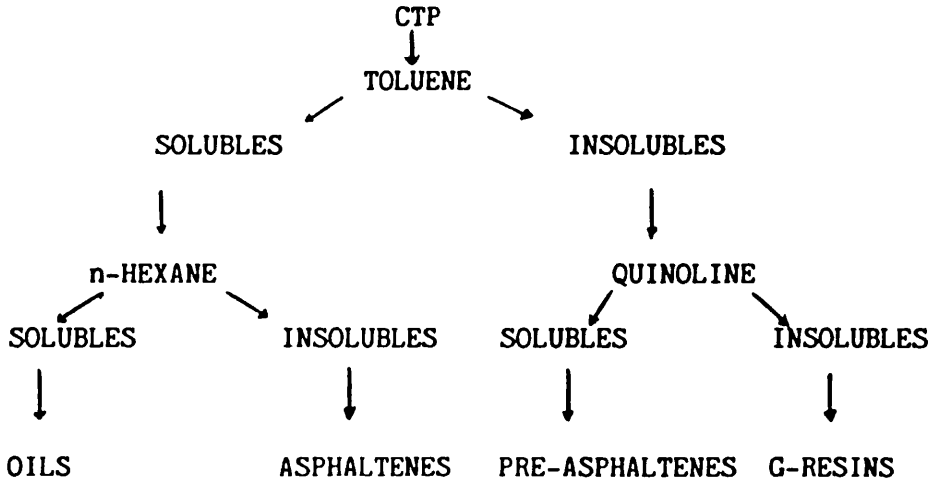


The latter technique gives the average molecular weight and the former technique gives information on molecular size

distribution and type. During solvent fractionation, the solvent can have a profound influence on tar and pitch compounds leading to precipitation and coagulation (55). A typical pitch analysis is presented in tables 2.3a and 2.3b. The aliphatic and aromatic character of the pitch is determined by infrared spectroscopy and proton and $^{13}C$ NMR spectroscopy (54,55, 57,58).

TABLE 2.3a Characteristics of SCT, PP AND CTP (ref. 49)

| | SCT Pitch | Petroleum Pitches (1) | Petroleum Pitches (2) | Coal Tar Pitches (1) | Coal Tar Pitches (2) |
|---|---|---|---|---|---|
| 1. Physical Characteristics | | | | | |
| Sp. gr. | 1.265 | 1.223 | 1.260 | 1.270 | 1.259 |
| Softening Point (R&B) °C | 110 | 117 | 110 | 101 | 113 |
| Coking Value at 550°C (wt %) | 52.0 | 54.0 | 56.0 | 56.6 | 59.7 |
| Ash Content (%) | 0.100 | 0.150 | 0.21 | 0.200 | 0.300 |
| Benzene Insolubles (%) | 27.0 | 8.0 | 30.0 | 41.98 | 48.7 |
| Quinoline Insolubles (%) | 2.5 | 0.5 | 11.5 | 21.7 | 26.0 |
| Viscosity (%) (cps) at 160°C | 3000 | 1400 | 2050 | 1116 | 840 |
| 2. Chemical Characteristics | | | | | |
| Aromatic Carbon (atom %) | 78 | 82 | 80 | 89 | 88 |
| Aromatic Protons (%) | 50 | 57 | -- | 84 | 86 |
| Benzylic Protons | 37 | 34 | -- | 13 | 11 |
| Paraffinic Protons | 12 | 9 | -- | 3 | 3 |
| Carbon/Hydrogen Atomic Ratio | 1.37 | 1.44 | 1.57 | 1.77 | 1.76 |

TABLE 2.3b Molecular weight distribution of SCT, PP AND CTP (ref. 49)

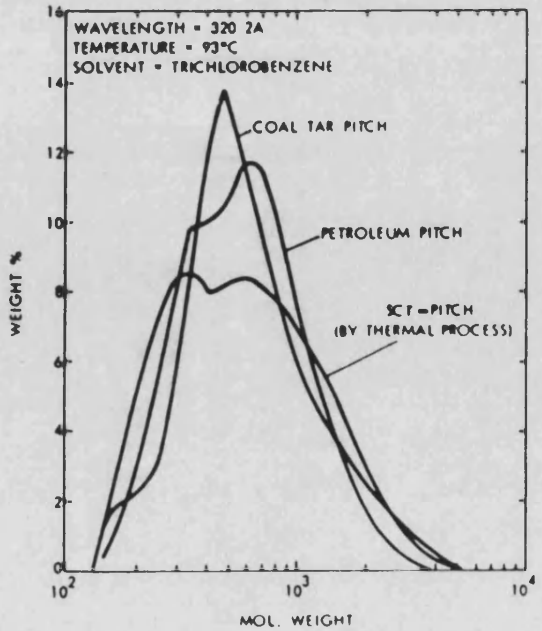

Chemical analysis has shown that the most complex molecules in CTP have an atomic mass unit (a.m.u.) <3000. Infrared studies indicate that the condensed aromatic molecules contain a number of benzene rings joined to each other by single bonds or methylene bridges, giving a 'ring-chain' structure. Aromatic hydrocarbons, either unsubstituted or substituted, with one or more methyl groups attached to the nucleus, represent the largest class of material. Hetrocyclic compounds containing oxygen, nitrogen or sulphur occur in smaller amounts. The aromatics are mainly (90%) of the benzene, naphthalene, anthracene and phenanthrene series. Phenols and paraffins range from 5-25%, depending on the source of the coal tar.

High aromatic content is essential for obtaining a good coke yield since aliphatic groupings tend to volatilise during pitch pyrolysis. Various techniques exist for improving the coke yield which is known to depend on the pressure, heating rate and sample size. High values of these conditions permit radical recombination reactions. Thus, vapourisation of low molecular weight carbon compounds i.e. paraffins, olefins and aromatics, is reduced and aromatisation, chemical polycondensation and cross-liking reactions to form high molecular weight carbon compounds, is increased. The method of pitch preparation from the raw material has a strong influence, especially with respect to percentage aromaticity, molecular weight distribution, viscosity and coke yield. Pressure has also been found to effect moulded carbon articles. The pressure effects may be summarised as follows: 1) maximum coke yield is obtained at 100 bars and a

temperature of 550°C; 2) the temperature of pyrolysis is lowered; and 3) segregation of the insoluble components of CTP (which forms mesophase) from the insoluble components ( which are unable to form a mesophase). High pressure hinders volatilisation of low molecular weight compounds, which are thus retained as a solvent phase of low viscosity and from which further large molecules are generated by condensation reactions. Thus, nucleation, growth, coalescence and re-orientation of the lamellae making up the mesophase are enhanced, as shown by enlarged areas of optical microscopy. However, pressures greater than 100 bar tend to impart only minor benefits (59,60).

Various additives and air-blowing techniques have also been used for increasing the percentage aromatic content and coke yield. Thus, benzotri-chloride has been reported to decrease the percentage porosity while chloro and nitro compounds increase the density of the binder carbon. Although little evidence is available to explain the effect of the additives on the pitch, the additives are presumed to aid condensation reactions which lead to increased viscosity, enabling adequate mesophase formation and a high coke yield (61, 62).

In summary, efficient pyrolysis of hydrocarbons should involve control of: 1) degradation or primary pyrolysis i.e cracking of all non-aromatic hydrocarbons to smaller molecules; and 2) synthesis reactions or secondary pyrolysis; a) aliphatic side chains can also undergo cracking or cyclisation, and b) condensation of aromatics to form polycyclic aromatic systems.

## 2.2.2 Formation of Mesophase

The microstructure and properties of graphitic materials are determined by the microstructural characteristics of an ordered intermediate fluid stage termed, the 'carbonaceous mesophase'. The mesophase was first described by Brooks and Taylor (63) as a plastic stage which appeared in the temperature range 370-500°C during pitch pyrolysis. The chemistry of the mesophase is directly linked to the chemistry of the starting materials (63, 64). Due to the complexity of pitch pyrolysis, data on the chemistry of carbonisation and mesophase formation have been compiled by research on a numerous variety of pitches. Single component systems containing individual aromatic ring structures such as naphthalene, arthracene and phenanthrene have also been investigated. Thus acenaphthylene, which is a component of CTP (13), upon heating to above 200°C, polymerised to polyacenaphthylene, structure 2, fig.2.10. Further heating lead to formation of polyarenes such as the fluorocyclenes, 4, via the dimer, 3 and to the stable planar decacyclene, 6. Further dimerisation, trimerisation etc. yield a viscous liquid consisting of a complex series of high molecular weight molecules. From within this liquid isotropic melt, small spherulites, consisting of a congregation of about 50 high molecular weight molecules (a.m.u. >1000) become evident, giving rise to a two phase emulsion. The spherulites represent the liquid crystal phase and can reversibly associate/dissociate depending on the temperature. However, at a certain critical stage the process becomes irreversible with the equilibrium being shifted towards

sphere formation i.e. insoluble material deposition, which is termed the mesophase. The critical stage has been linked to the critical concentration of large molecules at which transition to a liquid crystal phase is dominant. Thus mesophase formation is a process of supersaturation of large molecules.

Polarised light microscopy of polished cross-sections has been used to provide information on nucleation, growth and coalescence of the mesophase. Buechler (65) used quenching hot-stage to cool rapidly from the temperature at which mesophase formed to room temperature, thereby freezing the mesophase. The cooled mesophase was sectioned and the bulk morphology examined and compared with the surface morphology.

FIG.2.10 Formation and degradation of polyacenaphthylene, 2, via fluorocyclene, 4, decacyclene, 6 and zethrene, 7 (ref.13)

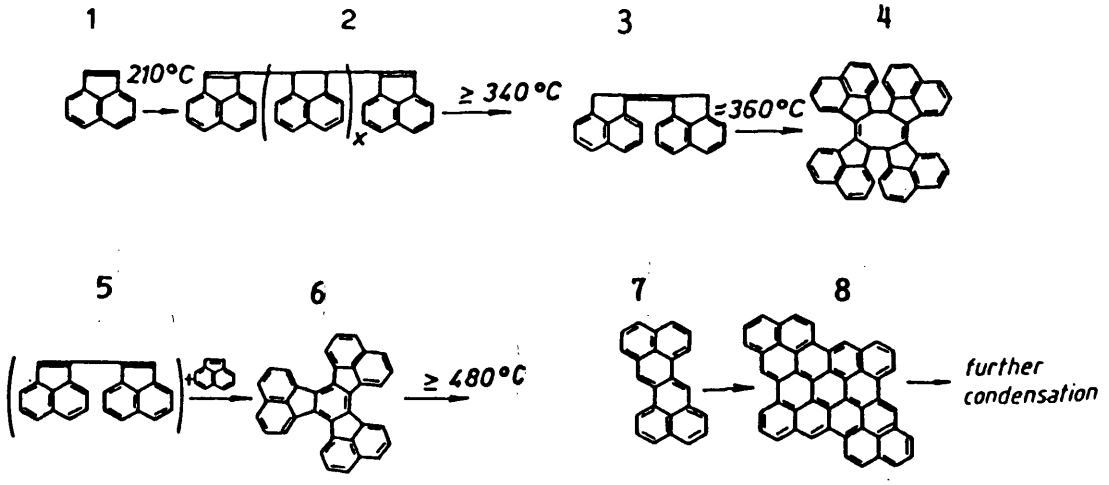


It was found that structural ordering prevalent in the bulk mesophase was responsible for optical texture observed in the resultant pitch coke. Extensive structural ordering being

represented by the large optical texture (domains >60um in diameter).

Several differences exist between mesophase formation and crystallisation phenomena of conventional liquid crystals. The latter is dependent on the following observations: 1) crystallisation can be achieved by temperature lowering i.e. reduction in kinetic energy; 2) Coulombic forces of attraction between constituent molecules operate in the crystal and 3) constituents of the liquid are chemically stable. In contrast, mesophase formation has been linked to these observations: 1) mobility of the molecular species is lowered not by decrease of temperature but by increasing the temperature i.e. due to formation of high molecular weight molecules; 2) large van der Waals forces are required to maintain the stability of the liquid crystal and 3) constituents of the liquid crystal are very reactive.

Two factors of utmost importance for generation of liquid crystals are the formation of large molecular units (a.m.u. >1000) and planar arrangement of these units. If the size of these units is not large enough, then the van der Waals forces would not be sufficient to hold the molecules together. Furthermore, if the molecules are non-planar then a physical steric barrier would prevent maximisation of the specified forces. Thus biphenyl groups, arising from phenanthrene, enable easy bond rotation which prevents permanent parallel arrangement of the aromatic system and hence, a coke of inferior graphitic nature.

Conversely, anthracene, which forms various bianthryls via radical reactions, also contains biphenyl bonds which, however, are unable to rotate due to steric hindrance. Hence the aromatic rings adopt a planar arrangement involving a parallel stacking of the molecules. The existence of long range molecular order is the only crystallographic requirement for mesophase formation. The resulting semi-coke, by further modification of the structure, can be made graphitic by heat treatment at high temperatures, or by the use of catalysts. If the reactivity of the system is too high, extensive polymerisation can occur within the fluid pitch at a temperature which is too low for establishment of the liquid crystal. Hence the resultant carbon will be isotropic, as in the case of carbon prepared from PF resins. Similarly, air-blowing or air-oxidation at low temperature, is used to increase coke yield by promoting cyclisation of alkyl side chains and aromatic polymerisation i.e. coupling of aromatic nuclei by methylene or ether bonds (66). However, excessive oxygen leads to formation of oxidation rims where the pitch remains isotropic. The oxygen content of the original material has a dominant effect on both the mechanism of formation of carbon texture and on its graphitisability . Furthermore, presence of oxygen containing groups, such as phenolics, can also lead to isotropic, non-graphitisable carbon generation.

Air-blowing of pitches or addition of dehydrogenating agents e.g. alkali metals, vanadium, oxidising agents such as dinitrotoluene, ferric, halogens and sulphur, must be closely monitored to prevent excessive cross-linking. If excessive

cross-linking is permitted, pitch pyrolysis will proceed at such a rapid rate and low temperature that the plastic phase would be insignificant and an infusible, in the extreme case, coke is obtained. When sulphur is used as a cross-linking agent, the reaction involving removal of sulphur as hydrogen sulphide and combination of low molecular weight species, which contribute to the mesophase, is preferred over the reaction involving sulphide bridge formation, which leads to excessive cross-linking. When polished cross-sections of isotropic carbons are viewed under polarised light, no visible structure or texture is evident. Pores are detected but represent remains of gas bubbles formed prior to carbonisation. Similar examination of anisotropic (graphitisable) carbon reveal a highly textured surface, the texture and the anisotropy in the various grains being clearly outlined by the polarised light. Each grain is continuous, although distortions are evident, as flow-lines or striations mark the coke particle surface. The striations are thought to represent outlines of microcracks of the individual grains, as the anisotropic material solidifies from the isotropic pitch melt.

### 2.2.3 Growth of Mesophase

Over a particular temperature range, 400-500°C for CTP, the large lamellar molecules present in the isotropic fluid at a critical concentration, undergo homogeneous nucleation to generate the liquid crystal phase. This process is not analogous to 'seeding' as in conventional liquid crystallisation. However, addition of particulate matter, such as carbon black, MgO etc. will enhance the growth but not nucleation of the spherulites. At onset of nucleation, details of the number of ring systems, their method of bonding and their size within the lamellar molecules are reported to be unimportant (67). Mesophase formation is also independent of: 1) pitch composition- as indicated by the ease of mesophase formation by substances of quite different chemical composition e.g. CTP, asphaltenes, PVC and polycyclic aromatic compounds (68); 2) physical carbonisation i.e. quiescent or turbulent, rapid stirring may however, influence the shape of the spheres but not their actual growth. Conversely, mesophase growth is dependent on the size and planarity of the molecules, the temperature and fluidity of the system (to allow diffusion and orientation of the molecules).

As the pyrolysis temperature is increased, further large molecules separate out as nucleating spheres, the aromatic molecules exhibiting a considerable degree of molecular ordering and are arranged into stacks of parallel arrays. The spheres increase in size by agglomeration with neighbouring spheres and internal polymerisation, thus increasing the extent of mesophase

at the expense of the isotropic liquid melt (69). The mesophase eventually solidifies to a semi-coke between 500-550°C, although the temperature range is influenced by the initial rate of heating. The semi-coke still contains 10% volatile material which will be evolved during further heat treatment, leading to formation of shrinkage cracks within the coke. The spheres of lamellar structure have a circular outline but deviations from circularity occur with increasing sphere/isotropic liquid ratio. Impurity particles (fine particulate materials are known to be present in some pitches) may physically retard sphere enlargement, while over-sized spheres tend to crack and fragment. The spheres have a complex internal structure which is slowly stabilised due to the high viscosity of the mesophase. As two spheres coalesce, a structure is formed containing lamellae of uniform orientation with interconnecting zones of mesophase, in which the lamellae curve around sharply. This structural arrangement is referred to as a mosaic structure and the coke is said to be anisotropic.

In summary, mesophase formation proceeds via several stages: 1) generation of high molecular weight, planar, aromatic molecules within the liquid melt; 2) parallel arrangement of the large molecules due to dispersion effects; 3) growth of the planar molecules; 4) agglomeration of the above molecular structures to form liquid spherulites and 5) coalescence of the spherulites leading to formation of an insoluble mesophase of anisotropic texture, which solidifies to a semi-coke.

## 2.2.4 Graphitisation

When the semi-coke is heated the mosaic texture and lamellar orientation making up randomly stacked and defective graphite sheets, are converted into perfect, defect-free, hexagonal graphite sheets, as shown by the appearance of a strong 101 peak in the x-ray pattern. Graphitisation, as described above, is a modification of the structure developed during carbonisation, and varies widely with starting material. The volatiles (10wt%) enclosed in the semi-coke are evolved in the temperature range 600-800$^{o}$C, leading to an increase of material density and generation of shrinkage cracks. The latter are responsible for the low reported values of the coefficient of thermal expansion, CTE, for anisotropic carbons. Further heat treatment involves minor weight losses due to removal of edge carbon atoms, heteroatoms and hydrogen and structural changes (70). The latter includes rotation and smoothing out of layers, removal of defects such as voids and cracks. This annealing mechanism, operating at the graphitisation temperature (>2000$^{o}$C), is thought to mainly involve diffusion of carbon atoms by a vacancy mechanism (71).

High resolution electron microscopy, HREM, and x-ray diffraction studies have been used to provide the following data on the anisotropic carbon lattice: at 500$^{o}$C Lc=1-1.5nm; $d_{002}$ = 0.344nm; at 1000$^{o}$C Lc=1.5-2.0nm, La= 5nm and at >2000$^{o}$C La and Lc increase further due to extensive growth of the layers and increase of the stack height. La is the basal plane distance, Lc is the stack height and $d_{002}$ is the inter-lamellar spacing or

Bragg distance. Lc always remains less than La. The graphitisation temperature may be lowered by the use of catalysts (71-74). The metal catalyst is thought to dissolve the carbon atoms, therby allowing them to reform as extensive graphite sheets which can stack perfectly (73-76).

## 2.3 FIRE RETARDANTS

### 2.3.1 Combustion Inhibition of Polymeric Materials by Fire Retardants

The basis of this work is to increase the oxidation resistance of resin carbons by incorporating into the resin carbon chemical compounds, or additives, which are known to act as fire retardants when added to polymers. To aid selection of suitable additives, a literature survey on fire retardants was carried out.

Flammability has been an important social and scientific problem from the earliest times. The Egyptians had coated wood with a solution of alum to render it fire resistant, while Gay-Lussac, 1821 (77) recommended a solution of ammonium chloride, ammonium phosphate and borax as a fire retardant for linen and jute. The increasing application of polymers as construction materials in home furnishing, domestic and industrial buildings, appliances, fabrics and transportation vehicles have been accompanied by demands for stringent safety regulations. A report by the "National Commission of Fire Prevention and Control" provided the following U.S. fire statistics: 12,000 lives lost annually due to smoke and toxic gas inhalation; 300,000 fire injuries; 1 billion dollars for burn injury treatment; 11.4 billion dollars in fire cost and 3.3

billion dollars in productivity loss (78). The resulting sociological pressure has encouraged the developement in technology and engineering of new heat resistant molecules, polymers and commodoties which are inherently flame resistant (79, 80).

Present day fire retardants mainly contain seven key elements of the periodic table viz. boron, aluminium, nitrogen, phosphorus, antimony, bromine and chlorine. Research efforts to find new and improved fire retardent agents for polymers have concentrated mainly on these elements and new ways of incorporating them. However, certain compounds of barium, zinc, tin, silicon and sulphur have been claimed to be effective in some polymers, especially when used in conjunction with one of the seven key elements. New heat-resistant materials have been developed in specialised areas e.g. the space industry, where refractory oxides of titanium, zirconium, hafnium, molybdenum etc. have been successfully applied as sacrificial or ablative coatings on the surface of re-entry vehicles. Protective layers of iridium have been described successful after 2000h at 1400°C (81) Composite layers consisting of $Mo/Al_2O_3/Pt$ were found to be effective at 1425°C between 20 and 4500h (82). With other oxide and metallic coatings protection life times of only a few hours at temperatures upto 1600°C are reported (83-86). Due to the cost of coatings of precious metals, high melting silicides are being regarded as promising ablative materials. Thus $TiSi_2$-coatings (87) as well as $Al_2O_3/MoSi_2$ layers (88) were reported to protect graphite from oxidation for more than 100h at 1400°C (table 2.4)

Table 2.4 Metallic coatings used for inhibition of graphite oxidation (ref.83)

| Coating Material | Method of preparation | Test results in air (lifetimes) |
|---|---|---|
| Ir | Melting;<br>Slurry Dipping technique;<br>CVD | up to 2200°C<br>> 100 h<br>1400°C > 2000 h |
| Mo + Pt | Electrodeposition | ------ |
| $Mo/Al_2O_3/Pt$ | Plasmaspraying | up to 1425°C<br>20 – 4500 h |
| $MgO + ZrO_2$ | Simultaneous flame spraying | 1200°C – 1300°C<br>some hours |
| $Cr_2O_3$; HfC; $ZrB_2$, $HfO_2$ | Plasmaspraying | 1650°C<br>some hours |
| SiC | Pack-Diffusion | 1650°C<br>some hours |
| $TiSi_2$ ; $MoSi_2$ | Hot Pressing | 980°C – 1500°C<br>> 100 h |
| $TiC/MoSi_2$ | CVD + Plasmaspraying<br>+ Hot pressing | 1200°C > 1000 h<br>1500°C > 400 h<br>1700°C > 200 h |

A number of guidelines exist for developing an ideal fire retardant system: 1) low price, colourless, odourless, easily incorporated and compatible with no adverse effect on the polymers properties; 2) stable to heat and light; 3) a low rate and amount of smoke generation; 4) low toxicity and combustibility of combustion gases; and 5) permanent or non-migratory in nature. These guidelines have been developed on the basis of information regarding: 1) chemical and physical properties of the polymer; 2) phases of the polymer degradation; 3) combustion of the polymer and its dependence on the nature of the degradation products; 4) chemical and physical properties of the fire

retardant compositions and their interaction with the polymeric substrate.

Fire retardants are usually classified according to : a) method of incorporation or b) mechanism of combustion inhibition:

Class a): 1) reactive fire retardants; these are monomer(s) containing a heteroelement capable of confering some degree of flame retardancy by becoming an integral and permanent part of the polymer. They are less used because of the additional reaction step and changes in the physical properties of the polymer.

2) additive fire retardants; compounds containing elements with known flame retarding properties which are incorporated into the polymer system by physical mixing (as a solution in a solvent or as a slurry from water), or by radiation processing (90,91).

Class b: 1) fire retardants inhibiting flame reactions (vapour phase inhibitors): Vapour phase inhibition involves release of a chemical agent which inhibits free radical reactions involved in the flame formation and propagation.

According to Hastie (92) the vapour mechanism is characterised by the following observations; 1) inhibition is dependent on the nature of the oxidant but is independent of the polymer structure; 2) the fire retardant element is not retained in the polymer; and 3) the fire retardant does not change the

composition or amount of volatiles. Class b: 2) condensed phase inhibition; the condensed phase mechanism is characterised by the following criteria (based on the effect of phosphorus containing fire retardant); 1) the volatile composition is changed; 2) inhibition is sensitive to polymer structure but insensitive to the nature of the oxidant i.e. nitrous oxide or oxygen; 3) increased char formation; and 4) the fire retardant element is retained in the substrate.

During condensed phase inhibition, the additive alters the polymer decomposition chemistry leading to the formation of a thermally stable, insulating surface char or intumescent glassy coating. The glass coat isolates the bulk of the polymer from the high temperature and to an extent the gaseous oxidant. Beneath the char, an underlying degradation zone forms where the polymer undergoes melting, vapourisation and oxidation with the accompanying heat changes, fig.2.11. (93).

The ablative performance of a polymer is influenced by its composition and structure. Thus, a high oxygen, nitrogen and hydrogen content of the polymer wil increase the char oxidation rate. This oxidation rate decreases with increasing carbon content but is also influenced by the environment. A further mechanism of inhibition involves fire retardants which degrade endothermally, producing copious amounts of non-combustible gases e.g. HCl, $NH_3$, HBr, $SbCl_3$,$H_2O$, and $CO_2$. The latter either smother the flame or dilute the gaseous fuel from polymer decomposition to below the ignition temperature.

## 2.3.2 Flammability Evaluation

In practise, the evaluation of flame retardancy of many polymer systems and end use conditions is difficult and only semiquantitative methods are available. Thus, the limiting oxygen index (LOI) standard tests (ASTM D2863, BS2782-141) have been developed to provide flammability data which may relate to an actual fire situation, table 2.5 (94, 95). With regards to the flammability tests, various facts emerge: 1) oxygen accessibility under test conditions is usually less than that encountered in actual fires; 2) air velocity and temperature about a burning object in a real fire are usually higher; and 3) the tests depend on a number of parameters not controlled in a real fire situation e.g. sample geometry, burning time, fluidity and dripping of molten polymer, char formation and orientation of the polymer with respect to the flame. Useful information can however, be obtained by combining the results of several complimentary flammability tests. Thermoanalytical methods have also been used for flammability evaluation and are fast, reproducible techniques (96). The LOI test is a measure of the minimum concentration of oxygen in an oxygen-nitrogen atmosphere, which is necessary to initiate and support a flame for more than three minutes, a polymer is considered to be flammable if LOI < 25:

LOI= (volume oxygen/volume oxygen + volume nitrogen) x 100

TABLE 2.5 LOI values for a few polymers (ref. 97)

| POLYMER | LOI | CHAR YIELD (wt%) |
|---|---|---|
| phenolic resin (kynol) | 35 | 60.4a |
| polyoxymethylene | 15 | 0.0b |
| polymethylmethacrylate | 17 | 0.0b |
| polyfurfuryl alcohol | 31 | 54.4a |
| polytetrafluoroethylene | 95 | - |
| carbon/graphite | 56-54 | - |

a, b; condensed and vapour phase decomposition respectively

In summary, at least five speculative modes of action have been proposed for fire retardation: 1) gas theory; generation of non-combustible gases which dilute the flame oxygen supply and exclude the oxygen from the polymer surface; 2) thermal theory; radicals or molecules from additive degradation react endothermally with flame species or substrate species, the additive decomposes endothermally; 3) chemical theory; the additive degrades into free radical acceptors which interfere with flame chain reactions; 4) coating theory; non-volatile char of low thermal conductivity and high reflectivity, or a liquid barrier, is formed, which minimises oxygen diffusion to the condensed phase and also reduces the heat transfer from the flame to the polymer; and 5) physical interaction theory; finely divided particles or solid interfaces which may form endothermally and lower the net heat of combustion or reduce flame propagation

by altering the course of gas-phase reactions and lead to less reactive radicals. Many fire retardant systems act by a complementary combination of these mechanisms operating at different stages of polymer combustion.

### 2.3.3 Pyrolytic Decomposition Temperature Profile

The mechanism of combustion inhibition by a fire retardant is obviously related to the mode of polymer degradation. The latter is a very complex process involving several inter-related and inter-dependent stages. However, three fairly distinct stages can be detected: 1) upon heating the polymer fragments to yield combustible gaseous products (fuel gas); 2) the fuel gases burn in the surrounding oxidant containing atmosphere; and 3) a fraction of the heat of combustion is transferred back to the solid or molten polymer, therby maintaining a steady supply of fuel gases. Polymer properties which affect the heating and combustion processes include the glass transition, Tg, melting, Tm and decomposition, Td, temperatures, specific heat and thermal conductivity. These bulk properties are of particular significance at the advanced stages of combustion when the temperature of the polymer reaches higher levels and the processes of heat generation and convection begin to control the course of combustion. At the three critical temperatures, Tg, Tm and Td, a polymer undergoes phase transitions associated with significant changes in physical properties, such as thermal conductivity, modulus, viscosity and density. Depending on their chemical

structure, different polymers have different tendencies to react with oxygen at elevated temperatures.

Theoretically, combustion inhibition can be achieved by suppression of one or more of the stages of polymer degradation by chemical, physical (or both) processes. Those polymers which degrade by thermal fragmentation alone i.e. non-oxidative degradation, such as polystyrene and polymethylmethacrylate, can be stabilised by addition of fire retardants which interfere with the transfer of heat back to the polymer. The additive may be of a type which promotes depolymerisation due to the presence of heat labile chemical bonds which undergo preferential disintegration from the original polymer. This process removes heat from the combustion zone and facilitates melting (98-100). In the case of polymers decomposing by a thermo-oxidative route, combustion inhibition can be achieved by mechanisms that exclude the oxidant (air) from the polymer surface. Borates and phosphates are thought to function by this and other, mechanisms. In both cases, a glassy coat forms on the polymer surface so that the diffusion of oxygen through this layer becomes the rate determining factor, fig.2.11. The efficiency of an additive is related to its ability in matching the decomposition temperature profile of the substrate, often referred to as the 'right place at the right time' theory (101). Fig.2.12 displays the decomposition temperature profile of a metal amine additive and a urethane foam. Although only about 50% of the additive degrades in the desired region, the gases evolved are essentially non-combustible viz. ammonia, nitrogen and ammonium chloride.

These gases act as inert diluents for the flammable combustion products. A combination of additives may be used to match the substrate decomposition temperature profile more precisely.

FIG.2.11 Heat changes involved upon formation of a glassy coating

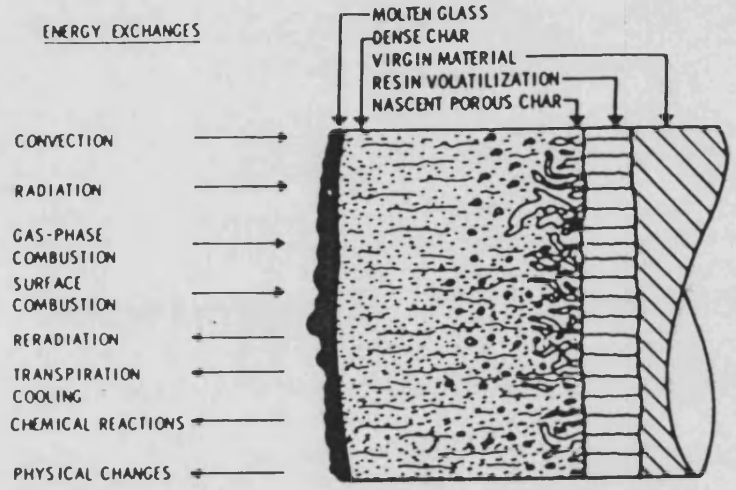


FIG.2.12 TGA curves of hexamminocobaltic chloride and flexible urethane foam (shaded area), (ref.102)

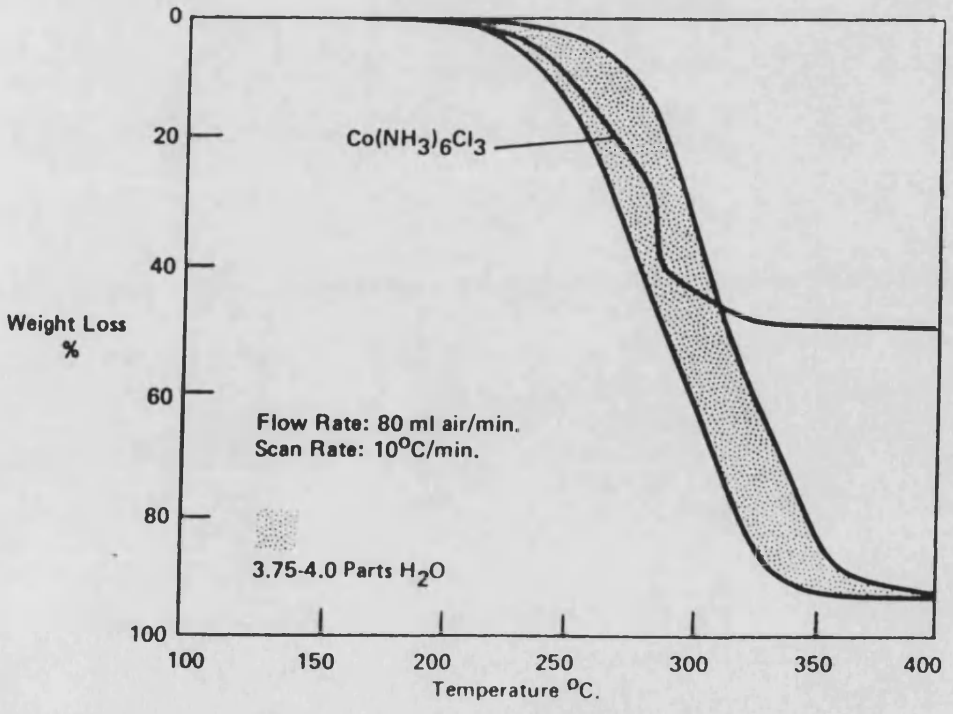

The basis of polymer flammability and approaches to fire retardation has been outlined. The following section presents a review of the various classes of fire retardant systems commercially available. The review has been limited to cover the application of these additives to the phenolic resins.

## 2.4 Combustion Inhibition of Phenolic Resins

### 2.4.1 Introduction

Phenolics are intermediate in their combustion behaviour between most of the vinyl systems and the so called non-flammable, heat resistant polymers. In fact, in fibre form, phenolics have been reported to exhibit a high degree of heat resistance (103). As previously mentioned, polymer combustion proceeds through several stages. These are inter-related owing to variations in the external heat source, the surrounding atmosphere and the polymer geometry and characteristics. While surface oxidation, which is exothermic is the predominant mode of phenolic degradation, thermal fragmentation or pyrolysis also occurs immediately below the polymer surface, at elevated temperatures. These two processes proceed until a heat resistant carbon char is formed. Heat transfer through the char layer is probably different from that of the unheated resin. Hence, decomposition of the char through volatile product formation becomes very complex. It probably involves radical reactions leading to

formation of a new char and volatile species which must percolate through this char and into the combustion zone. Radical trapping reactions can thus reduce the amount of combustible material reaching the combustion zone.

By considering the mechanism of phenolic resin degradation, appropriate chemical, or physical, modifications can be used to elevate the resin's thermal stability. The first process is to control or eliminate the formation of combustible volatiles. The second step is to modify the system such that diffusion of volatiles into the combustion zone is inhibited. In general terms, the majority of the chemistry of combustion is the chemistry of the resin below 500°C. This involves chemical changes leading to more (or less), char and less (or more), combustible volatile products. An understanding of this chemistry is essential for developing a method for controlling polymer flammability (see section 2.1). When ignited, cellular phenolic retains a strong carbonaceous char corresponding to a very highly knit, cross-linked structure and the presence of a large aromatic content. Phenolic foams are not ignitable when exposed to an open flame source. However, under prolonged exposure to heat, phenolic foams will smolder and char until consumption is nearly complete. This process is called 'punking'. Non-punking can be achieved by retarding or interfering with the further combustion of this char. Hence, additives which effect phenolic resin decomposition must act in the condensed phase and includes inhibitors, inert fillers and protective coatings.

Nonpunking or after-glow in phenolic foams can be achieved by the addition of boric acid or boric anhydride, with oxalic acid as the catalyst (104). Also phosphates, aluminium trichloride trihydrate (105), antimony oxide/halogen synergens (106), organic amides (107) and polyhydroxylated and/or polyaminated derivatives of a polychlorinated diphenyl, which is added at the phenol-aldehyde condensation stage (108). Borates and phosphates are believed to interfere with the solid phase oxidation reactions which lead to the formation of carbon oxides, inhibiting either the initial production of surface oxides or the highly exothermic conversion of carbon monoxide to the dioxide. This is achieved by the formation of a nonvolatile glassy barrier at the surface which minimises oxygen diffusion to the condensed phase and also reduces heat transfer to the polymer.

### 2.4.2 Halogen Based Additives

Most of the technology concerning combustion inhibition of phenolics, involve either the incorporation of substances known to exhibit fire retardant properties, into the backbone structure of the polymer or, the addition of various compounds or combinations of compounds into the resin system to impart fire retardant characteristics. When incorporated into the polymer structure, halogen atoms promote hydrogen-bonding and structural rigidity. They also take part in dehalogenation reactions at elevated temperatures, therby providing cross-linking sites for increased char formation. Upon pyrolysis the gaseous halogen products are decomposed in the ignition zone and tend to smother

or dilute the flame. As in other polymer systems, bromine based compounds tend to be more effective than their chlorine based counterparts. Halogens have been incorporated into the phenolic resin by the synthesis of halogenated resins or by the addition of halogen containing materials to the preformed phenolic resin. Thus, a mixture of 50% phenol and 50% of a mixture of predominantly 2,3-dichlorophenol, 2,4-dichlorophenol and 2,6-dichlorophenol, with formaldehyde was reported to form a chlorinated phenolic resin. The latter was used as a paper impregnating material and was found to be self-extinguishing and non-punking when ignited (109,110). Alternatively, direct halogenation of preformed phenolic resins produced halogen-containing polymers with enhanced thermal stability. Modification of the aldehydic portion with halogen-containing moities e.g. condensation of phenol with p-bromo benzaldehyde at elevated temperatures produced polymers with enhanced self-extinguishing characters (111). Chlorinated polyphenols (112) and other chlorinated phenyl ring compounds (113) when mixed with phenolic resins, also increased the latters thermal stability.

### 2.4.3 Boron Based Additives

Phenolic resins modified with boric acid, boric oxide or borate and metaborate salts (zinc, magnesium, sodium etc.), have been observed to exhibit improved thermal resistance (114, 115). The majority of these compounds inhibit in the condensed

phase and in some cases gas phase inhibition has also been reported. A surface coating of the additive will promote char reactions thereby reducing the amount and rate of combustible volatiles in the ignition zone. When boric acid is added to the liquid resin phase or impregnated into partially cured resin systems, it reacts with the phenolic hydroxyl groups to form borate esters with the elimination of water. These esters promote char formation decomposition reactions as well as retention of the boric oxide surface coating, during high temperature exposure of the phenolic resin.

FIG.2.13 The phenolic resin/boron structure responsible for promoting thermo-oxidative resistance in phenyl borate

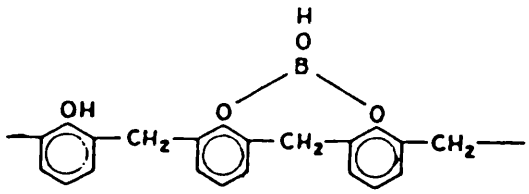


CYCLIC BORATE ESTER

Phenyl borates are usually prepared by reacting an aryl borate with paraformaldehyde (80-120°C) followed by addition of HMTA and further heating at ~200°C. Thus, by heating 3mole p-aminophenol with 1mole boric acid in xylene and distilling off formed water as an azeotropic mixture, tris-p-aminophenyl borate is obtained. This is reacted (3h) with formaldehyde at 70°C in the presence of an acid catalyst and the resulting red resin cured by addition of HMTA at 200°C to give a final, highly cross-linked system. Presently, boron modified resins are only used as ablative coatings and in brake linings (116).

### 2.4.4 Phosphorus based additives

Phosphoric acid or ammonium phosphates are added to phenolic resin lacquer, or wood, rendering them self-extinguishing (117). Thus, when glycerol phosphate acidic ester, formed on mixing one equivalent of phosphoric acid with two equivalents of glycerol, was mixed with 20% by weight of phenolic resin, a flame resistant material was obtained (118). When a phenolic resin/phosphorus additive system is heated, the additive usually decomposes in the temperature range 200-500°C forming phosphoric acid which decomposes to the oxide forming the so called glass coating. The resin itself degrades to a cross-linked carbon skeleton, in this temperature range. The glass coating, similar to that proposed for boric oxides, retards the rate of diffusion of volatiles to the resin surface and their subsequent diffusion into the pyrolysis zone. The decreased diffusion rate of these volatiles permits radical trapping reactions to form the carbon char, by

thermal crosslinking.

Stabilisation by phosphorus additives takes place primarily, but not exclusively, through: 1) formation of organophosphorus/phenolic ester moities which promote polymer cross-linking, fig.2.14; and 2) formation of the glass coating by phosphorus oxides which retards escape of volatiles into the combustion zone and concurrent diffusion of oxygen towards the polymer surface (119). Normally, esterification of novolaks of high -OH functionality with polyfunctional inorganic phosphoric and boric acids, or with phosphorus oxyhalides results in gelation.

FIG.2.14 Organophosphorus/phenolic ester linkages responsible for increased flame resistance.

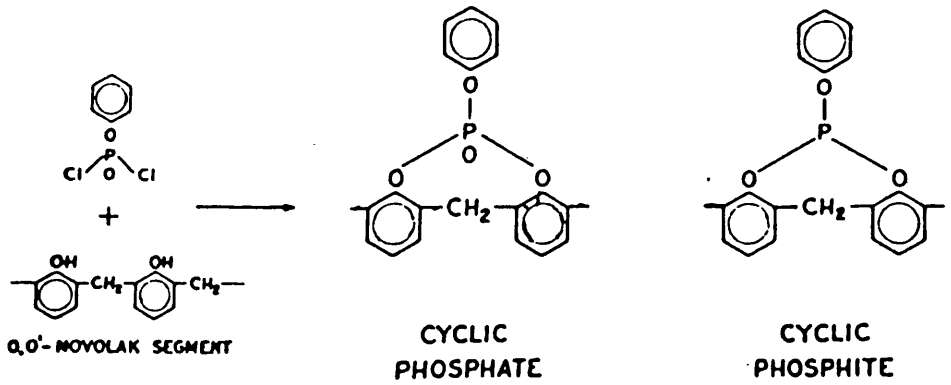

By using bisphenols and bifunctional derivatives of phosphoric acid or phosgene, linear polymers can be obtained (120). Furthermore, it has been reported that 'high ortho' novolaks can be extensively esterified with bifunctional compounds (121), while random novolaks were found to gel at a low level of esterification. Intermolecular cross-linking with phosphoric acid (also boric acid and diphenylsilyl dichloride) is dominant in random novolaks, while the ortho counterparts, which involve intramolecular esterification, yield thermally stable 8-membered ring structures fig.2.14

Phosphorus containing additives are more superior than halogen based compounds, especially when used in oxygenated polymers, in terms of light stability, effect on viscosity, thermal stability etc. The element phosphorus resembles carbon in its electronegativity and its preferred co-ordination number of four, such that, incorporation of phosphorus into organic polymers alters their properties only slightly. In general properties enhanced by phosphorus incorporation include: 1) reduced flammability; 2) increased adhesion; and 3) increased solubility in polar solvents. The additive diammonium phosphate (DHAP) available commercially as Monsanto's 'Phos-chek R P/30' (122) is reported to decompose as shown in fig.2.15. Ammonia and water are evolved in the range 200-225$^{o}$C. A highly condensed polyphosphoric acid is thought to form and undergo no further weight loss below 600$^{o}$C. Above this temperature, an azeotropic $P_4O_{10}.H_2O$ mixture boils off. The loss due to ammonia evolution ranges from 2.8% to 14.3% by weight, depending on the heataing rate. The relatively

small amount of available ammonia in the ammonium phosphates on a weight bases, appears to rule out the functioning of these additives in the gas phase of the burning process.

**FIG.2.15 Thermal degradation route of DHAP (ref.123)**

$$(NH_4)2H_2PO_4 \xrightarrow{147\ ^oC} H_3PO_4 + NH_3$$

$$2H_3PO_4 \xrightarrow{216\ ^oC} H_2O + H_4P_2O_7$$

$$H_4P_2O_7 \xrightarrow{>600\ ^oC} H_2O + P_2O_5$$

Little (124) reported, in simplified form, that phosphoric acid reacted in the condensed phase via the mechanism presented in fig.2.16. The phosphorus reacts preferentially with carbon, such that the net heat liberated is considerably less than that obtained from direct oxidation of carbon to the dioxide.

**FIG.2.16 Reactions of phosphoric acid (ref. 124)**

$$2H_3PO_4 + 5C \longrightarrow 2P + 5CO + 3H_2O$$

$$4P + 5O_2 \longrightarrow 2P_2O_5$$

$$P_2O_5 + 5C \longrightarrow 2P + 5CO$$

Lyons (125) reported that ammonium phosphates yield phosphoric acids which, as polyphosphoric acid, form ester links with oxygen containing polymers, resulting in the formation of a carbonaceous char with a corresponding reduction in the amount of flammable tars produced. The char formation involved catalytic dehydration of the hydroxyl groups, esterification by the polyphosphoric acids formed and finally crosslinking and skeletal rearrangement. The polyphosphoric acids also eliminate

after-glow. The polyacid being very viscous, is thought to be an excellent film forming substance that can coat the surface. This glassy coat retards the diffusion of oxygen into the reactive layers of carbon. However, enhanced charring rather than the glassy coating is a more likely mechanism for suppression of after-glow.

It has been reported that impregnating carbon (phenolic resin and furfuryl alcohol) and graphite grades with metal based phosphorus compounds, followed by a heat treatment between 350°C and 800°C, resulted in improved thermal oxidation resistance of these materials (126). Previous to this, in a U.S. patent, Johnson (127) reported a method of incorporating phosphate additives viz. tricresyl, iso-octyl, methyl, tributyl and ethyl acids. This process involved addition of the additive to pyrolysed carbon and graphite articles, with a coal tar pitch, followed by rebaking to 900°C. The baking temperature was limited to 1200°C to prevent volatilisation of the phosphorus containing radicals from the final graphite and carbon.

### 2.4.5 Nitrogen based additives

It is well known that amino resins are less flammable than phenolic resins (107). Therefore, by incorporating a variety of nitrogen containing materials into the phenolic resin, the thermal stability of the latter should be improved. Incorporation of aniline results in a high char yield which is found to be nitrogen rich i.e when heated to 900°C a 65% by weight of the

original polymer is obtained. The thermal-oxidative behaviour of this aniline-modified phenolic resin at temperatures upto 200°C showed a lower extent and rate of oxidation at methylene links and a higher retention of the thermally stable nitrogen portion of the system (128). The incorporation of formaldehyde dicyandiamide condensate, melamine and sulphonamide, into a phenolic resin foam composition also produces a fire resistant system. In each of these cases, the nitrogen additive is thought to function as a cross-linking agent through radical trapping reactions. The overall behaviour of these systems is probably similar to phosphorus and boron containing additives (129).

### 2.4.6 Sulphur Based Additives

Sulphur modified phenolic resins can be obtained by a direct reaction between phenol and sulphur in the temperature range 130-230°C under alkaline conditions followed by further cross-linking with HMTA, or resole additives (130). Sulphur modified phenolic resins have no wide spread commercial use although 4,4-thio-bis(3-methyl-6-tertbutyl)phenol is used as an antioxidant. By reacting dihydroxydiphenylsulphone with formaldehyde, a resin with improved heat resistance is obtained.

### 2.4.7 Silicon Based Additives

Silicon modified PF resins were reported to show improved thermal resistance as early as 1941 (131). Nevertheless, the high cost of available organic silicon compounds and the

relatively high level of incorporation (~10%), required before significant improvement in flame resistance became apparent, prevented these systems from being widely used. In a U.S. patent Dannels (132) suggested a method for improving the thermal stability of phenolic resins. This involved introducing a silicon moiety into the structure of the resin by an esterification reaction (similar to borate and phosphate esterification). The esterification reaction yield a non-sticky brittle resin having 3.7% silicon. This is pulverised, mixed with 10% HMTA and cured to a hard infusible resin by heating to 160°C.

Beecher (40) observed that an ablative material of fibre-glass reinforced PF resin adequately protected vehicles subjected to atmospheric re-entry at hypersonic velocity. In the initial decomposition reaction, about 10-12% by weight of the material gasified leaving the same amount of the original weight of the material as carbon in the glass matrix. The gases, larger molecucles i.e cresols, phenols, and smaller molecules i.e. carbon monoxide, methane etc. arising from polymer decomposition, entered the boundary layer. The net result of this mass addition was a reduction by about 20% in heat transfer to the unaffected plastic.

By impregnating carbon-carbon composites with a phenolic resin having a silicon group, a marked increase in oxidation resistance was reported (133,134). It was postulated that the silicon group was converted to the thermally stable Si-C upon pyrolysis. Silicon atoms can be introduced into the resin chain instead of

the thermally labile methylene linkage by reaction with polysilylphenols (135). Alternatively, siloxanes may be reacted with the phenolic hydroxyl to yield stable Si-O bonds fig.2.17 (136).

FIG.2.17 Silicon modified phenolic resin

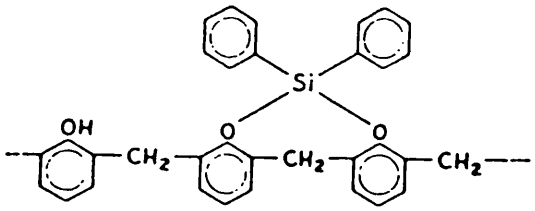


CYCLIC SILANE DIOL DERIVATIVE

## 2.4.8 Miscellaneous Additives

### 2.4.8.1 Oxide Based

Apart from antimony oxide a few other metal oxides have been found useful, either alone or in combination with antimony oxide (126) and a halogen, as a fire retardant system. The most important of these is hydrated alumina $Al_2O_3.3H_2O$ which is often used in conjunction with chlorine as a fire retardant for phenolic rubber products and polyester (137). The inhibition mechanism is thought to involve $AlCl_3$ generation which in turn acts as a source of inhibiting halogen radicals in the gas phase (108). An alternative and more plausible explanation for combustion inhibition is endothermic dehydration of alumina

hydrate in the condensed phase, releasing about 35% water which dilutes the gaseous products of polymer decomposition below the ignition point. To facilitate this mechanism, alumina hydrate is incorporated in relatively large amounts and acts as a heat sink imparting a non-specific inhibiting effect on polymer decomposition.

A synergistic effect between hydrated alumina and tris(2-chloroethyl)phosphate has been reported by Green (138). In allylic polymers containing chlorine and $Al(OH)_3$, the addition of magnesium oxide, $MgO$, was found to reduce smoke evolution by these resins from 1% to 0.4% by weight (139,140). The oxides of zinc, Fe(III) and titanium (in conjunction with $Sb_2O_3$) have been claimed to lower or accelerate the decomposition of chloroparaffins (used in coatings) and polyurethanes. An extensive report on the application of metal oxides has been compiled by Pitts (141).

### 2.4.8.2 Carbonate and Bicarbonate Based

Only a few carbonates and bicarbonates have been used as commercial additives for polymers. This is due to the tendency of the bicarbonates to decompose at temperatures lower than normally used in the course of polymer processing. Conversely, carbonates of calcium and sodium used as cheap inert fillers for some polymers, are thermally too stable to exhibit significant fire retardant effects in most polymer systems (96,109).

## Summary

The available literature emphasizes the following additive systems for use in phenolic resins: phosphorus as phosphoric acid is an ester and anhydride forming reactant which promotes cross-linking through thermal bond rupture, the phosphate ester is a good 'leaving group'. Also in the presence of heat and oxygen, a polyphosphate surface coating forms over the polymer, thus preventing escape of combustible volatiles into the pyrolysis zone and, most important, reduces diffusion of oxygen into the polymer mass. Antimony, arsenic and bismuth are thought to exhibit similar retardation chemistry. The presence of these elements, combined with oxygen in the polymer mass, provide additional sites for hydrogen bonding. In the case of multiply bonded units eg P=O, an increase in thermal stability is obtained owing to the highly endothermic dissociation of these groups. With halogens and phosphorus, or antimony, a synergistic effect has been reported. It is thought that antimony and phosphorus stabilize in the condensed phase and in the presence of a halogen, form heavy gaseous products which inhibit gas phase combustion and upon decomposition, form effective radical scavengers.

Halogens, namely chlorine and bromine, when incorporated into the polymer mass probably enter into dehydrohalogenation processes at elevated temperatures, thus promoting char forming and cross-linking reactions. On pyrolysis, the halogen gases formed are further decomposed in the oxidation area to form radical scavengers or, in the presence of such materials as

phosphorus and antimony, heavy gases which act as flame smothering agents. Boron, being an effective ester forming element is thought to react similar to phosphorus. Boron oxide forms a glassy coat over the polymer surface, thus retarding combustion. At elevated temperatures, boron functions as a good cross-linking agent.

Presently most of the chemical bases for combustion inhibition are speculative. However, by combining the mechanisms of both oxidative and thermal degradation of the resin and additive, along with resin/additive interaction, useful information can be obtained.

Candidate fire retardants were selected on the basis of the following properties: 1) ability to withstand resin processing and product manufacture (this rules out additives which were likely to volatilise during carbonisation e.g. bicarbonates, amine and sulphur based retardants); 2) chemically incorporated into the structure of the phenolic resin e.g. esterification with boric acid or phosphoric acid; and 3) readily available as a commercial chemical. The additives which will be incorporated into the PF resins with the aim of obtaining a stable resin-based carbon are listed in table 2.5.

Table 2.5 Fire retardants to be used with PF resins (32,91,136-139)

| Fire Retardants |
| --- |
| dihydrogen ammonium phosphate |
| tris(2-chloroethyl)phosphate |
| tris(2,3-dichloropropyl)phosphate |
| tributyl phosphate |
| tri-N-iso-octyl phosphate |
| tritolyl phosphite |
| tri-iso-octyl phosphite |
| silicon-based (Z6018) |
| boron-based (MT59) |

# CHAPTER 3 EXPERIMENTAL

## 3.1 MATERIALS

### 3.1.1 The Phenolic Resins and Model Compounds

Phenol formaldehyde, PF, resins were supplied by Borden (U.K.) Ltd., North Baddesley, Southampton. Data on these resins is presented in table 3.1. The novolak TPSX4 is a yellow powder containing 10wt% of hexamethylene tetra-amine, HMTA, $[(CH_2)_6 N_4]$ or HEXA. PR77 is a red-brown viscous novolak in a solution of monoethylene glycol and water. PR77i is similar to PR77 but contains no solvent. Resins FRD2298 and FRD2244 are low molecular weight novolaks, while PA65 is a liquid resole. Two model compounds were also used viz. hydroxymethylphenol or saligenin and methylol phenol or dihydroxydiphenylmethane, DDM, Koch Light Laboratories Ltd., Haverhill, Suffolk. A boron containing novolak, MT59 and a silicon containing novolak, Z6018, were also studied as candidate precursors for generating oxidation resistant carbons. Z6018 was a Dow-Corning silicone resin described as a hydroxyl functional resin of low molecular weight. MT59 was synthesised at Borden (U.K.) Ltd. laboratories by a simple esterification reaction (see Knop and Scheib p.95 ref.9).

### 3.1.2 The Pitches

Three pitch materials were used viz. petroleum pitch, PP,

designated "Croda Hydrocarbon ESSO", coal tar pitch, CTP, designated 1.5 NESS and dolobus pitch, DP, which is a form of coal tar pitch and was provided by Borden (UK) Ltd. Both PP and CTP were supplied by Prof. H. Marsh, Northern Carbon Research Laboratories, University of Newcastle-Upon-Tyne.

### 3.1.3 The Fire Retardants

In order to allow uniform mixing of the fire retardant into the resin, liquid type of additives were selected. However, results are also reported for a solid additive i.e. dihydrogenammonium phosphate, DHAP. Some of the properties of the additives are presented in table 3.2.

## 3.2 Curing of the PF Resins and Additive Modified Resins

The novolak TPSX4 was placed in an aluminium foil packet and cured in an oven open to the atmosphere. PR77 was heated to 80°C on a hot plate to lower the viscosity to 2-5 poise and subsequently, 10wt% HMTA cross-linking agent was stirred in, ensuring a homogeneous distribution. The mixture was then poured into a cold mould and oven cured. The solvent free analogue PR77i was ground, sieved and 10wt% HMTA mixed in prior to resin cure. The model compounds saligenin, sal, and DDM were similarly cured after addition of 15wt% of HMTA. The resole PA65 was cured by simple heating, without addition of cross-linking agent. The novolaks FRD2244 and FRD2298 are semi-solids at room temperature because of their low molecular weight. They were freeze dried in

a slush bath of dry ice and methanol at -20°C, and then ground to the required particle size (500-850um). HMTA, 15wt% was stirred in and the resulting mixture was placed in the aluminium foil and oven cured.

Various resole /novolak compositions were prepared by direct mixing of the two components followed by oven curing. The resole was PA65 while the novolaks were either TPSX4 or PR77. Z6018 was obtained as a solid powder and was thus cured as obtained. MT59 was ground and then oven cured. The solid DHAP and the liquid organophosphorus compounds were directly mixed into the resins prior to the cure. The various curing schedules used are presented in table 4.1.

## 3.3 Bulk Carbonisation

The carbonisation apparatus, fig.3.1, consists of a block furnace containing a horizontal mullite tube (70cm long; 3.3cm diameter). The pitch or resin were ground to the required particle size and placed in open boat-shaped crucibles with a capacity of 7g. The crucible was positioned centrally in the work tube. The ends of the latter were water cooled and sealed with stainless steel end caps. A stream of nitrogen gas (BOC, M.30-NG grade 98%), flow rate 200ml/min, was passed through the work tube during heating and cooling. A chromel-alumel thermocouple, placed centrally in the furnace and in contact with the outside of

the work tube, was connected to a temperature programmer, Eurotherm Type 120. The latter was set to give a linear heating rate of 2°C/min. The samples were heated to 970°C and held at that temperature for 5min. The block furnace had a maximum safe working temperature of 1200°C. Nevertheless, repeated heating to 970°C caused the heating element to be burnt out on several occassions. To carbonise a greater amount of sample a larger quartz glass crucible and a carbolite furnace (134cm long; 7cm diameter) were used, Carbolite, Sheffield, England. The method of operation and apparatus layout are similar to fig.3.1 although the temperature programmer was more versatile, permitting several heating and/or cooling rates or segments, Programming Unit 802KB, Control and Readout Ltd., Worthing, Sussex.

The nitrogen gas was dried and de-oxygenated by passing it through a molecular sieve, Type 3A, Hopkin and Williams Ltd., and an oxygen trap, Phase Separation Ltd., respectively. The exit gases were passed through a Dreschel bottel system in order to trap carbonised products. The oxygen trap consisted of coiled aluminium tubing packed with reduced cuprous oxide. The trap was regenerated after de-oxygenating one and a half cylinders of gas by reducing the formed copper oxide with hydrogen gas (BOC M.30-NG 98%). The trap was placed in an oven and purged with flowing hydrogen gas (200ml/min) for 5min. The oven temperature was then raised to 150°C whilst maintaining the hydrogen flow rate. The water which was formed condensed in the vent line. The regeneration was continued for 5h at 150°C until the vent gas was free of moisture. When reconnecting the oxygen trap into the

inert gas line, the trap inlet was connected to the nitrogen gas to purge residual hydrogen from the de-oxygenator. Finally, the trap outlet was connected to the end of the furnace by copper tubing.

FIG.3.1 A block diagram of the bulk carbonisation apparatus

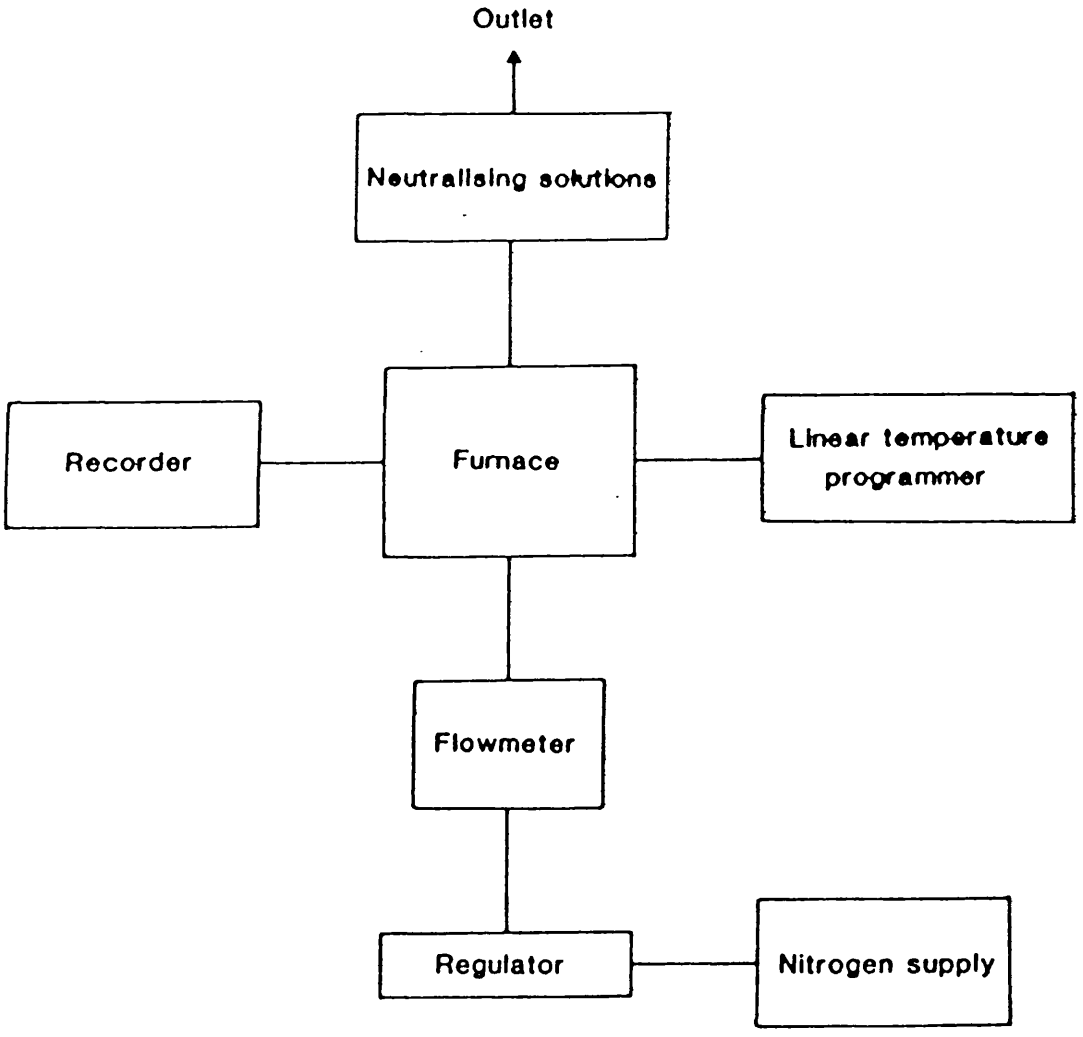


## 3.4 High Temperature Heat Treatment, (HTT)

The resin carbon, or pitch carbon, 10g, particle size

500-850um, previously carbonised at a temperature of 970°C, was placed in a graphite crucible and the latter carefully positioned in a high temperature 1000A series graphite element resistance furnace, Astro Industries Inc., Santa Barbara U.S.A., and evacuated using a rotary pump, Edwards Vacuum Products Ltd. Helium gas, BOC, London, flow rate 30ml/min, was admitted into the furnace chamber and the furnace heated electrically. The samples were subjected to the following additive (i.e. the material heated to 1200°C was then used for 1500°C etc.) temperatures; 1200°C, 1500°C and 1700°C. The electrical current was increased at a rate sufficient to give a temperature rise of 20°C/min. The final temperature was maintained for 20min. The temperature was measured using a Cyclops 52 portable thermometer, or optical pyrometer, Minolta Land Pyrometers Ltd, Japan.

The optical pyrometer was aimed and focused at the viewing spot, a transparent opening leading to the furnace where the crucible was positioned, and the thermal radiation emitted was presented as a digital read-out. For measuring temperatures in excess of 1200°C, dark lens were placed in the eye-piece of the pyrometer to protect the eyes from the high energy radiation. The pressure in the furnace was maintained below 10psi by operation of a vent.

## 3.5 THERMAL ANALYSIS

### 3.5.1 Thermogravimetric Analysis (TGA) of Carbonisation and Oxidation

The Stanton Redcroft TG750 thermo-balance, fig.3.2, was used to obtain a direct plot of weight loss versus temperature from the temperature range of ambient to 1000 $^{o}$C. The heart of the instrument is an electronic bridge circuit maintained in continuous balance by a servo-system.. The head unit magnetically balances the torque produced by the change in sample weight. As the latter changes, a proportional current flows through the head and operates an indicating meter. This provides an electrical output which is used to operate a pen recorder. The sample is heated by a micro-furnace (20mm long, 12mm diameter), fig.3.2, made from chrome-plated brass and water-cooled by a number of inter-coonected vertical channels.

The furnace is constructed from mineral-insulated nichrome wire sheathed in inconel. The sheath of the furnace is in direct contact with the water-cooled body of the unit via the end connectors. A platinum resistance sensor is carefully positioned in contact with the furnace well and is used as the temperature controller. The sample is placed in a platinum pan, 6mm diameter,· and the sample temperature is measured by a plate-type Pt-13%Rh/Pt thermocouple carried in a twin-bore alumina rod. The plate is positioned carefully 0.5mm below the sample pan and

suspension. The capacity of the balance is 1g.

The Stanton Redcroft TG750 allows both isothermal and non-isothermal experiments to be carried out using programmable heating (or cooling) rates from 1°C/min to 100°C/min. The Stanton Redcroft BD9 potentiometric two-channel recorder measures temperature as a signal which was received from the sample thermocouple, and the signal from the balance output which provides a record of the weight loss at the corresponding temperature. For thermogravimetric, TG, studies of carbonisation, samples of cured resins, or pitch, were placed in a previously zeroed sample pan and heated at a linear rate of 15°C/min to 1000°C. The inert atmosphere was provided by flowing nitrogen gas (50ml/min) which was dried and deoxygenated as described for bulk carbonisation. A similar procedure was used to carry out TG studies of non-isothermal oxidation of the carbons in flowing air, delivered by a peristaltic pump (MHKE Model 11). Heating rates, air-flow rates, sample weight and particle size were varied to determine the most suitable conditions for TG studies. During isothermal oxidation studies, the sample was rapidly heated to the required temperature, at 100°C/min, in a nitrogen atmosphere. By operation of a suitable valve the atmosphere was then switched to oxygen (air) and the isothermal TG run recorded.

Fig.3.2 A diagramatic representation of the thermobalance

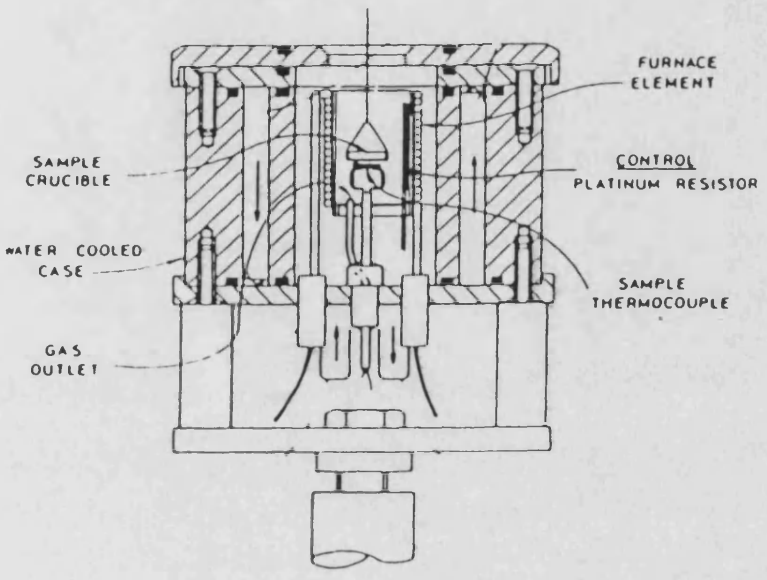

### 3.5.2 Differential Scanning Calorimetry, (DSC)

The resin TPSX4 (10mg) was placed in a platinum sample pan and the latter sealed and carefully positioned in the heating cell of the DSC instrument, DuPont Instruments, 910 DSC, 9900 Computer/ Thermal Analyser. For curing studies, the temperature was increased to 130$^{o}$C at 4$^{o}$C/min and maintained for the required period. A DSC trace was obtained showing the occurrence of resin curing. To determine the presence of residual, uncured resin, a second DSC scan was obtained for the resin, and for the previously oven-cured resin samples, using a scanning procedure of 8$^{o}$C/min to 300$^{o}$C. The latter scan, which was below the decomposition temperature of the phenolic resin, was used to provide an indication of the glass transition temperature, Tg, and hence a measure of the extent of resin cure.

## 3.6 CHEMICAL ANALYSIS

### 3.6.1 Energy Dispersive Analysis of X-Rays (EDAX)

The System

A Linkan 10 000 analyser fitted with a solid state lithium drifted-silicon detector (LZ-S) was coupled to a JEOL JSM 35-C electron microscope, enabling energy dispersive analysis of x-rays (EDAX) to be performed using a 'SEMI- QUANT' programme available on the instrument. During operation an electron beam was directed at a point on the specimen causing it to emit x-rays. The latter, which are characteristic of the emitting element, were analysed by the solid state detector and the results printed out as a spectra of peaks. The peak intensity provided a semi-quantitative measure of the amount of element detected. An SEM micrograph of the specimens was also obtained showing the presence of the elements as white spots on a dark background.

The specimens (particle size 500-850um) were mounted in resin, Mounting Resin-2, Struers, Denmark, and hot-pressed, 70$^{o}$C, 10 ton/in$^{2}$. The resin-embedded specimen was then then ground and polished to obtain a flat section. During analysis standard conditions were maintained viz. current $10^{-10}$ amps; voltage 15kV and scanning time 100s.

### 3.6.2 Elemental Analysis

Elemental analysis was performed using the Elemental Analyser (Carlo Erba, model 1106). The sample (1mg) was ground to a fine powder and subjected to elemental analysis for carbon, hydrogen and nitrogen (using the built-in gas chromatography). Direct measurement of the remaining elements known to be present, e.g. oxygen or the additive elements could not be measured due to lack of facilities. A rough estimate of these elements was thus obtained from the mass balance.

## 3.7 TEXTURAL CHARACTERISATION

### 3.7.1 Scanning electron microscopy (SEM)

The particulate specimens (particle size: 500-850um) were secured to aluminium dish specimen holders using 'Quick dry colloidal graphite', (Polaron Equipment Ltd., Watford, Hertfordshire), and the latter was affixed to a base plate with DAG conducting paint (Agar quick dry silver paint, Agar Aids, Stanstead, Essex). This ensured good electerical contact between the specimen and the analysing equipment, a JEOL JSM-35C SEM which was funded by SERC. On several occassions a JEOL T330 SEM, which was a more automated electron microscope was used. The SEM provided a visual image on the screen which was photographed at different magnifications.

In electron microscopy, an electron beam is directed at the sample to obtain an image. The pitch and resin carbons were both sufficiently good conductors, thus preventing accumulation of charge. However, the phenolic resins were unable to conduct away the incident electrons which tended to accumulate leading to a build-up of charge and hence, inter-particle repulsion. This motion of the particles lead to blurred images. The problem of charge build-up was overcome by the application of a thin gold coat on the particle surface, to conduct away the charge, using a Sputter Coater (Edwards S150B).

### 3.7.2 Determination of the Total Surface Area (TSA) from gas adsorption isotherms

The most common method for determining the specific surface area (TSA or BET) is by gas adsorption. The techniques frequently used are gravimetric or volumetric. Both techniques have been used in the present work and a description of the apparatus and method is presented.

### 3.7.2.1 Gravimetric Techniques: Spring and Microbalance

The Spring balance

The spring balance was a M$^{c}$Bain spring type and is shown in fig.3.3. The pyrex glass outer-case was attached to a framework secured to a wall. The tubes, J, were attached by cup and socket 'O' ring joints, T, which allowed easier tube manipulation. The use of four tubes allowed simultaneous analysis of four different samples. Low pressures ($10^{-4}$ to 100 Torr) were measured by a highly accurate (0.12% of the reading) capacitance pressure gauge (MKS Baratron Model No.270). A further check of adsorptive pressure was provided by a Pirani gauge (LKB Autovac Model No.3294B). Presence of leaks and completion of outgassing were verified by use of these pressure gauges. Pressures in the range 100-760 Torr were measured by a mercury manometer, N. A tap, M, isolated the manometer from the system, thus reducing the possibility of sample contamination by mercury vapour. During adsorption, the manometer was kept isolated until required.

The pumping system consisted of a rotary pump, A, (Edwards Vacuum Products Ltd.), backing a water-cooled diffusion pump, B. In the event of a power failure, a built-in protection unit served to isolate the vacuum system and allowed the rotary pump back to atmospheric pressure. Oil-vapour back-streaming was reduced by incorporation of a liquid nitrogen trap, D, and a water-cooled baffle valve, E. Large quantities of gas could be removed from the system via a by-pass line, C, thus protecting the diffusion pump. A one-litre bulb, G, acted as a secondary

reservoir of adsorptive, permitting small amounts of gas to be introduced into the system. The system used pyrex springs which were previously annealed under a load of 0.5g at 470 $^{o}$K for 10h, to counteract their known tendency to creep under stress. Spring sensitivities were measured using standard weights and recording the extensions with a cathetometer. This was able to detect a minimum spring movement of $\pm$30um, which corresponds to a minimum detectable weight change of $\pm$50ug. Any displacement of the cathetometer with respect to the sample could be detected by reference to a fiducial fibre suspended within each spring.

A weighed amount of carbon, 200-350mg, was placed in the aluminium foil bucket, L, fig.3.3, and the latter suspended from a fine glass fibre connected to a helical spring. Sample outgassing was performed under vacuum at 528$^{o}$K (12-14h), by wrapping heating tape around the sample area of the hangdown tube and controlling the temperature by means of a variac heater. Completion of outgassing was checked by isolating the system and detecting any pressure change (>0.01 Torr) on the pressure gauge. After allowing to cool, the hangdown tubes were immersed in liquid nitrogen (77$^{o}$K). High purity adsorptive (nitrogen gas) was dried by passing it through a column of type 3A molecular sieve, before being admitted to the system. Equlibiration times were indicated by cessation of spring extension and constancy of the pressure readout.

After outgassing and thermostatting to the relevant adsorption temperature, the sample weight was determined by measurement of

the spring extension using the cathetometer. The extension in length was then converted to its equivalent in gramms using the spring sensitivity, which was obtained by spring calibration using standard weights.

**The Vacuum microbalance**

The vacuum microbalance (CI Electronics Ltd. Mark 2 Model B) was directly attached to the system by modification of the case, P. Since balance movement is controlled by a light sensitive servo-mechanism, constant light intensity was achieved by shading the microbalance assembly with aluminium foil. A PTFE 'O' ring sealed tap allowed microbalance isolation and hence operation of either spring or microbalance jointly or separately. The maximum sensitive range of 0-25ug full scale deflection (fsd) was difficult to utilise because of building vibrations. Measurements were thus made in the range 0-100ug fsd. The microbalance was more sensitive than the spring balance with a minimum detectable deflection of $\pm$2.5ug. The microbalance was used for samples having surface areas less than $100 m^2 g^{-1}$.

Gravimetric techniques are prone to error during both weight and pressure measurements. Thermal transpiration effects were limited to the hangdown fibres by keeping the sample immersed at least 10cm beneath the coolant surface. Corrections to pressure measurements were necessary over certain pressure ranges and were accordingly calculated (Appendix 2). Buoyancy effect discrepancies were found to be less than 1% of the weight increase

upon adsorption at all pressures for the spring balance and were thus neglected. The level of liquid nitrogen was maintained at a maximum by continual addition. Only when the samples were at temperature and being pumped were zero extensions measured. The initial readings were given a period of equilibration times ranging from 1.5h to 2.5h depending on the sample. The remaining readings were taken after 10-15min intervals.

FIG.3.3 A block diagram of the Gravimetric apparatus

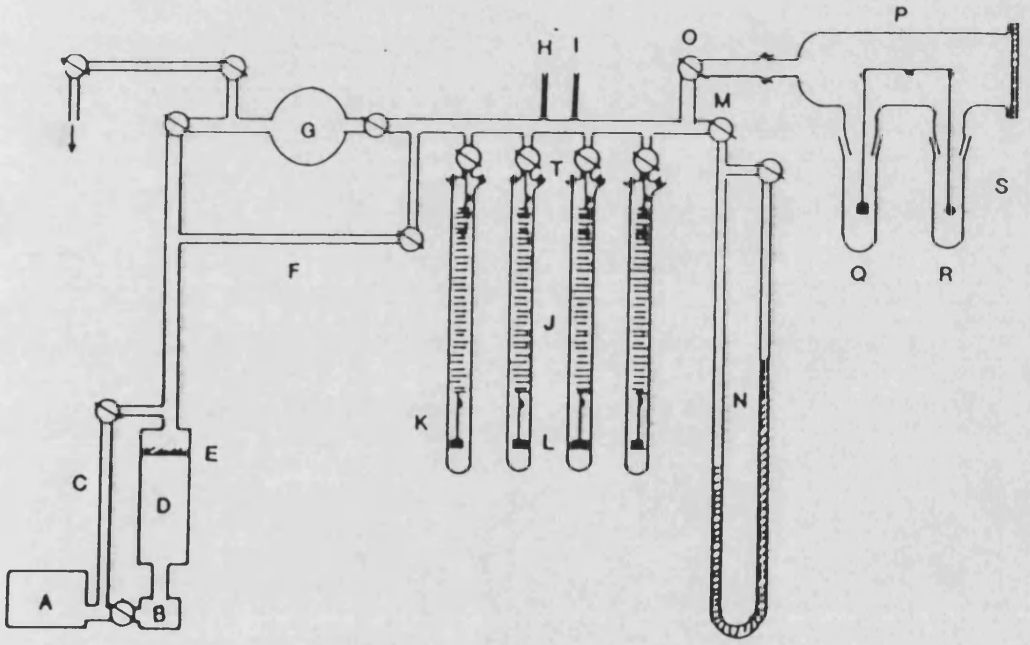


A Rotary pump
B Oil diffusion pump
C By-pass line
D Liquid nitrogen trap
E Baffle valve
F By-pass line
G One litre volume
H Pirani head
I Baratron head
J Hangdown tubes
K Sample support fibre
L Samples
M Manometer isolation tap
N Mercury manometer
O Microbalance isolation tap
P Microbalance case
Q Sample pan
R Counterweight pan
S Sample support fibre
T 'O'ring joints

### 3.7.2.2 Volumetric Technique

The apparatus was constructed of glass, including the valves, and was evacuated to $10^{-6}$ Torr by operation of a rotary pump and an oil-diffusion pump. The sample container was a long necked flask of narrow bore size to prevent sample particles entering the inter-connecting capillaries. The pressure readings were taken from an MKS Baratron, Type 170M-250 instrument. A simplified version of the apparatus is presented in fig.3.4.

The sample was oven-dried (115°C/over-night) and an accurately weighed amount was added to the sample container. This was connected to the apparatus at A and sample out-gassing continued at 250°C, over-night. By operation of the appropriate valves a dossage of the adsorptive was introduced into the capillary section, B. With the sample container isolated, the adsorptive was admitted to the bowl system C1-C5, D1-D6 and capillaries, E,(the dead volume) in the constant temperature chamber, F, and the pressure recorded using the barometer, G. The mercury level in either of the bowl systems, C or D, was raised, e.g. from C1 to C2, thus reducing the available volume and the gas pressure was recorded. The mercury was removed from the bowl, i.e. C2 back to C1 and the pressure recorded. This was repeated until reproducible pressure readings were obtained. The latter procedure provided a means of testing for system leaks.

The sample valves, J,K, were opened and individual points on

the isotherm were obtained by raising the mercury level in the bowl system and hence increasing the pressure of gas incident on the sample. An equilibration time of 1-1.5h was allowed before the first pressure reading was recorded. Consecutive readings were obtained after 10min intervals. The volume of the bowl system and capillaries connecting them to the sample container (the dead volume ) was previously known.

The container volume was determined by using helium gas due to its small atomic size and inertness. The pressure readings from the Baratron was corrected using a calibration plot of $P_{actual}$ versus $P_{Baratron}$, where $P_{actual}$ is the pressure measured by a mercury manometer. The series of pressure, P and volume, V readings were used to plot a graph of PV vs P, see Chap.7 fig.7.1b. The slope of the latter graph is a measure of the container volume. Helium gas was removed from the sample and container by further evacuating and degassing at 250$^{o}$C for 1.5h. Nitrogen gas was then admitted to the sample and the isotherm plotted over the BET pressure range (0.05 to 0.30 Torr).

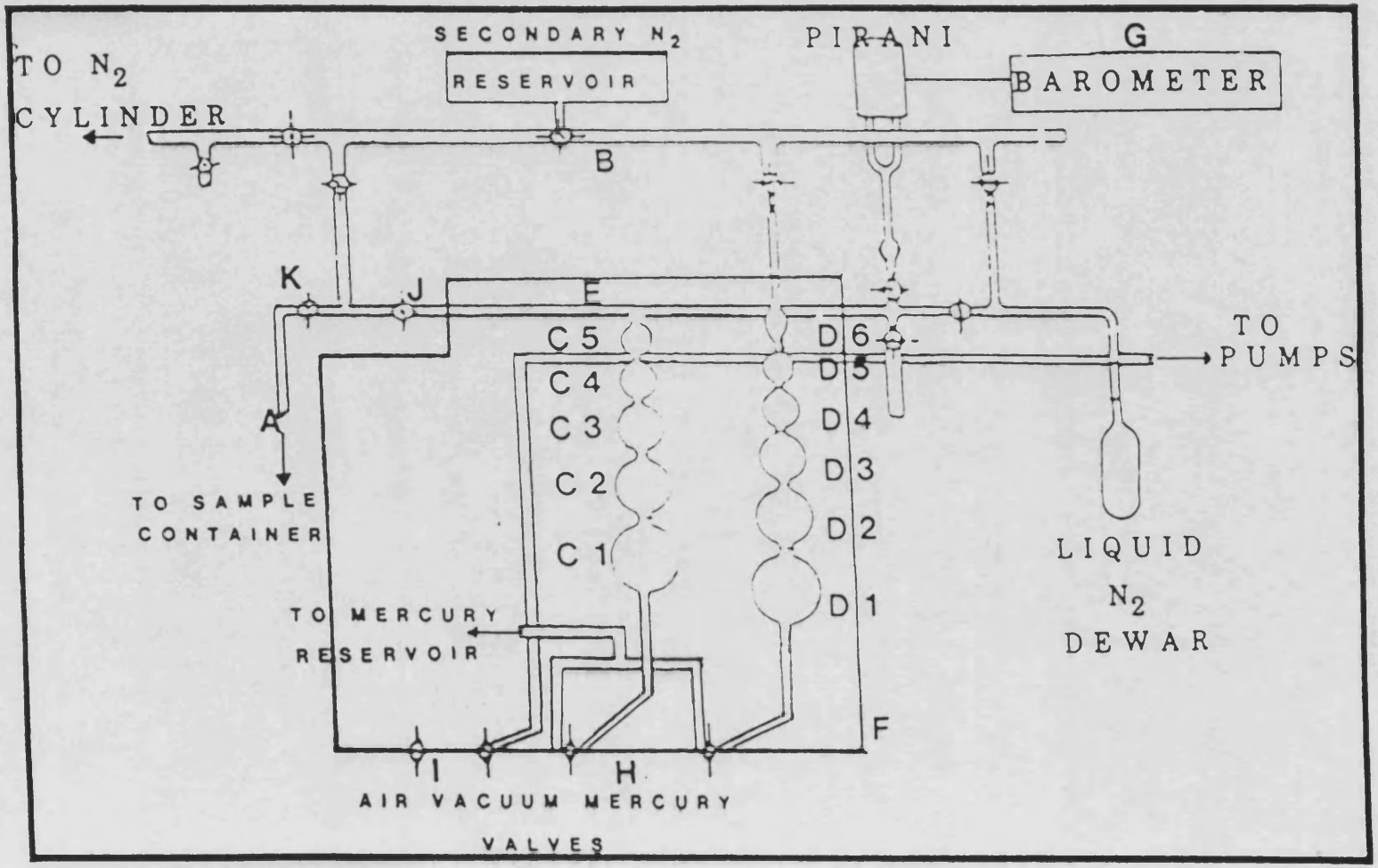


FIG.3.4 A simplified diagram of the Volumetric apparatus

### 3.7.3 Mercury Porosimetry

The particulate sample (particle size 500-850um) was oven dried (115$^{o}$C/over-night) and an accurately weighed amount was added to the dilatometer. The dilatometer was evacuated to $10^{-3}$ Torr over a period of 2h. Highly pure, freshly distilled mercury was then slowly added to the dilatometer taking care to prevent formation of air-bubbles. The vacuum was removed in stages to atmospheric pressure and the mercury level made upto the mark by means of a syringe in the dilatometer before carefully positioning the latter in the mercury porosimeter (Carlo Erba 200 Automatic Porosimeter). The sample was then subjected to pressures ranging from 200 to 2000kg/cm$^{2}$. The weight of sample used depended on the expected surface area. Thus pitch carbons were expected to have a low surface area, hence 10-15g were used. Resin carbons were expected to show larger surface areas hence smaller amounts were employed, e.g. ~2g.

### 3.7.4 Quantitative Image Analysis

#### 3.7.4.1 The System

A quantitative study of porosity was undertaken using computer-aided-image-analysis. The apparatus consisted of a computer controlled Joyce-Loebl Magiscan 2A system coupled to a Zeiss Ultraphot 11 optical microscope. The samples were illuminated with a tungsten-filament lamp operating in reflective mode. The two dimensional image from the microscope was

presented on the Magiscan screen by a two-dimensional light intensity function, F(x,y), where x and y denote spatial co-ordinates. The value of F, ranging from 0-64, at any point (x,y) is proportional to th brightness or 'grey level' of the image at that point. The image is stored in the memory of the Magiscan as a matrix whose row and column indices identify a point in the image and the corresponding matrix element value represents the grey level at that point. The elements of this array (making up a 512x512 square) are referred to as picture elements or pixels. The image-matrix of brightness values is calculated mathematically by a computer system to give void (pores and cracks) measurements. The highest magnification is with a (40x2) objective, when the side of a single pixel is 0.23um. In order to eliminate video camera noise, void images containing less than 6 pixels were ignored. Thus the minimum area detected was [$6x(0.23)^2=0.32um^2$] and the corresponding minimum diameter resolved for circular images was >0.64um.

### 3.7.4.2 Sample Preparation

The particulate sample, 500-850um, was secured by embedding in slow setting 'Metset' mounting plastic, Metset Resin/SW, Metallurgical Services Laboratories Ltd, Surrey. To ensure a single layer of particles and to prevent their random dispersion throughout the mould, the following technique was adopted: 1) the mould bottom was thinly coated with the resin/hardener mixture and left to gel, 2) the sample particles were applied as a single layer and secured by addition of a top thin layer of the

resin/hardener and the assembly left to gel, and 3) the mould was then completely filled with the resin/hardener and left to gel for 24h at room temperature. The fully-hardened assembly was removed from the mould and secured in a metallic holder, nine at a time, ready for particle sectioning by grinding. Wet grinding was performed using silicon carbide paper fixed onto a Pedemax-2 automatic grinding wheel, Struers Denmark. After grinding, the specimens were washed and debris removed using an ultra-sonic cleaner. Further polishing was performed using a 1um DP-spray, DP-Lubricant Red and a 1um polishing wheel, Struers Denmark.

TABLE 3.1 Properties of the PF resins and model compounds[1]

| Resin | F/P Ratio | Catalyst Type + HMTA Added (wt%) | Molecular Weights $M_w$ | $M_n$ | $M_z$ | Dispersivity |
|---|---|---|---|---|---|---|
| TPSX4 | 0.8 | sulphuric acid (10) | 2100 | 700 | 3550 | 3.0 |
| PR77[2] | 0.6 | sulphuric + alicyclic acids (10) | 850 | 465 | 1305 | 1.8 |
| PR77i | | same as PR77 | | | | |
| FRD2244 | 0.5 | oxalic/salicyclic (2/5) acids (15) | 553 | 370 | 800 | 1.5 |
| FRD2298 | 0.3 | as FRD2244 | 320 | 250 | 410 | |
| PA65[2] | | | 435 | 240 | 775 | 1.8 |
| Saligenin[3] | | (15) | | | | |
| DDM[3] | | (15) | | | | |

1 information on the PF resins was supplied by Borden (UK) Ltd
2 PR77 was a 80wt% novolak in a solution of monoethylene glycol and water, PA65 was a resole in an aqueous solution
3 saligenin or hydroxymethyl phenol, and DDM or dihydroxydiphenylmethane, were supplied by KOCH Light Laboratories, Suffolk

TABLE 3.2 Properties of organophosphorus additives and additive modified novolaks[a]

| Notation | Full name + chemical formula | Properties Purity (%) | BP (°C) | FP (°C) |
|---|---|---|---|---|
| TDCP[b] | tris(1,3-dichloropropyl)phosphate $(C_3H_5Cl_2O)_3$ P(O) | 97 | 200[f] | >230 |
| TCEP[b] | tris(2-chloroethyl)phosphate $(ClCH_2CH_2O)_3$ P(O) | 97 | 330 | 232 |
| TBP[c] | tributylphosphate $[CH_3\ (CH_2)_3O]_3$ P(O) | 97 | 289 | 196 |
| TTPhate[c] | tritolylphosphate $(CH_3C_6H_4O)_3$ P(O) | 90 (mixture of isomers) | 265 - | - - |
| TTPhite[c] | tris(2-tolyl)phosphite $(CH_3C_6H_4O)_3$ P | 97 | 201 | - |
| TIOP[c] | tri-iso-octylphosphate $[CH_3(CH_2)_7O]_3$ P(O) | 97 | 216 | 217 |
| TNOP[c] | tri-N-octylphosphate $[CH_3(CH_2)_7O]_3$ P(O) | 97 | - | - |
| DHAP[d] | dihydrogenammoniumphosphate $(NH_4)H_2\ PO_4$ | (analar grade) | | |
| Z6018[e] | Dow-Corning silicone resin (solid) | | | |
| MT59[e] | boron 6.7wt%; HMTA 10wt%; free phenol 13.2wt%; molecular weight $M_w$ 1650, $M_n$ 440 $M_z$ 3180; dispersivity 3.8 | | | |

a the organophosphorus additives were colourless, highly toxic liquids with irritant vapours
b source: Alpha Products/Thiokol Ventron Division
c source: Aldrich Chemical Co. Ltd
d source: British Drug Houses Ltd, Poole, Dorset
e source: Borden (UK) Ltd, North Baddesley, Southampton
f boiling point with decomposition

# RESULTS AND DISCUSSION

## (CHAPTER 4 TO CHAPTER 7)

# CHAPTER 4 CURING, CARBONISATION AND OXIDATION RESISTANCE OF THE RESINS AND RESIN AND PITCH CARBONS

## 4.1 Introduction

The results of studies of the carbonisation of pitch carbons and resin carbons, unmodified by addition of fire retardants are presented in this chapter. The organisation of the chapter follows the logical sequence of curing, carbonisation and oxidation. In addition to comparing a range of resin and pitch carbons, detailed studies of effects of cure schedule and of co-polymerisation of resoles and novolaks on the production and properties of resin carbons were made. The results of these studies are also presented in this chapter.

## 4.2 Curing of the Resins

### 4.2.1 Curing Weight Loss of the Resins

Initially the resins were cured according to the schedule specified by industry viz. 110°C for 16h, denoted as 110/16, for DDM, Sal, FRD2298 and FRD2244; 150/1.5 for PR77, PR771 and TPSX4 and 130/16 for PA65 (see table 3.1 for resin specification). Subsequently, multiple stage cures were used, see table 4.1 for the cure schedules and the notation used. Inspection of table 4.2 shows that for 110/16 cure the low molecular weight novolaks FRD2298 and FRD2244 and the model compounds undergo higher weight

losses on curing than the high molecular weight novolak TPSX4. This may reflect volatilisation of low molecular weight species, i.e. monomers or partially polymerised oligomers (in the case of the low molecular weight compounds). A similar trend is obtained when comparing the 150/1.5 curing of TPSX4 and the medium molecular weight novolak PR77, table 4.2. The difference in weight loss on curing PR77 and PR77i at 150/1.5 also reflects the presence of solvent in the former case. The resole PA65 has the highest weight loss on curing reflecting evaporation of the solvent and evolution of the volatiles.

### 4.2.2 Differential Scanning Calorimetry, (DSC)

In the present research, differential scanning calorimetry, DSC, was used to determine the effect of temperature and time on the extent of cure of novolaks and to determine the glass transition temperature, Tg, which is a measure of the cross-link density (9). Fig.4.1 shows the DSC trace obtained for the uncured novolak TPSX4; the cross-linking peak is clearly evident spanning the temperature range 140-160$^{o}$C. The literature for cross-linking of acid catalysed PF resins report a similar single exothermic peak between 150-160$^{o}$C (due to both cross-linking and condensation reactions), (142-144). Upon running a DSC scan (8$^{o}$C/min to 300$^{o}$C) of the oven cured material, a broad endotherm due to removal of adsorbed water was observed, which masked the Tg, fig.4.2. However no residual cross-linking peak over the temperature range 140-160$^{o}$C was evident. When a second DSC scan was performed, clear and similar glass transition temperatures in

the range 113.7-117.4°C were obtained, fig.4.4, implying similar levels of cross-linking. Literature values of Tg for phenolic resins range from 35-75°C for low molecular weight novolaks to >300°C for highly cross-linked resoles (9). The Tg is reported to be highly dependent on the rate of scanning, i.e. the slower the scan rate the higher is the value of Tg. The latter may explain the difference in Tg values obtained in the present research.

For resins cured at 4°C/min to 130°C and held isothermal for different time periods, the first DSC scan showed the presence of a residual cross-linking peak, fig.4.3, which did not appear during the second scan and similar Tg values were obtained, fig.4.5. The latter Tg values were similar to those shown in fig.4.4. The results of Fig. 4.4-4.5 indicate that, if uncured resin is present within the sample bulk, then residual curing extending to 300°C will take place during pyrolysis. DSC data illustrate that for TPSX4 resin the conditions employed during oven cure, i.e. time and temperature, were sufficient to obtain similar levels of resin cure.

## 4.3 Carbonisation of Pitches and Resins

The thermogravimetric, TG, curves and carbon yields obtained after carbonisation of the pitch and cured resins are presented in Fig. 4.6 and 4.7 respectively, and table 4.2. The TG data are presented as fractional weight loss, $\alpha$, versus temperature, T°C, graphs where;

$$\alpha = (Wo-W_t)/W_o$$

where $W_o$ is the initial sample weight and $W_t$ is the weight at time t. Time and temperature are linearly related by the heating rate, $\beta$. The standard conditions used for TG pyrolysis studies are similar to oxidation studies (section 4.4). FRD2298, Sal and DDM exhibit similar decomposition curves and their bulk carbon yield is similar to each other and to TPSX4, i.e. 61-62wt%. The bulk carbon yield is slightly lower than the TG carbon yield. The carbon yield of PR77 and PR77i are lower compared to the other resins while PA65 shows the highest bulk and TG yield, i.e. 65wt%.

The minor low temperature weight loss (<120°C) observed for the resins is probably due to loss of moisture. Between 140-300°C the observed high rate of weight loss for the solvent containing PA65 and PR77, especially the latter, is due to solvent evaporation. In this temperature range, the other compounds show a weight loss which may be due to loss of entrapped oligomeric species in addition to evolution of $NH_3$, unreacted HMTA and monomers and water of condensation as further residual polymerisation takes place. Between 320-420°C, the weight remained more or less constant and above this temperature, there is a very rapid weight loss corresponding to a maximum rate of oxidative degradation, i.e. the region where char forming reactions become dominant. This region spans 420-620°C and is referred to as a region of maximum reaction rate.

Carbonisation of the pitches, fig.4.6, is a single stage process of distinctly different character to carbonisation of the

resins. The main weight loss occurs at lower temperatures and over a narrower temperature range, $\Delta T$, than for the resins. Thus for pitches $\Delta T$ =200-550°C and for the resins $\Delta T$ =200-800°C. This difference probably reflects the higher oxygen content of the resins. The significant high temperature weight loss for the resins, which is not complete at 1000°C, probably results from elimination of residual oxygen as CO and $CO_2$. The bulk carbon yields from the pitches (40-44.5wt%) are substantially lower than that observed for the resins. CTP is more aromatic than PP and this may explain the slightly higher yield of CTP carbon. However, the lowest yield is obtained from DP, which is a form of CTP. This discrepancy may reflect a low molecular weight distribution in the case of DP since its TG curve is displaced to lower temperatures compared to PP and CTP.

## 4.4 Oxidation of Resin and Pitch Carbons

A number of experimental parameters will influence the shape of the TG curve, i.e. heating and air-flow rates, particle size and sample size. An extensive survey of these parameters was carried out to select a suitable range of operating parameters. As a result of this survey the following conditions were chosen: heating rate 15°C/min, air-flow rate 50ml/min, initial sample weight 10mg, and initial sample particle size 500-850um. In an attempt to provide a concise quantitative summary of the TG oxidation data, the following arbitrary terms are defined: $T_{0.05}$, $T_{0.5}$ and $T_{0.95}$ being the temperature at which the weight loss fraction is 0.05, 0.5 and 0.95 respectively. $T_{0.05}$ provides

an index of the onset of oxidation and $T_{0.05}$-$T_{0.95}$ indicates the temperature range of oxidation. The TG oxidation curves of several resin and pitch carbons are presented in Fig. 4.8 and 4.9. Rates of oxidation of carbons were obtained from the slope of the weight loss curve, $d\alpha/dT$, at $T_{0.5}$; the oxidation rate $(d\alpha/dt) = (d\alpha/dT)\beta$, where $\beta$ is the linear heating rate (144-145). The rate of oxidation can be expressed as:

$$d\alpha/dt = k\ f(\alpha) \quad \ldots\ldots\ldots\ldots\ldots 1)$$

where k is the rate constant and $f(\alpha)$ is a function of the weight loss. Assuming that k can be represented by the Arrhenius equation, i.e.

$$k = A \exp(-Ea/RT) \quad \ldots\ldots\ldots\ldots 2)$$

where Ea is the activation energy for the oxidation reaction, A is a pre-exponential factor and R is the gas constant. Combination of equations 1 and 2 gives equation 3;

$$d\alpha/dt = f(\alpha)\ A \exp(-Ea/RT) \quad \ldots\ldots\ldots 3)$$

At constant $\alpha$, $f(\alpha)$ may be assumed to be constant so that equation 3 becomes;

$$\ln(d\alpha/dt)_{\alpha} = \ln[f(\alpha)A] - Ea/RT \quad \ldots\ldots\ldots 4)$$

In this work equation 4 is tested by plotting $\ln(d\alpha/dt)_{0.5}$ versus $1/T_{0.5}$ for different carbons. The results are plotted in fig.4.10 and show reasonable conformity to equation 4. Fig.4.10 also illustrates the ranking in reactivity of the resin carbons, with TPSX4 being the most reactive and Saligenin the least reactive. The lower reactivity of the pitch carbons is also illustrated. Although the reactivity of pitch carbons is similar to the most reactive resin carbons, their reactivities occur at a much higher temperature. This is supported by the similarity of

the activation energies for oxidation of the resin and pitch carbons viz. 64.2±6.3 kJ/mol and 61.2±5.6 kJ/mol, respectively. These values are in good agreement with literature values quoted for the air oxidation of glassy carbon and graphitic pitch carbons, i.e. 54.4 kJ/mol (47).

An illustration of the reproducibility of TPSX4 and pitch (CTP) carbons is presented in fig.4.11. This figure also shows that CTP exhibits a superior oxidation resistance to TPSX4 with $T_{0.5}$ values of 831°C and 680°C, respectively, table 4.2. Fig.4.8 shows the oxidation curves of the various resin carbons. The novolaks exhibit similar oxidation curves with $T_{0.5}$ values ranging from 680°C for TPSX4 to 748°C for FRD2244, table 4.2 (i.e. referring to $T_{0.5}$ values obtained for the industrially-utilised cure schedules). The resole PA65 exhibits an unusual oxidation curve with a low $T_{0.05}$ and the highest $T_{0.5}$ value among the resin carbons.

## 4.5 Effects of Cure Schedule on Carbonisation of Resins and Oxidation of the Resin Carbons

In order to determine whether the differences in thermal behaviour between the resins were linked to differences in the cure schedule, the effects of various cure schedules were investigated. The schedules used are presented in table 4.1. The results of the study are presented in tables 4.2-4.4 and Fig. 4.8, 4.12-4.19. For the model compounds, weight losses upon curing generally increase with increasing severity of the cure

schedule, table 4.4b, whereas there are no clear trends in carbon yield. The model compound saligenin, subjected to either single stage, fig.4.12, or multiple stage, fig.4.13, cures exhibited similar thermograms upon carbonisation. The same temperature zones defined previously, are evident viz. 200-420$^{o}$C representing an induction period of low weight loss followed by a temperature zone in which a maximum rate of weight loss is observed. A final high temperature zone of declining weight loss, as carbon is converted to a stabilised form, is also clearly defined.

For saligenin, the first three PC1 cure schedules yield carbons of low $T_{0.5}$ compared to the single stage cures, fig.4.12 and 4.14. However, further heating of the PC1 cured resin to 200/5min PC1 enhanced the $T_{0.5}$ value. The two stage cures, PC2 and PC3 gave a carbon of similar oxidation resistance to the 200/5min PC1 carbon. There is no consistent pattern of effects of cure schedule on carbonisation and oxidation resistance in the case of the intermediate molecular weight novolaks PR77 and PR77i, fig.4.19. For PR77 postcuring increased the carbon yield significantly, table 4.4, but there is no effect on carbon yield for PR77i. Conversely the oxidation resistance increased with postcuring of PR77i but not for PR77. For the latter, the single stage cure, 130/16, gave the most stable carbon. It is interesting to note that, apart from the PC3 schedule, the oxidation resistance of the solvent containing PR77 is consistently higher than the solvent-free PR77i for each cure schedule.

For TPSX4, low temperature single stage cures viz. 100/24 and 110/16, resulted in a lower curing weight loss and a lower carbon yield than the higher temperature cures, 150/1.5 and 180/24. This is also illustrated by the effects of progressive curing by schedule PC1, table 4.4b which shows an increasing weight loss with severity of the cure. Upon pyrolysis the shape of the single stage, fig.4.15 and the multiple stage cures, fig.4.17 are similar and exhibit weight loss rates and temperature zones which are not very different from each other. There is no clear trend on the oxidation resistance of TPSX4 for the various cure schedules. Thus for single stage cure, fig.4.16, the extended high temperature schedule, 180/24, gave a carbon of high $T_{0.5}$, although the most stable TPSX4 carbon was given by PC2. The results for the resole PA65 are presented in the next section.

## 4.6 Effect of Resole/Novolak Co-polymerisation on Carbonisation and Oxidation Resistance

Upon curing the resole PA65, a high weight loss was observed due to solvent evaporation. Upon pyrolysis, a high carbon yield compared to the novolaks and pitch carbons was obtained, table 4.2. The shape of the thermogram for PA65 pyrolysis is similar to the other resin carbons, although an unusual oxidation curve was obtained, fig.4.8, characterised by a low $T_{0.05}$ and a $T_{0.5}$ which approached the pitch carbons. In contrast, TPSX4 and PR77 carbons yield high $T_{0.05}$ values but lower $T_{0.5}$ values upon

oxidation. For these reasons, studies were performed on various PA65/novolak compositions. Using the novolak TPSX4 the curing weight loss increased with increasing PA65/TPSX4 ratio, table 4.5. The highest carbon yield was obtained for co-polymers with the ratio PA65/TPSX4 > 1. Fig.4.20 shows the influence of PA65/TPSX4 ratio on carbonisation. At temperatures below about 400°C, the Tg curves are very similar but above this temperature, the curves for the co-polymer are displaced to higher temperatures compared to the curve for TPSX4 alone. The PA65-90/10-TPSX4 composition, designated PT, shows a rapid weight loss which extends into the high temperature region and is still incomplete at 1000°C.

Fig.4.21 compares the oxidation resistance of TPSX4 carbon to the carbons prepared from resins with the ratio PA65/TPSX4 < 1. The thermal stability of the co-polymer carbons is clearly inferior to TPSX4 carbon. However, the $T_{0.05}$ value is improved compared to PA65 alone. The oxidation curves for carbons prepared from PA65/TPSX4 > 1, fig.4.22 show that there is a general trend of increased oxidation resistance with increasing level of PA65. The most stable carbons are obtained for PA65/TPSX4 ratios in the range 80/20 to 90/10. Fig.4.23 illustrates the reproducibility of the PT system, starting from the resin stage of manufacture. The carbon represented by the number 5 oxidation curve had been cured under a nitrogen atmosphere and in a small volume Carbolite furnace. This is in contrast to oven cures, open to the atmosphere, employed for the other resins. The effect of cure schedule on the oxidation resistance of PT carbon is presented in

fig.4.24 and table 4.6. Data on single stage cure of PA65 alone is included for comparison. PA65 cured using the schedule 180/24 gave a carbon of high $T_{0.5}$, however the latter carbon could not be reproduced as consistently as the co-polymer carbon, PT. Furthermore, using the schedule 130/16, the co-polymer gave a carbon of higher $T_{0.5}$ compared to PA65 alone.

There is no clear trend of curing weight loss and bulk carbon yield with cure schedule for PT. However the 180/24 schedule showed the lowest curing weight loss and bulk carbon yield, higher $T_{0.05}$ and a slightly improved $T_{0.5}$. Briefly, the most stable carbon was produced by the extended single stage cure schedules 130/16 and 180/24. The multiple stage postcures all had a detrimental effect on the oxidation resistance of PT.

When the high molecular weight novolak TPSX4 was replaced by the medium molecular weight PR77 as a co-polymer with PA65, no improvement in oxidation resistance and a decreased carbon yield compared to the analogous PT co-polymer was observed, fig.4.25, table 4.5. The results show that addition of HMTA cross-linking agent significantly improved $T_{0.5}$, although not to the same level as observed for PT.

## 4.7 Discussion of Results

The weight loss during carbonisation involves oxidative degradation even in an inert atmosphere, due to the high oxygen content of the resins. At higher temperature, fragmentation reactions also occur. Pyrolysis at elevated temperatures depends on the thermal stability of the dihydroxydiphenylmethane unit. Thus all polycondensates (resoles and novolaks) should behave similarly, i.e. show the same route and extent of pyrolysis once the curing processes are complete (133). This prediction is supported (using TPSX4 resin as an example) by the similarity of the glass transition, $T_g$ values, and by the shapes of the carbonisation thermograms, which are clearly distinct from the carbonisation of the pitches.

Since the low molecular weight volatiles are removed by diffusion, equilibrium conditions can be attained at the higher temperatures when the rate of volatile species generation is high. Under such conditions the evolved species tend to participate in thermally-induced postcuring reactions as they would not have time to diffuse out of the solid matrix. Postcuring is further aided by the charring tendency (and hence diffusion inhibition) of phenolic resins (146). Reaction scheme 1 illustrates a possible mechanism for weight loss during carbonisation of the resins.

The non-homogeneity of the pitches, i.e. presence of volatile aliphatics and aromatics, accounts for the low carbon

yield compared to the resins. The difference in carbon yield between the pitches is probably based on the presence, or absence, of large polynuclear and non-volatile aromatics. Thus PP is known to be less aromatic than CTP and DP and hence shows a correspondingly lower coke yield. Pyrolysis of the pitches shows a low temperature weight loss, ($<200^{o}C$), which has been linked to removal of adsorbed water and oxides of carbon. This is followed by a region of high rate of weight loss when 75% of the volatile matter is evolved, including the lighter condensable hydrocarbons. The plastic mesophase is also thought to form at this stage as oxygen, (or sulphur, which is a known contaminant of coal tar pitches), bridges are broken and the aromatic lamellae become mobile. As aromatisation of the char proceeds, large hexagonal carbon platelets are developed representing the involatile coke residue. The mineral matter present in the pitches is also converted to the metal oxides at this stage.

Reaction Scheme 1: The mechanism for weight loss during carbonisation of phenolic polycondensates in an inert atmosphere

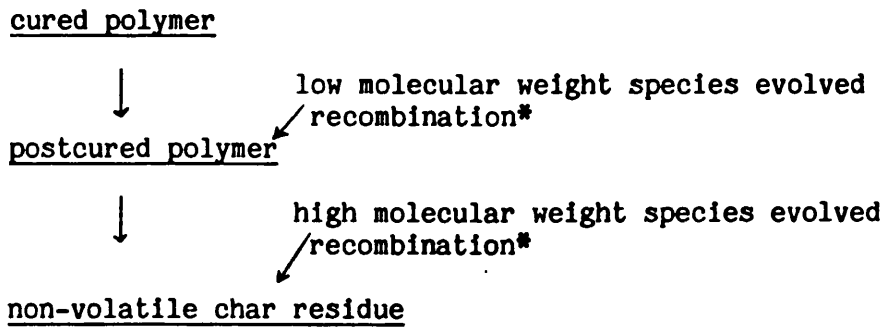


* The percentage recombination is dependent on several factors viz. environment, rate of temperature increase, rate of gas flow, ability of the resins to char and solvent evaporation.

During resin and pitch pyrolysis, the following changes are postulated to occur in the resulting carbon; 1) increase in porosity, 2) increase in average macropore size, and 3) decrease in average micropore size due to volatile recombination. The changes in porosity are considered in more detail in Chap.7.

The thermograms (weight loss versus temperature) for non-isothermal oxidation studies of resin and pitch carbons were of similar shape and showed the presence of three distinct reaction zones (147-148). By reference to Fig. 4.8 and 4.9, the following zones were evident: zone 1- low temperature oxidation; 590-650$^{o}$C for the resins (excluding PA65) and 700-800$^{o}$C for the pitches, zone 2- maximum oxidation rate; 650-800$^{o}$C for resins and 800-930$^{o}$C for pitches and zone 3- reduced high temperature rate of weight loss; 800-880$^{o}$C for resin and 930-1000$^{o}$C for the pitches.

During the initial weight loss, the rate of oxidation increases with increase of temperature and is independent of the diffusion of oxygen to the interior of the carbon surface, i.e. via pores and cracks. This initial oxidation (zone 1) has been reported to drastically increase the surface area of the carbon (43, 149). Similarly, Linares-Solano reported that gasification (oxidation in air) during manufacture of active carbons from olive stones, resulted in an increase of volume, widening of micropores and eventual destruction of the narrower micropores (150). Further gasification results in complete destruction of the mesopores and eventually macropores (151-152). This explains

the rapid increase in the rate of oxidation (zone 2), which ultimately becomes equal to the rate of diffusion of oxygen through the changing pore structure. The concentration of oxygen thus becomes depleted within the carbon network. Hence the reaction rate at higher temperature decreases and becomes dependent on the diffusion of oxygen to the carbon surface and mass transport of the product gases, CO major and $CO_2$ minor. Furthermore, the amount of carbon remaining in the high temperature region is less than initially present during the early stages of oxidation.

The difference in oxidation resistance observed between the resin carbons is probably linked to differences in the initial structure of the carbon. Since the resin carbons are chemically similar, as shown by the similarity of the carbonisation curves and were more-or-less cured to the same extent, as suggested by the $T_g$ values, their reactivity will be related to the heterogeneity of the surface. The chemical similarity of the resin carbons is further implied by the straight line Arrhenius-type graph, fig.4.10. The difference in reactivity between the resin carbons is probably due to differences in the pre-exponential factor A. One possible factor affecting the value of A is the specific surface area of the carbons. This is considered in Chap.7. Similar considerations apply to the pitch carbons, although the latter exhibit a lower reactivity than the resin carbons.

Studies of PA65/TPSX4 ratio, Fig. 4.20-4.23, show that in general, increasing the resole content has a progressively beneficial effect on oxidation resistance which reaches a maximum in the range PA65/TPSX4 80/20 to 90/10 (weight%). Cured resoles are cross-linked by a process which evolves less gas (evolution of which is aided by solvent evaporation) than is the case with novolaks. Thus it is possible that progressive addition of resole to novolak will produce a co-polymer of high cross-link density which will lead to a more stable carbon. This line of argument would lead one to suppose that the pure resole when cured would produce the most stable carbon. However this is not the case under the curing conditions studied, i.e. 130/16 for the resole/novolak co-polymers. Nevertheless, when the resole is subjected to the slower cure schedule 180/24, the resulting resin does produce a stable carbon. Since the slower cure schedule is expected to aid more complete and uniform loss of volatiles, the high oxidation resistance of the PA65 carbon implies that the oxidation resistance of the resin carbons is linked to a physical factor, i.e the surface area and pore structure. The latter are reported to act as centres for the initiation of carbon oxidation (43, 147, 150, 153-154).

Curing of the co-polymer in a Carbolite furnace, under a nitrogen atmosphere, gave a carbon of reduced oxidation resistance compared to the co-polymer cured in an oven open to the atmosphere. Although nitrogen is not expected to have a profound influence on the extent of resin cure, it is suggested that the restricted space of the Carbolite furnace prevented complete

removal of the condensation products, which remain trapped in the polymeric network. Upon pyrolysis, the entrapped volatiles are released in large amounts thus destroying the carbon structure. Furthermore, curing in an inert atmosphere has been reported to effect the char yield. Pre-oxidation, which occurs in phenolic resins cured in air, increases the char yield and gives more bulky and harder residues compared to resins cured under non-oxidative conditions (155-157).

In summary, the chemical similarity of the resin carbons is supported by the similar shape of the carbonisation thermograms. The difference in oxidation resistance observed between the resin carbons must therefore be linked to a physical difference in the actual carbon structure, i.e. as caused by the evolution of volatiles. The higher oxidation resistance of the pitch carbons compared to the resin carbons, excepting PA65 and PT, is probably due to their more ordered, graphitic structure and low surface area. The enhanced oxidation resistance observed for the resole and the co-polymer PT carbon is postulated to be due to the possession of a uniform, although non-graphitic, carbon structure of low surface area arising from the use of an extended high temperature cure schedule, i.e. 130/16 and 180/24.

TABLE 4.1 Schedules used for resin curing *

a) Single Stage Cure Schedules

| Temperature (°C) | Time (h) | Notation |
|---|---|---|
| 100 | 24 | 100/24 |
| 110 | 16 | 110/16 |
| 130 | 16 | 130/16 |
| 150 | 1.5 | 150/1.5 |
| 180 | 24 | 180/24 |

b) Multiple-Stage Cure Schedules

| | |
|---|---|
| 100/24 + 130/12 + 140/5 + 150/2.5 + 200/5min | PC1 |
| 150/0.5 + 180/1 | PC2 |
| 150/1 + 180/0.5 | PC3 |
| 130/16 + 150/1 + 180/1 | PC4 |
| 110/16 + 180/1 | PC5 |

* The 180/24 schedule involved a heating (and cooling) rate of 8°C/h followed by an isothermal hold at the final temperature for 10 min. The remaining schedules involved a heating rate of 4°C/min followed by an isothermal hold for the period listed.

TABLE 4.2 Single stage curing weight loss of the resins, bulk carbon yield and oxidation resistance of the resin and pitch carbons

| Precursor | Cure-Type | Curing Loss (wt%) | Carbon Yields* (wt%) TG | Bulk | $T_{0.5}$ (°C) |
|---|---|---|---|---|---|
| Resin Carbons | | | | | |
| DDM | 110/16 | 5.3 | 63.0 | 60.8 | 709 |
| SAL | 100/24 | 10.4 | | 58.8 | 728 |
| " | 110/16 | 12.7 | | 60.9 | 743 |
| FRD2298 | 110/16 | 6.5 | 62.5 | 61.2 | 718 |
| FRD2244 | 110/16 | 10.1 | 62.5 | 61.8 | 748 |
| PR77 | 150/1.5 | 10.0 | 53.0 | 44.9 | 728 |
| " | 130/16 | 6.3 | | 58.2 | 728 |
| PR77i | 150/1.5 | 3.3 | | 56.4 | 705 |
| TPSX4 | 150/1.5 | 2.6 | 62.0 | 59.0 | 680 |
| " | 100/24 | 2.2 | | 55.0 | 690 |
| " | 110/16 | 2.6 | | 55.9 | 770 |
| " | 130/16 | 3.9 | | 59.4 | 683 |
| " | 180/24 | 4.1 | | 57.5 | 773 |
| PA65 | 130/16 | 26.2 | 65.0 | 65.3 | 840 |
| " | 180/24 | 26.9 | | 65.8 | 915 |
| Pitch Carbons | | | | | |
| CTP | | | 40.0 | 44.5 | 831 |
| DP | | | 34.0 | 40.1 | 860 |
| PP | | | 38.0 | 42.8 | 854 |

* The bulk carbon is the yield after carbonisation in the furnace to 970°C and the TG yield is the carbon remaining after TG pyrolysis to 1000°C

TABLE 4.3 Data on the oxidation resistance of resin carbons cured under different schedules compared to the pitch carbons

| Carbon | Cure Schedule | $T_{0.05}$ | $T_{0.5}$ °C | $T_{0.95}$ | Oxidation Rate $R_{0.5}$ $x10^{-3}$ $s^{-1}$ |
|---|---|---|---|---|---|
| DDM | 110/16 | 626 | 709 | 826 | 1.48 |
| SAL | " | 636 | 743 | 871 | 1.07 |
| FRD2298 | " | 625 | 718 | 822 | 1.38 |
| FRD2244 | " | 645 | 748 | 873 | 1.09 |
| PR77 | 150/1.5 | 630 | 728 | 838 | 1.29 |
| PR77i | " | 618 | 705 | 786 | 1.66 |
| CTP | | 733 | 831 | 865 | 1.951 |
| DP | | 749 | 860 | 954 | 1.62 |
| PP | | 766 | 854 | 940 | 1.66 |

TABLE 4.4a Multi-stage curing weight loss of the resins, bulk carbon yield and oxidation resistance of the carbons

| Resin-Type | Cure-Type | Curing Loss (wt%) | BC Yield (wt%) | $T_{0.5}$ (°C) |
|---|---|---|---|---|
| SAL | PC1 | 13.7 | 59.9 | 800 |
| | PC2 | 13.5 | 59.0 | 806 |
| | PC3 | 14.7 | 59.8 | 808 |
| DDM | PC1 | 4.5 | 58.3 | 730 |
| | PC2 | 3.2 | 57.3 | 745 |
| | PC3 | 4.2 | 58.3 | 749 |
| PR77 | PC2 | 12.1 | 53.8 | 720 |
| | PC3 | 10.4 | 54.1 | 728 |
| PR77i | PC2 | 4.7 | 55.3 | 715 |
| | PC3 | 5.2 | 59.6 | 745 |
| TPSX4 | PC1 | 3.5 | 58.3 | 705 |
| | PC2 | 2.9 | 57.3 | 788 |
| | PC3 | 4.2 | 58.3 | 749 |

4.4b Curing weight loss at each stage of PC1

| PC1 Stage: | 130/12 | 140/5 | 150/2.5 |
|---|---|---|---|
| SAL | 12.9 | 13.3 | 13.52 |
| TPSX4 | 2.7 | 2.9 | 3.07 |

TABLE 4.5 Effect of Resole/Novolak ratio on bulk carbon yield and oxidation resistance (cure schedule: 130/16)

| PA65 | TPSX4 | Curing Loss | BC Yield | $T_{0.05}$ | $T_{0.5}$ |
|---|---|---|---|---|---|
| (wt% ratio) | | (wt%) | (wt%) | ($^oC$) | |
| 0.0 | 100 | 3.9 | 59.4 | 620 | 683 |
| 16 | 84 | 5.8 | 59.1 | 678 | 798 |
| 20 | 80 | 6.2 | 61.5 | 434 | 515 |
| 33 | 67 | 7.4 | 61.4 | 444 | 530 |
| 40 | 60 | 9.6 | 62.5 | 505 | 580 |
| 50 | 50 | 12.7 | 61.8 | 480 | 595 |
| 60 | 40 | 15.2 | 62.4 | 497 | 640 |
| 75 | 25 | 19.2 | 64.3 | 472 | 700 |
| 80 | 20 | 20.3 | 65.1 | 381 | 898 |
| 84 | 16 | 21.3 | 65.9 | 482 | 878 |
| 90 | 10 | 23.1 | 64.4 | 773 | 890 |
| 95 | 5.0 | 24.2 | 64.5 | 452 | 810 |
| 100 | 0.0 | 26.2 | 65.3 | 423 | 840 |
| PA65 | PR77 | | | | |
| 90 | 10 | 16.1 | 61.5 | 435 | 724 |
| 90 | 10(a) | 19.5 | 62.9 | 445 | 811 |
| 80 | 20 | 17 | 60.9 | 432 | 826 |
| 0.0 | 100(b) | 6.3 | 58.2 | 695 | 728 |

a, b; 1 and 10wt% HMTA, respectively were added

TABLE 4.6 Effect of curing schedule on curing weight loss, bulk carbon yield and oxidation resistance of PT

| a) Single Stage Cure | Curing Loss | BC Yield | $T_{0.05}$ | $T_{0.5}$ |
|---|---|---|---|---|
| | (wt%) | (wt%) | ($^oC$) | |
| 130/16(a) | 26.2 | 65.3 | 423 | 840 |
| 180/24(b) | 26.9 | 65.8 | 805 | 915 |
| 130/16 | 23.1 | 64.4 | 773 | 890 |
| 150/16 | 25.5 | 66.0 | 455 | 798 |
| 180/24 | 16.9 | 60.5 | 797 | 902 |
| b) Multi-stage Cure | | | | |
| PC2 | 24.4 | 65.0 | 432 | 773 |
| PC3 | 23.9 | 64.8 | 413 | 773 |
| PC4 | 26.4 | 67.8 | 484 | 584 |
| PC5 | 24.8 | 65.3 | 432 | 776 |

a,b PA65 alone, (b was difficult to reproduce)

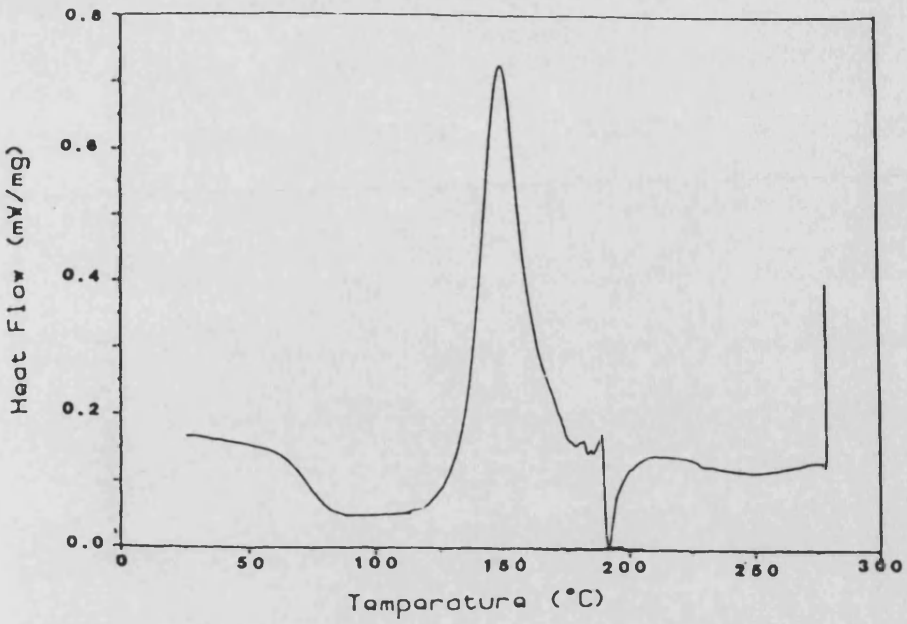


FIG.4.1 Polymerisation of TPSX4 showing the position of the cross-linking peak

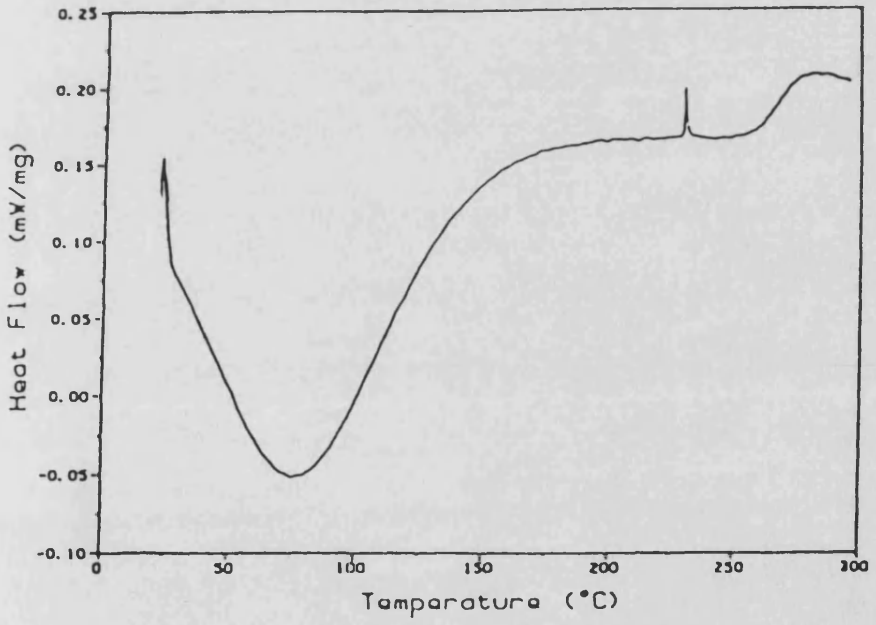


FIG.4.2 DSC trace of TPSX4 resin previously cured using the schedule 150/1.5 (note the absence of the cross-linking peak)

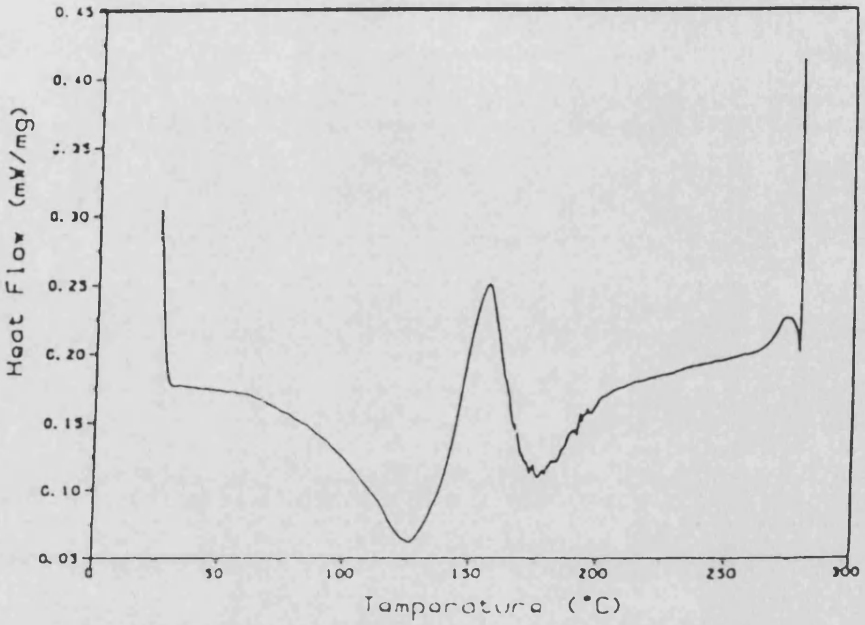


FIG.4.3 DSC trace of TPSX4 resin previously cured at 130°C for 240min.

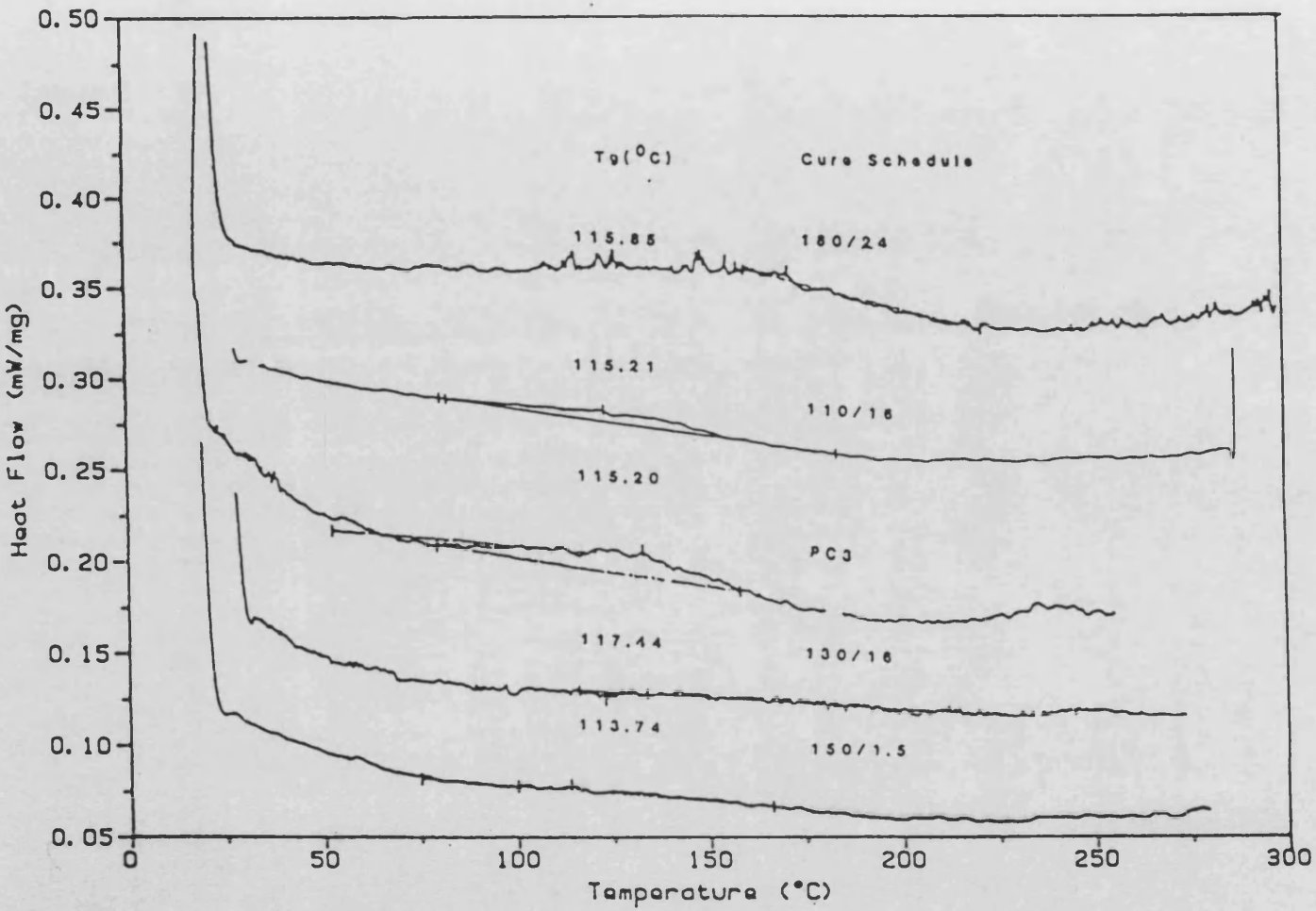


FIG.4.4 Glass transition temperatures of TPSX4 resin previously cured using the schedules listed

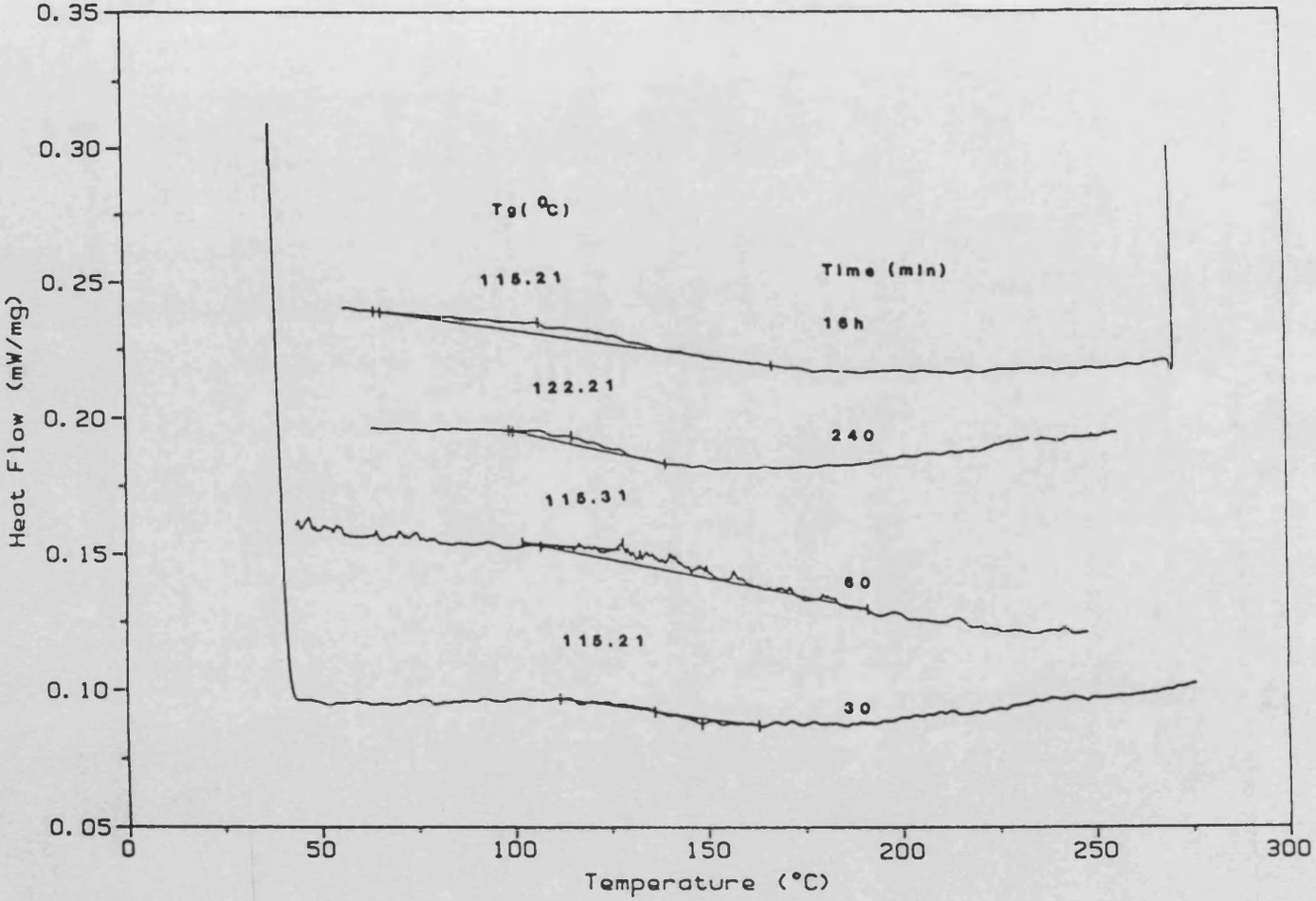


FIG.4.5 Glass transition temperatures of TPSX4 resin cured isothermally at 110℃ for the times listed

FIG.4.6 Pyrolysis of the pitches

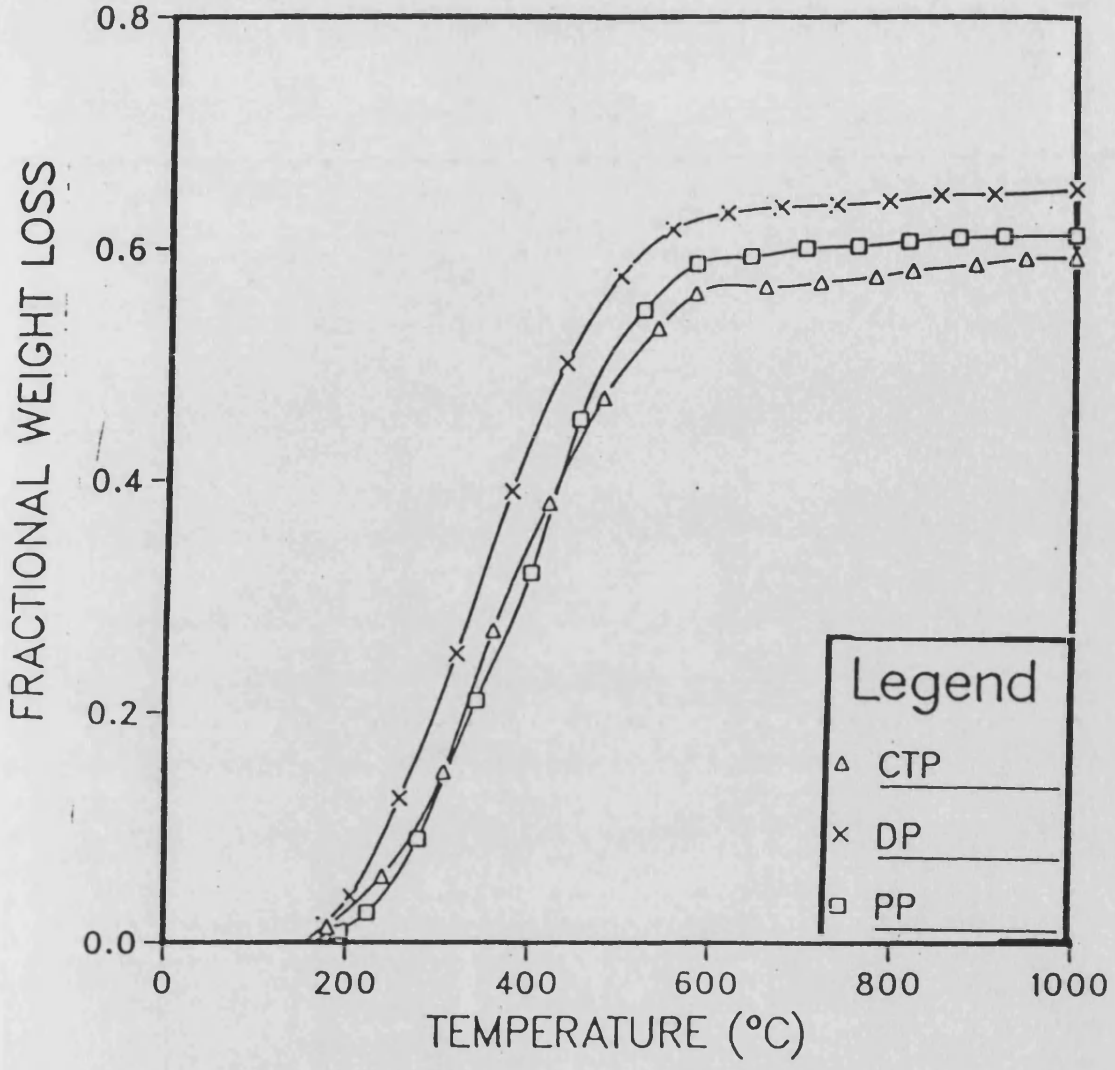

FIG.4.7 Pyrolysis of the model compounds and PF resins

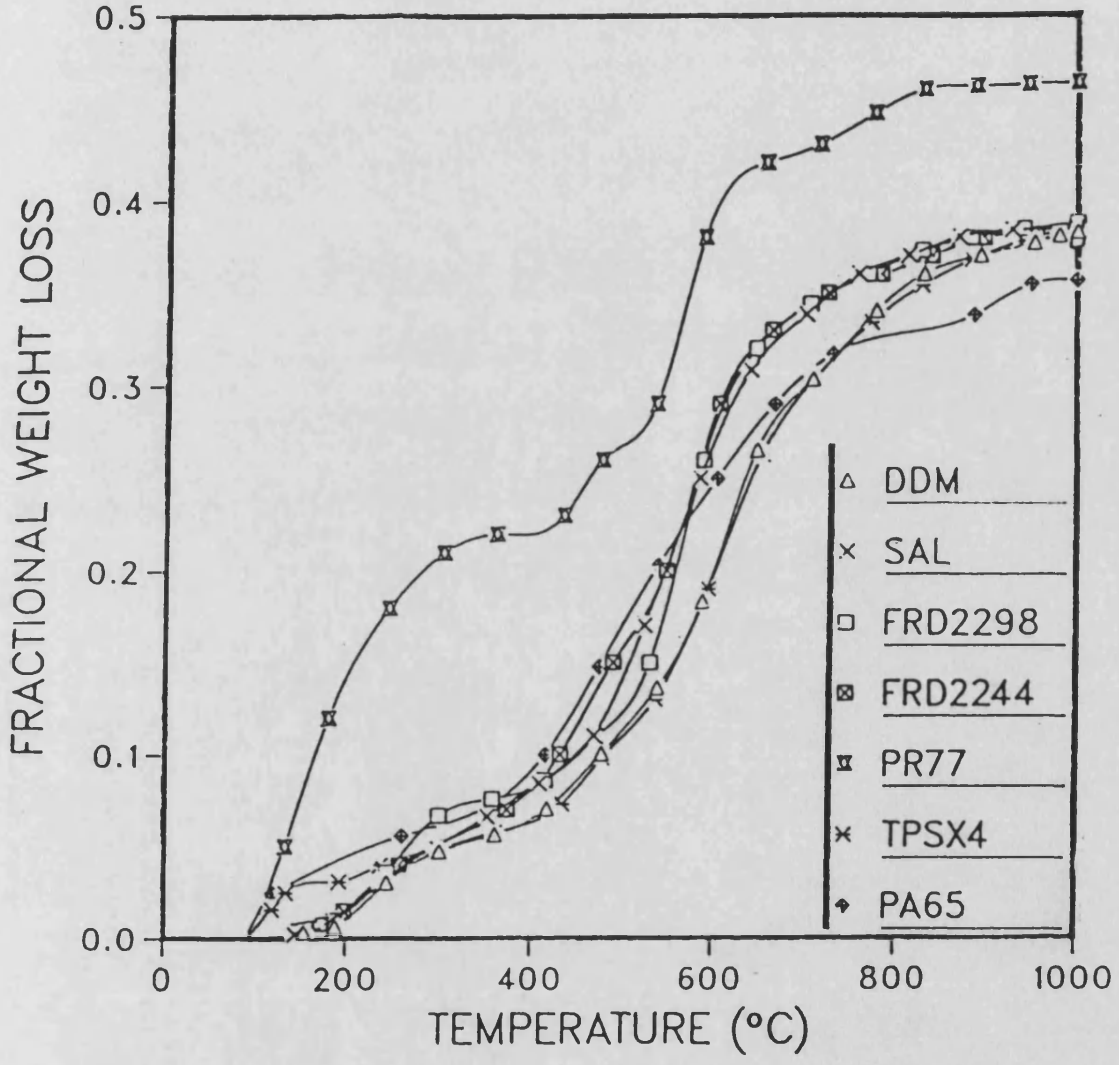

FIG.4.8 Oxidation resistance of the model compounds and PF resin based carbons

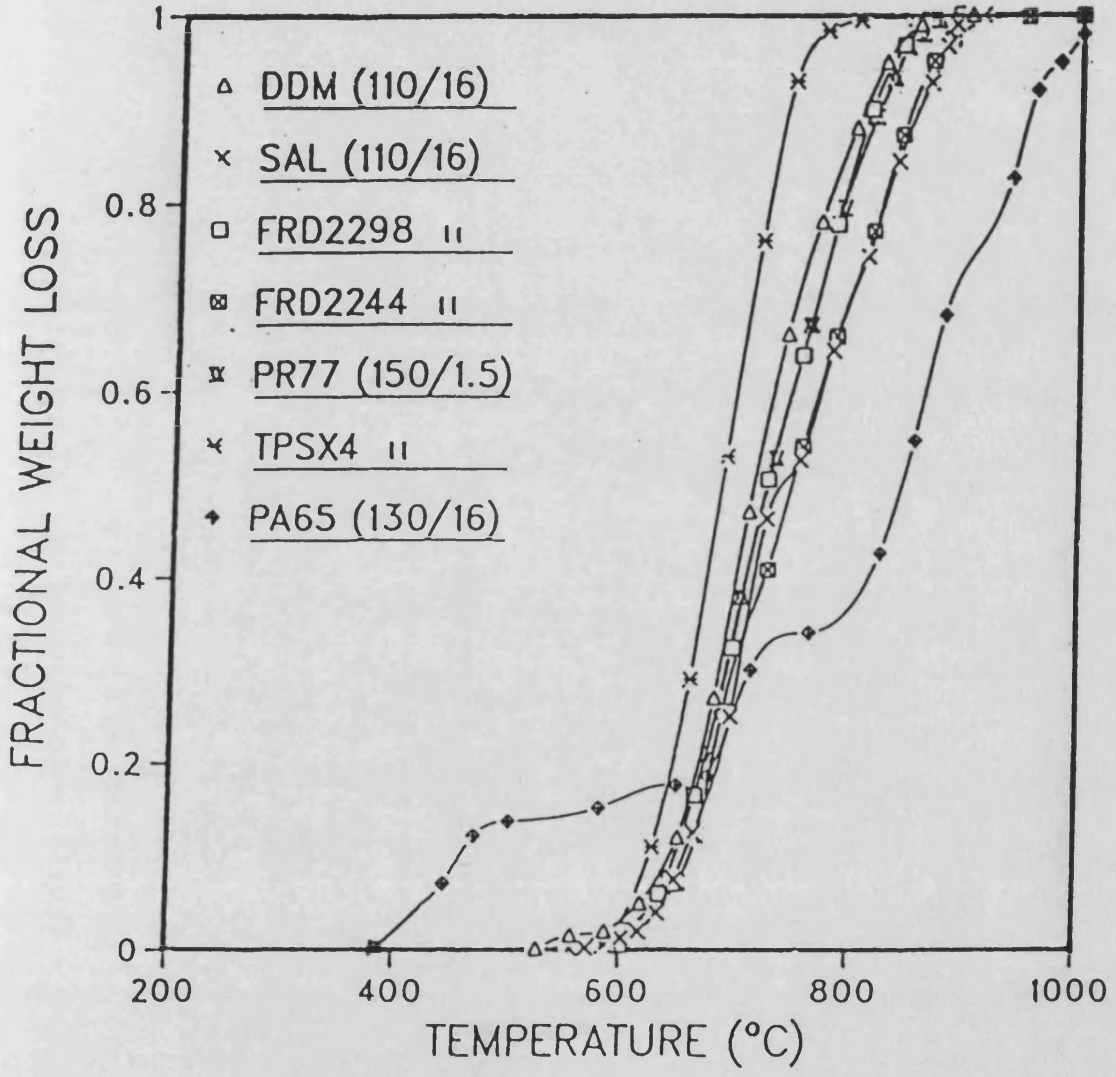

FIG.4.9 A comparison of the oxidation resistance of the pitch carbons

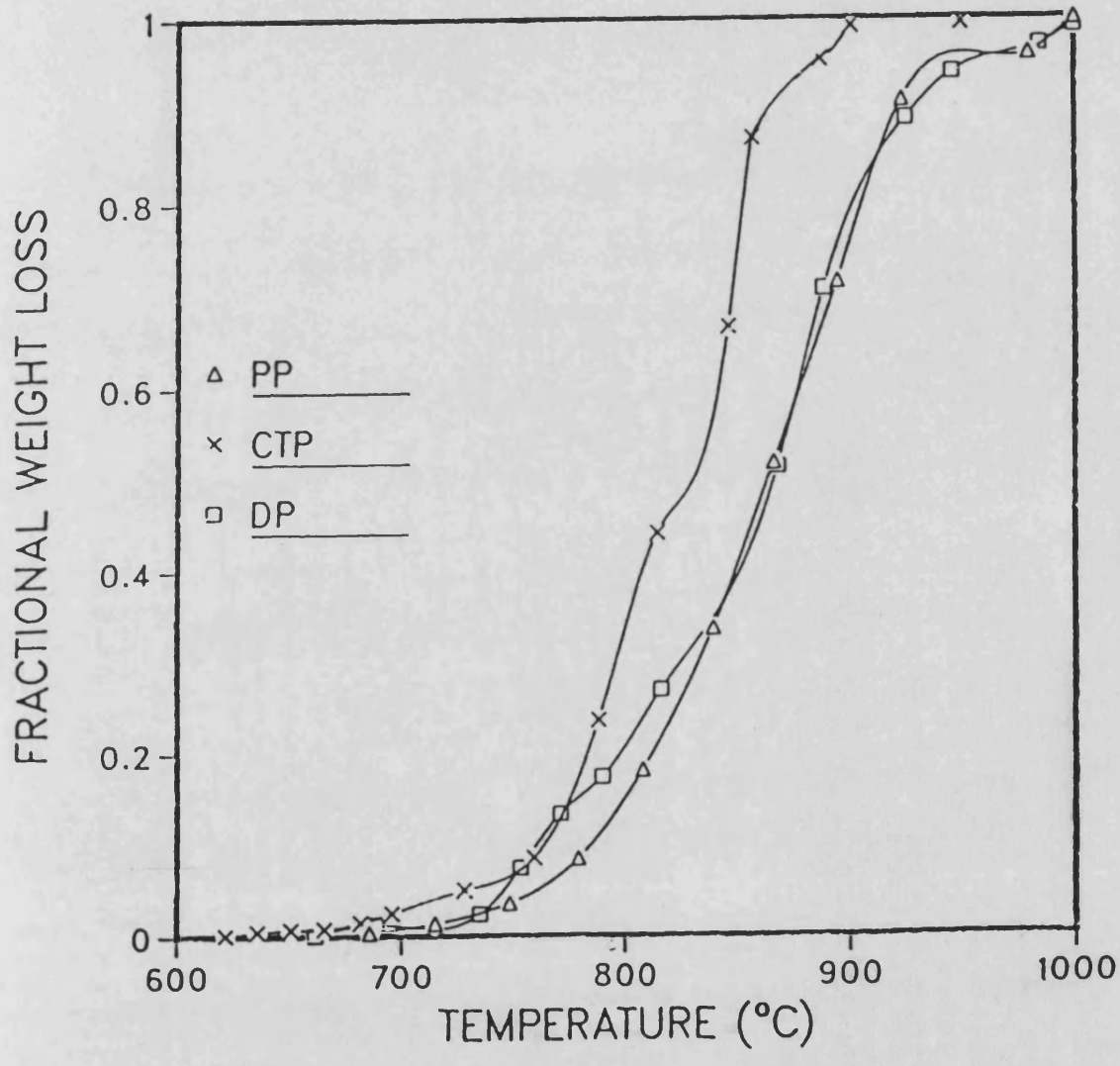

FIG.4.10 Determination of the Activation energy from non-isothermal carbon oxidation thermograms

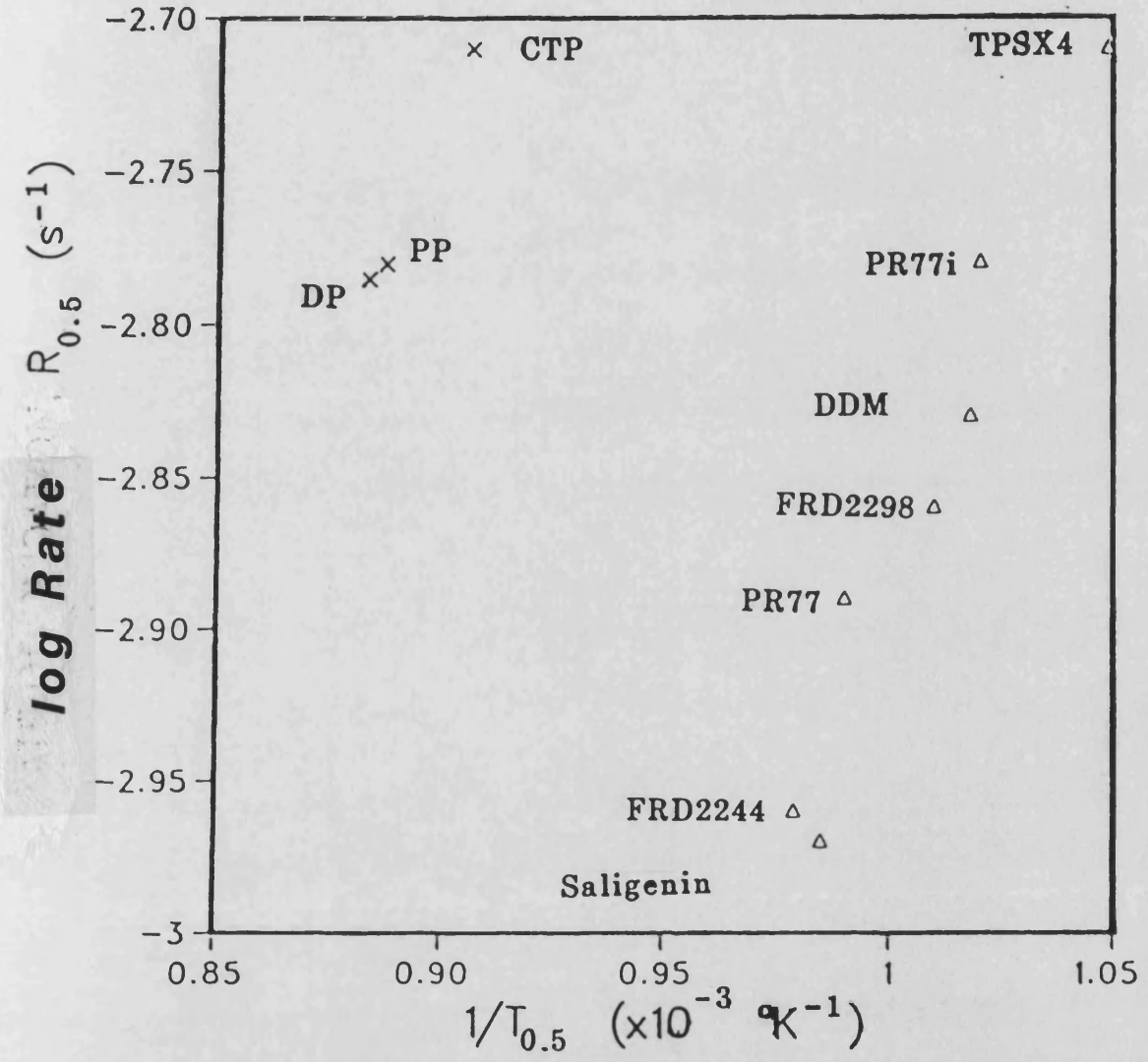

FIG.4.11 An illustration of the reproducibility of TPSX4 and CTP carbons and a comparison of their oxidation resistance

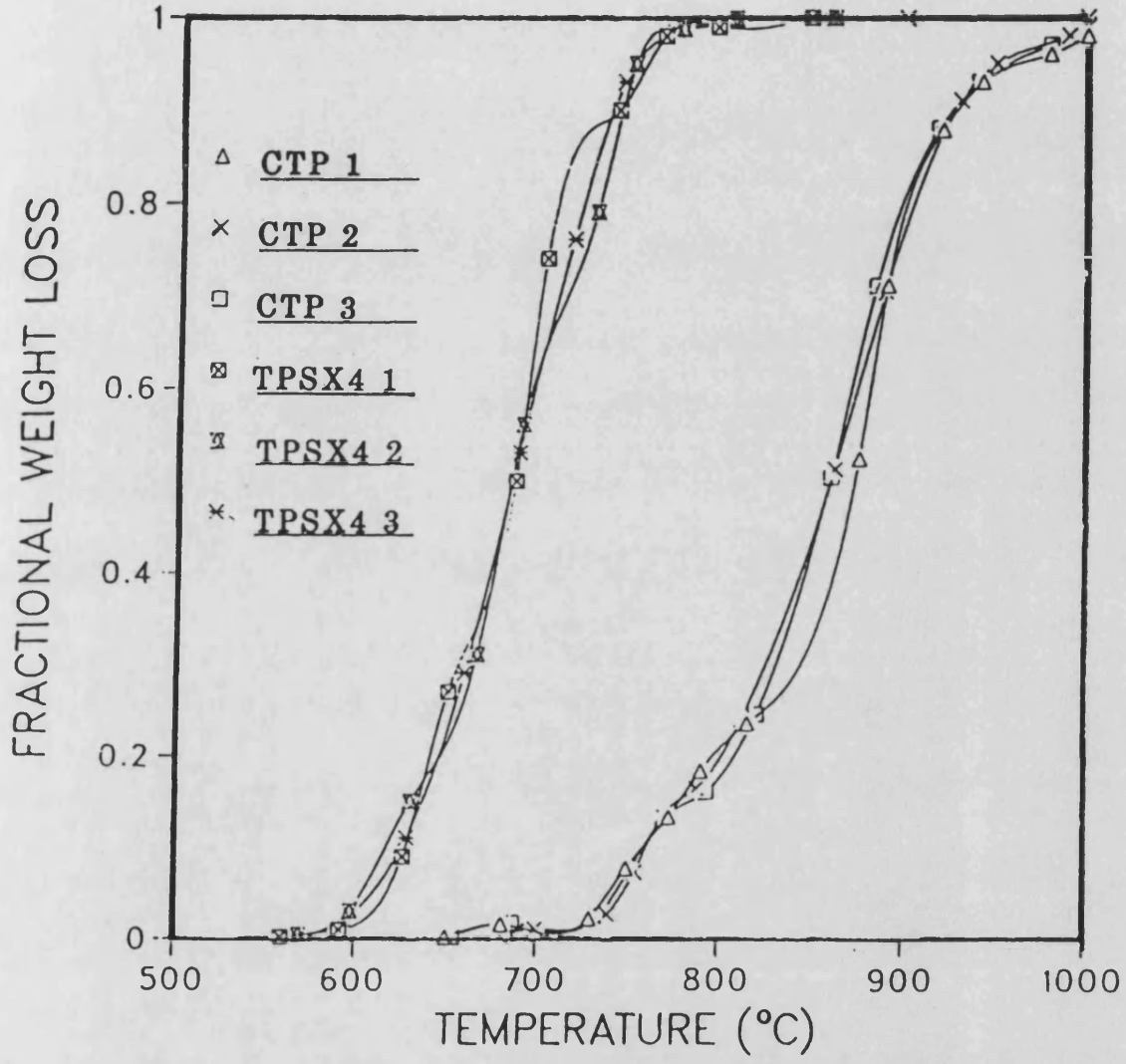

FIG.4.12 Effect of single stage cure on pyrolysis and oxidation resistance of Saligenin

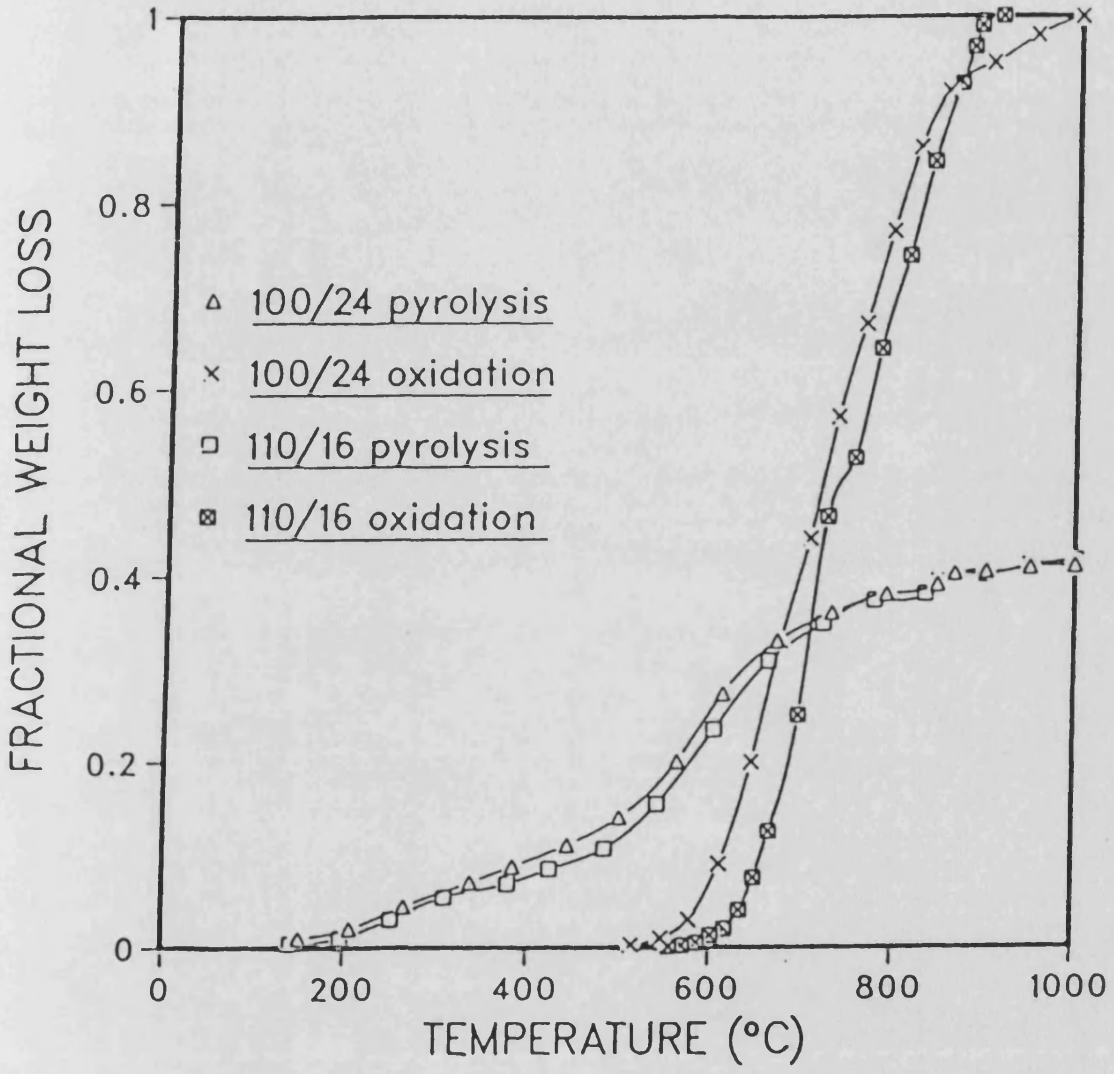

FIG.4.13 Effect of multi-stage cure on pyrolysis of Saligenin

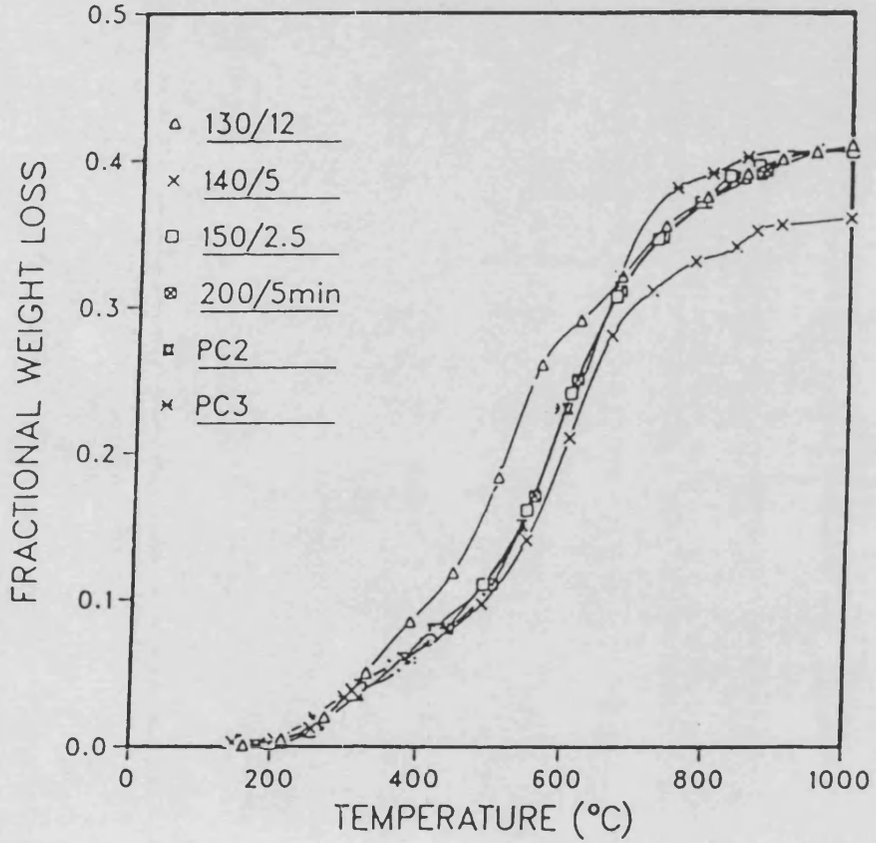


FIG.4.14 Effect of multi-stage cure on the oxidation resistance of Saligenin

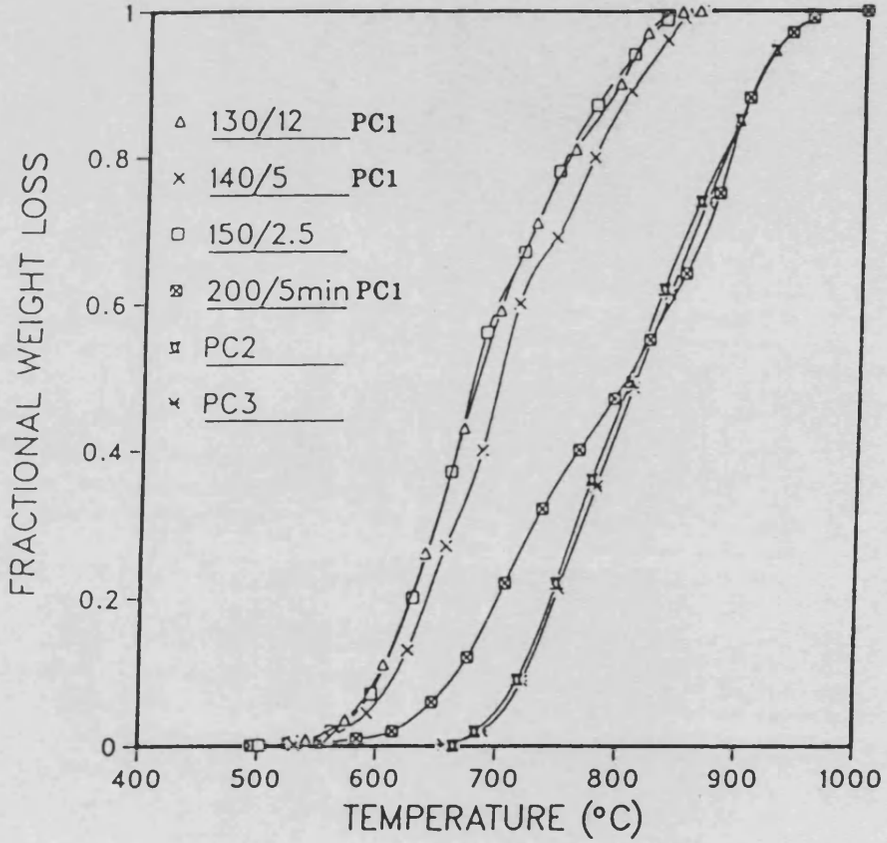

FIG.4.15 Effect of single stage cure on the pyrolysis of TPSX4

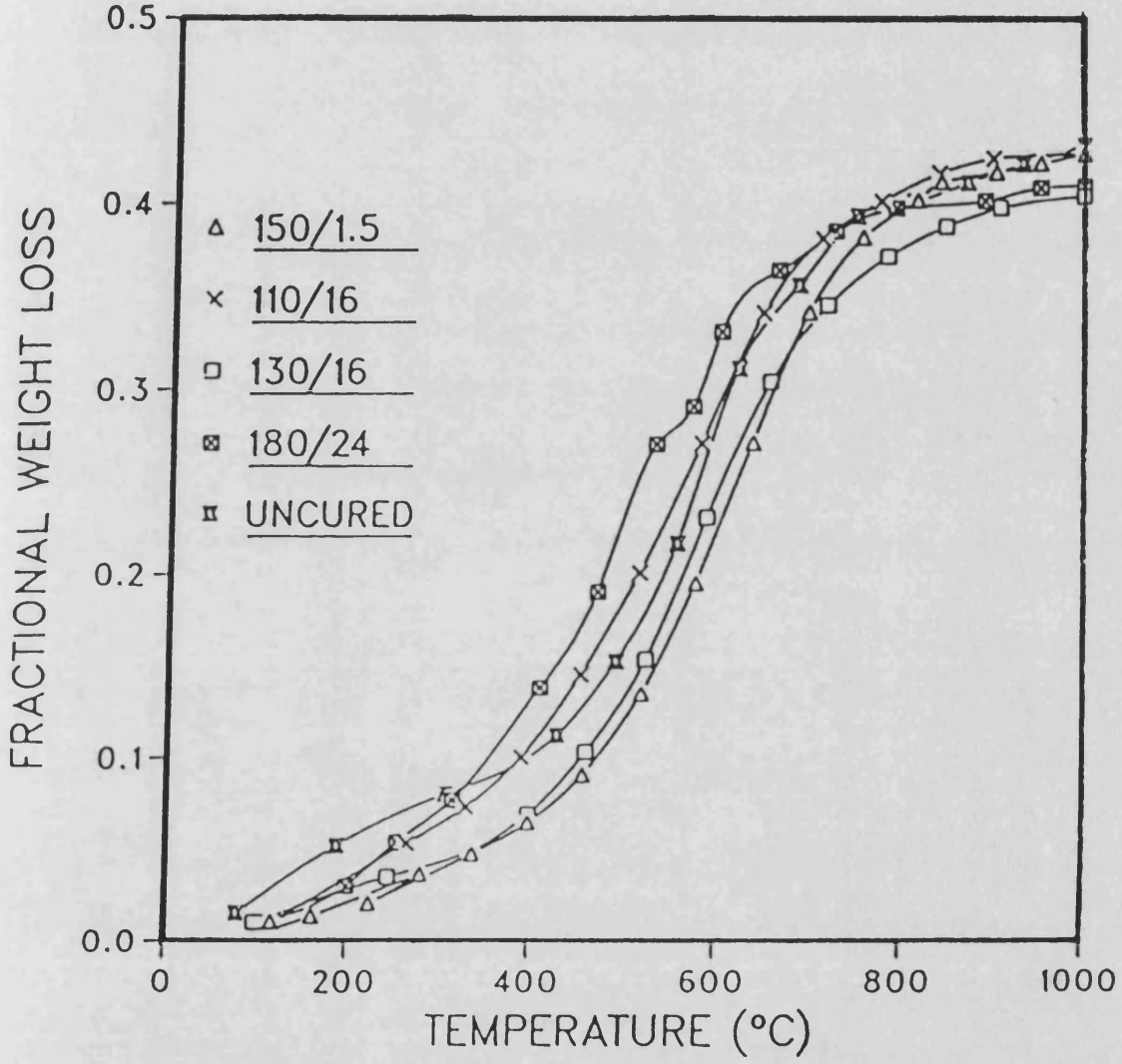

FIG.4.16 Effect of single stage cure on the oxidation resistance of TPSX4 carbon

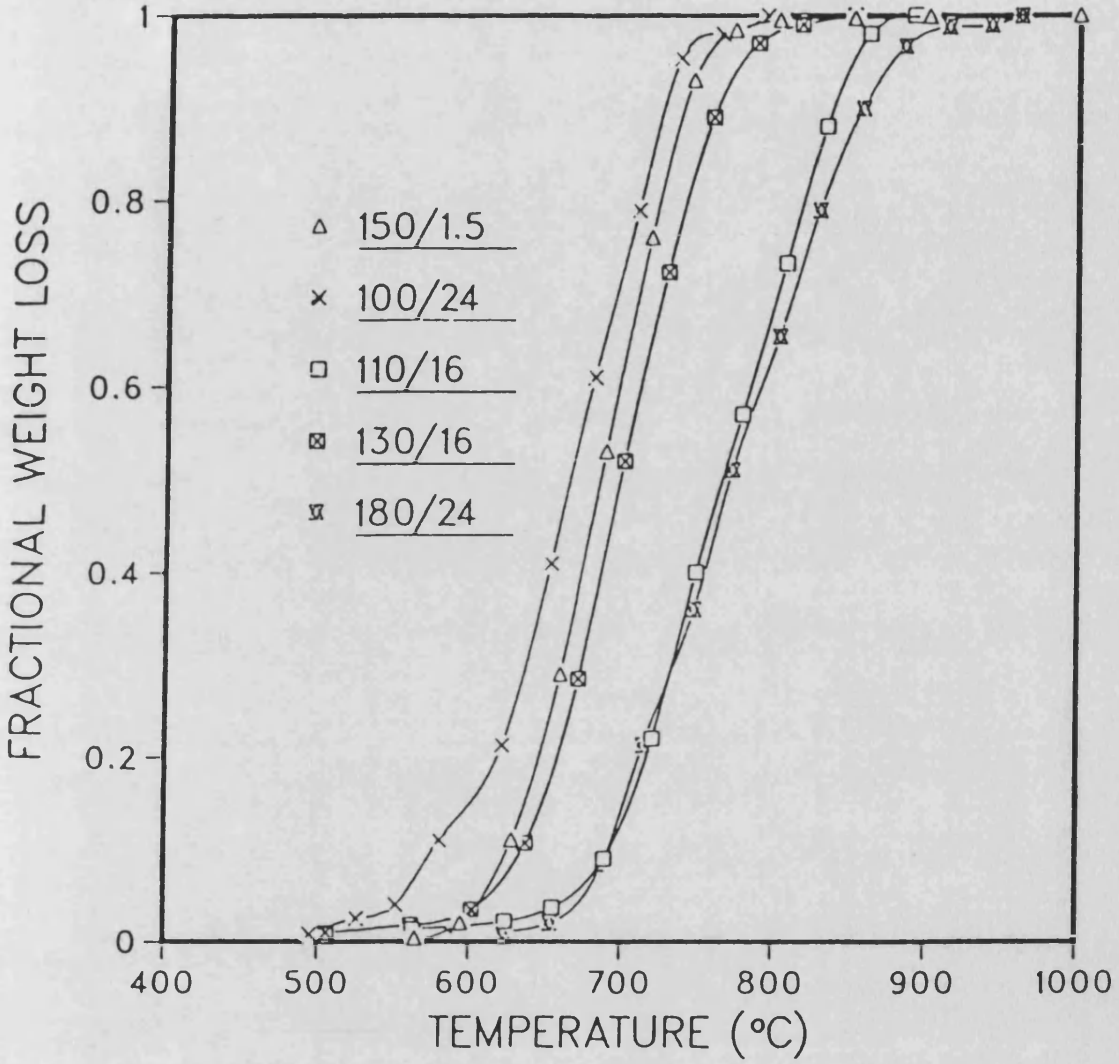

FIG.4.17 Effect of multi-stage cure on pyrolysis of TPSX4

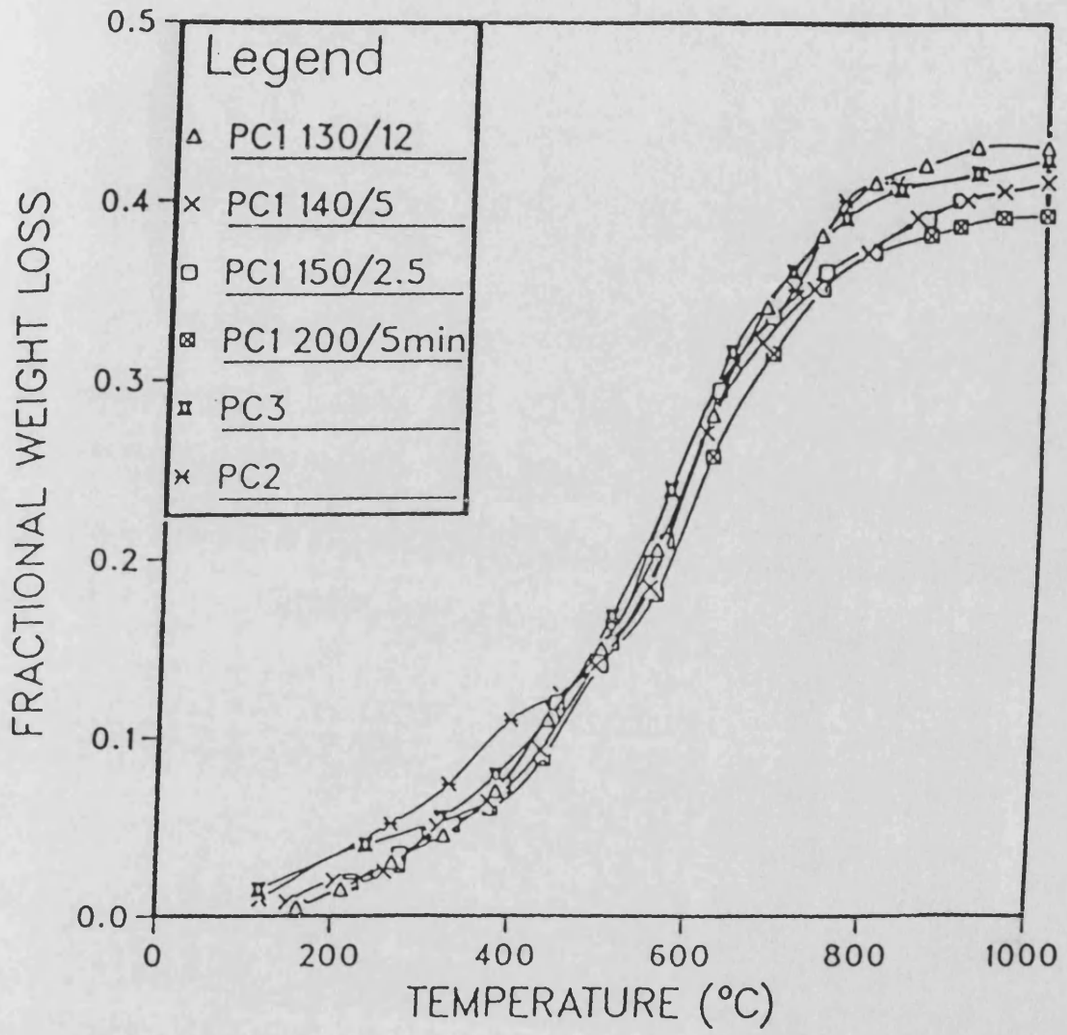

FIG.4.18 Effect of multi-stage cure on the oxidation resistance of TPSX4 carbon

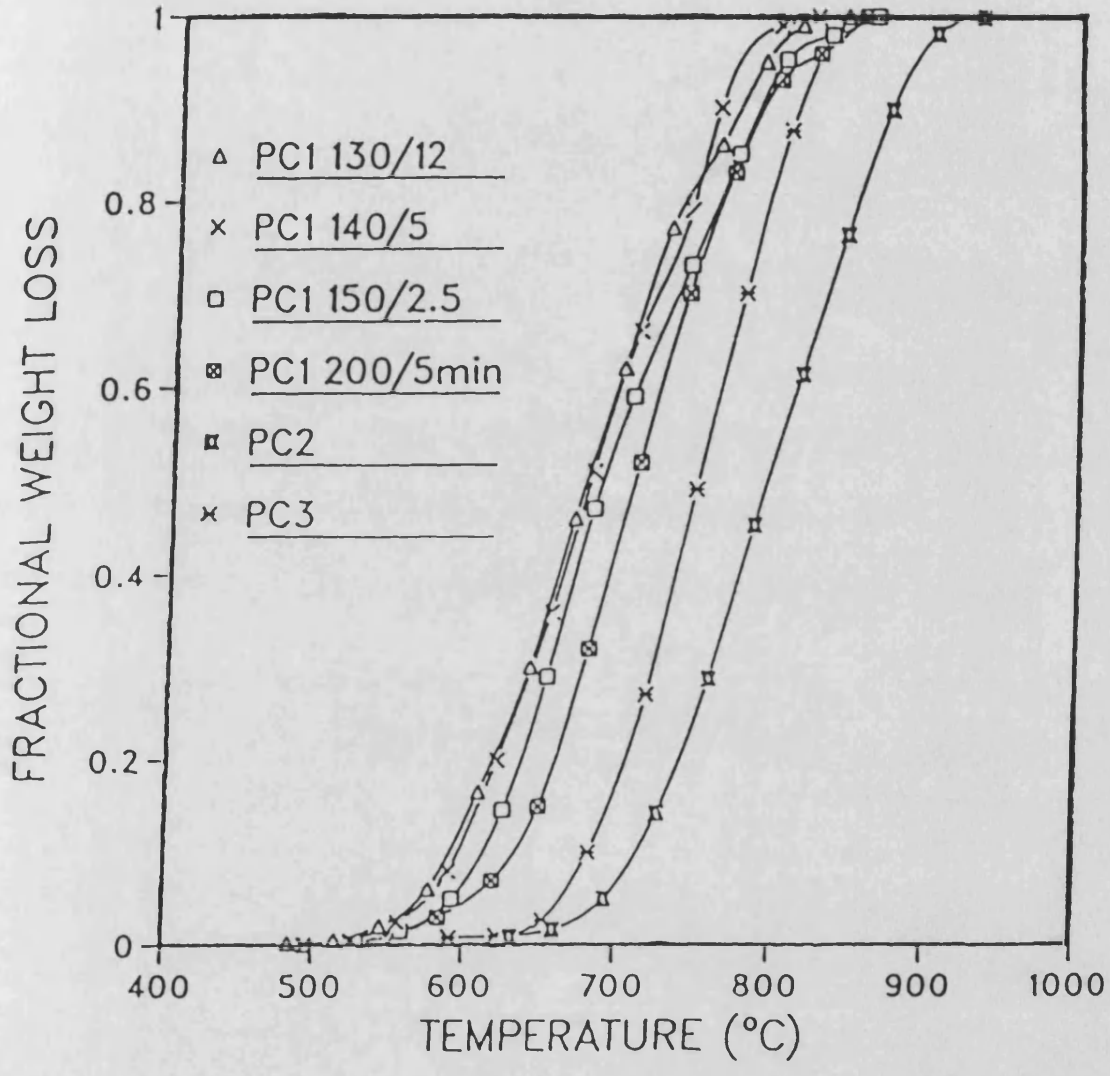

FIG.4.19 Effect of cure schedule on the oxidation resistance of PR77 and PR77i

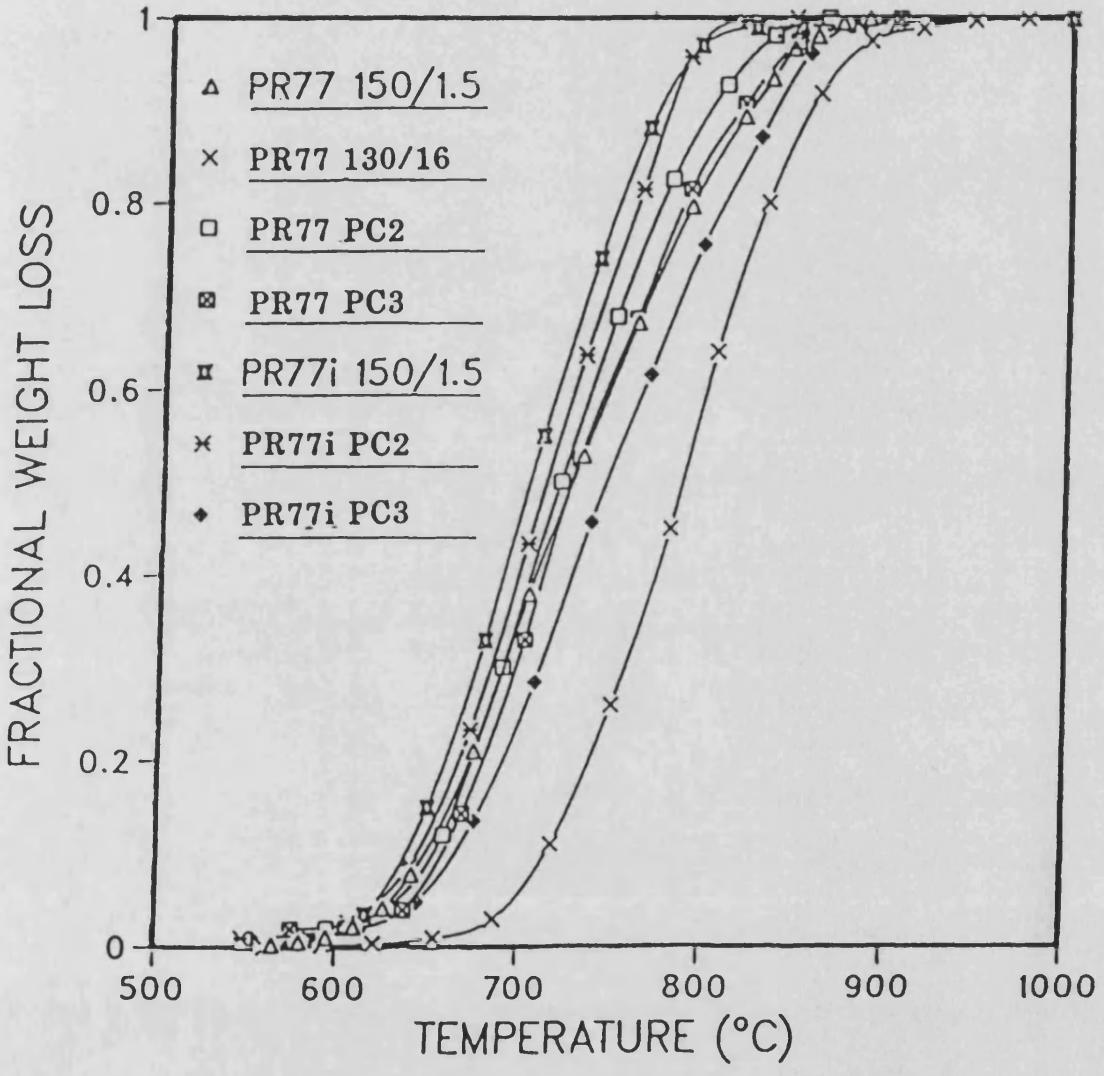

FIG.4.20 Pyrolysis of various PA65/TPSX4 compositions compared to PA65 and TPSX4 alone

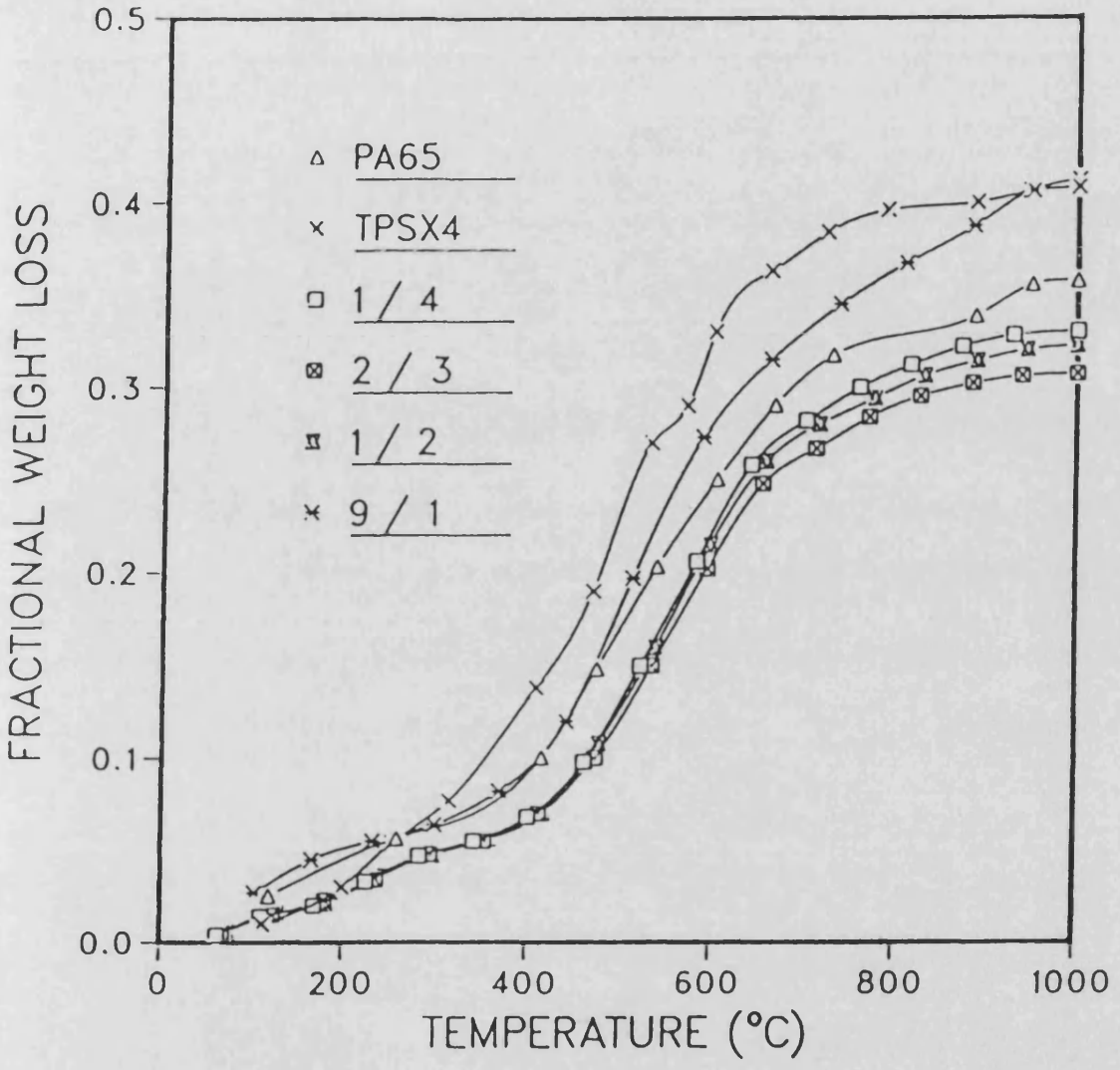

FIG.4.21 Oxidation resistance of the co-polymer (PA65/TPSX4 ratio <1)

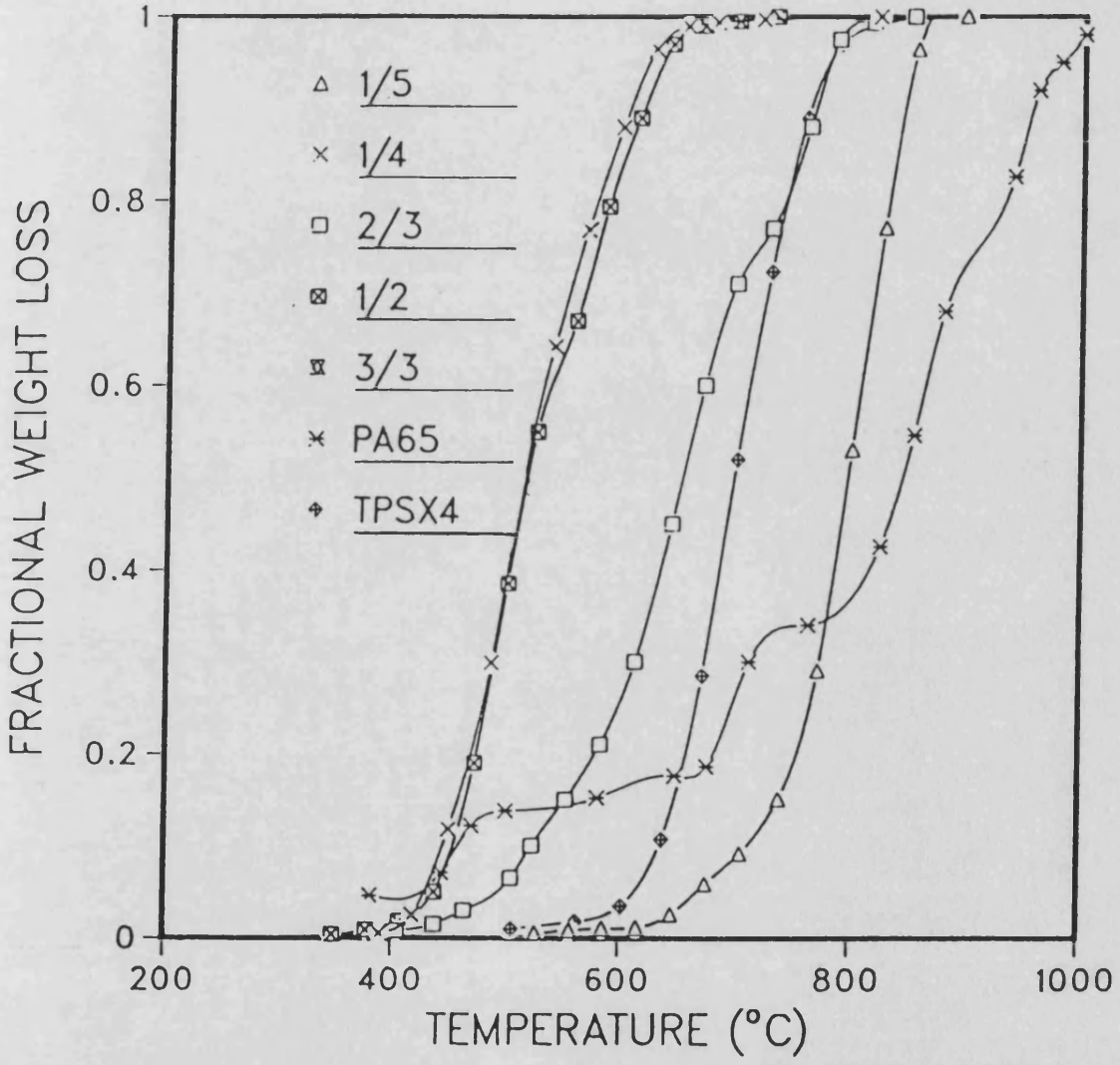

FIG.4.22 Oxidation resistance of the co-polymer (PA65/TPSX4 ratio > 1)

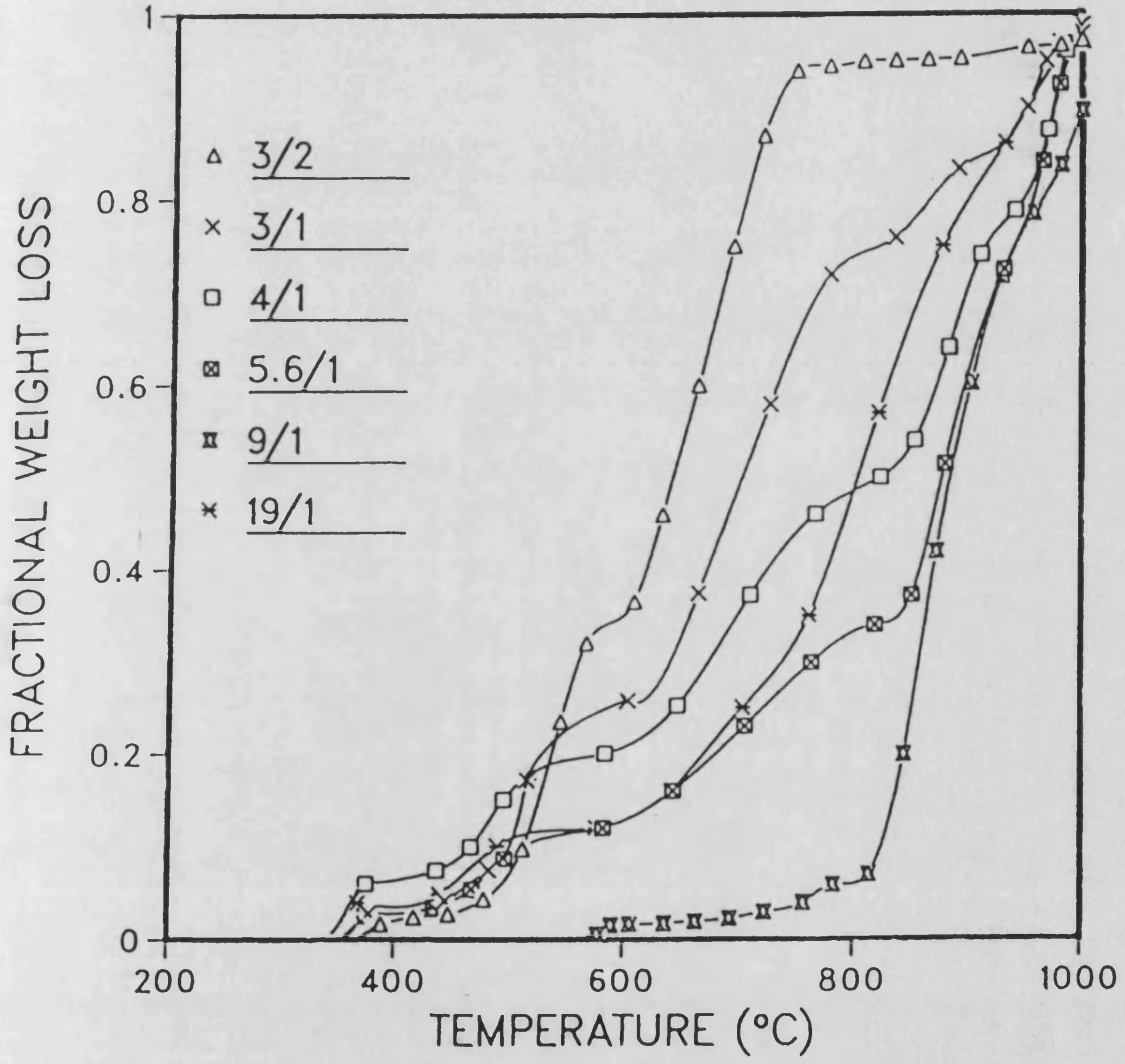

FIG.4.23 An illustration of the reproducibility of PT carbon prepared from the resin stage of manufacture

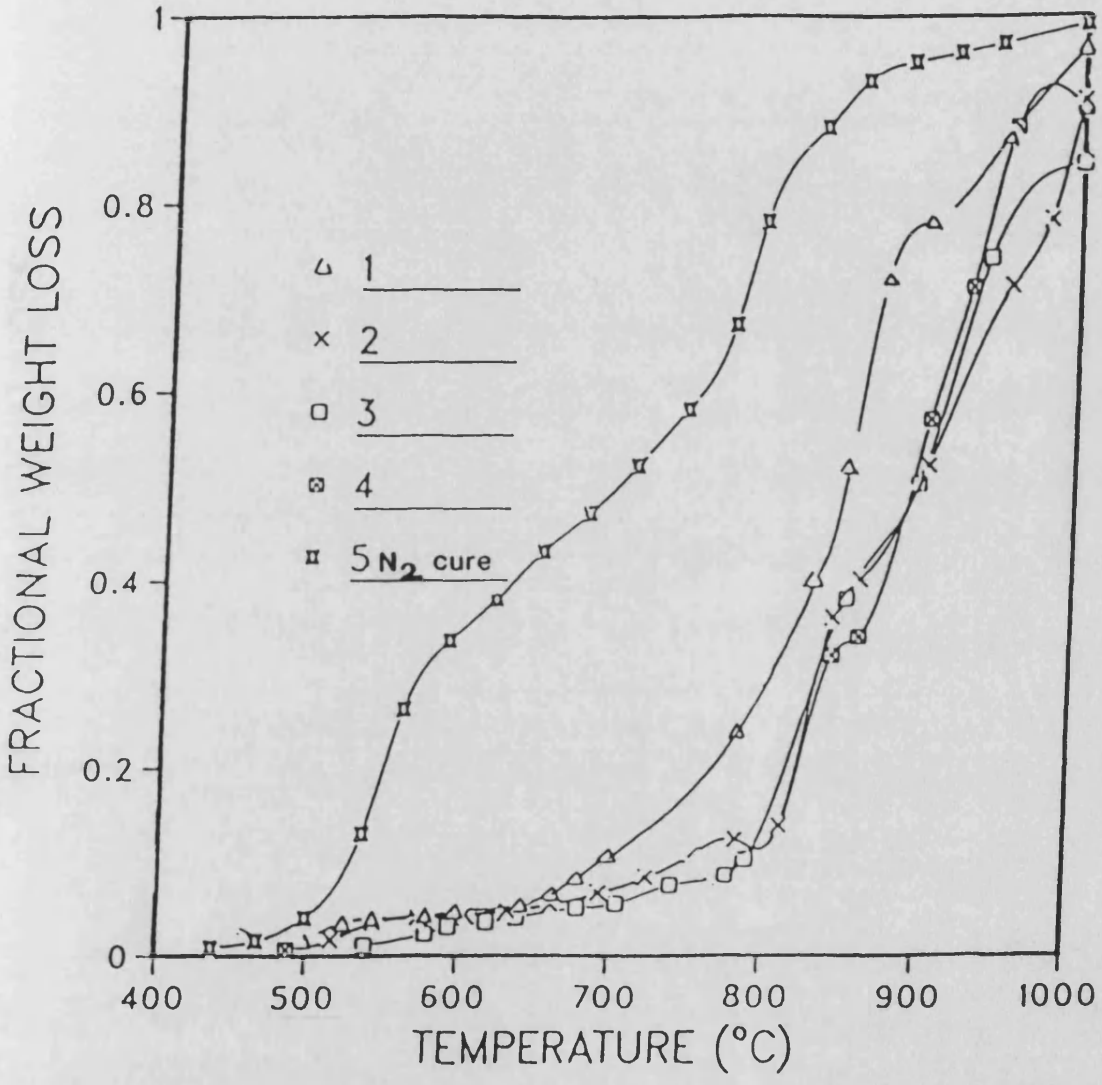

FIG.4.24 Effect of cure schedule on the oxidation resistance of PT

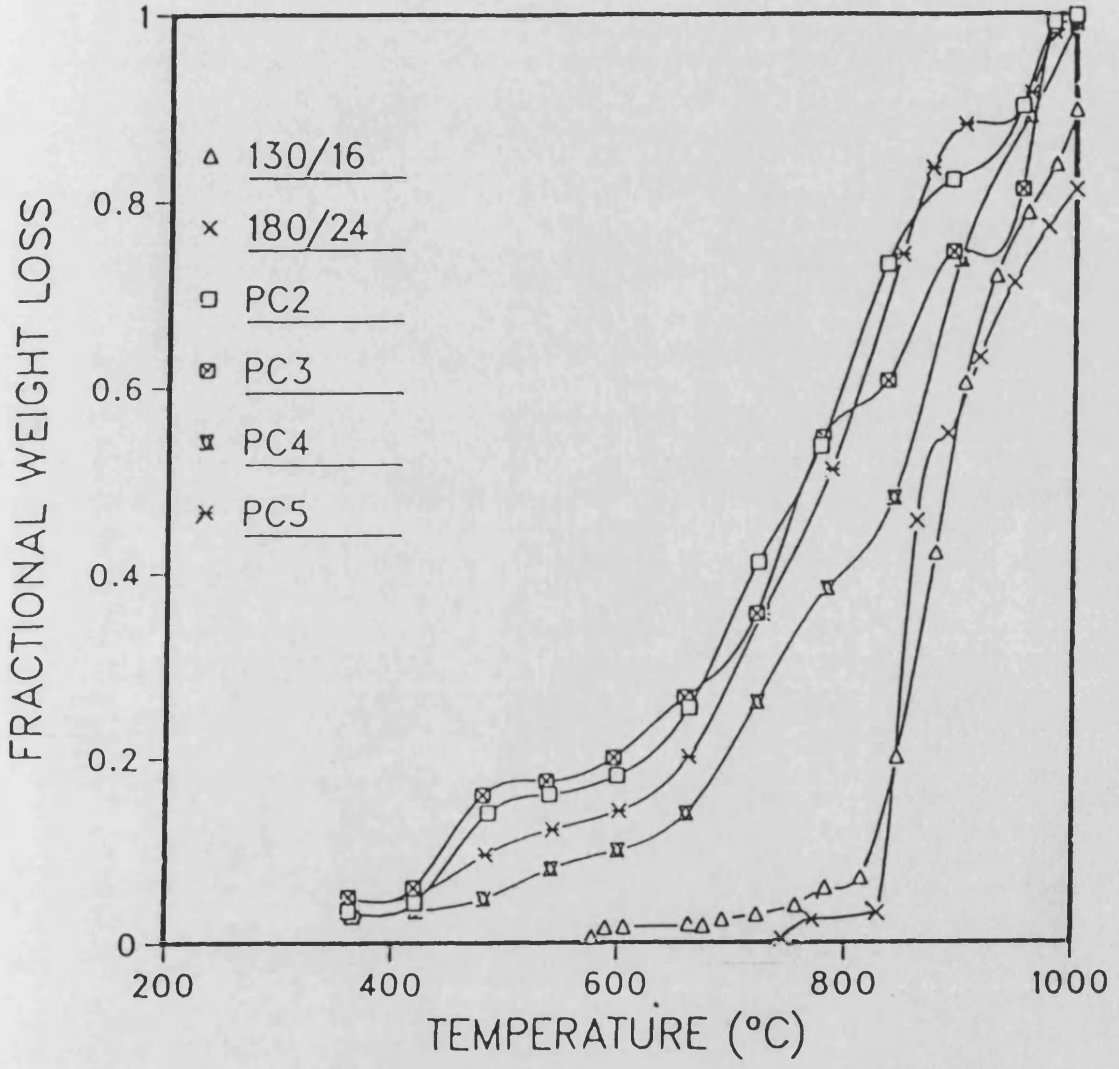

FIG.4.25 Oxidation resistance of the PA65/PR77 co-polymer compared to PT

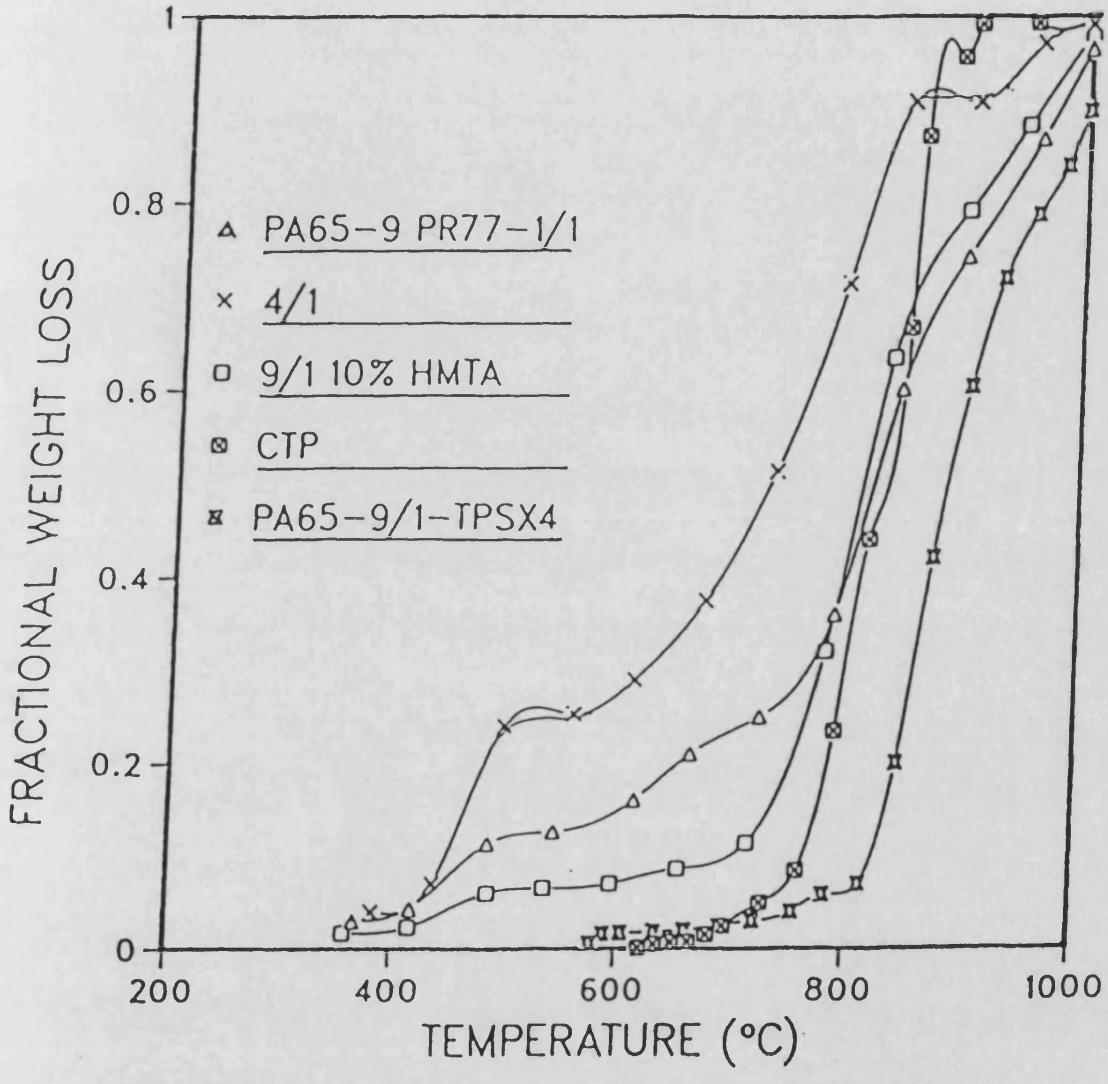

FIG.4.26 Relation between carbon oxidation resistance and PA65/TPSX4 ratio

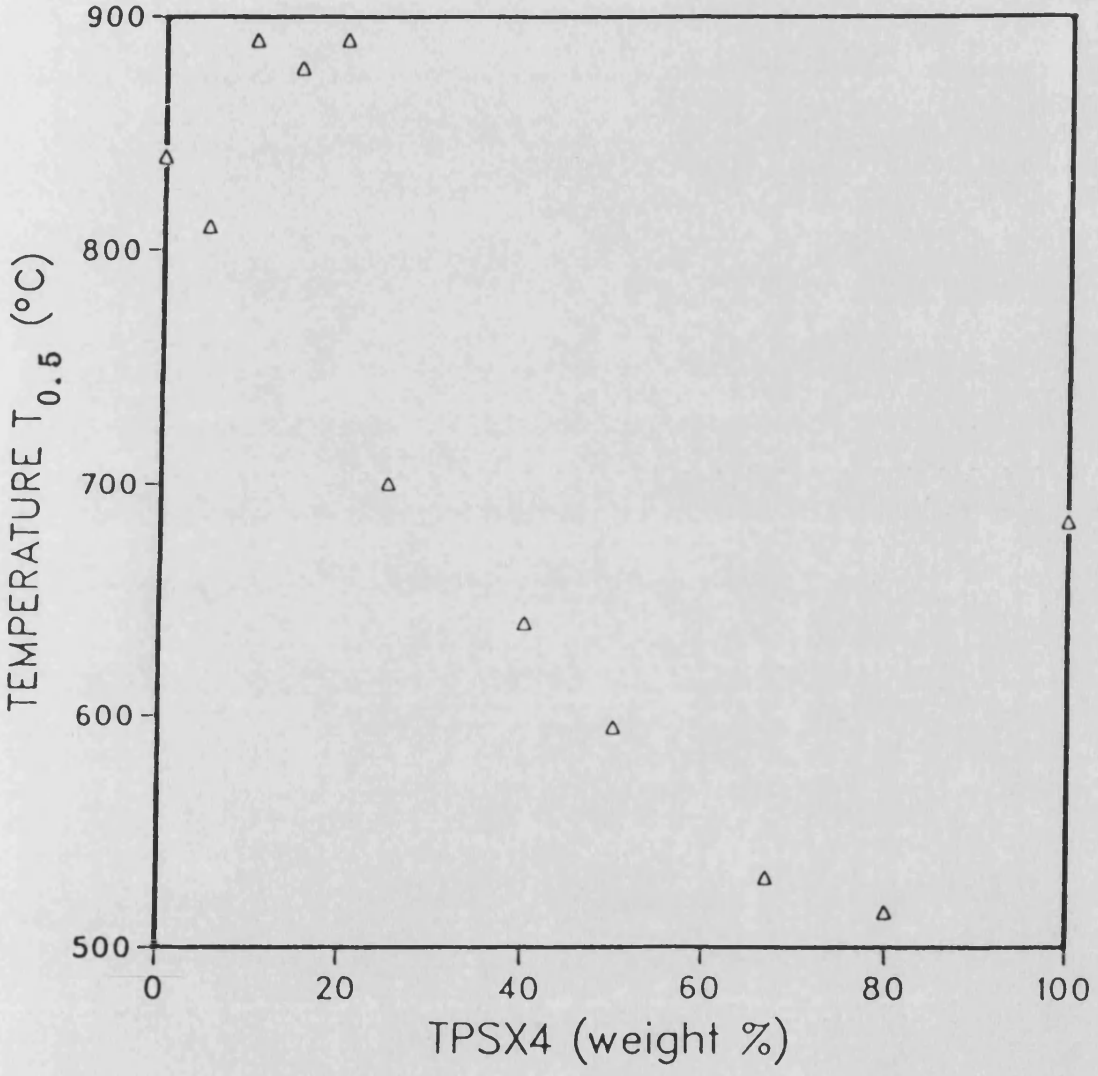

# CHAPTER 5 EFFECTS OF FIRE RETARDANT ADDITIONS ON RESINS: Curing, Carbonisation and Oxidation Resistance

## 5.1 Introduction

The effect of additives on curing weight loss and carbon yield from the PF resins and the oxidation resistance of their carbons are presented. The data are presented separately for the inorganic metal-based modified resins viz. the silicon-containing resin Z6018 and boron-containing resin MT59, and the organophosphorus-modified resins. The solid additive, dihydrogen ammonium phosphate, DHAP, produced only minor benefits when added to the novolak TPSX4, prior to resin curing, fig.5.1. Hence the work on this additive was discontinued.

## 5.2 The Silicone Resin Z6018

Curing of the silicone Z6018 resulted in a resin which was easy to grind, with a low curing weight loss. Pyrolysis gave a carbon in high yield which exhibited an oxidation resistance superior to the pitch carbons and other PF resin carbons, table 5.1, fig.5.2. The solid residue remaining after oxidation at 1000$^{o}$C was 68wt%, a high proportion of which was presumed to be silica (see Chap.6). Analogous to resole/novolak studies, experiments were carried out to assess whether the benefits obtained from Z6018 could be retained by co-polymerisation with

conventional resins. However, co-polymerisation of upto 10wt% of Z6018 with the resole PA65 and the co-polymer PA65-90/10-TPSX4 (i.e. PT), had a deleterious effect on oxidation resistance and carbon yield, although the oxidation resistance of the co-polymerised resin carbons is still comparable with the pitch carbons. Fig.5.3 shows the progressive improvement in oxidation resistance with addition of Z6018 to TPSX4, although the benefits after the higher additions are only marginal when compared to unmodified TPSX4 resin carbon. The carbon yields are enhanced for the Z6018/TPSX4 co-polymer compared to TPSX4 carbon. Table 5.1 shows the contradictory effects of different curing schedules on the oxidation resistance of Z6018/saligenin co-polymer resin carbons. The two stage cure PC3 reduces the oxidation resistance of the carbon compared to the single stage cure.

## 5.3 The Boronated Resin, MT59

The oxidation resistance of the boronated, ortho-novolak carbon is inferior to DP carbon upto 800°C, fig.5.4a. Above this temperature the rate of oxidation of DP carbon shows a rapid increase, while oxidation of MT59 remains more-or-less constant. Consequently, MT59 carbon becomes more heat resistant despite the increasing temperature and leaves a solid residue at 1000°C of 49wt%, cf. DP residue of < 1wt%. Addition of excess cross-linking agent, HMTA 10wt%, improves the carbon yield from 56wt% to 65wt%, while the solid residue at 1000°C of the resulting carbon decreases to 20wt%, and the $T_{0.5}$ value decreases from 985°C to 760°C. Postcuring of the HMTA modified MT59 novolak produced

minor beneficial effects, table 5.2, while co-polymerisation of MT59 resin with PA65 gave a carbon in high yield although the oxidation resistance was much reduced compared to MT59 carbon, table 5.2, fig.5.4b. The performance of the PA65-50/50-MT59 co-polymer carbon was similar to CTP, and in the high temperature region, i.e. > 800°C, approached the oxidation resistance of the most stable pitch carbon, DP, with a stable residue at 1000°C of 25wt%.

## 5.4 The Organophosphorus Modified Phenolic Resins

The effect on oxidation resistance of several resin carbons modified by the organophosphorus class of additives is presented in Fig. 5.5-5.11a,b and tables 5.3-5.5. Table 5.6 presents TG information on thermal degradation of a few organophosphorus additives. The data show that the additives start decomposing, and hence start functioning as fire retardants, well below the decomposition temperature of fully cured phenolic resins viz. <300°C. The similarity in the shapes of the TG curves, of the additive modified resins, implies a similar mode of degradation. The TG plot for the PT/additives fig.5.5, containing a phosphate functional group appear to have a deleterious effect on the oxidation resistance compared to unmodified PT carbon. In the high temperature range, the rate of oxidation declines for the PT/TNOPhate and PT/TTPhate carbons, (see table 3.2 p.93 for identification of the additives), which is in contrast to oxidation of the DP carbon. The PT/TTPhite significantly improves the oxidation resistance of the co-polymer yielding a solid

residue at 1000°C of 29wt%, table 5.3. The effects of 20wt% TDCP addition on oxidation resistance of several resin carbons are presented in fig.5.6 and table 5.4. The results show an improvement in $T_{0.5}$ in the order:

PT > PA65 > Saligenin > TPSX4

The first three carbons having oxidation resistances superior to CTP. The initiation of oxidation for PT/TDCP carbon occurs at a lower temperature compared to the unmodified carbon but there is an appreciable increase in $T_{0.5}$. The improved oxidation resistance is further verified by the high percentage of residue remaining after oxidation at 1000°C. The effects of 20wt% additions of other organophosphorus compounds to PA65 and PT resins are shown in fig.5.7 and table 5.3. As with TDCP, additions of these compounds to the resins reduce the carbon yields, however, addition of TBP and TCEP have remarkably beneficial effects on oxidation resistance of the carbons, $T_{0.5}$ being in excess of 1000°C and $T_{0.05}$ is also significantly improved. The high amount of solid residue remaining after oxidation at 1000°C is a further indication of the enhanced oxidation resistance. Reproducibility of the TG curves for oxidation of 20wt% of TDCP and TCEP modified resin carbons, is presented in Fig. 5.8 respectively. These curves were obtained from individual carbon samples prepared independently, starting from the resin stage of manufacture.

The effect of concentration of TDCP and TCEP on the oxidation resistance of various resin carbons is presented in Fig. 5.9-5.11 a,b and tables 5.4-5.5. Fig.5.9 shows that 10% TDCP addition to

TPSX4 produces only a minor benefit. However, 20wt% addition significantly improved the oxidation resistance in the high temperature range. Additions of 10-20wt% TDCP to PA65 and PT yield carbons of enhanced oxidation resistance compared to CTP, fig.5.10, although addition of 5wt% TDCP to PA65 has a deleterious effect. The effects of TCEP additions on PA65 and PT show carbons exhibiting high oxidation resistances as the concentration of the additive was increased, fig.5.11a,b. The most stable additive modified resin carbons are presented in fig.5.12, showing the superior oxidation resistance compared to DP carbon. Fig.5.13 shows the carbonisation curves of the most stable additive modified resin carbons. The similar shape of the curves implies a similar mode of resin/additive decomposition.

## 5.5 Discussion

The results showed an exceptionally high carbon yield from the novolak Z6018. However, oxidation of the resulting carbon showed that after ~40% weight loss, almost pure white silica particles, which were visibly distinct from the black carbon particles, were obtained. The silica particles were stable to further weight loss despite prolonged isothermal heating. This implies that the precursor resin must initially contain a high level of silicon. The boronated ortho-novolak, MT59, gave a carbon yield which was slightly inferior to the novolak TPSX4. The difference is probably linked to additional minor weight losses associated with decomposition of boric acid.

The carbon yields of resins modified by organophosphorus additives were significantly decreased. The carbon yield was linked to the the percentage of fire retardant added, i.e. high yields were obtained at low levels of addition and vice versa. Additives having aliphatic and aromatic groups were associated with a lower carbon yield compared to the halogen containing compounds. This is due to the ability of halogen containing compounds to promote radical recombination reactions, thus increasing the carbon yield (see Chap.2.1). The reduced carbon yield compared to the unmodified resin carbons is probably linked to loss of aliphatic, or aromatic, groups making up the fire retardant, which are known to decompose to form polyphosphoric acid (106-109).

Initiation of the oxidation of organophosphorus modified resin carbons, fig.5.12, occurs at a lower temperature compared to the pitch carbons. However, their rates of oxidation do not increase so steeply with rising temperature. It is known that oxidation inhibition by organophosphorus and boron-containing compounds can result from the growth of a glassy surface layer which acts as a barrier to diffusion of reactant and product gases (118, 158-162). The similar shapes for each modified resin, of the pyrolysis, fig.5.13, and oxidation curves suggests that the various additives inhibit oxidation in a similar manner. The weight loss curve of the modified resin carbons is stepped, e.g. PT/20-TCEP, fig.5.12. This suggests formation of a type of barrier which decreases the rate of weight loss despite the increasing temperature. This is in contrast to the shape of the oxidation curves for the unmodified PT and DP carbons. The latter

carbons show an induction period for initiation of oxidation and is followed by an increased rate of oxidative weight loss.

It is postulated that boric acid when impregnated into partially cured phenolic resin, reacts with the phenolic hydroxyl group to form borate esters with the elimination of water, reaction 1 (133).

**Reaction 1: Proposed mechanism for intra-molecular esterification of o,o'-novolak showing reactive para positions which are available for HMTA cure**

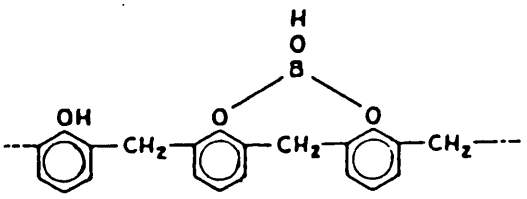


cyclic borate ester

The esters are expected to enhance char formation decomposition reactions as well as the retention of the boric oxide surface coating during high temperature exposure of the phenolic resin. Kobayashi (163) has reported that high temperature exposure leads to molecular changes in the initially formed borate ester. The latter is thought to convert to a form of boron oxide in the temperature range 1200-1400°C, while in the range 1600-1800°C boron carbide structures have been detected. Above 2000°C some of the boron forms a solid solution with carbon therby promoting graphitisation and hence, enhanced oxidation resistance (164). The organophosphorus compounds are also thought to form phosphorus esters with hydroxylated resins (133, 165, 166), reaction 2.

Reaction 2: Simple cyclic esters formed by reaction with the phenolic hydroxyl group

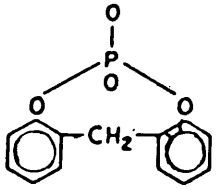

cyclic phosphate

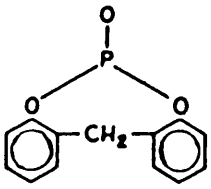

cyclic phosphite

Since flammability of a phenolic polymer involves a series of complex reactions, i.e. thermal and oxidative degradation, it is reasonable to predict that stabilisation by phosphorus containing compounds occurs in two very general ways both of which involve formation of a comparatively high-cross-linked-density structure as degradation proceeds. Since the phosphorus containing additives degrade between 200-500°C, table 5.6, polyphosphoric acid and a cross-linked carbon skeleton is expected to form at these temperatures. With diffusion of polyphosphoric acid and organophosphorus fragments to the surface, it is reasonable to propose a phosphorus oxide coating on the polymer surface. This coating would have a profound effect on the rate of diffusion of volatiles to the surface and their subsequent evaporation into the pyrolysis zone. Since the diffusion rates would be slowed down, radical trapping reactions to form char should be more favourable.

In summary, stabilisation by phosphorus and boron takes place primarily, but not exclusively, first by the formation of additive-phenolic ester moieties which promote thermal polymer cross-linking, thereby retarding volatile formation, and second, by the surface coating behaviour of the phosphorus or boron oxides, which would be expected to render the carbon self-extinguishing. The increase in oxidation resistance of the carbon with increasing concentration of additives is probably linked to the formation of a correspondingly thicker surface coating. Improvements in the oxidation resistance of the silicon containing novolak has also been attributed to formation of a silica glass layer, followed by high temperature conversion to silicon carbide (167). It has been reported that oxidation resistance is reduced due to mismatch of the thermal expansion coefficients of the $SiO_2$-layer and the carbon materials thus leading to spalling upon cooling, and hence catastrophic subsurface oxidation of the underlying material, as observed in the present work. The oxidation resistance of the latter system can be improved by use of additives which form liquids upon oxidation, thereby filling up the cracks in the $SiO_2$ layer and reducing the ease of diffusion of the oxygen to the carbon surface (167).

TABLE 5.1 Carbonisation of Z6018 resin and co-polymers and oxidation resistance of the carbons

| Z6018 (wt%) | Cure-Type | Curing Loss (wt%) | BC Yield (wt%) | $T_{0.5}$ (°C) | SOLID* (wt%) |
|---|---|---|---|---|---|
| 100 | 130/16 | 5.5 | 74.6 | >1000 | 67.9 |
| TPSX4/co-polymer | | | | | |
| 0 | 150/1.5 | 3.8 | 59.4 | 683 | 0.0 |
| 2 | " | 3.4 | 62.2 | 653 | 1.0 |
| 10 | " | 3.3 | 67.3 | 695 | 4.3 |
| 20 | " | 3.1 | 65.2 | 700 | 9.0 |
| PT/co-polymer | | | | | |
| 0 | 130/16 | 18.6 | 64.6 | 890 | 2.5 |
| 10 | " | 19.8 | 63.3 | 783 | 6.0 |
| PA65/co-polymer | | | | | |
| 0 | 130/16 | 23.5 | 65.3 | 840 | 2.0 |
| 10 | " | 22.1 | 63.7 | 785 | 3.0 |
| Saligenin/co-polymer | | | | | |
| 0 | 110/16 | 12.7 | 60.9 | 750 | 0.0 |
| 10 | 150/1.5 | 13.4 | 67.2 | 804 | 4.0 |
| 10 | 150/1+180/1 | 13.9 | 67.1 | 766 | 4.2 |

* solid residue after the TG oxidation run to 1000°C

TABLE 5.2 The carbonisation of boronated ortho-novolak resin MT59 and co-polymers and oxidation resistance of the carbons

| Resin-Type | Cure-Type | Curing Loss (wt%) | BC Yield (wt%) | $T_{0.5}$ (°C) | Solids* (wt%) |
|---|---|---|---|---|---|
| MT59 | 130/16 | 5.6 | 56.0 | 985 | 49.0 |
| MT59-9/1-HEXA | 150/1.5 | 6.9 | 65.0 | 760 | 20.0 |
| " | PC3 | 7.6 | 65.6 | 772 | 18.0 |
| MT59-5/5-PA65 | 130/16 | 17.9 | 69.8 | 790 | 25.3 |
| MT59-1/9-PA65 | " | 22.0 | 65.1 | 647 | 6.0 |
| PA65 | " | 26.2 | 65.3 | 840 | 2.0 |

* Solids residue after the TG oxidation run to 1000°C

TABLE 5.3 Effects of 20wt% organophosphorus compound additions to PT on carbon yield and oxidation resistance (cure schedule: 130/16)

| Additive[1] | Curing Loss (wt%) | BC Yield (wt%) | $T_{0.5}$ (°C) | Solids[2] (wt%) |
|---|---|---|---|---|
| TDCP | 19.2 | 55.0 | 967 | 40.8 |
| TTPHOSPHATE | 19.2 | 51.6 | 813 | 13.0 |
| TTPHOSPHITE | 19.6 | 50.6 | 923 | 29.0 |
| TBP | 22.6 | 53.0 | >1000 | 63.2 |
| TCEP | 18.7 | 54.0 | >1000 | 74.2 |
| TNOP | 19.8 | 50.3 | 798 | 5.0 |
| TIOP | 24.5 | 50.9 | 702 | 1.0 |

1 see table 3.2 for identification of the additives
2 solids residue after the TG oxidation run to 1000°C

TABLE 5.4 Effect of TDCP addition to resin curing weight loss, carbon yield and oxidation resistance (cure schedule:130/16)

| TDCP (wt%) (Resin) | | Curing Loss (wt%) | BC Yield (wt%) | Solids* (wt%) | $T_{0.5}$ (°C) |
|---|---|---|---|---|---|
| Sal | 15 | 11.4 | 56.0 | 0.3 | 884 |
| TPSX4 | 10 | 4.1 | 58.4 | 0.0 | 730 |
| " | 20 | 5.1 | 57.8 | 1.0 | 783 |
| PA65 | 5 | 21.7 | 57.6 | 4.0 | 682 |
| " | 15 | 17.3 | 55.4 | 16.0 | 878 |
| " | 20 | 21.8 | 49.4 | 21.8 | 900 |
| PT | 10 | 21.5 | 58.8 | 4.5 | 865 |
| " | 15 | 18.5 | 58.6 | 20.7 | 895 |
| " | 20 | 19.2 | 55.0 | 40.8 | 967 |
| P/PR77[a] | 20 | 16.9 | 52.3 | 18.3 | 864 |

* solids residue after the TG oxidation run to 1000°C
a PA65-90/10-PR77

TABLE 5.5 Effect of TCEP addition to PA65 and PT on curing weight loss, carbon yield and oxidation resistance

| TCEP (wt%) | Curing Loss (wt%) | BC Yield (wt%) | Solids* | $T_{0.5}$ (°C) |
|---|---|---|---|---|
| PA65 | | | | |
| 5 | 19.5 | 56.2 | 18.0 | 820 |
| 10 | 19.3 | 56.4 | 27.0 | 894 |
| 20 | 20.3 | 53.8 | 73.0 | >1000 |
| PA65-90/10-TPSX4 | | | | |
| 5 | 24.5 | 61.3 | 19.0 | 823 |
| 10 | 24.7 | 59.1 | 28.0 | 910 |
| 20 | 24.6 | 53.3 | 74.2 | >1000 |

* solids residue after the TG oxidation run to 1000°C

TABLE 5.6 Oxidation weight loss data for some organo-phosphorus fire retardants

| Additive | TG Weight Loss Temperature (°C) 1wt% | 5wt% | 10wt% |
|---|---|---|---|
| tris(2-chloroethyl)phosphate | 140 | 170 | 190 |
| tris(2,3-dibromopropyl)phosphate | 215 | 270 | 290 |
| tris(dichloropropyl)phosphate | 160 | 208 | 234 |

FIG.5.1 Effect of dihydrogenammonium phosphate on the oxidation resistance of TPSX4 carbon

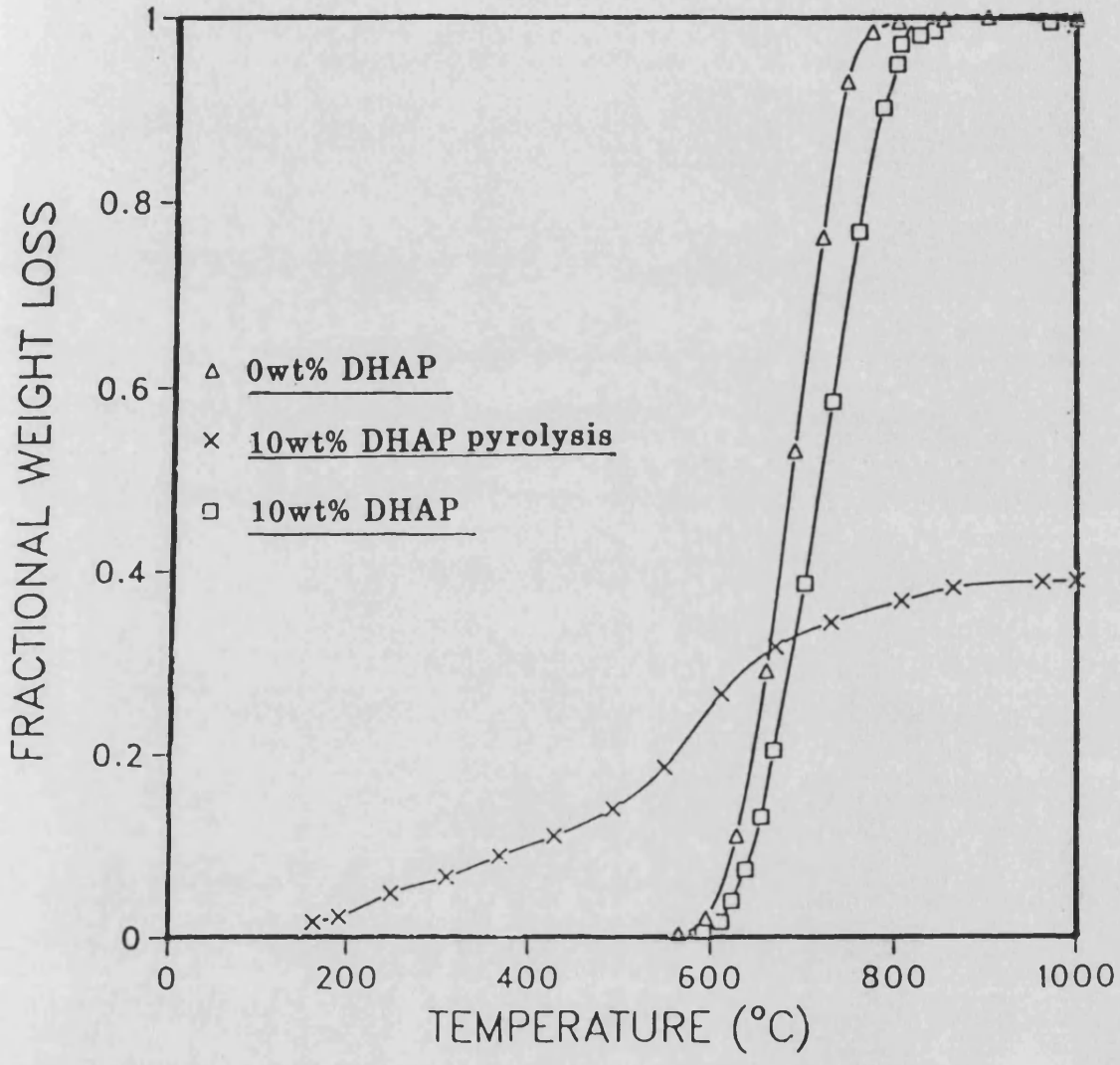

FIG.5.2 Pyrolysis and oxidation resistance of Z6018

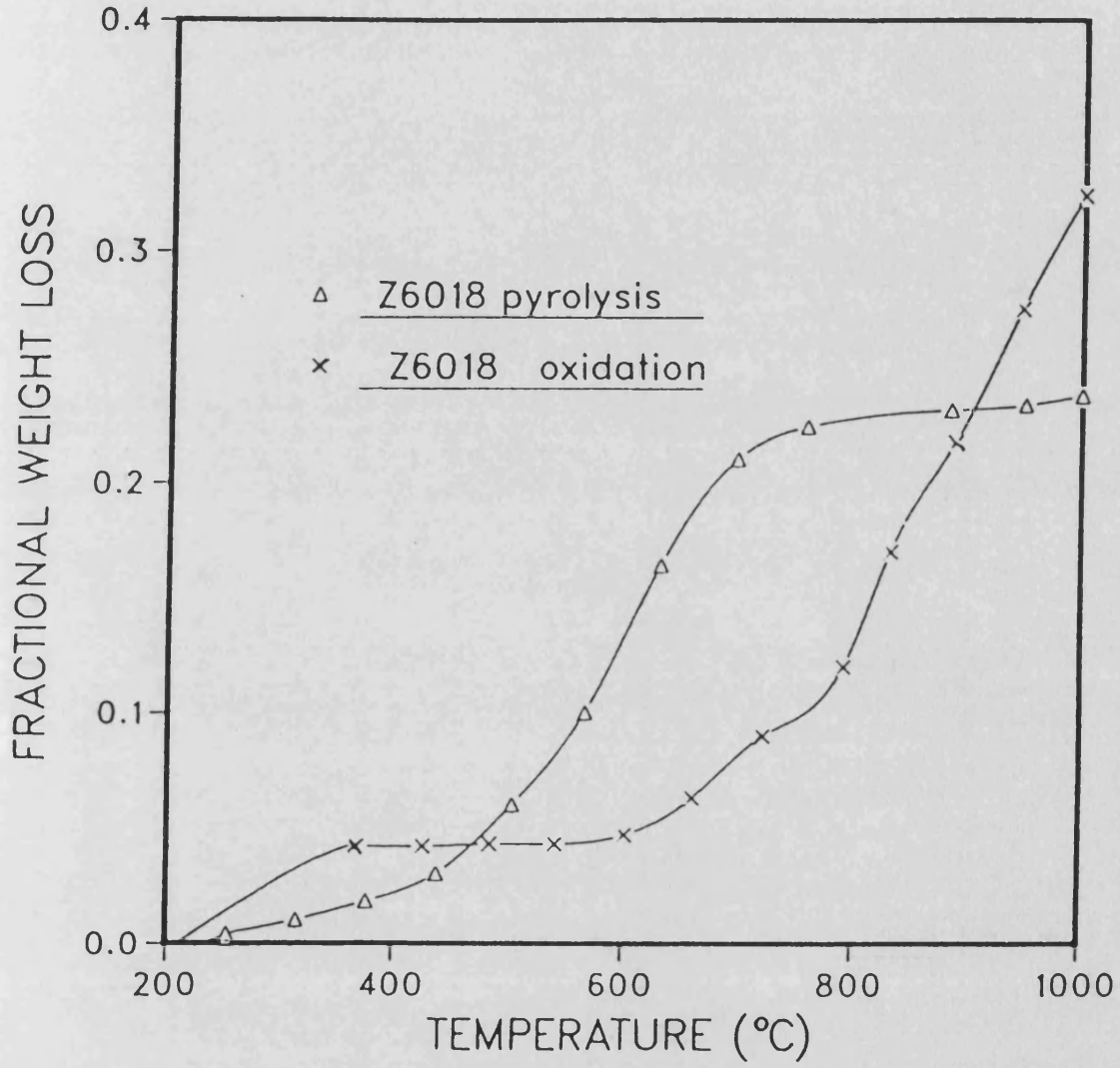

FIG.5.3 Oxidation resistance of PF resins co-polymerised with Z6018

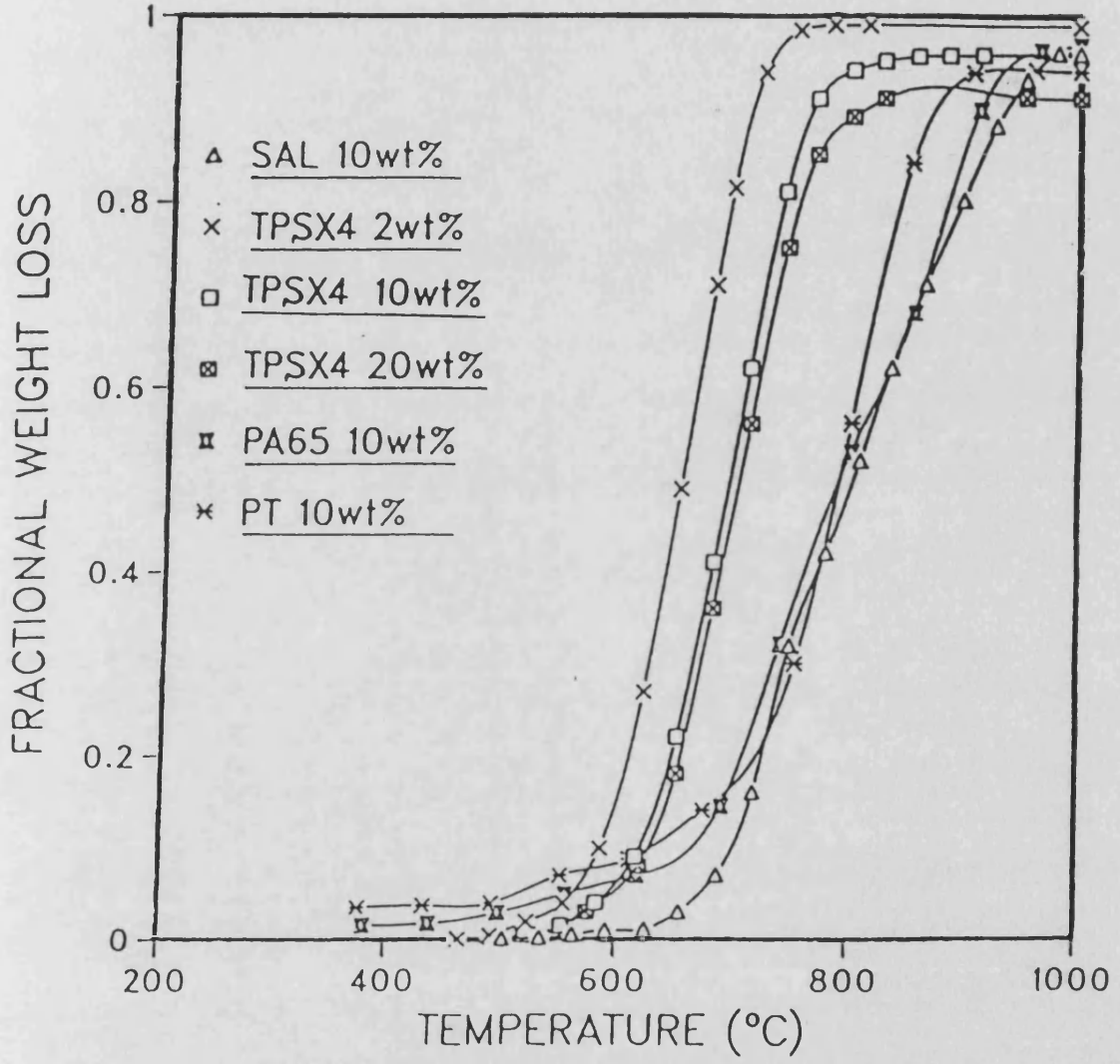

FIG.5.4a Pyrolysis and oxidation resistance of MT59 and effect of HMTA addition

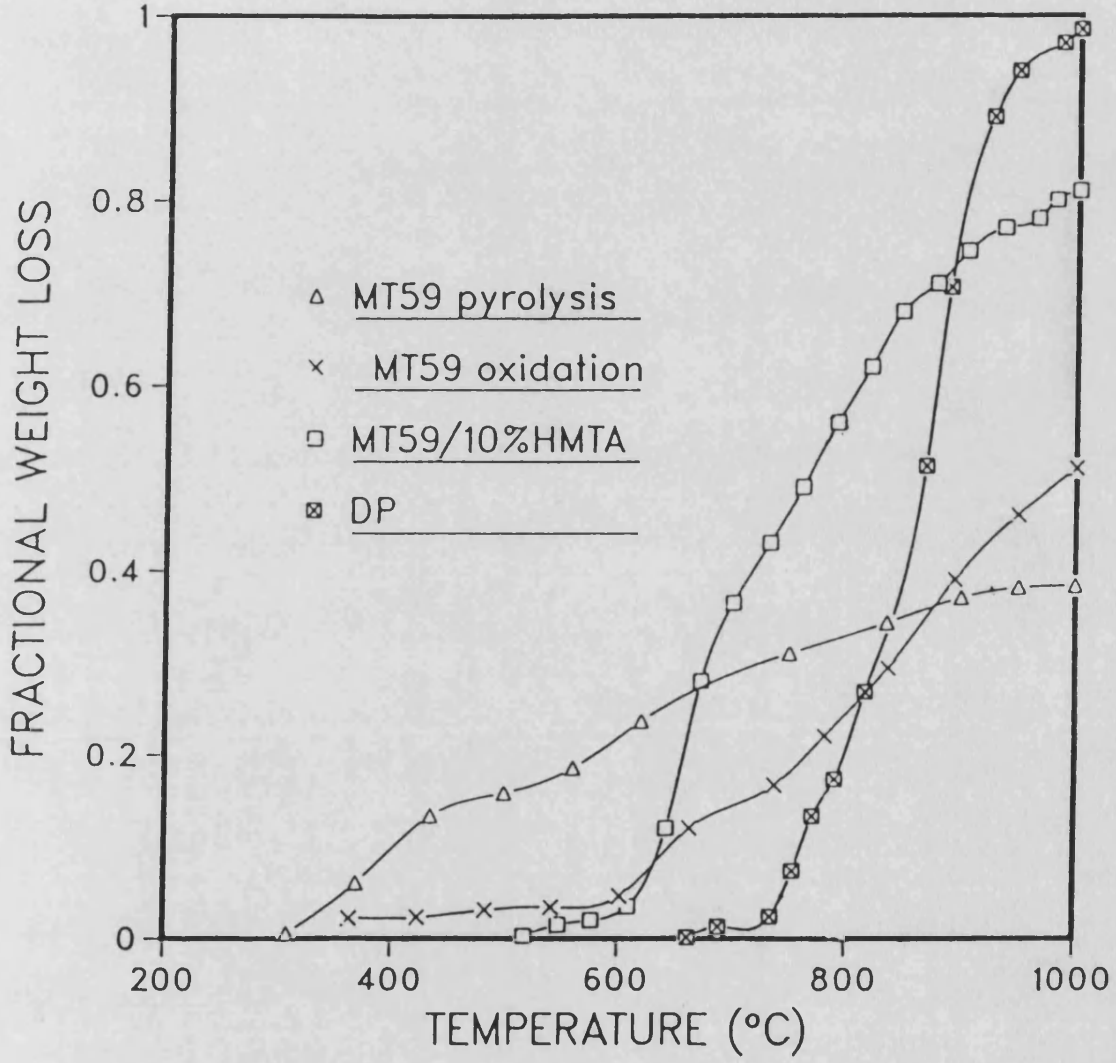

FIG.5.4b Oxidation resistance of PA65 co-polymerised with MT59

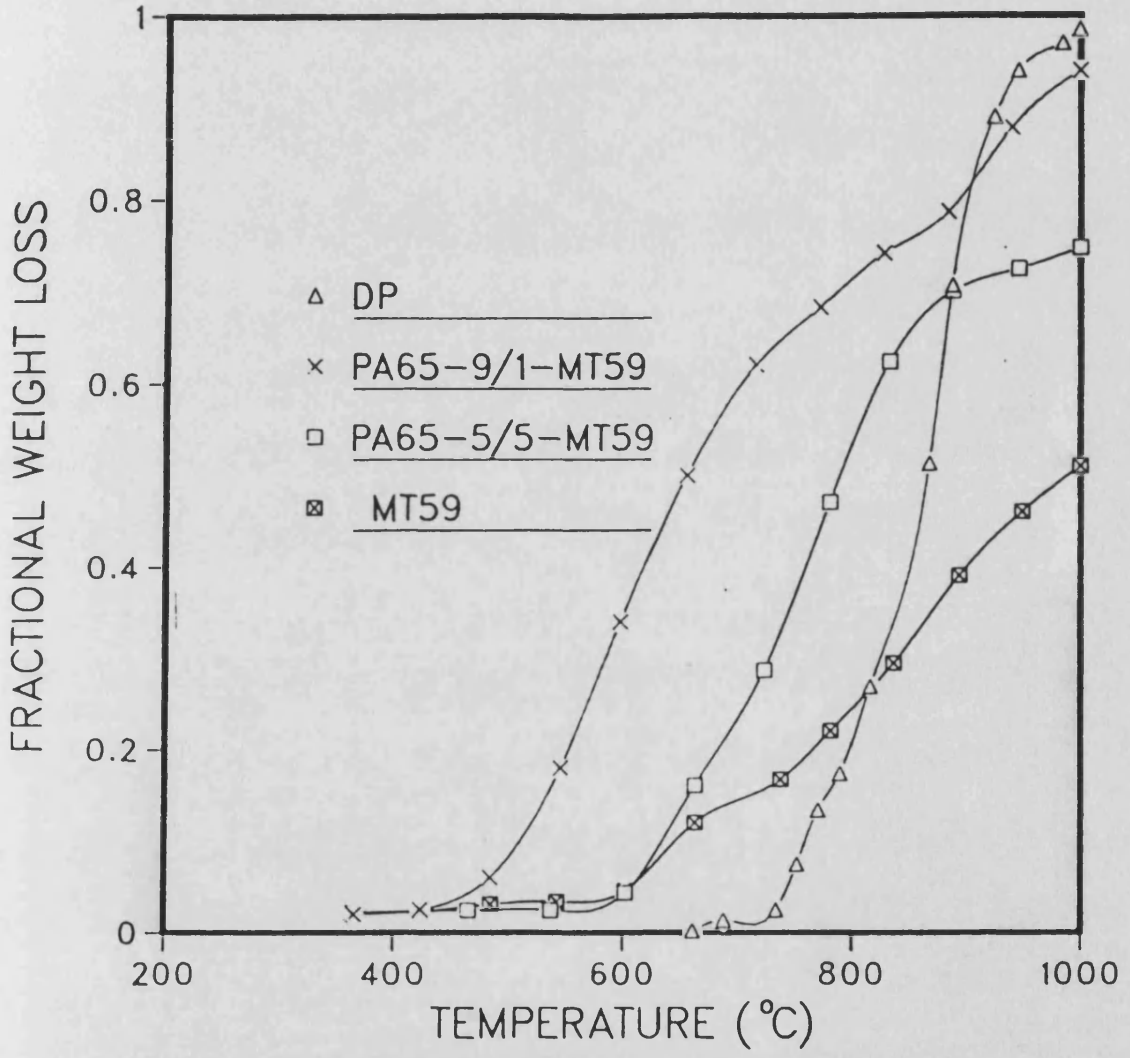

FIG.5.5 Effect of organophosphorus additives on the oxidation resistance of PT carbon (20wt% added before resin cure)

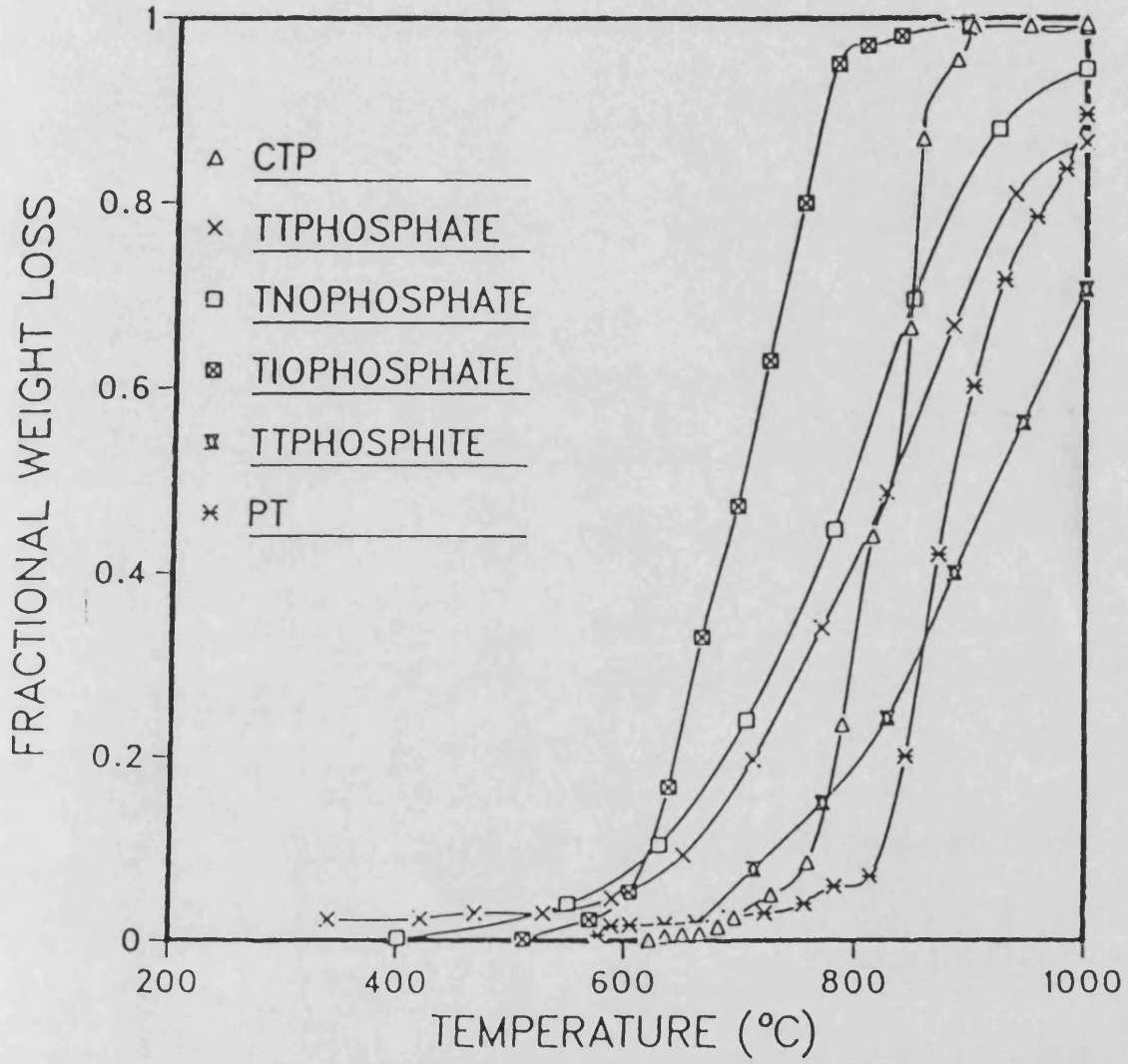

FIG.5.6 Oxidation resistance of PF resins mofied with TDCP (20wt% added at the resin stage)

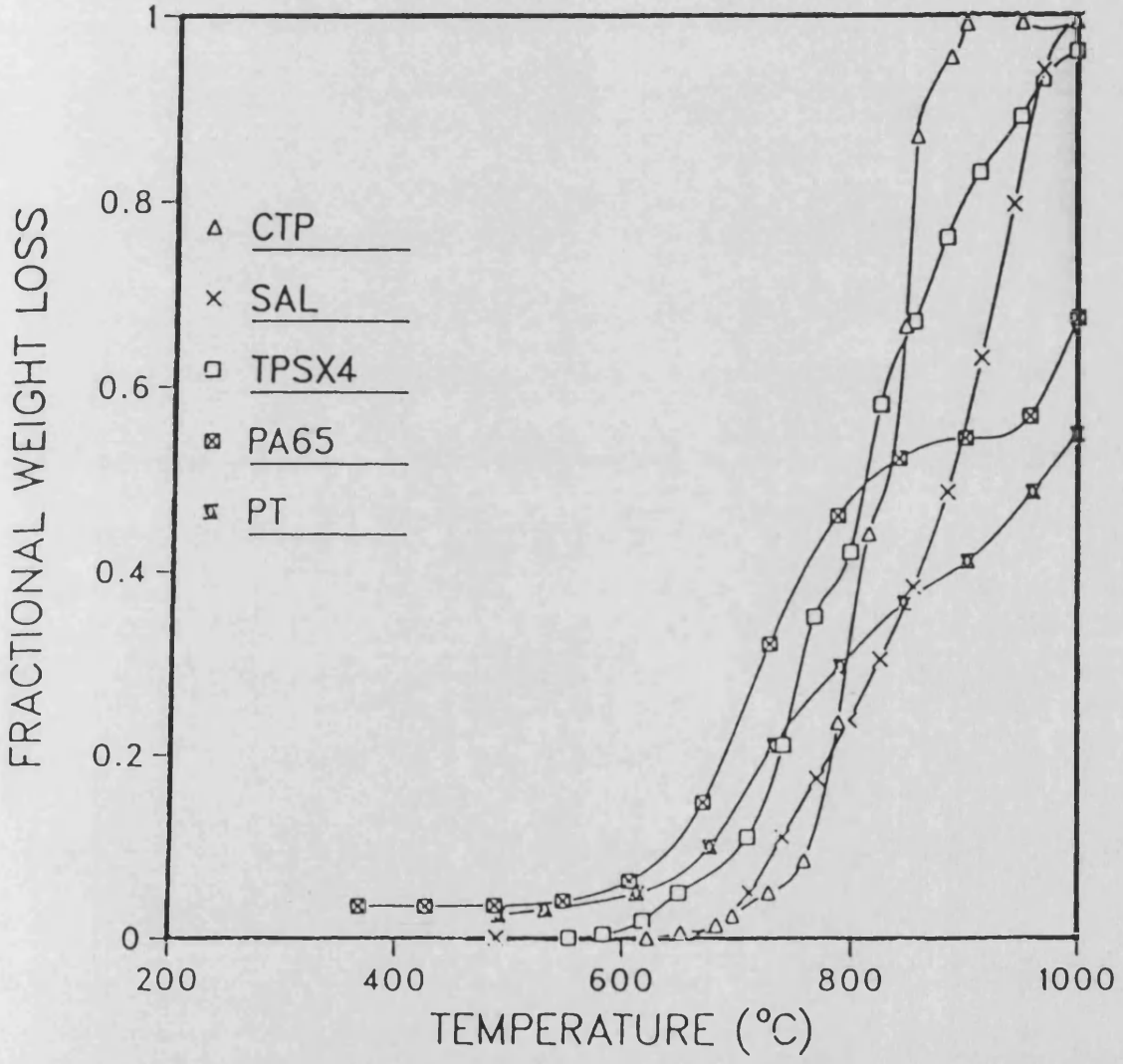

FIG.5.7 Oxidation resistance of PA65 and PT resins modified with organophosphorus additives (20wt% added before resin cure)

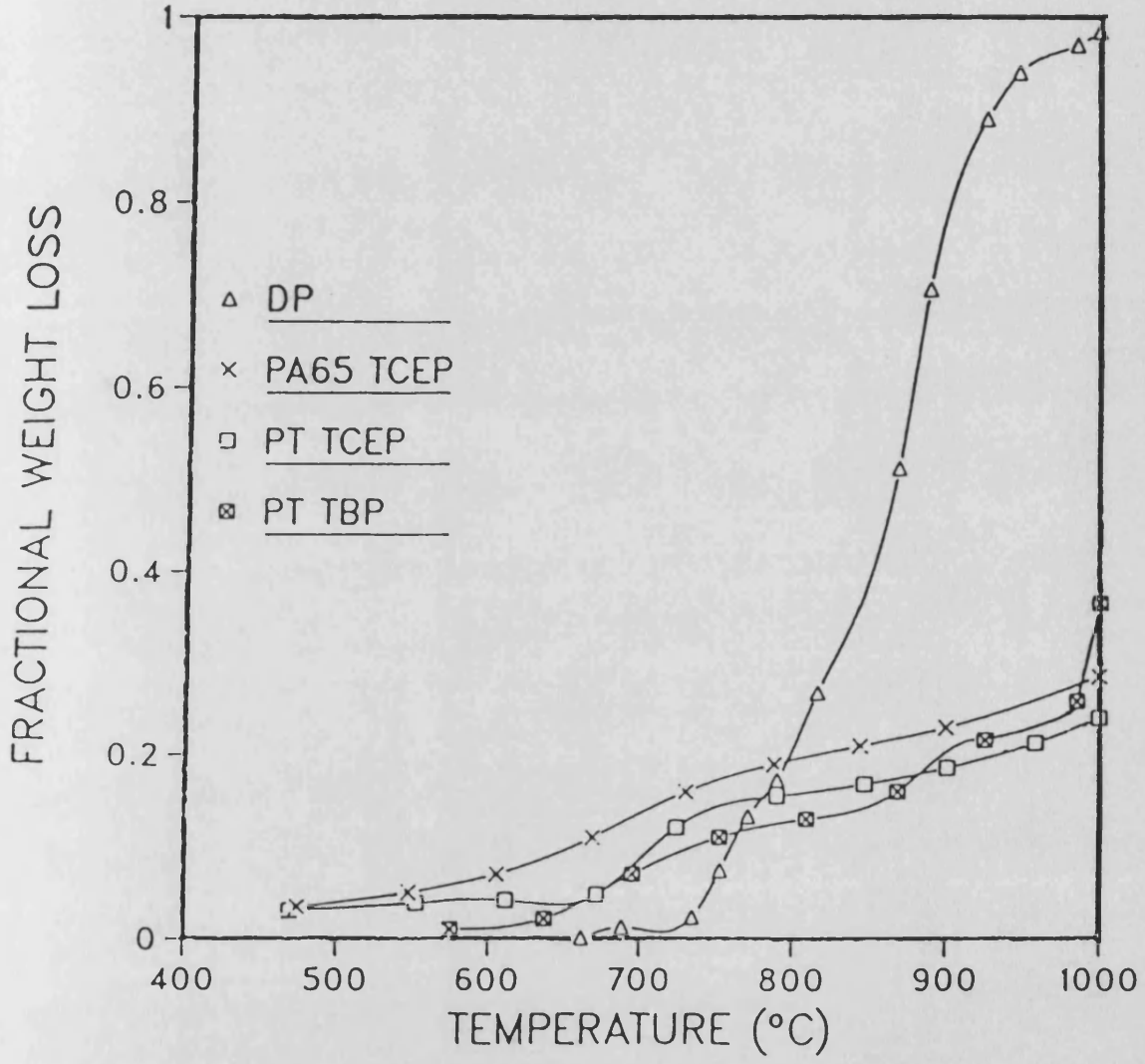

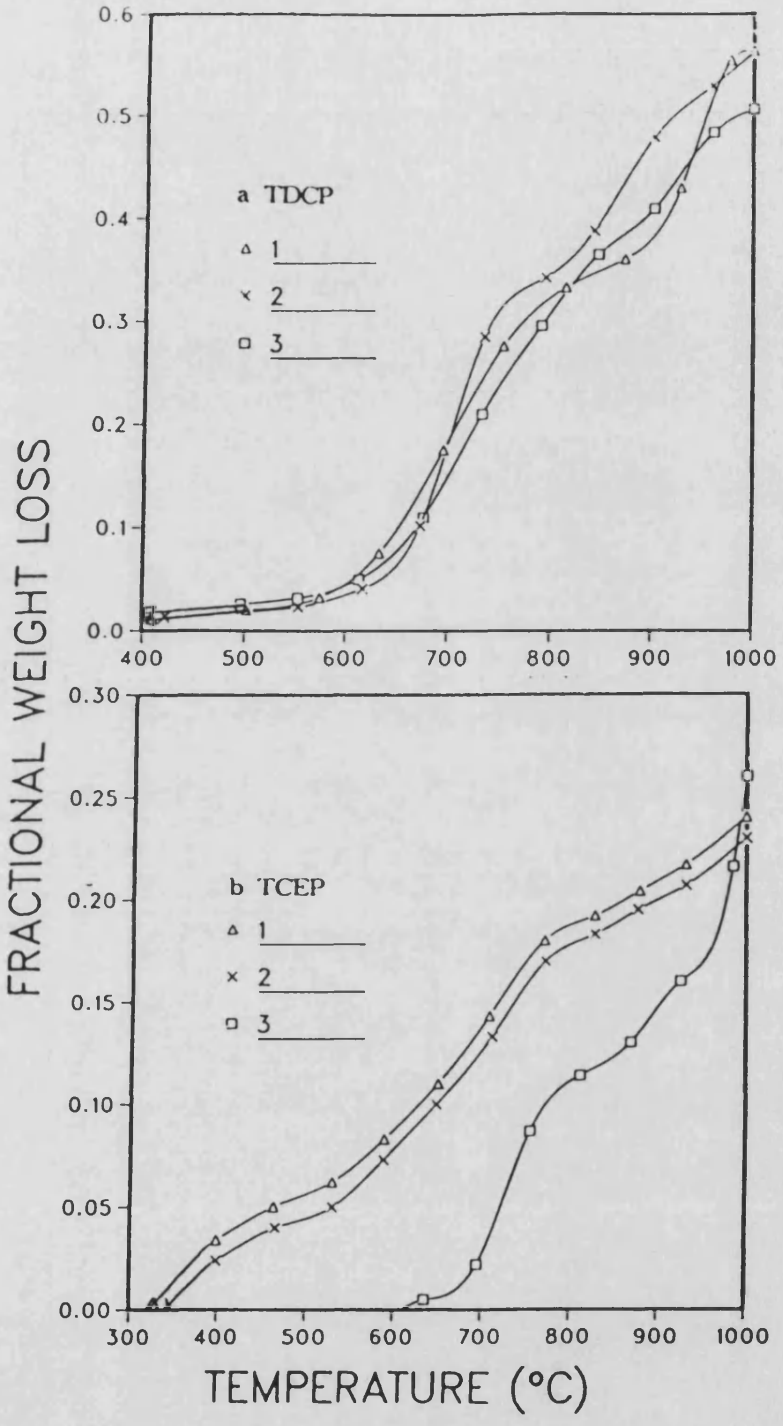


FIG.5.8 An illustration of the reproducibility of carbon prepared from PT resin and 20wt% additive (cure schedule:130/16)

FIG.5.9 Effect of TDCP additions on the oxidation resistance of TPSX4 carbon

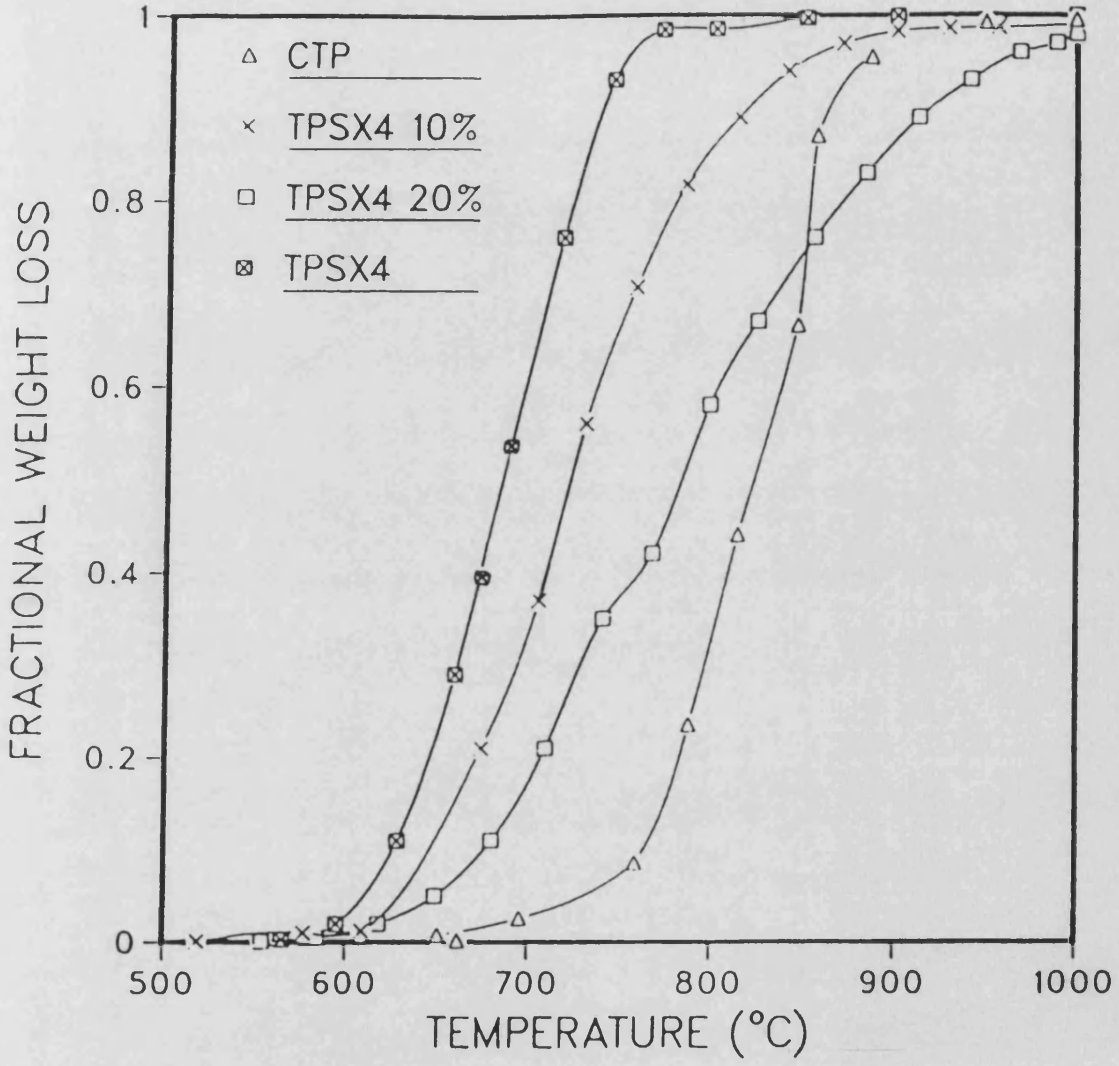

FIG.5.10 Effect of TDCP additions on the oxidation resistance of PT and PA65

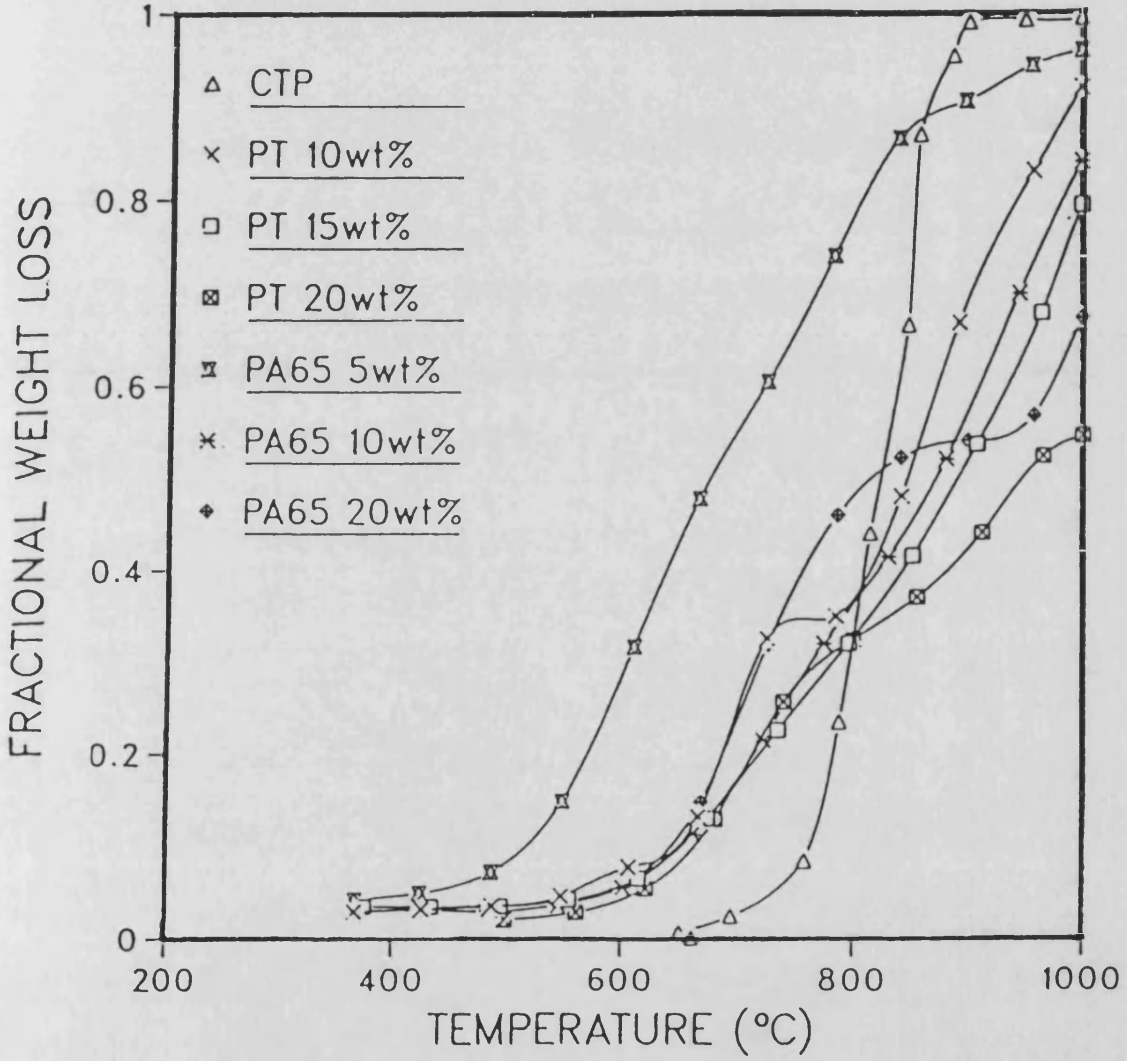

FIG.5.11a Effect of TCEP additions on the oxidation resistance of PA65

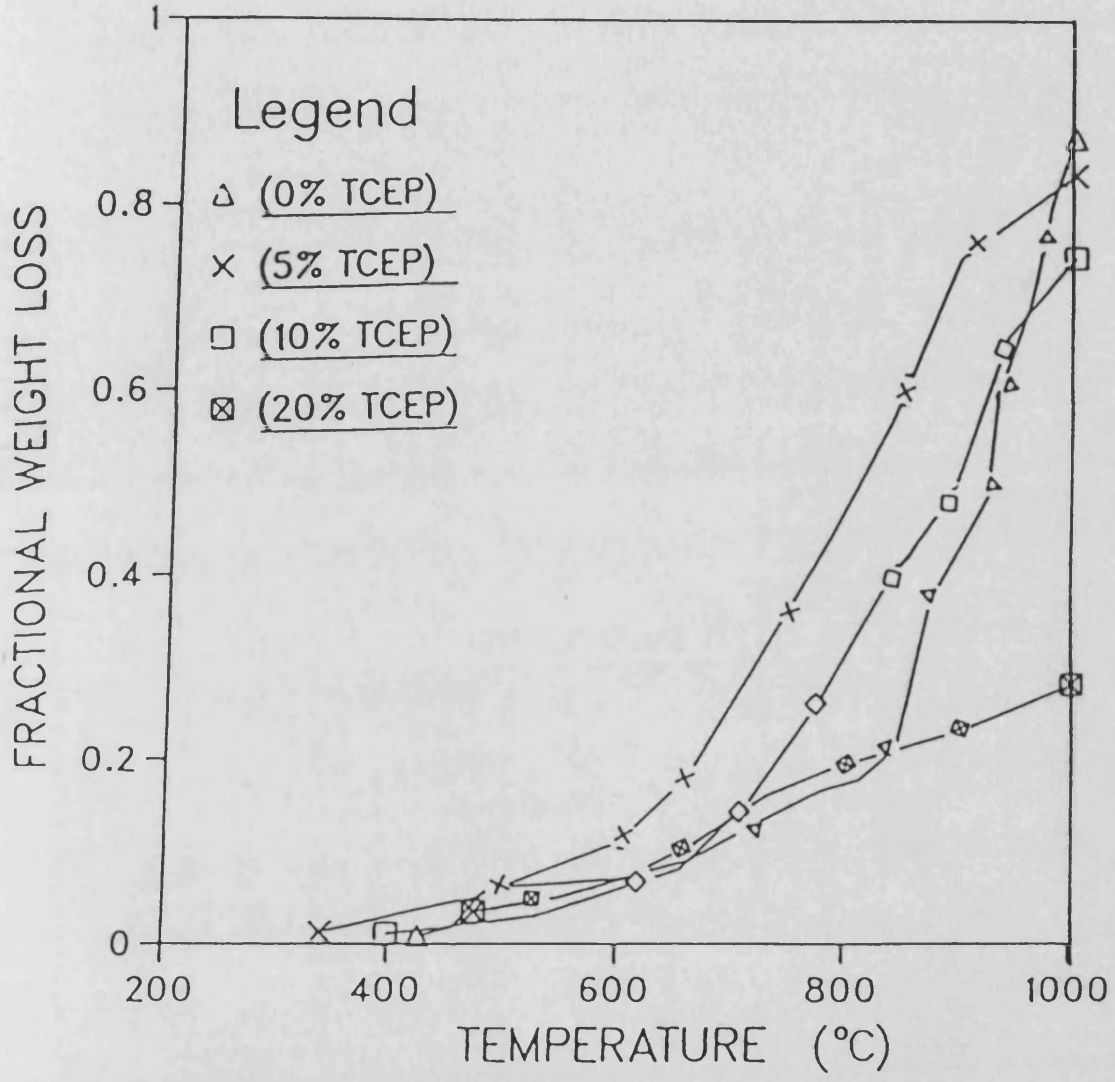

FIG.5.11b Effect of TCEP additions on the oxidation resistance of PT

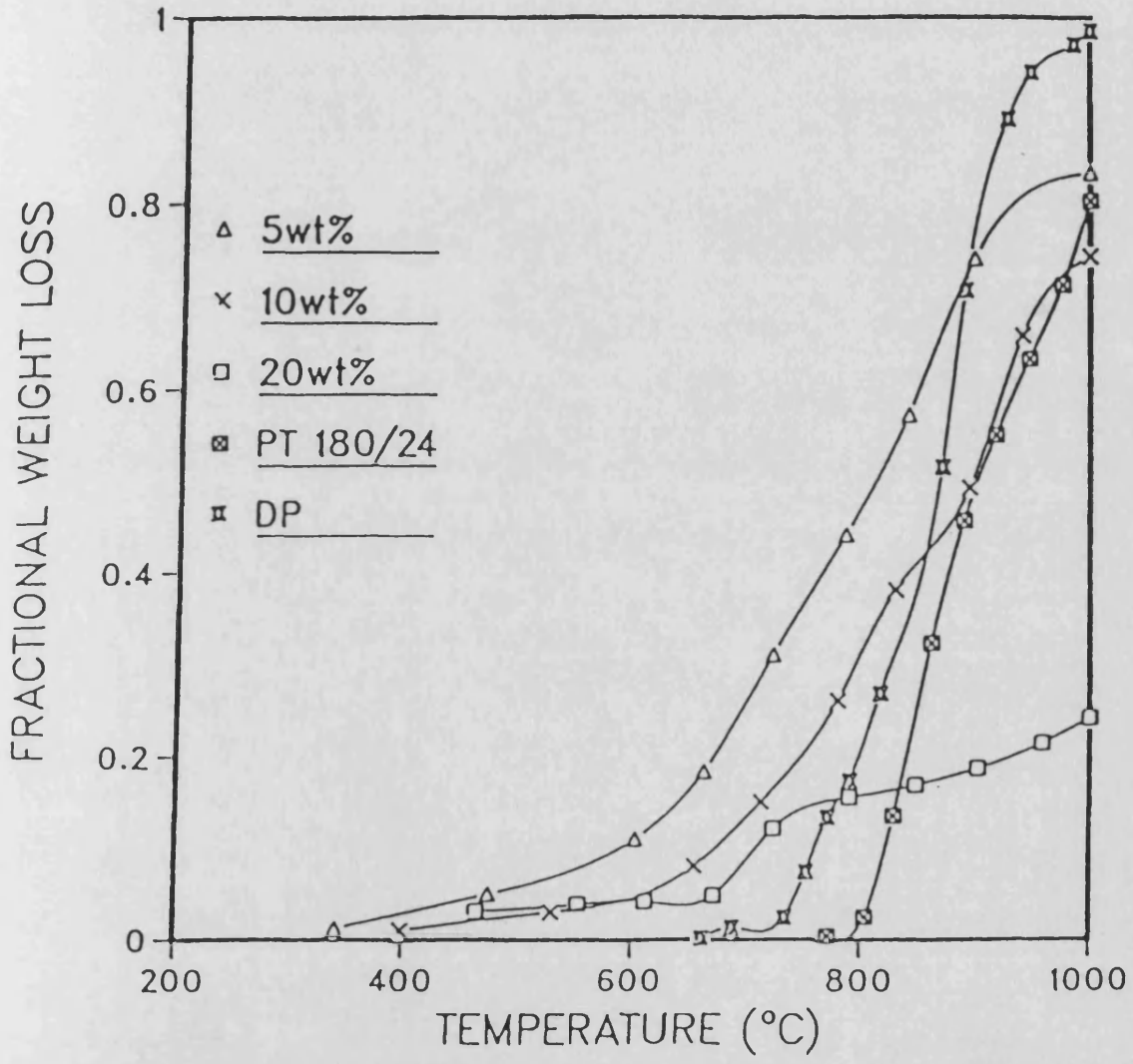

FIG.5.12 A comparison of the oxidation resistance of the most stable additive modified resin and pitch carbons

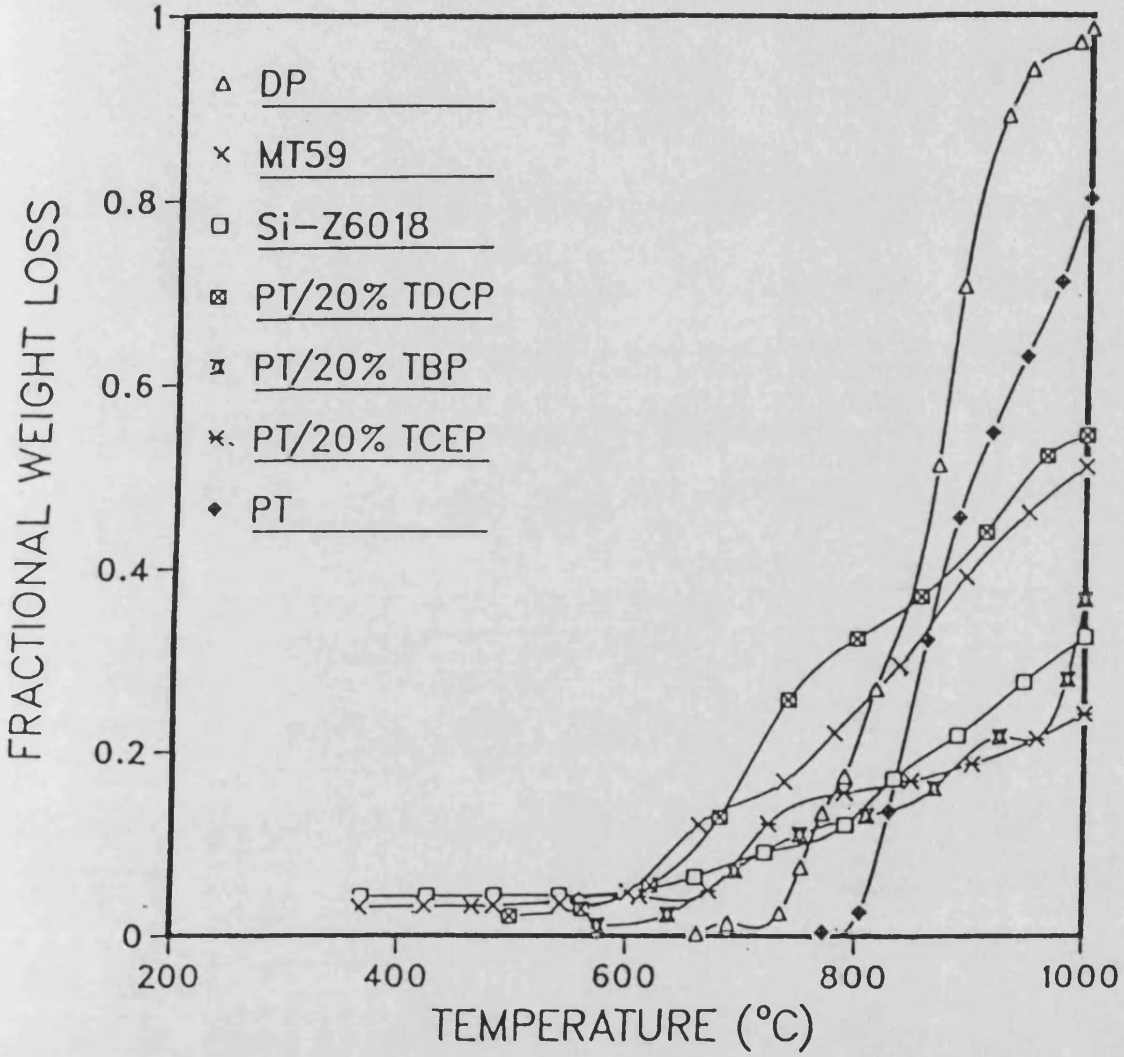

FIG.5.13 Pyrolysis of selected additive modified resins (cure schedule:130/16)

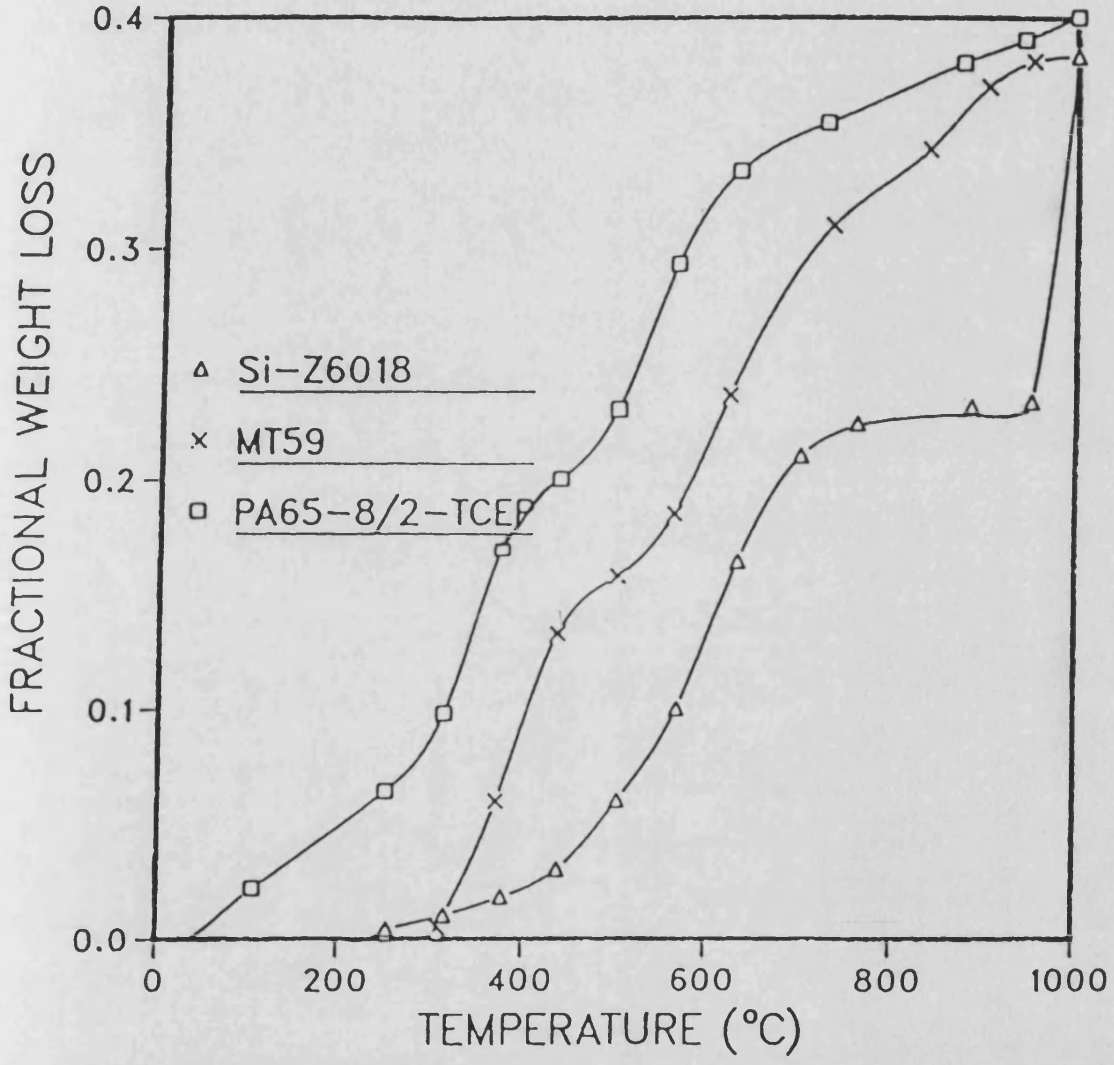

# CHAPTER 6 RESULTS: HIGH TEMPERATURE HEAT TREATMENT, (HTT); ISOTHERMAL OXIDATION STUDIES, EDAX AND CHEMICAL ANALYSIS

## 6.1 Effect of Heat Treatment Temperature on Carbon Yield and Oxidation Resistance of the Resin and Pitch Carbons

### 6.1.1 Results

Casting operations, continuous or interrupted, for the manufacture of high quality steels require high furnace temperatures viz. 1650-1700$^{o}$C. For this reason the resin carbons and pitch carbons were subjected to high temperature heat treatment, HTT, in an inert atmosphere (nitrogen gas flowing at 200ml/min), ranging from 970-1700$^{o}$C. The results of the study are presented in table 6.1a-6.1b and Fig. 6.1-6.3. The carbons were prepared by initial carbonisation of the cured resin (180/24), to 970$^{o}$C followed by further heat treatments to higher temperatures. For this reason, the results for the 970$^{o}$C material are those obtained from the carbon which was used for further HTT studies rather than the average values presented in Chap.4.

For DP carbon there is a gradual increase in oxidation resistance with increasing HTT, fig.6.1. Excluding the initial weight loss during carbonisation to 970$^{o}$C, the weight loss during

heat treatment from 1200°C to 1700°C was only 2wt%. The solid residue after oxidation at 1000°C increases with HTT from 0.1wt% to 15wt% for the 970°C and 1700°C heat treated carbons, respectively. The effects of progressive heat treatment upon the least stable novolak resin carbon, TPSX4, were similar to the DP carbon, although it does not achieve the same degree of thermal stability. TPSX4 carbon shows the greatest improvement in oxidation resistance with increasing HTT. Thus upon increasing the heat treatment from 970°C to 1700°C, $T_{0.05}$ and $T_{0.5}$ values improved by 35.3% and 24.2%, respectively compared to 14.0% and 11.5% improvements observed for DP carbons. The weight loss during the heat treatment in the range 1200°C to 1700°C for TPSX4 carbon, was also low, 2.9wt%, although the residue remaining after oxidation to 1000°C increased from zero to 13wt%, for the 970°C and 1700°C heat treated material.

The co-polymer, PT, showed significant improvements in oxidation resistance as HTT increased, although the 1500°C heat treated carbon showed anomalously low $T_{0.5}$ values. The most striking observation is the great increase in residue remaining after oxidation at 1000°C for the PT carbon subjected to 1700°C heat treatment viz. 64wt%, (cf. similarly treated DP carbon which yields 15wt% residue). The additive modified carbon, PA65/TCEP, showed the highest weight loss during heat treatment from 1200°C to 1700°C, i.e. 7.4wt%. However this was more than compensated by the overall superior oxidation resistance exhibited by this carbon-type compared to the other pitch or resin carbons. Furthermore, HTT improved the $T_{0.05}$ value to that approaching DP

carbon, fig.6.2, while the residue remaining after oxidation at 1000°C for each of the heat treated materials was very high (>71wt%). The results for the carbons heat treated at 1700°C are compared in fig.6.3.

### 6.1.2 Discussion

The results for effect of HTT on the carbons are in good agreement with the observations of Kipling (168) and Strickland-Constable (148), i.e. HTT improves the oxidation resistance of the carbons. Chang and Rhee (43) attributed the decrease in reactivity of pitch and resin-based carbons with increase of HTT to various factors viz. 1) a reduction in total and accessible active surface areas, 2) an increase of graphitic character, 3) changes in pore structure (annealing, i.e. removal of microporosity and other structural defects) which would ultimately affect the diffusion rates of oxygen, carbon-oxygen complexes etc. (169), and 4) a decrease in the level of catalytic impurities.

Inherent impurities are known to either promote or inhibit the oxidation resistance of pitch and resin carbons (170). Metallic impurities promote catalytic oxidation of carbon by lowering the activation energy, Ea. The primary metallic impurity in pitch ash is silicon (20-50wt% of the ash), with Ca, Fe, Co, Ni and V being of secondary importance, (171-173). The reactivity of some metals, e.g. Au and Fe, is only appreciable if they are near a crystallographic defect (172). HTT reduces catalytic

impurity effects by either volatilisation of the metal or its conversion to an inactive compound such as the carbide. The latter is reported to become deposited in pores, thus rendering the carbon more impermeable to diffusion of reactant gases (174).

Masters and McEnaney (169), report that HTT has a significant effect on the porosity and structure of a cellulose carbon. Measurements of the pore width, mean layer stack height, Lc and interlayer spacing $d_{002}$ at 1397°C gave the following information: 1) the pore width increased, and 2) Lc and $d_{002}$ were unaffected. This was associated with an initial lateral growth of the layer planes which removed localised distortions. Further HTT increased Lc with $d_{002}$ unaffected, implying a growth of stack height. This resulted in a collapse of some of the ultramicropores and conversion of open micropores to closed micropores, i.e. sealing off the intrinsic porosity. Strickland-Constable (148) referred to the latter process as conversion of reactive sites to less reactive sites. Thus pitch carbon becomes more graphitic in nature while for the resin carbon, the polymer chains, which are arranged in highly defective layer planes, cross-linked by aliphatic groupings, have coalesced to form narrow ribbons of condensed aromatic molecules which stack above each other to form stabilised microfibrils.

The weight loss upon heating from 970°C to 1700°C for the resin and pitch carbons was low and reflects loss of residual hydrogen, heteroelements and aliphatic carbon groups attached to the edges of the layer planes. The higher weight loss observed

for the additive modified resin carbon probably represents additional loss of the fire retardant decomposition compound. The great increase in oxidation resistance and amount of solid residue after oxidation at 1000°C, for all carbons is observed for the 1700°C heat treated material. This is due to the fact that inter-ribbon cross-link breakage (for resin carbons), and hence release of strain energy, has been reported to occur at ~1500°C and is followed by conversion of open microporosity to closed microporosity. The materials heated below this temperature have a pore structure which is not very different to the material heated at 970°C and thus exhibit quite similar oxidation resistances.

HTT does not appreciably affect the oxidation resistance of the additive modified carbons after the initial improvement, i.e. the 1200°C, 1500°C and 1700°C heat treated materials show very similar oxidation curves. This similarity implies that the additive-derived surface coating, which is assumed to form, and indeed retained despite the increasing HTT, has a more dominant effect on reducing carbon oxidation than the structural changes outlined above. Had the latter been more important, differences in oxidation resistance between the higher and lower heat treatment temperatures would have become apparent, as observed for the unmodified resin carbons and the pitch carbon.

Fig.6.3 depicts the oxidation resistance of the various carbons heat treated at 1700°C. The higher stability of the co-polymer PT and additive modified carbon PA65/TCEP compared to DP carbon is clearly evident. The plot shows that the difference

in performance observed between the resin and pitch carbons heat treated at the lower temperature, 970°C, is narrowed at the higher (service) temperature, 1700°C. The greatest improvement in oxidation resistance is observed for the least stable TPSX4 carbon viz. the $T_{0.5}$ value is enhanced by 35.3%. The pitch carbons are not expected to achieve a pure graphitic structure due to lack of mutual orientation and greater average spacing between adjacent layers compared with graphite. Thus DP carbon heat treated at 1700°C fails to give the expected high oxidation resistance.

TABLE 6.1 Effect of heat treatment temperature on thermal properties of resin, additive modified resin and pitch carbons

a) Effect of HTT on the oxidation resistance of the carbons

| Carbon | Weight Loss Temperature (°C) | Heat Treatment Temperature (°C) 970 | 1200 | 1500 | 1700 |
|---|---|---|---|---|---|
| DP | $T_{0.05}$ | 752 | 749 | 849 | 875 |
| | $T_{0.5}$ | 860 | 846 | 952 | 972 |
| | $T_{0.95}$ | 950 | 934 | >1000 | >1000 |
| TPSX4 | $T_{0.05}$ | 518 | 562 | 639 | 800 |
| | $T_{0.5}$ | 710 | 748 | 799 | 936 |
| | $T_{0.95}$ | 824 | 858 | 936 | >1000 |
| PT | $T_{0.05}$ | 500 | 646 | 584 | 736 |
| | $T_{0.5}$ | 700 | 866 | 836 | >1000 |
| | $T_{0.95}$ | 896 | 989 | 956 | >1000 |
| PA65/TCEP | T0.05 | 600 | 727 | 733 | 747 |
| | T0.5 | >1000 | >1000 | >1000 | >1000 |
| | T0.95 | >1000 | >1000 | >1000 | >1000 |

b) Effect of HTT on weight loss and carbon yield

| | Carbonisation weight loss (wt%) 970 | [1200-1700 (°C)] | Solid residue after TG-oxidation for each HTT (wt%) 970 | 1200 | 1500 | 1700 °C |
|---|---|---|---|---|---|---|
| DP | 40.2 | 2.0 | 0.0 | 2.0 | 11.0 | 15.0 |
| TPSX4 | 56.3 | 2.9 | 0.0 | 0.0 | 0.0 | 13.0 |
| PT | 61.5 | 6.4 | 0.2 | 0.2 | 4.0 | 64.0 |
| PA65/TCEP | 53.8 | 7.4 | 71.5 | 74.9 | 75.0 | 75.0 |

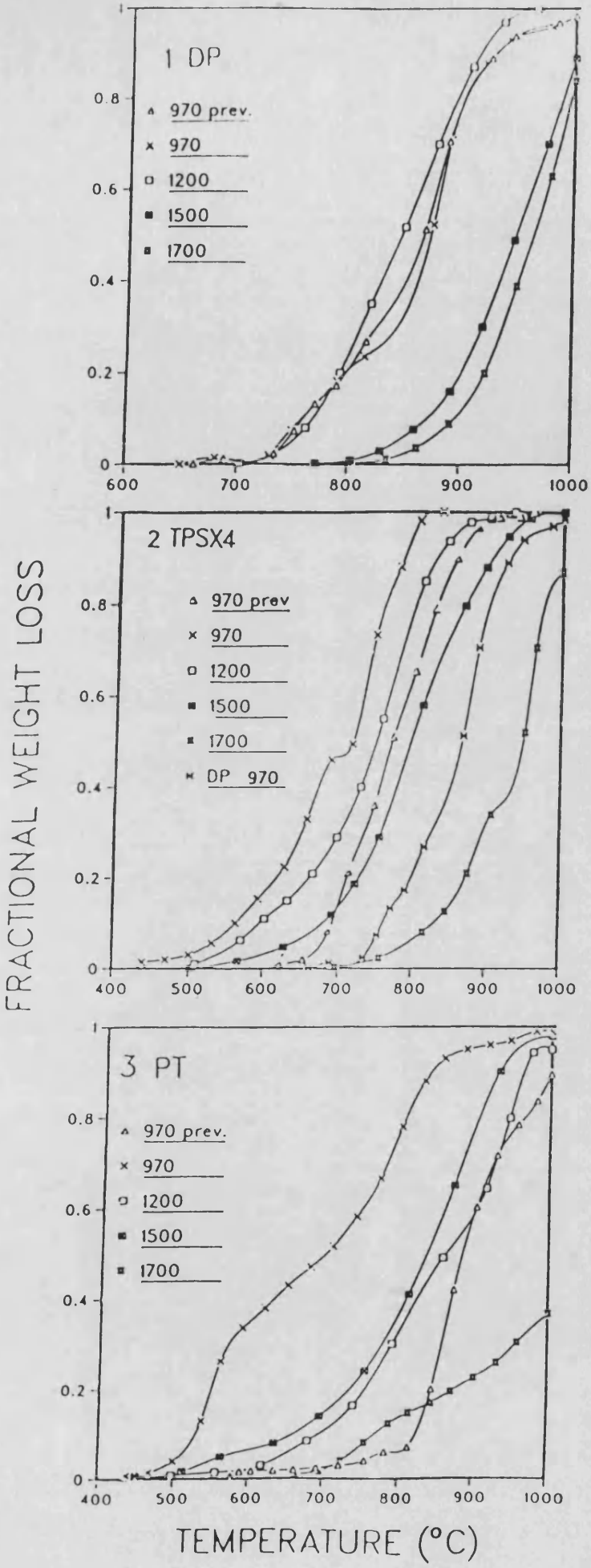


FIG.6.1 Effect of HTT on the oxidation resistance of the carbons

FIG.6.2 Effect of HTT on the oxidation resistance of PA65-80/20-TCEP carbon

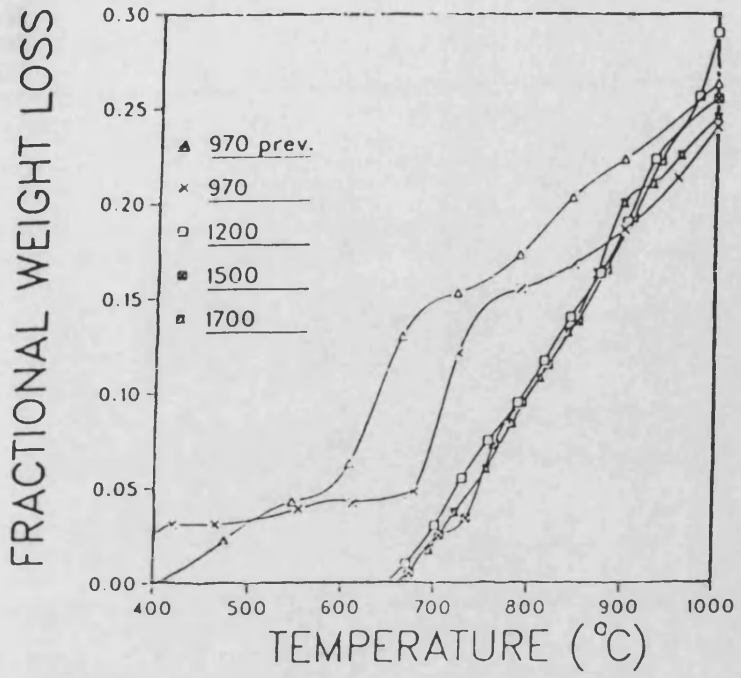


FIG.6.3 A comparison of the oxidation resistance of the carbons heat treated at 1700 C with DP carbon heat treated at 970 C

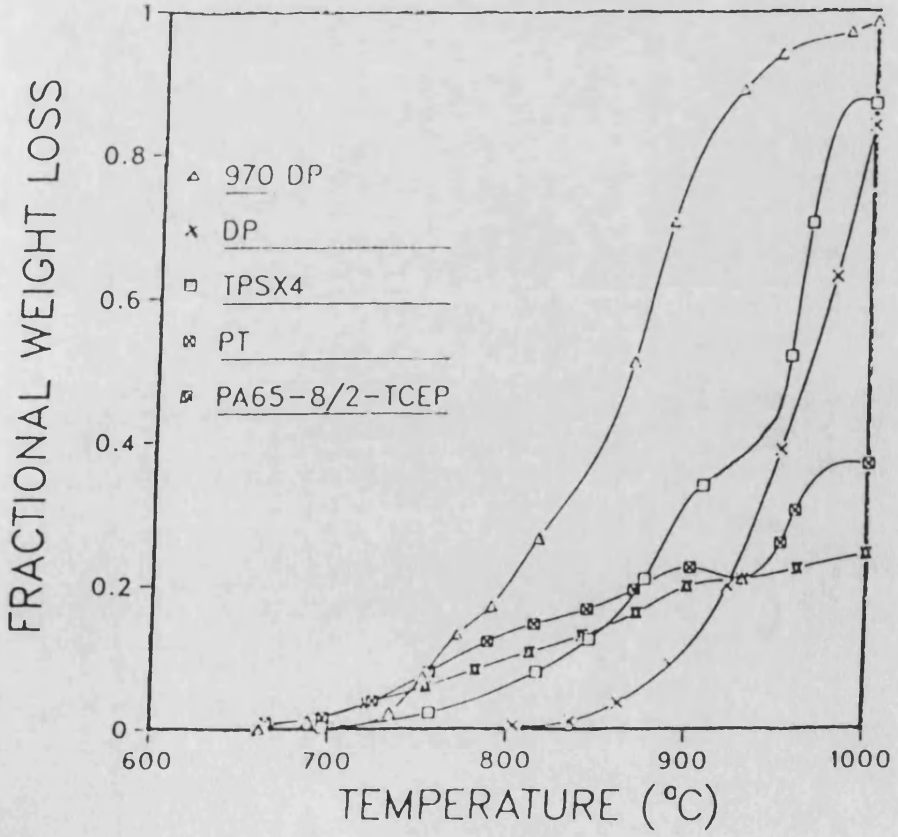

## 6.2 Isothermal Oxidation Studies: Results and Discussion

In the temperature range 900-1000$^{o}$C the isothermal rates of oxidation for DP and unmodified resin carbons, were very similar, i.e. the weight loss vs time curves are almost superimposed. Thus in the high temperature range, the rate of carbon oxidation is diffusion controlled, i.e. diffusion of oxygen to the carbon surface, and the kinetics of oxidation show a very low dependence on the temperature. TPSX4 carbon had the lowest $T_{0.5}$, as reflected by its rapid rate of burn-off even at the lowest temperature (700$^{o}$C). The increase in oxidation resistance for PA65, PT and the additive modified carbons is manifested by a separation of the weight loss vs time plots for the various isothermal temperatures, fig.6.4a,b. DP carbon is completely oxidised at each temperature, showing a maximum period of resistance to oxidation of 60min at 700$^{o}$C. In contrast PT/20-TCEP after exposure for 1200min at 700$^{o}$C still showed ~30% residual carbon. PT/TBP and MT59 also showed high amounts of carbon residue despite prolonged isothermal heating, table 6.2.

A simple method for comparing the oxidation resistance of the carbons involved calculation of the 'relative oxidation resistance', R(x), using the data from isothermal weight loss graphs, fig.6.4a,b. The resulting graph, fig.6.4c was obtained after corrections to the fractional weight loss for presence of residue, i.e. ash or unreacted carbon:

$$\alpha'(t) = (W_o - W_t / W_o - W_f)$$

where $\alpha'(t)$ is the fractional weight loss corrected for residue, $W_o$, $W_t$ and $W_f$ are the initial, time, t, and final, f, weight losses.

$$R(x) = t(x)_s/t(x)_c$$

where $t(x)_s$ and $t(x)_c$ represents the times required to reach x% weight loss by the sample, s, and the control, c, respectively. TPSX4 carbon, exhibiting the lowest oxidation resistance, was used as the control. The relative oxidation resistance R(x) was plotted against the oxidation weight loss x%. The results are presented in fig.6.4c, demonstrating the clear superiority of the PT/TCEP and MT59 resin carbons.

Oxidation rates from weight loss vs time graphs were obtained from the slope of the graph over the following ranges: $(\alpha_{0.05}-\alpha_{0.5})/(t_{0.05}-t_{0.5})$; $(\alpha_{0.05}-\alpha_{0.3})/(t_{0.05}-t_{0.3})$; and $(\alpha_{0.05}-\alpha_{0.1})/(t_{0.05}-t_{0.1})$

The corresponding Arrhenius-type plots are presented in fig.6.5a,b,c respectively. Oxidation of TPSX4 is so rapid that similar high rates were obtained. The Arrhenius plots all gave a low and similar Ea, i.e. 16.3-13.8kJ/mol, indicating that the rate of TPSX4 carbon oxidation is under gaseous diffusion control. Oxidation rates of DP carbon were similar in the high isothermal temperature range implying diffusion control, i.e. the rate of reaction increases faster than the diffusivity of the reactant gas. This represents a depletion of the reactant molecules along the pores and a corresponding increase in the concentration of the product gases due to limitations of gas diffusivity. Eventually

the concentration of the reactant falls to zero (all gas molecules entering the pores react), and a concentration gradient is observed with the rate controlling step being in-pore diffusion. Significantly lower rates were obtained at the lower temperatures due to gas diffusivity being greater than the rate of carbon oxidation, i.e. the oxidation was under chemical control. Consequently, the Ea at high temperature for DP carbon oxidation is less than that at lower temperature oxidation.

The Arrhenius plots for PA65 and PT carbons were similar and showed lower oxidation rates. The additive modified carbons exhibited lower rates of oxidation than the other carbons. At 700$^{o}$C PT/TCEP carbon had an oxidation rate lower by a factor of 43 compared to DP. Oxidation at 1000$^{o}$C for PT/TCEP was still lower than the rate at 700$^{o}$C observed for DP, i.e. by a factor of ~6. The Ea obtained from isothermal oxidation at ( $\alpha$ =0.05-0.5) is similar in magnitude, (for the carbons DP, PT and PA65, Ea = 53.2, 54.9 and 60.7kJ/mol, respectively), to the value reported from non-isothermal studies, i.e. Ea = ~61 and ~64kJ/mol for pitch and resin carbons, respectively, (Chap.4 fig.4.10), table 6.3. This implies that the mechanism of oxidation is similar for both pitch and resin carbons. Wallouch (175) reported the mechanism for graphitic oxidation as the removal of edge carbon atoms and blocking off of interconnected porosity. However, for glassy carbons, the latter proposal is not the complete story. Thus catalytic impurities and dynamic structural changes, i.e. creation of pores and enlargement of existing pores until they coalesce, will have a profound influence on the prevailing

mechanism (43, 148). Furthermore, the value of Ea is clearly dependent on the weight loss range selected, table 6.3, during calculation of the oxidation rates. The high Ea observed during onset of carbon oxidation, i.e. using the weight loss range (=0.05-0.1) implies chemical control and was expected to decrease in the final stages of carbon oxidation, which is under gaseous diffusion control. The latter is observed for DP carbon but not for the resin and resin-modified carbons.

Using the weight loss range selected by Chang (43), i.e. rates of oxidation calculated over the weight loss range ($=_{0.05}{}^{-}{}_{0.1}$), different Ea values were obtained for the resin and pitch carbons. Thus PA65 and PT showed Ea of ~57.4 kJol/mol compared to 134.0 kJol/mol for DP. The lower Ea values of the resin carbons implies a different mechanism of oxidation compared to the pitch carbons. The Ea values found for resin and pitch carbons are markedly lower than the values reported in literature, e.g. graphitic carbon, Ea =185.9 kJol/mol (153), and 219.8 kJol/mol (151,177)] and phenolic resin carbon, Ea =172.5 kJol/mol (176), 147.8 kJol/mol (43) and 161.6 kJol/mol (178)]. The lower Ea may reflect catalysis of the carbon oxidation by inorganic impurities comprising the ash. The additive modified carbon exhibit values of Ea which were similar to the resin carbons.

TABLE 6.2 Weight (%) carbon residue after oxidation in air at low and high temperatures

| Temperature (°C) | 1000 | | | 700 | | |
|---|---|---|---|---|---|---|
| Exposure time (min) | 100 | 500 | 1000 | 100 | 500 | 1000 |
| Carbon type | TG residue (weight %) | | | | | |
| DP | 0.0 after 13min | | | 0.0 after 60min | | |
| PT/20TCEP | 70 | 6.0 | <3.0 | 88 | 59 | 31 |
| PT/20TBP | 26 | 6.0 | <3.0 | 76 | 60 | 30 |
| MT59 | 62 | 36 | 21 | 76 | 51 | 37 |
| Z6018 | 60 | 56 | 53 | 71 | 58 | 55 |

TABLE 6.3 Activation energies obtained from isothermal oxidation rates (the rates were calculated over the shown weight loss ranges of the TG oxidation thermograms)

| Carbon type | (weight loss ranges) | | |
|---|---|---|---|
| | 0.05-0.1 | 0.05-0.3 | 0.05-0.5 |
| | Activation Energy, Ea, (kJ/mol) | | |
| DP | 121.4 | 63.6 | 53.2 |
| TPSX4 | 16.3 | 13.8 | 13.8 |
| PA65 | 46.5 | 62.8 | 60.7 |
| PT | 54.8 | 77.0 | 54.9 |
| PT/TBP | 67.8 | 51.1 | 68.2 |
| PT/TCEP | 67.4 | 54.9 | 64.9 |
| MT59 | 71.6 | 61.5 | - |

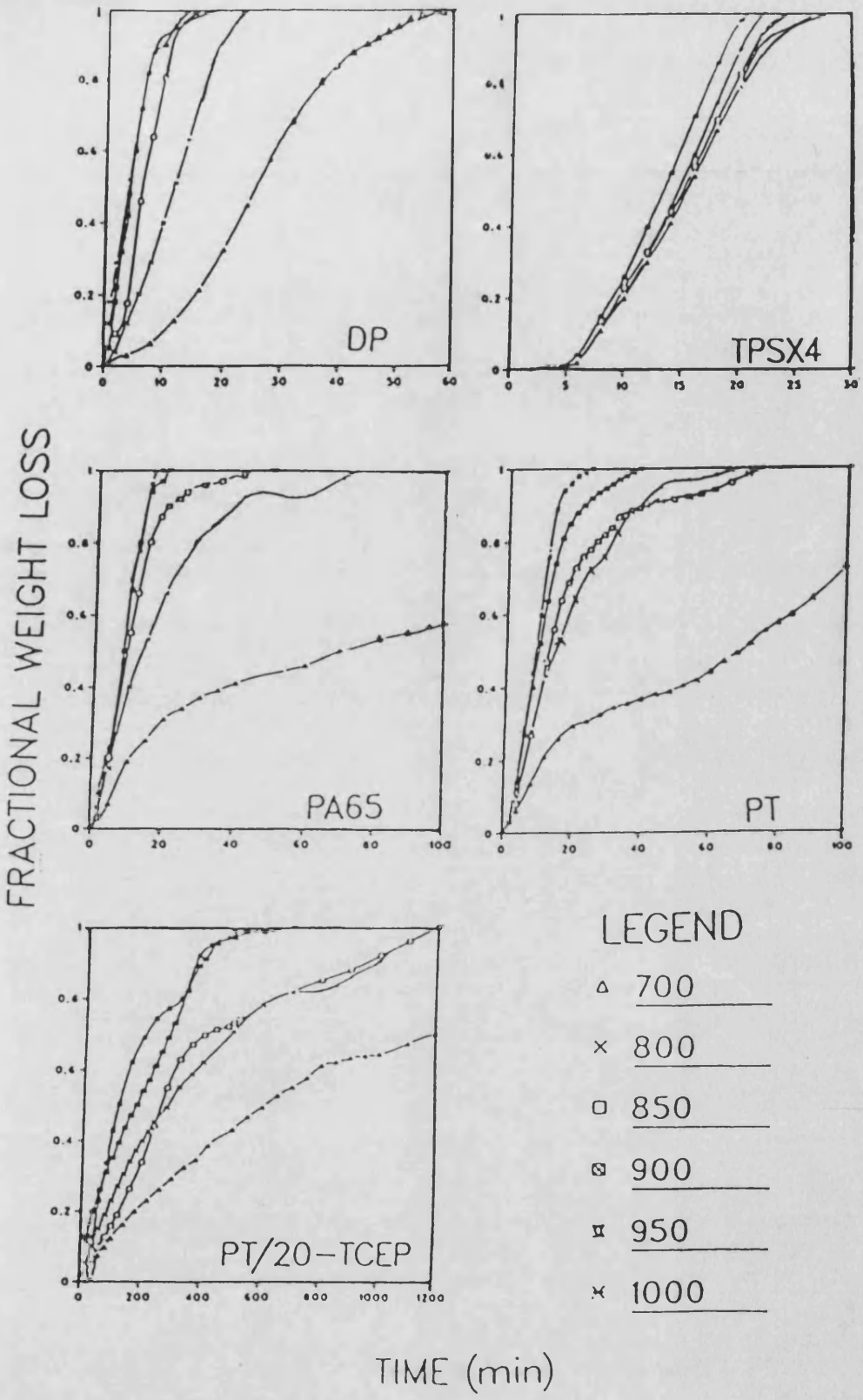


FIG.6.4a An illustration of the oxidation resistance of pitch and resin carbons under isothermal conditions

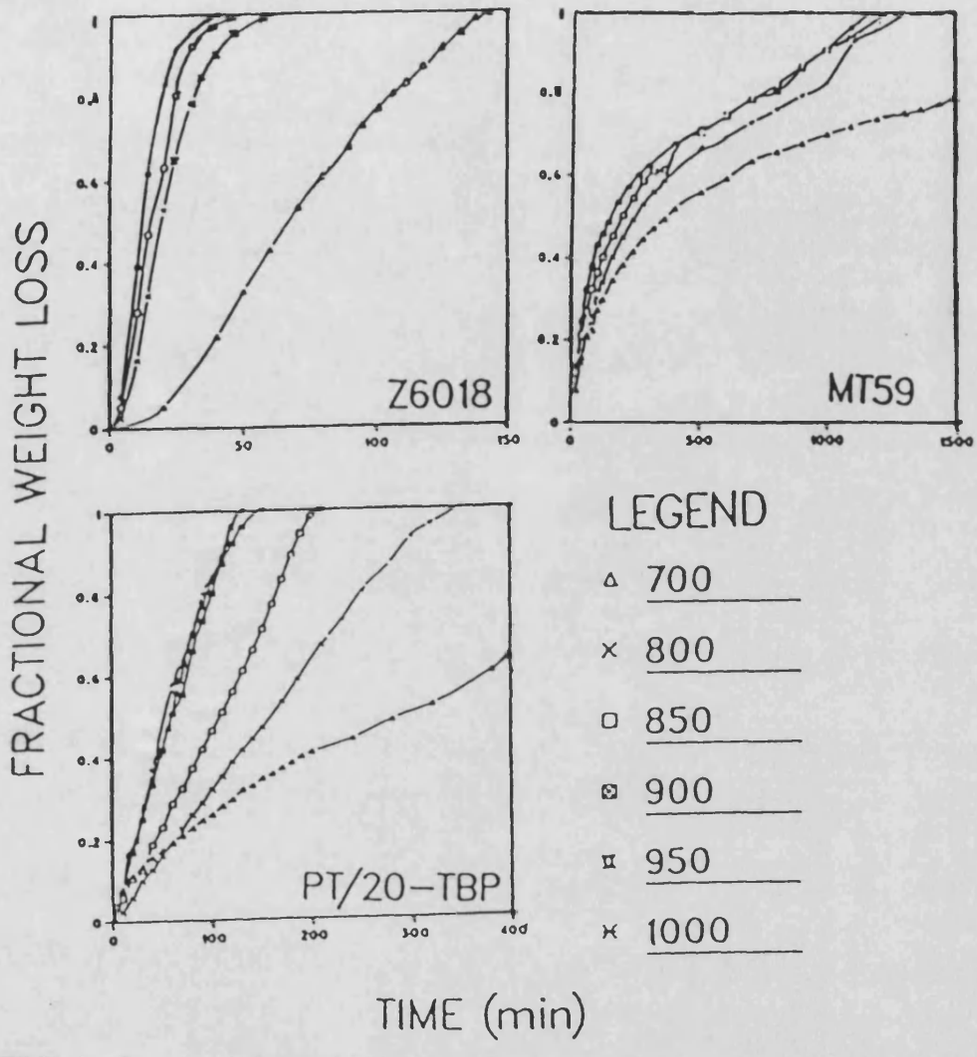


FIG.6.4b An illustration of the oxidation resistance of additive modified resin carbons under isothermal conditions

FIG.6.4c A comparison of the relative oxidation resistances of the resin and pitch carbons

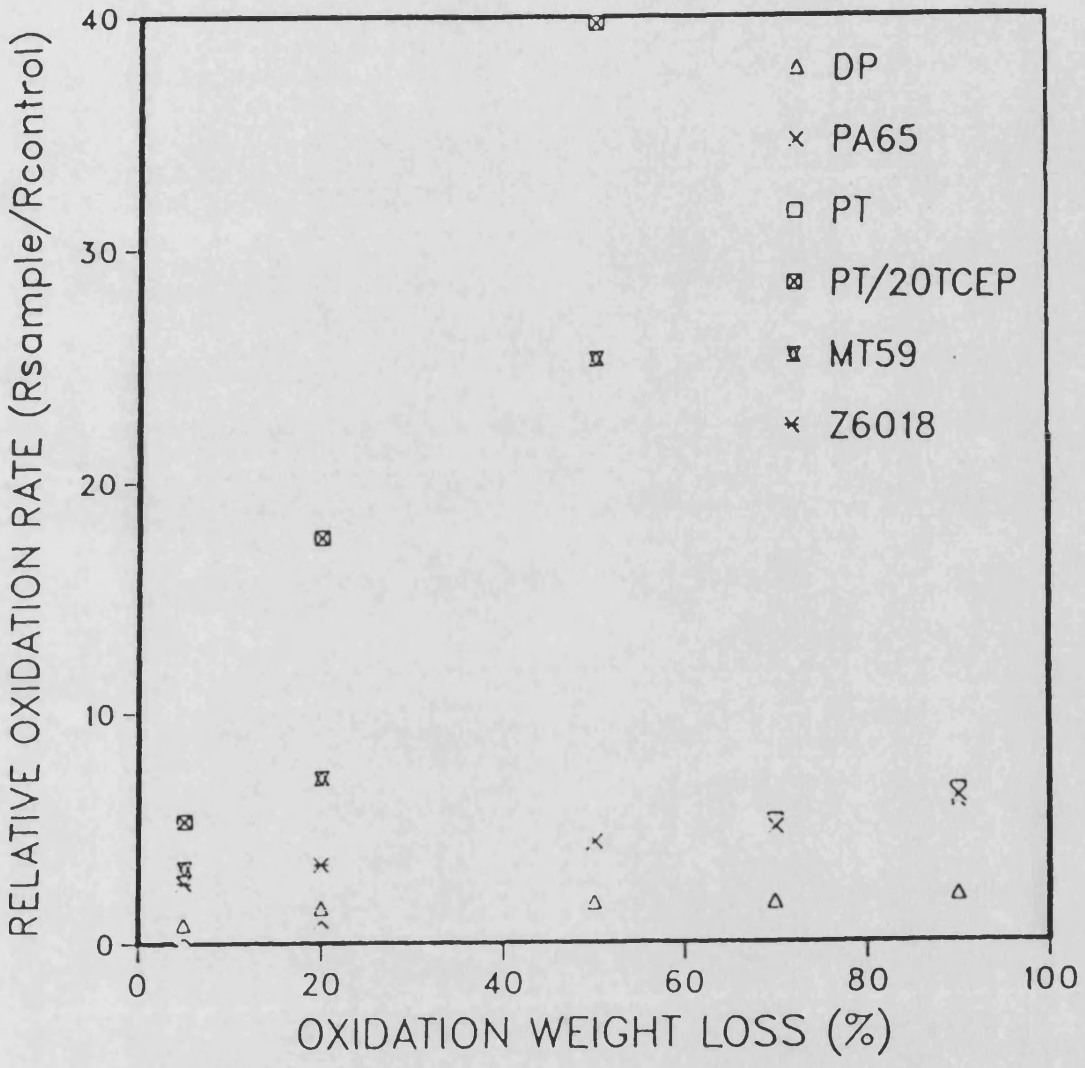

FIG.6.5 A comparison of the Activation energy, Ea obtained from different weight loss ranges of the isothermal weight loss thermograms; a) $\alpha_{0.05-0.5}$

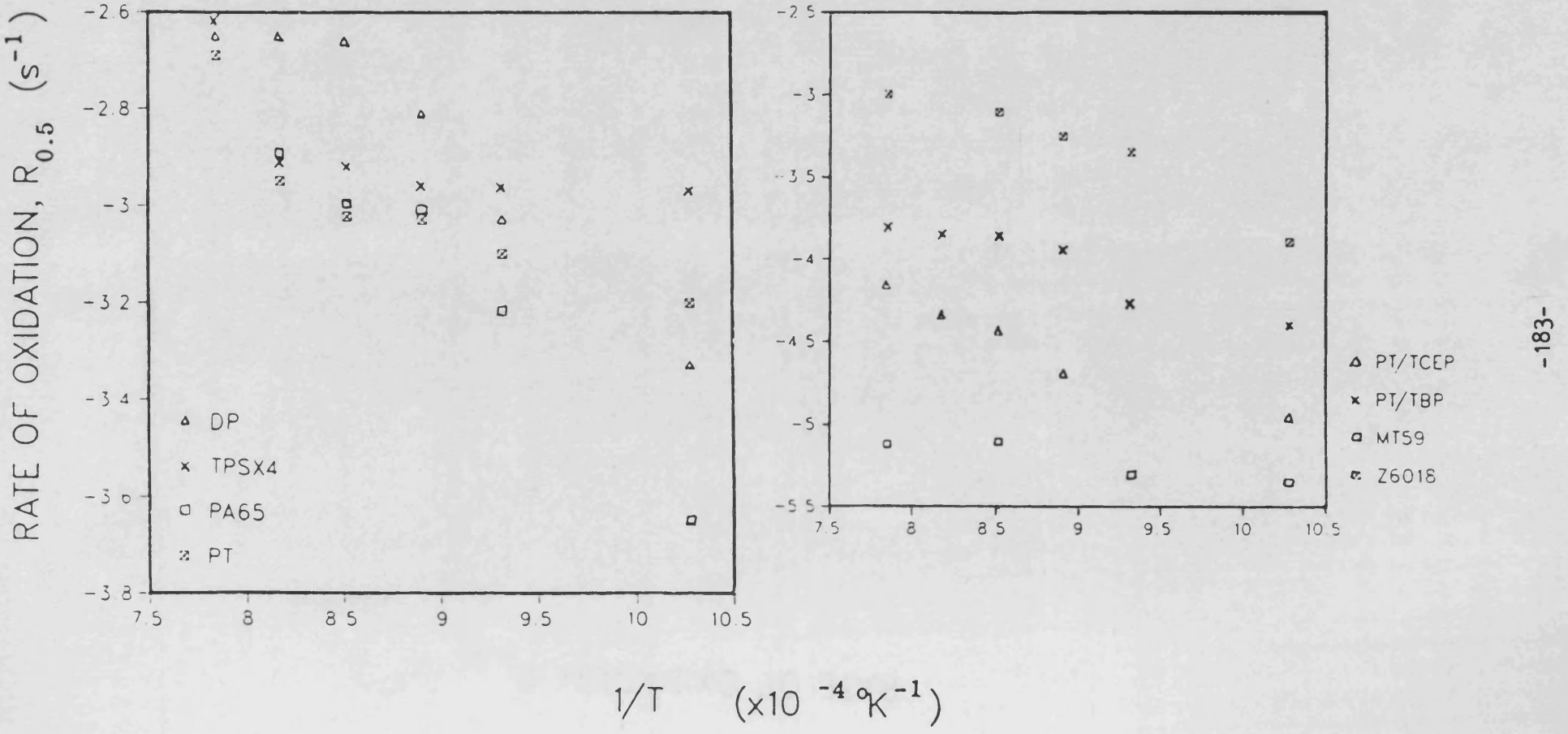

FIG.6.5 A comparison of the Activation energy, Ea, obtained from different weight loss ranges of the isothermal weight loss thermograms; b) $\alpha_{0.05\text{-}0.3}$

FIG.6.5 A comparison of the Activation energy, Ea, obtained from different weight loss ranges of the isothermal weight loss thermograms; c) $\alpha_{0.05-0.1}$

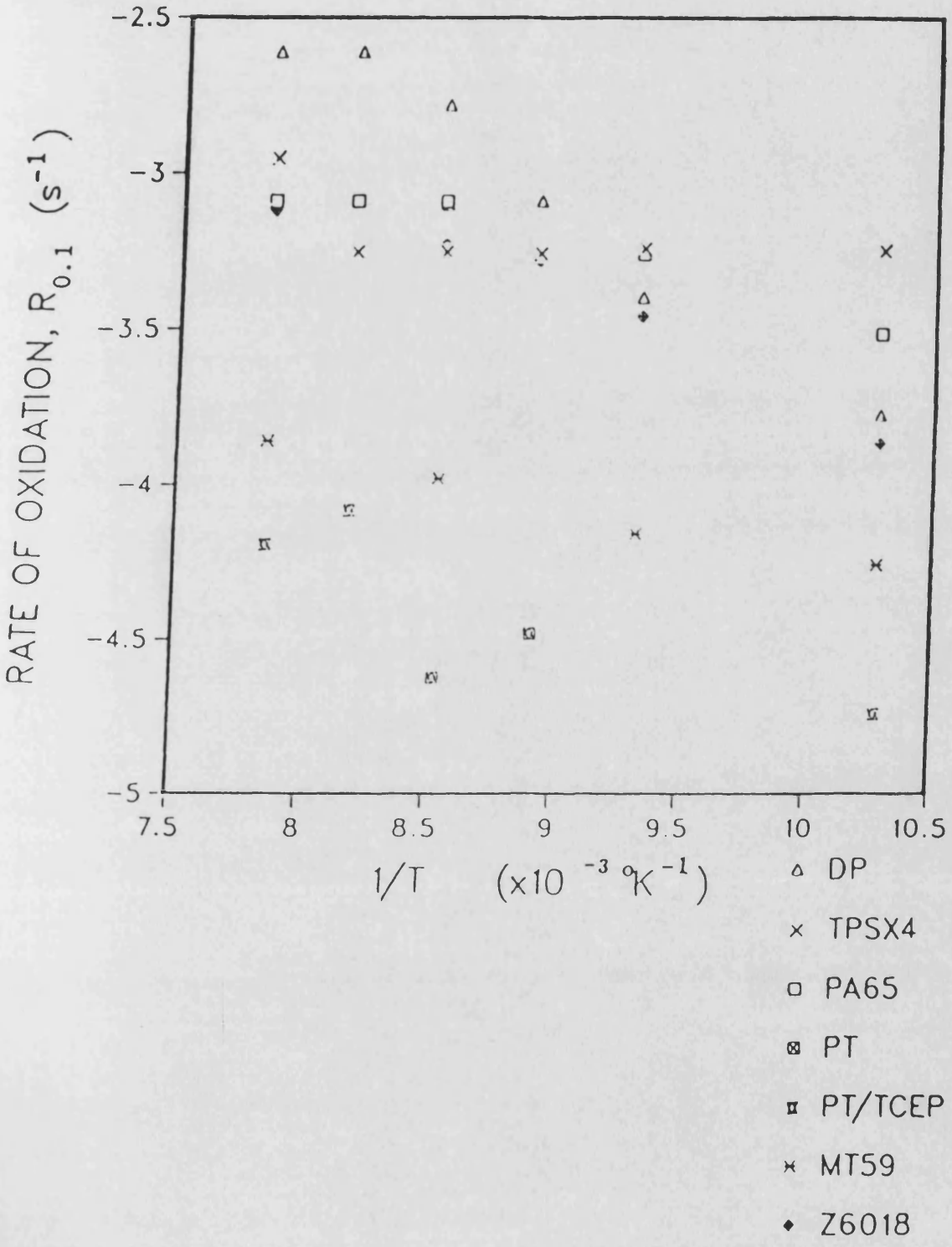

## 6.3 Energy Dispersive Analysis of X-rays: Results and Discussion

The spectra obtained from energy dispersive analysis of x-rays (EDAX), provided semi-quantitative information of the elements present in the material investigated. Fig.6.6a shows the high level of sulphur and low levels of nitrogen (which is estimated to be present despite peak overlap with carbon, see also C-H-N analysis, section 6.4), and oxygen in DP carbon. Silicon and sodium are also detected while the other inorganic elements were present at too low a concentration and were presumably masked by the background noise. For example, K, Ca and Fe are reported to be present as trace impurities in coal tar pitches, functioning as catalysts for carbon oxidation (151, 177-178). The spectra for PT carbon, fig.6.6b shows the presence of oxygen, sodium, sulphur and nitrogen. The latter three elements probably arise from the catalysts used, including the cross-linking agent, HMTA, added to TPSX4.

EDAX is useful for determining whether the chemicals present in the compound TCEP, added to the co-polymer PT at the resin stage, were retained following different levels of oxidation, Fig. 6.8a-d. Fig6.6b shows that the phosphorus, P, is not detected in the unmodified PT resin carbon. Presence of P in the organophosphorus modified resin is evident, fig.6.8a. Various authors (108, 109) have reported that organophosphorus compounds decompose to form oxides of phosphorus on the surface of the carbon substrate. Based on this argument, sectioning the sample particle (carbon), as required for EDAX studies, should have

produced a micrograph showing an annular ring of the additive element P. There is no evidence for this ring, instead a heterogeneous distribution of the additive element is apparent, fig.6.7, micrographs 1-2. Since the specimens, resin and carbons, were ground and polished, thus removing the additive (i.e. represented by P on the spectra and micrographs) from the surface, detection of the P confirms that the latter had entered the polymeric network structure of the carbon. It is suggested that as cross-linking and volatile gas evolution proceeds, during resin cure and carbonisation, the liquid fire retardant (i.e. considering organophosphorus additives) percolates the polymer network via generated pores and cracks. The Z6018 and MT59 contained resins chemically bound via ester bonds with the phenolic hydroxyl group.

EDAX studies showed that progressive oxidation of the additive modified carbon results in additive retention although its distribution becomes increasingly heterogeneous. Thus micrographs 3 and 4, which were obtained after 30% and 50% carbon oxidation, respectively, show high concentration of the element P at specific points, e.g. periphery, of the carbon particle. As the percentage oxidation increased, the level of the additive element P also increased. The oxygen level showed a concurrent increase, suggesting that some form of phosphorus oxide is present. Due to the heterogeneity of additive distribution, only semi-quantitative results are reported.

The spectral data of Fig. 6.8a-d was converted to a

histogram, fig.6.9, having arbitrary units, to show more clearly the variation of the additive with percentage oxidation. Table 6.4 contains data representing the ratio of the maximum peak height, obtained from fig.6.9, of the specified elements. Although the peak heights varied even when analysing different points on the same specimen, the results consistently showed the following order:

$$P_0 < P_{15} < P_{30} < P_{50}$$

where P is the additive element phosphorus, and the numbers represent the percentage carbon oxidation. Since the electron beam penetrates the specimen surface to a depth of only 1um, the decrease in the ratio (C/P) with increasing oxidation, suggests that the thickness of the additive (i.e. phosphorus oxide), on the carbon surface, increased.

EDAX spectra for the silicon modified carbon Z6018, showed a high level of silicon and oxygen, fig.6.10. The spectra of the same material after 40% oxidation shows the complete absence of carbon, while the silicon and oxygen levels were enhanced, fig.6.10. This confirms that the latter residue was entirely silica.

In summary, EDAX data indicates that the organophosphorus additive is retained in the carbon network despite the carbonisation at 970°C and extensive carbon oxidation. The EDAX micrographs, 1-4, show that the additive acts by forming a barrier, probably an oxide, on the carbon surface (i.e. plane and porous surface). The latter is thought to retard the

diffusion of the reactant gas to the carbon surface, thus increasing its oxidation resistance.

TABLE 6.4 Arbitrary values of peak maxima ratios for detected elements to show variation of the additive with carbon oxidation (data obtained from the histogram, fig.6.9)

| Carbon oxidation (%) | C/P | C/O | P/O |
|---|---|---|---|
| 0 | 3.22 | 7.85 | 2.44 |
| 15 | 0.30 | 0.59 | 1.96 |
| 30 | 0.21 | 0.36 | 1.74 |
| 50 | 0.05 | 0.11 | 2.11 |

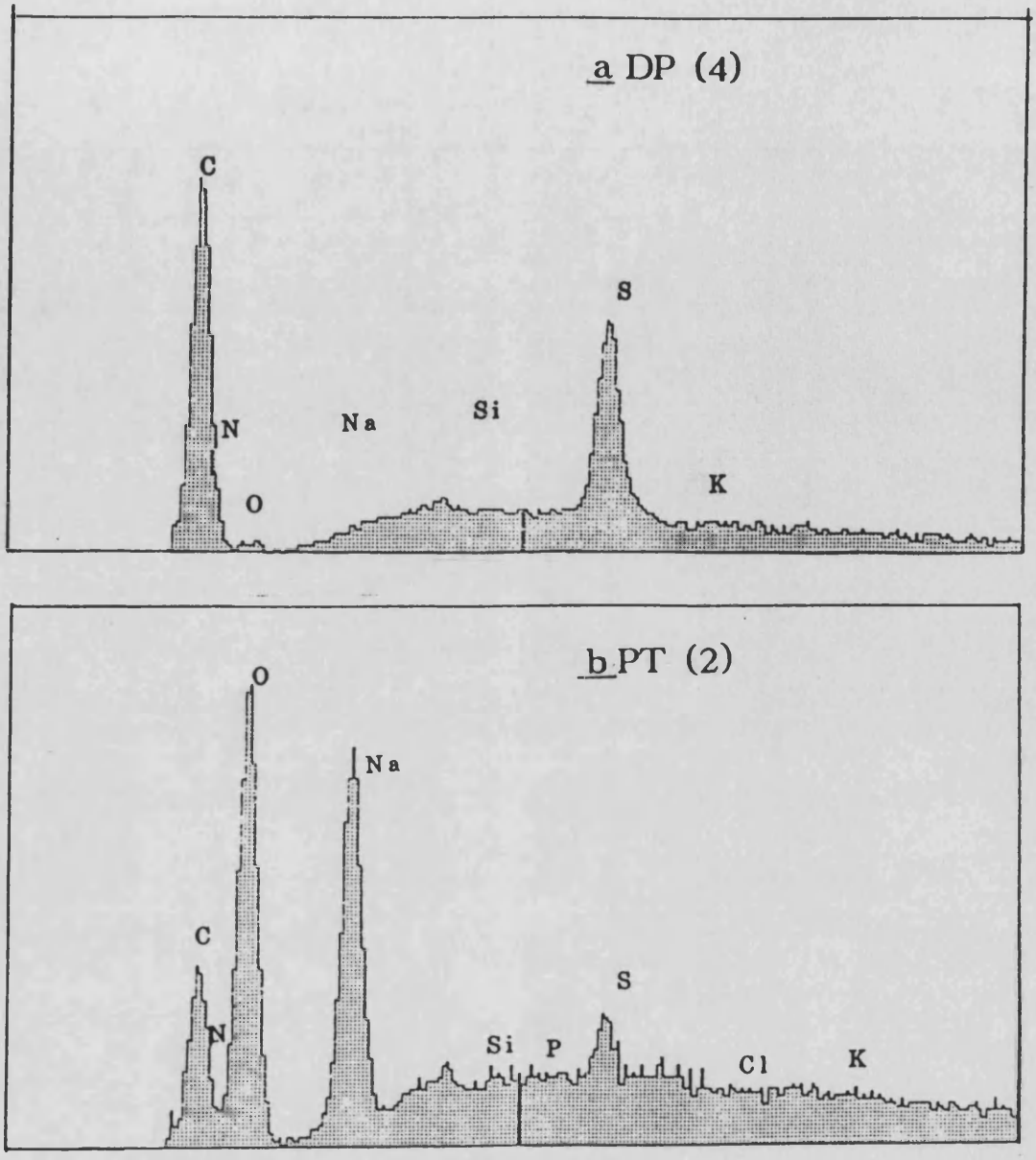


FIG.6.6 EDAX spectra of the unmodified copolymer PT carbon and DP carbon (x-ray intensities, ordinates, are on different arbitrary scales)

The numbers in brackets are the arbitrary values of the maximum peak intensity (used to construct FIG.6.9)

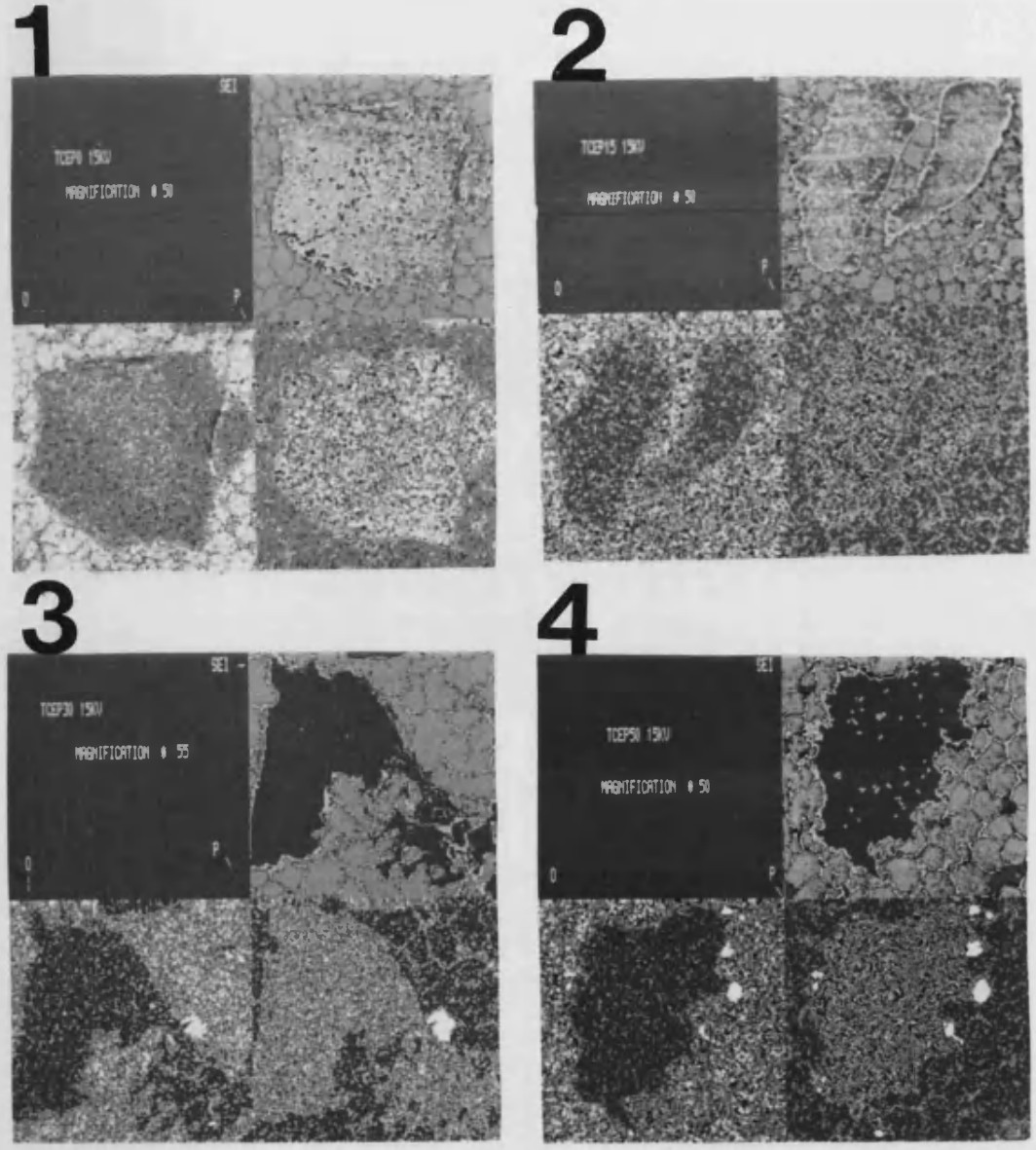


FIG.6.7 EDAX MICROGRAPHS SHOWING THE DISTRIBUTION OF THE FR TCEP AFTER VARIOUS LEVELS OF BURN-OFF OF THE COPOLYMER PT (the numbers after the notation represent percentage carbon oxidation e.g. TCEPo= 0% oxidation)

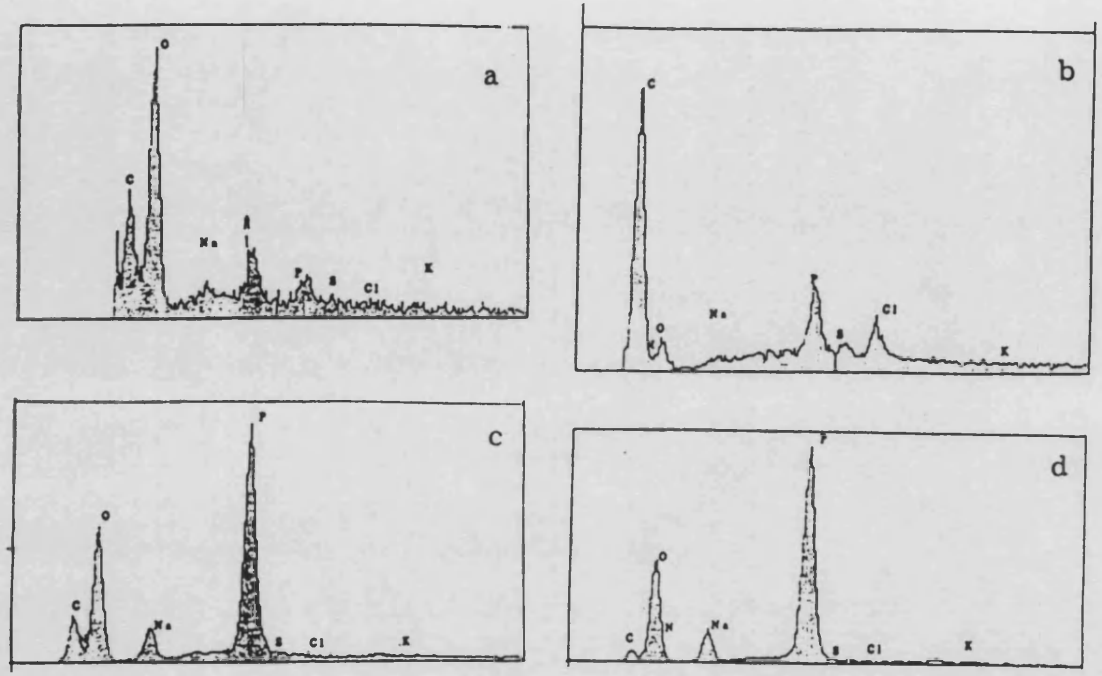


FIG.6.8 EDAX spectra showing distribution of the additive element in the copolymer PT-80/20-TCEP a Resin (0.5) b Carbon 0% oxidation (2) c Carbon 30% oxidation (4) d Carbon 50% oxidation (8)

The numbers in brackets are the arbitrary values of the maximum peak intensity (used to construct FIG.6.9)

FIG.6.9 Histogram showing the distribution of the various elements present in PT-80/20-TCEP following different degrees of oxidation **(each series of lines represents an arbitrary amount of the element remaining after 0%, 15%, 30% and 50% oxidation, respectively)**

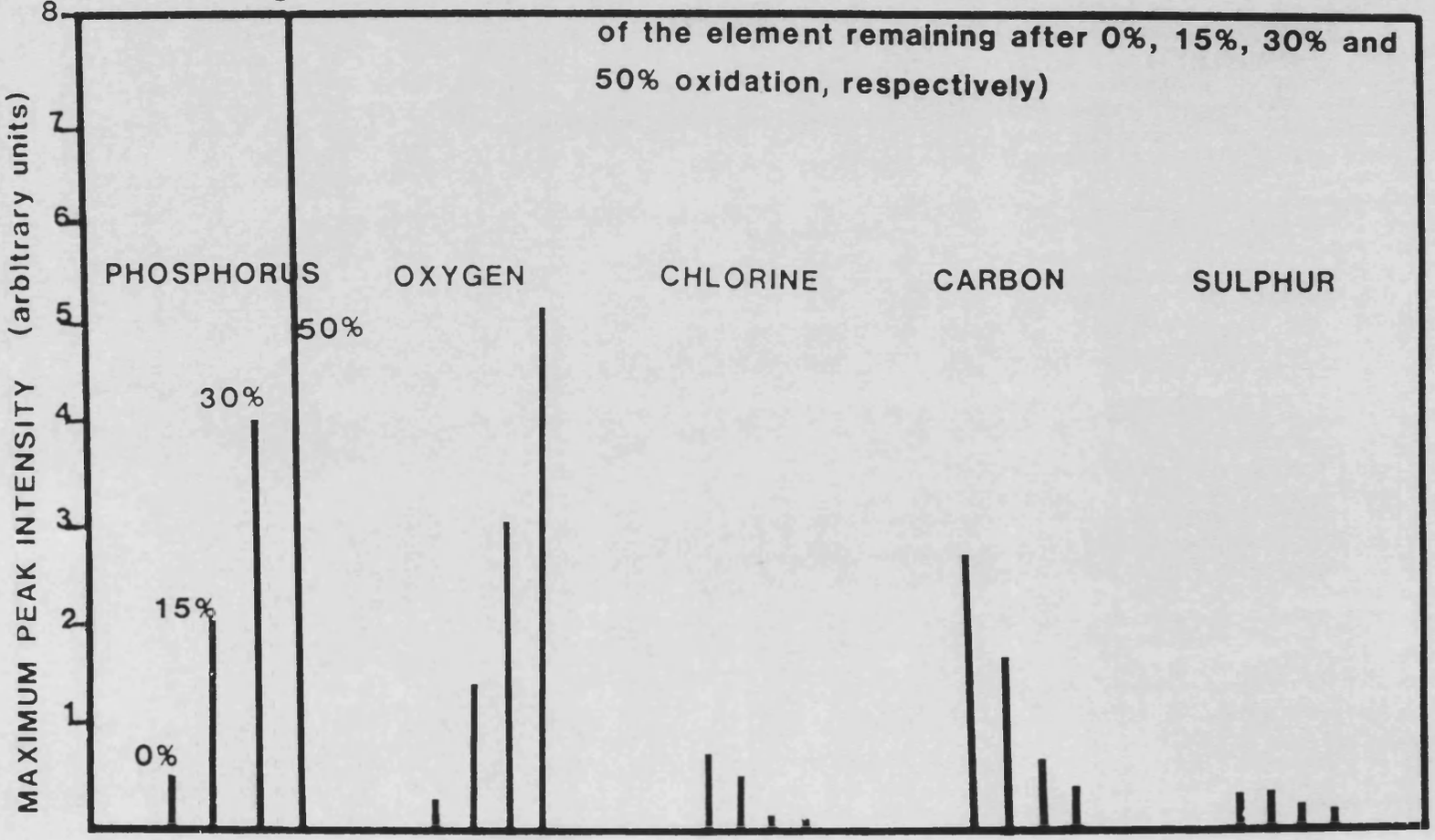

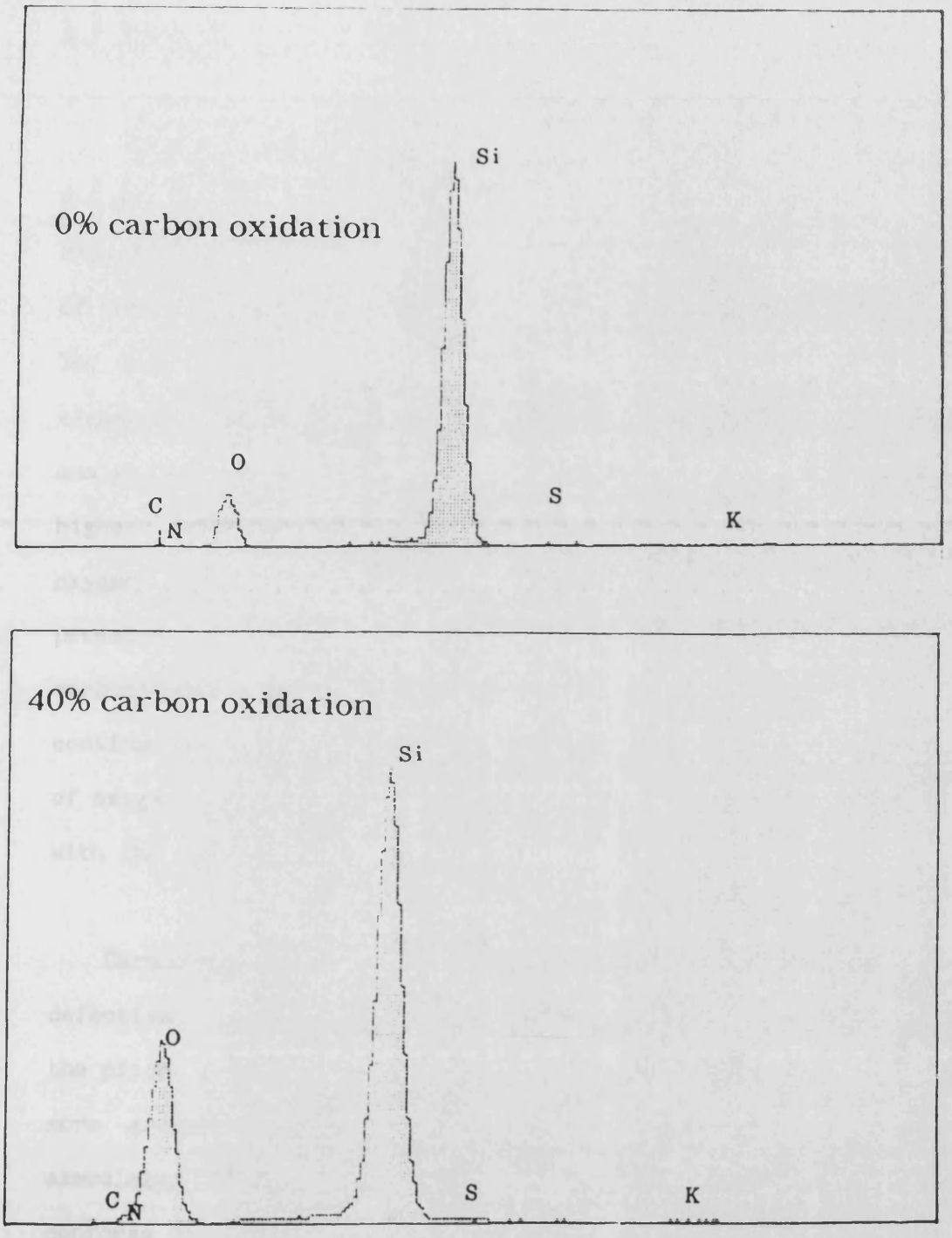


**FIG.6.10** EDAX spectra of the silicon modified carbon, Z6018

## 6.4 Chemical Analyses

Chemical analyses for carbon, hydrogen and nitrogen, i.e. C-H-N of the various materials are presented in table 6.5. Uncarbonised pitch shows a high level of carbon compared to some of the resin carbons, which upon pyrolysis is further increased. The mass balance [=(100-C+H+N)] represents the contribution from elements other than C, H, and N, including errors in the analytical method. The mass balance of the resin carbons is higher than the pitch carbons probably reflecting high levels of oxygen as well as minor (< 0.3%) inorganic impurities (33). The presence of oxygen in the resin carbons is supported by the carbonisation thermograms, e.g. Chap.4, fig.4.7, which show continuing weight loss even after heating to 1000°C. The presence of oxygen shows that the resin itself can act as an oxygen source with the result that pyrolysis is oxidative in nature (29).

Carbonisation of phenolic resins leads to a network of defective carbon layer planes which are randomly linked and for the pitch carbons, high temperature heat treatment produces a more graphitic structure. Thus high carbon content should be associated with a high thermal stability. Pitch carbon analyses conforms to the above postulate, however, PR77/10wt% HMTA, PA65 and the co-polymer PA65-90/10-PR77, although exhibiting high levels of carbon, show low levels of oxidation resistance.

C-H-N analysis of heat treated materials showed that,

generally, the carbon percentage increased with increase of HTT with a concurrent increase in $T_{0.5}$ for PT, PA65/TCEP and DP carbons, table 6.6. Hydrogen is eliminated by heat treatment and after the 1700°C treatment the hydrogen concentration falls to zero for the three materials. The decrease in mass balance for the heat treated materials is thus due to the loss of hydrogen as well as nitrogen, oxygen and inorganic impurities.

Elemental analyses of the modified resins give large mass balances indicating the presence of the additives in the resin, table 6.6. Upon carbonisation, the additives decompose with removal of the heat labile aliphatic groups, i.e. considering organophosphorus retardants, and retention of the inorganic (probably phosphorus oxide) compound(s). C-H-N analyses of PT/TCEP carbon showed that as the extent of carbon oxidation increased, there is a large increase in mass balance and a moderate decrease of carbon content. This reflects preferential loss of carbon with retention of the P containing residue, as shown by EDAX data, table 6.4.

The silicon containing novolak resin upon carbonisation shows a decrease in the carbon content from 52.13% to 34.30%, which is probably due to removal of oligomeric species and other carbon containing fragments, while the silicon containing moieties are retained. Oxidation to 40% burn-off yields a material which is entirely silicaceous, as shown by EDAX studies, and by failure to detect elemental carbon.

TABLE 6.5 Chemical analyses of the pitches and pitch and resin carbons

| | Carbon | Hydrogen | Nitrogen | Balance |
|---|---|---|---|---|
| Pitches | | | | |
| CTP | 92.3 | 4.37 | 1.16 | 2.17 |
| DP | 90.8 | 5.42 | 0.48 | 3.30 |
| PP | 89.3 | 5.29 | 0.28 | 5.13 |
| Pitch Carbon (BC 970°C) | | | | |
| CTP | 96.8 | 0.41 | 0.94 | 1.85 |
| DP | 97.7 | 0.14 | 0.31 | 1.85 |
| PP | 96.3 | 0.29 | 0.25 | 3.16 |
| Resins | | | | |
| TPSX4 | 75.3 | 5.79 | 2.45 | 16.46 |
| PR77/10-HMTA | 71.9 | 6.22 | 2.66 | 19.22 |
| PA65 | 72.1 | 5.56 | 0.82 | 21.52 |
| PT | 89.7 | 0.92 | 0.70 | 8.68 |
| Resin Carbons (BC 970°C) | | | | |
| TPSX4 | 84.9 | 1.43 | 0.65 | 13.02 |
| PR77/10-HMTA | 96.6 | 0.33 | 0.81 | 2.26 |
| PA65 | 85.7 | 0.86 | 0.50 | 12.94 |
| PT | 91.85 | 0.55 | 0.87 | 6.73 |

TABLE 6.6 Chemical analyses of DP carbon, additive modified resins, carbons, oxidised carbons and heat treated carbons

| | Carbon | Hydrogen | Nitrogen | Balance |
|---|---|---|---|---|
| Z6018 | | | | |
| resin | 52.13 | 0.06 | 4.94 | 42.87 |
| carbon | 34.30 | 1.04 | 0.17 | 64.49 |
| 40% oxidation | 0.27 | 0.05 | 0.01 | 99.67 |
| MT59 | | | | |
| resin | 68.40 | 5.40 | 0.09 | 26.11 |
| carbon | 78.1 | 0.74 | 0.68 | 20.48 |
| PA65/20-TCEP | | | | |
| resin | 61.8 | 5.35 | 0.57 | 32.28 |
| carbon 970°C | 86.0 | 0.54 | 0.52 | 12.94 |
| " 1200°C | 90.9 | 0.06 | 0.50 | 8.55 |
| " 1500°C | 92.0 | 0.01 | 0.41 | 7.58 |
| " 1700°C | 95.2 | 0.00 | 0.28 | 4.52 |
| PT/20-TCEP | | | | |
| resin | 62.1 | 4.93 | 0.86 | 32.12 |
| carbon 970°C | 85.0 | 0.38 | 0.52 | 14.10 |
| 15% oxidation | 80.2 | 1.03 | 0.76 | 18.01 |
| 50% oxidation | 78.9 | 0.74 | 0.64 | 19.72 |
| PT 970°C | 91.8 | 0.60 | 0.87 | 6.73 |
| 1200°C | 94.9 | 0.16 | 0.40 | 4.54 |
| 1500°C | 97.4 | 0.01 | 0.06 | 2.53 |
| 1700°C | 98.2 | 0.00 | 0.01 | 1.79 |
| DP 970°C | 97.7 | 0.14 | 0.31 | 1.85 |
| 1200°C | 97.8 | 0.08 | 0.21 | 2.21 |
| 1500°C | 97.9 | 0.00 | 0.13 | 2.27 |
| 1700°C | 98.2 | 0.00 | 0.01 | 1.79 |

# CHAPTER 7 TEXTURAL CHARACTERISATION

## 7.1 Scanning Electron Microscopy, (SEM)

The SEM micrographs are presented as plates. In plates P1-P5, prints are presented comparing the surface morphology of the resins, resin carbons and pitch carbons. Plates P6-P8 depicts various resin carbons after different extents of oxidation. Plates P8-P14 show the additive modified resins and their carbons after various extents of oxidation.

The effect of cure schedule on the surface morphology of TPSX4 resin is shown in plate P1, prints 1-4. The high-temperature, fast cure schedules PC3 and 150/1.5 give rise to a distorted, macroporous resin structure compared to the more uniform structure resulting from the lower temperature 110/16 and the slower 180/24 cure schedules. Plates P2-P3, prints 5-11 show the TPSX4 carbons and confirm that the structure established at the resin stage is, more-or-less, retained in the carbon. Plate P2 prints 5-8 show that the TPSX4 carbon particles are very porous due to the presence of large macropores with diameters of ~100um. The surfaces of carbons produced from resins cured at 180/24 and 110/16 contain fewer and smaller macropores. This reflects the lower porosity of the cured resins, prints 3,4. Plate P3, prints 12-14 show the presence of flow lines (due to melting), bubble-like macropores and shrinkage cracks usually associated with pitch carbons. Macroporosity is not evident in the cured

model compound saligenin and the resultant resin carbon, plate P4, print 17. The particulate surface shows indentations or surface channels which may have arisen due to shrinkage effects. The non-solvent containing PR77i resin shows the presence of macropores and surface swelling, print 16. The latter is probably caused by the build-up of pressure due to volatile gases trapped by the surface-cured resin. The PA65 and PT carbon surfaces appear to be fibrous with numerous interconnected indentations, plates P4-P5, prints 19-26. Macroporosity is not apparent.

Plate P6, prints 27-30 show that oxidation of TPSX4 carbon proceeds from the pores rather than the plane surface. The size of the pores increases with the extent of carbon oxidation. Prints 29-30, representing 50% oxidation, indicate generation of a large number of smaller pores. This is consistent with the reported observation that closed porosity, inherent to phenolic carbons, is converted to open porosity, (43). As oxidation of PA65 increases the surface appears increasingly fibrous with numerous indentations and pores being generated. The oxidised surface of PT shows distinct particulate matter apparently clinging to the carbon surface, P7, prints 35-37. Dust or impurity particles were ruled out due to their absence in PA65 and TPSX4 carbons. It is suggested that this particulate debris may have arisen as a consequence of separately polymerised TPSX4 novolak carbon, in contrast to the bulk co-polymer PT. After ~50% oxidation, two types of particles are evident in the PT carbon, P8, prints 38-40. One type exhibits a porous

sponge-like structure similar to TPSX4 while the second type contains elongated, interconnected and deep cracks. The latter particle indicates that oxidation causes build-up of stress (due to selective oxidation), which generates cracks leading to eventual powdering of the sample. A similar mode of glassy carbon oxidation has been previously reported by Heron (37).

The fire retardant is difficult to detect in the PT/TCEP resin from the SEM prints. However, evidence for the additive surface coating becomes apparent in the carbon, P8, prints 41-42. Addition of TCEP and TDCP to PT and PA65, P9, prints 43-46, results in generation of macropores of diameter 20-30um in the carbon which were absent in the unmodified carbons, e.g. PT, P5, prints 24-26.

Oxidation of the carbons was performed by isothermal heating at 1000$^{o}$C. At this temperature the additive is expected to decompose and form a surface coating on the carbon particles. The latter coating, P10-P11, prints 47-53, is clearly distinct from the particulate matter observed on the unmodifed PT carbon. The prints further show that the coating is continuous although non-uniform, i.e. globules of additive are evident. The latter may have been formed by either one, or both of the following routes:

1) Due to the high temperatures, the additive, although retained, begins to boil and upon cooling the surface bubble (or globule) morphology is retained. The globules thus represent regions of high additive concentration.

2) The glassy coating will be liquid at ~1000°C hence, the bubble structure may be due to evolution of CO from oxidation of the underlying carbon.

A bubble structure due to route 2 has been reported for coatings on carbon-carbon composites (184). Print 48 and to a lesser extent print 53, indicate that the additive also penetrates the carbon network via pores and cracks. Furthermore, as the percentage burn-off increased the additive surface becomes increasingly thicker.

As observed for the organophosphorus modified resin carbons the boronated carbon MT59 shows the presence of macropores, P11, prints 56-57. Oxidation of the carbon results in formation of a coating, which is particulate in nature rather than continuous, on the plane surface and on the pore walls, P12, prints 58,59. After 50% and 70% oxidation, particulate matter distinct from the parent particle, becomes evident. This distinctive material charges up rapidly as shown by its bright appearance compared to the carbon, and is probably a type of boron compound (164), P12, prints 60-62. The charged particles littering the carbon surface are distinguishable from the globular coating detected for the organophosphorus modified resin carbons. This may reflect a difference in the extent of crystallisation upon cooling between the boron oxide and phosphorus oxide coatings.

The surface texture of the silicon modified resin and its carbon is similar, P13, prints 63-65. After 15% oxidation large and deep cracks appear on the particle surface and a distinct

highly charged particle appears to separate from the parent (bottom left of print 66). As the percentage oxidation is increased, the charged particle becomes more dominant due to rapid carbon oxidation. The surface morphology of the charged particle is quite distinct from the carbon, P14, prints 68-69. Chemical analysis and EDAX measurements confirmed the latter particle to be entirely silica.

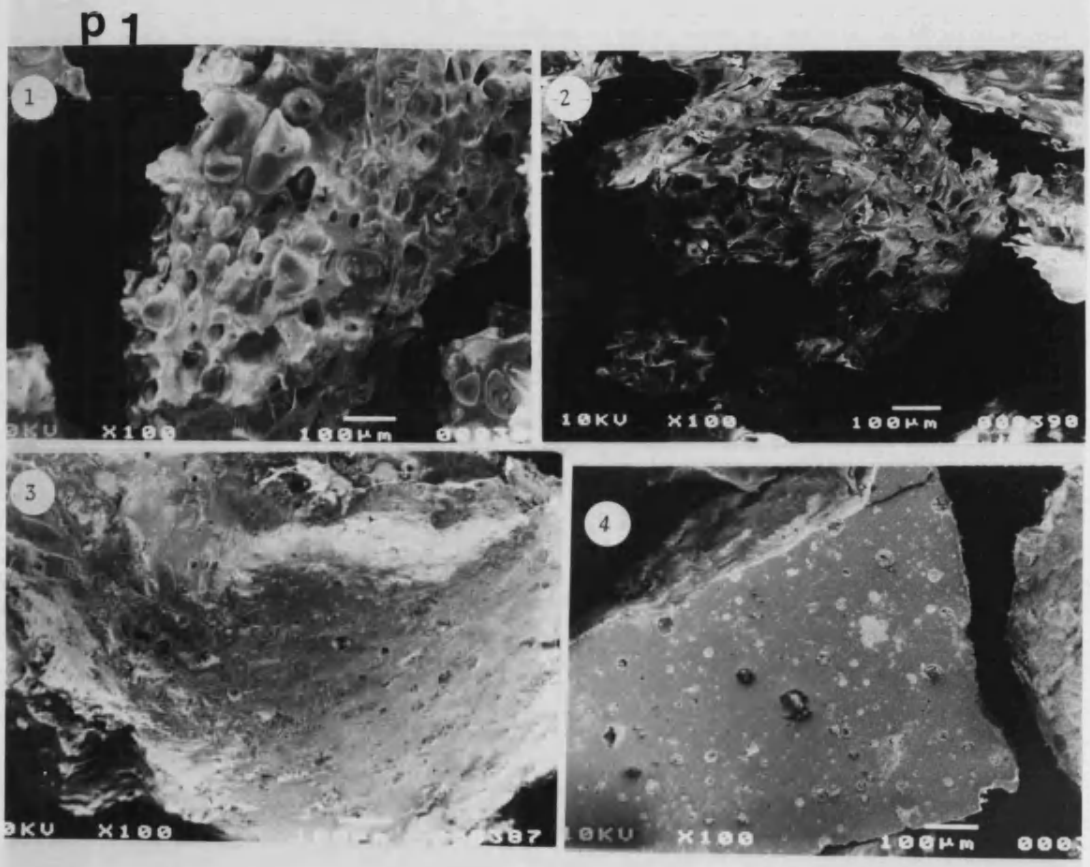


1 EFFECT OF CURE SCHEDULE ON THE SURFACE MORPHOLOGY OF THE NOVOLAK TPSX4

A) RESIN: 1) PC3 2) 150/1.5 3) 180/24 4) 110/16

p2

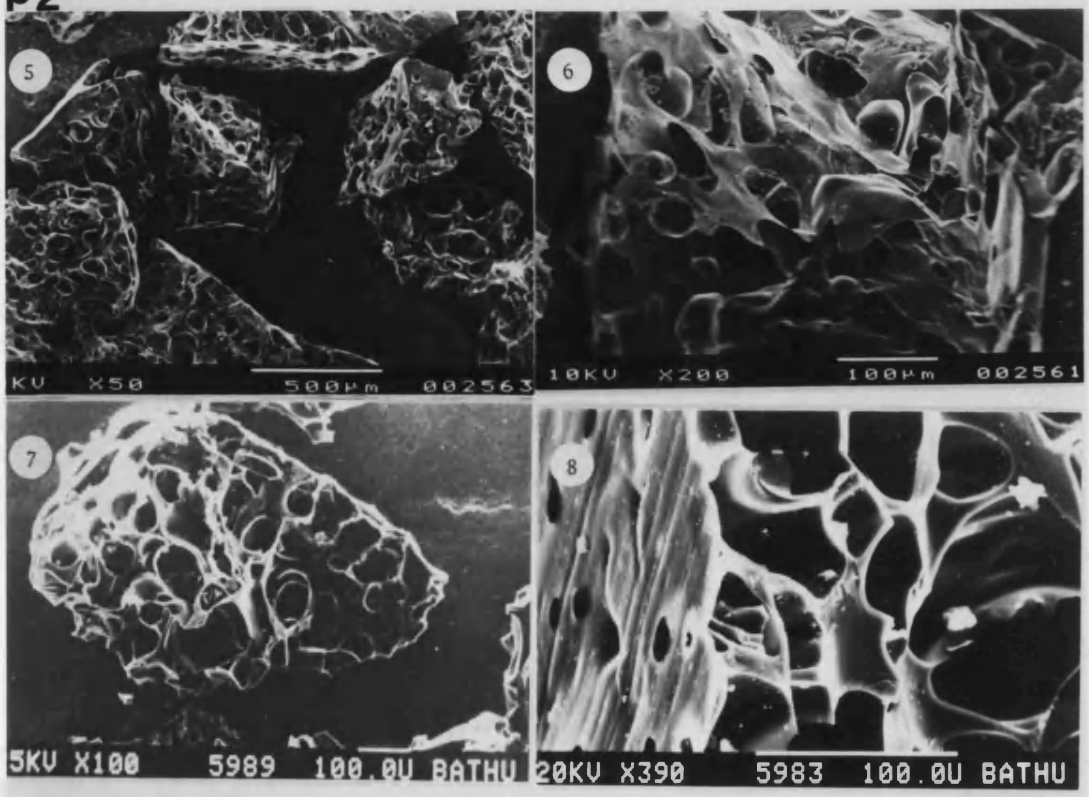


1 EFFECT OF CURE SCHEDULE ON THE SURFACE MORPHOLOGY OF THE NOVOLAK TPSX4

B) TPSX4 CARBON (BC 970): 5-6) PC3 7-8) 150/1.5

p3

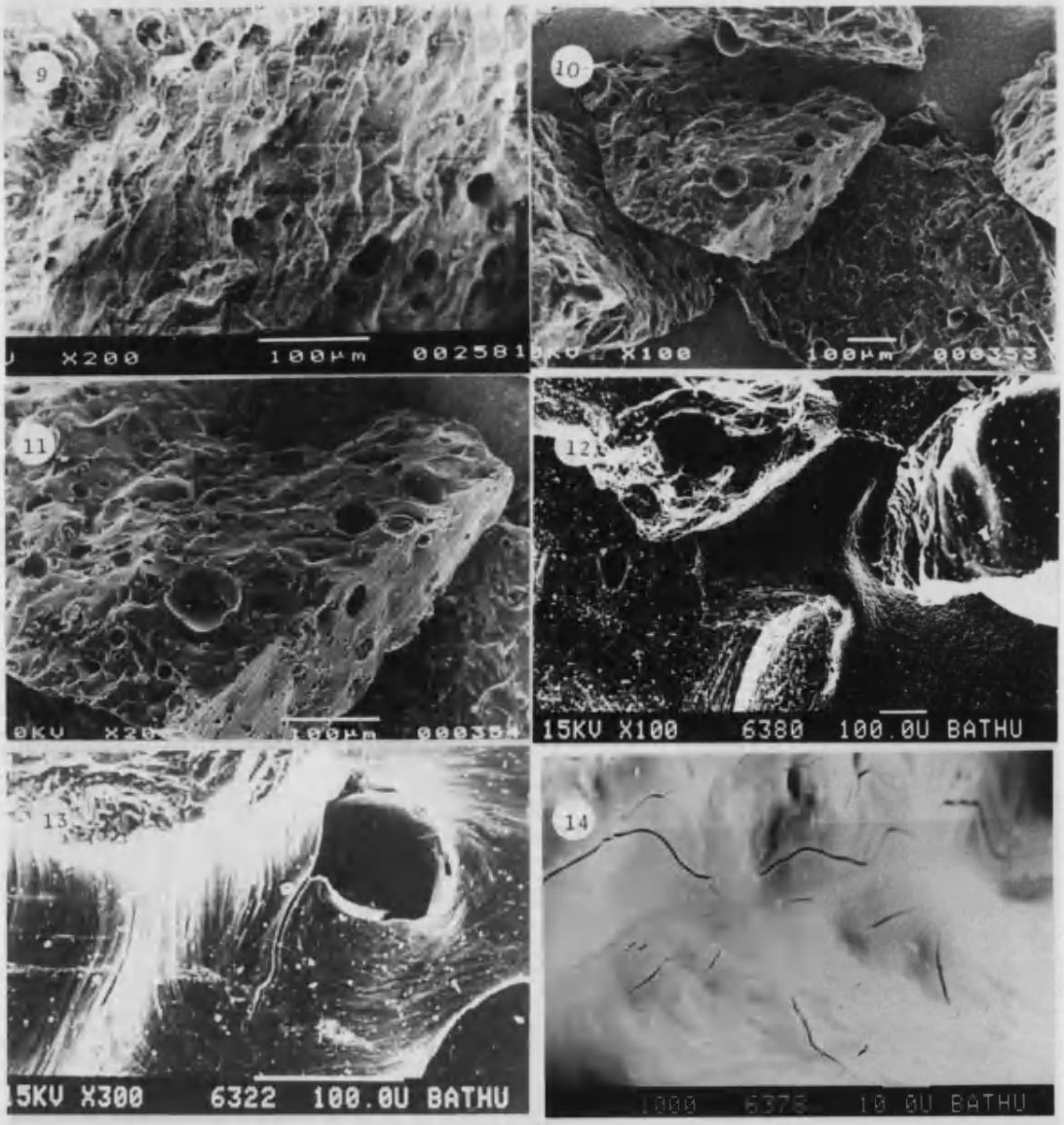


1 EFFECT OF CURE SCHEDULE ON THE SURFACE MORPHOLOGY OF THE NOVOLAK TPSX4: B)TPSX4 CARBON (BC 970); 9) 180/24 10-11) 110/16

2 SURFACE MORPHOLOGY OF THE PITCH CARBONS (BC 970): 12) DP 13) PP 14) CTP

p4

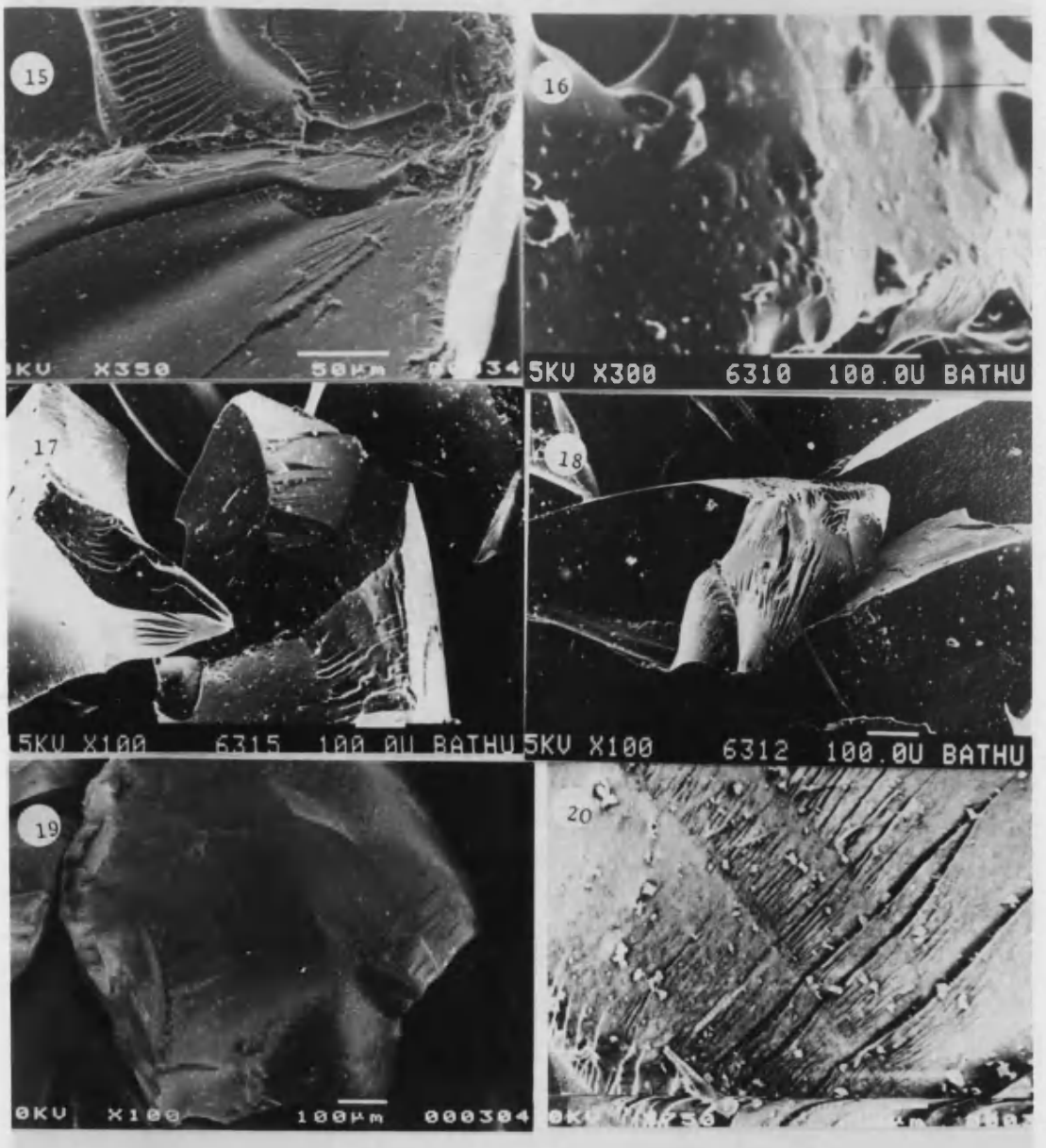


3 SURFACE MORPHOLOGY OF THE RESIN AND SALIGENIN CARBONS

15) PR77 16) PR77I 17) SALIGENIN 18) FRD2244

4 SURFACE MORPHOLOGY OF PA65

19-20) ~~RESIN~~ (180/24)

p5

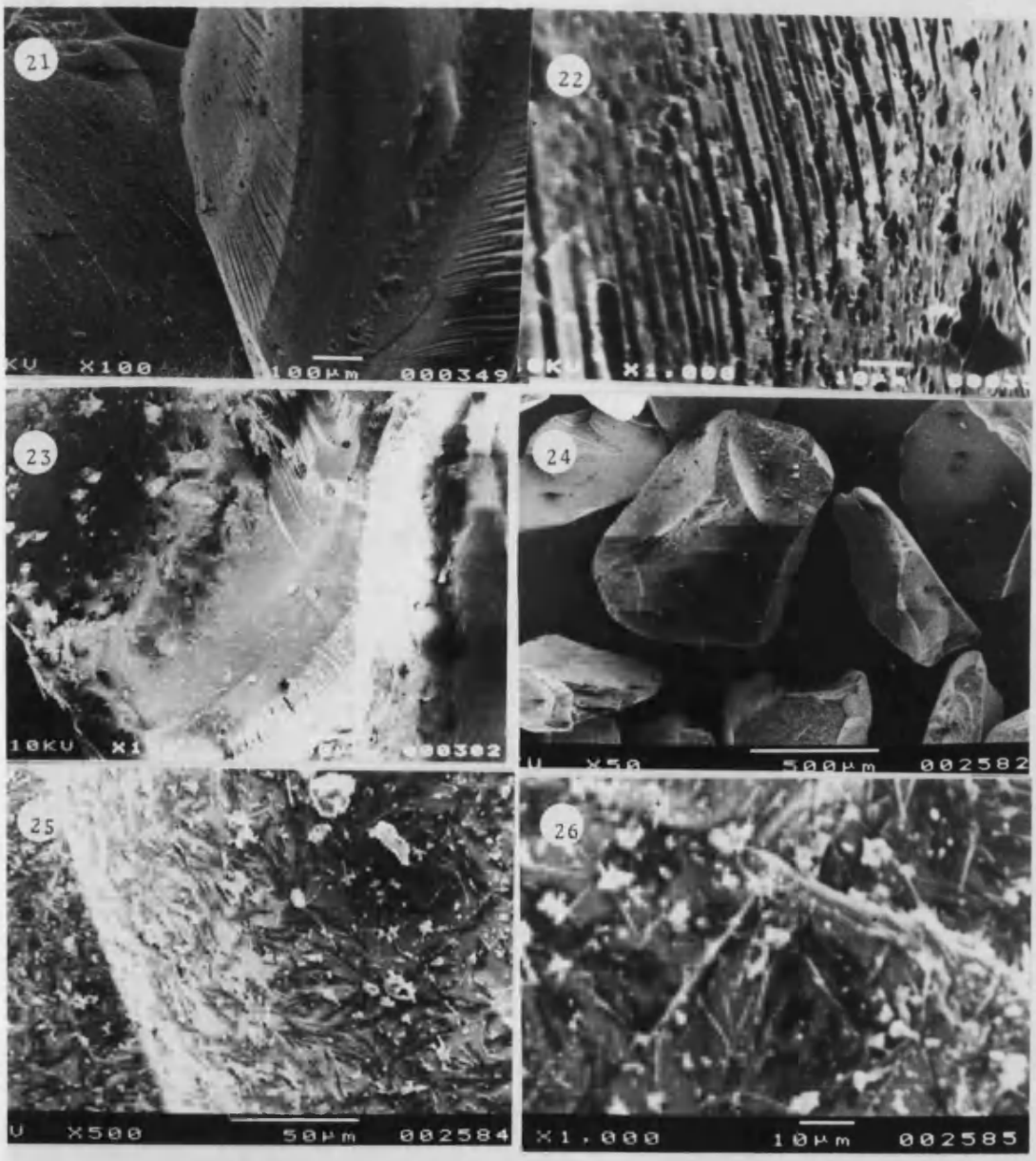


4 SURFACE MORPHOLOGY OF PA65 21-22) CARBON (BC 970)

5 SURFACE MORPHOLOGY OF THE RESOLE/NOVOLAK COPLOYMER (PT)

23) RESIN (180/24) 24-26) CARBON

p 6

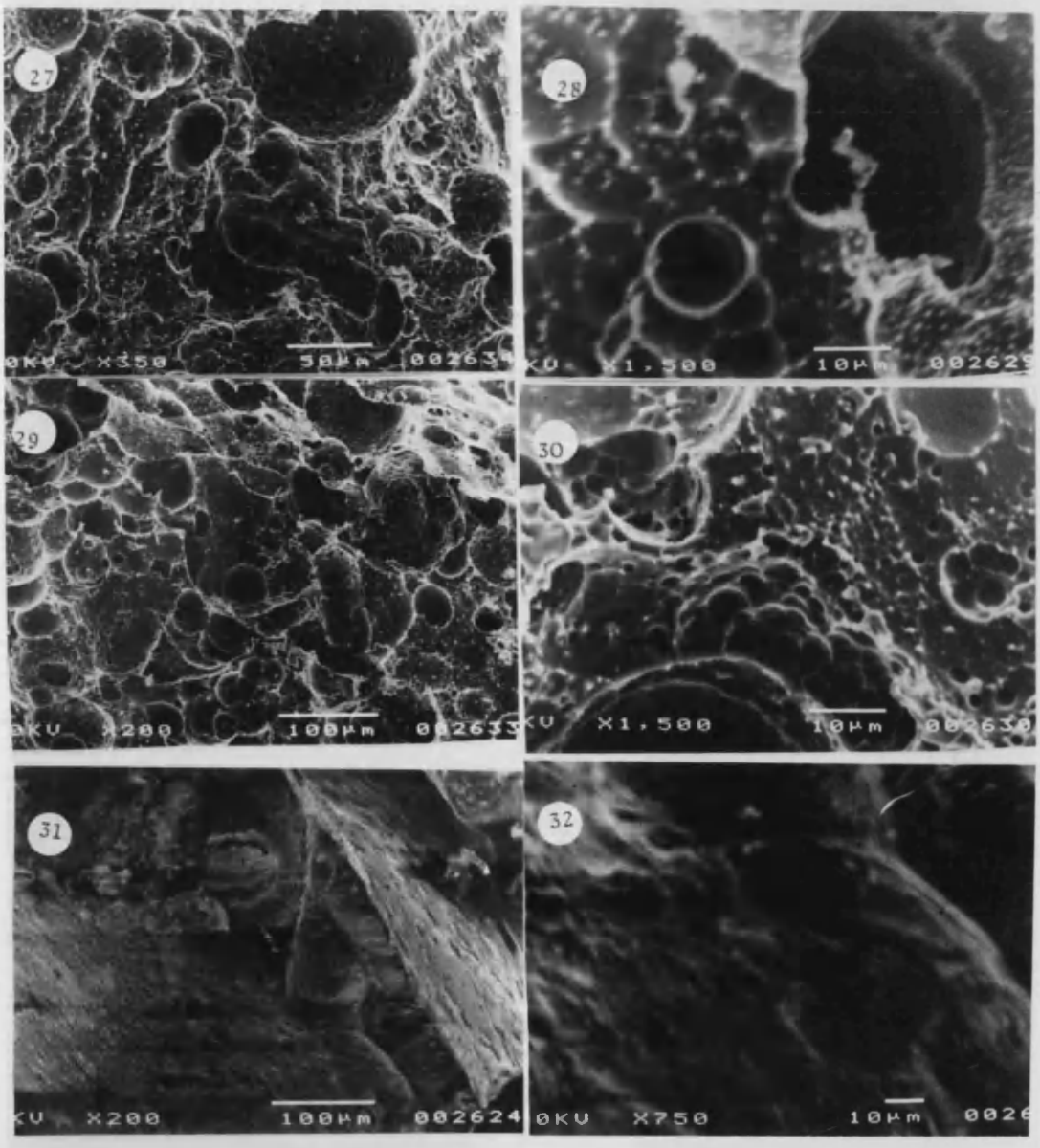


6.a EFFECT OF BURN-OFF (%) ON SURFACE MORPHOLOGY OF TPSX4 CARBON

27-28) 15% 29-30) 50%

6.b EFFECT OF BURN-OFF (%) ON THE SURFACE MORPHOLOGY OF PA65

31-32) 15%

p7

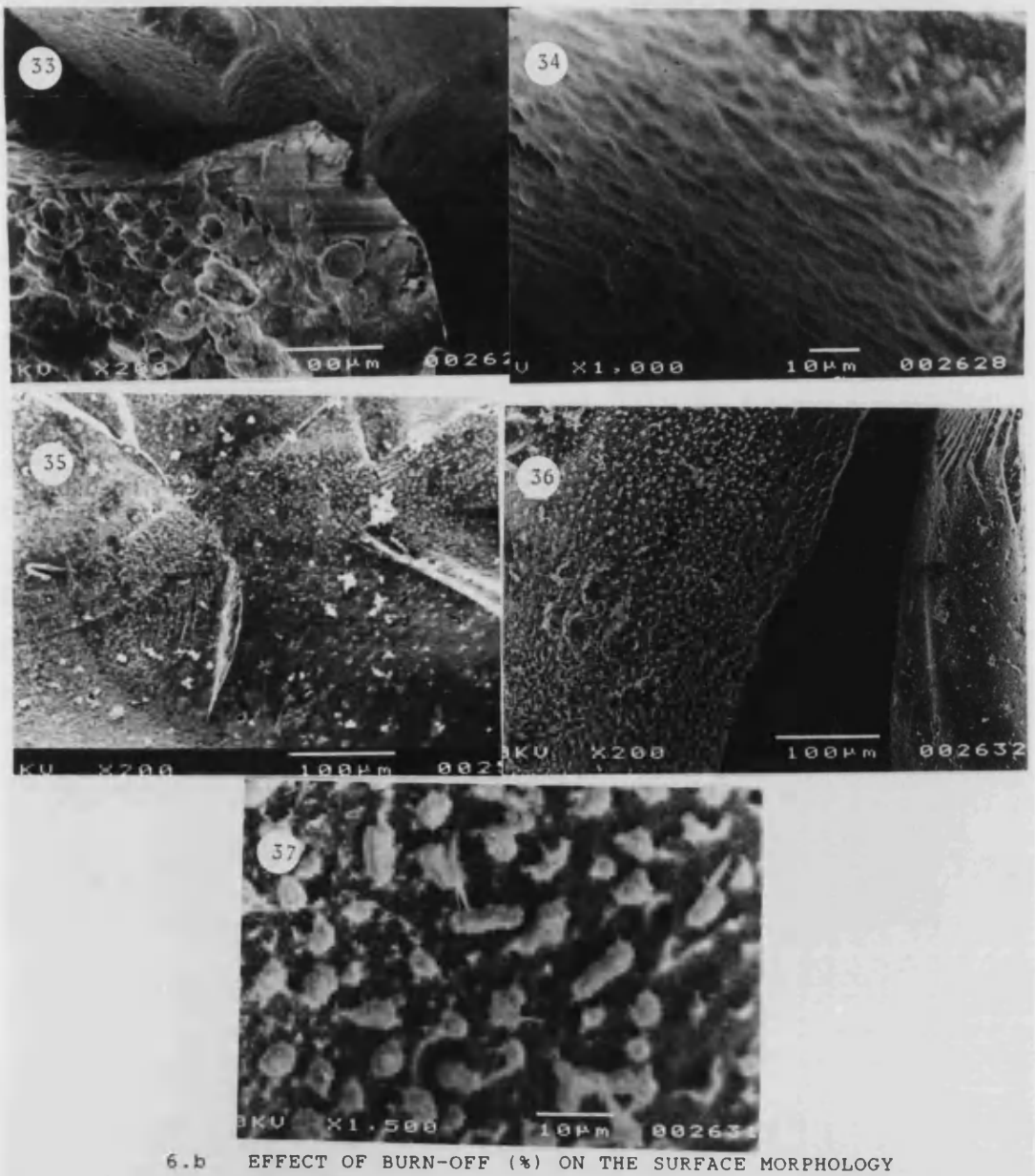


6.b EFFECT OF BURN-OFF (%) ON THE SURFACE MORPHOLOGY OF PA65

33-34) 50%

6.c EFFECT OF BURN-OFF (%) ON THE SURFACE MORPHOLOGY OF PT

35) 15% 36-37) 30%

p8


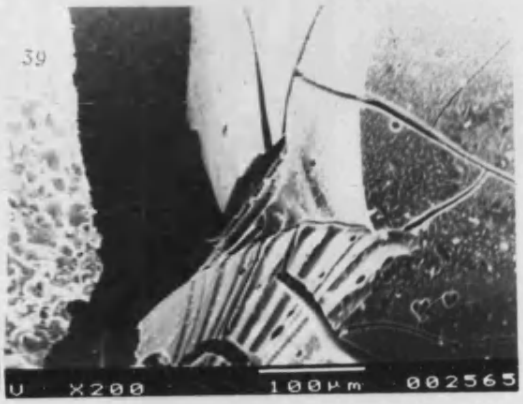



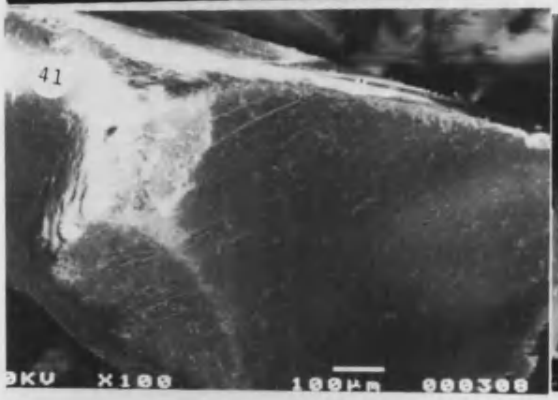


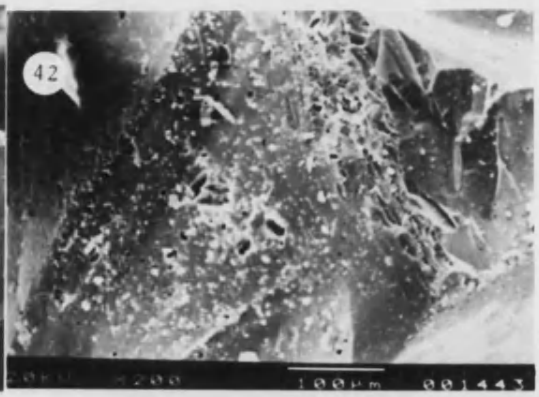


6.c EFFECT OF BURN-OFF (%) ON THE SURFACE MORPHOLOGY OF PT

38-40) 50%

7.a EFFECT OF TCEP (20%) DEPOSITION ON SURFACE MORPHOLOGY OF THE COPLOYMER PT

41) RESIN (180/24) 42) CARBON (BC970)

p9

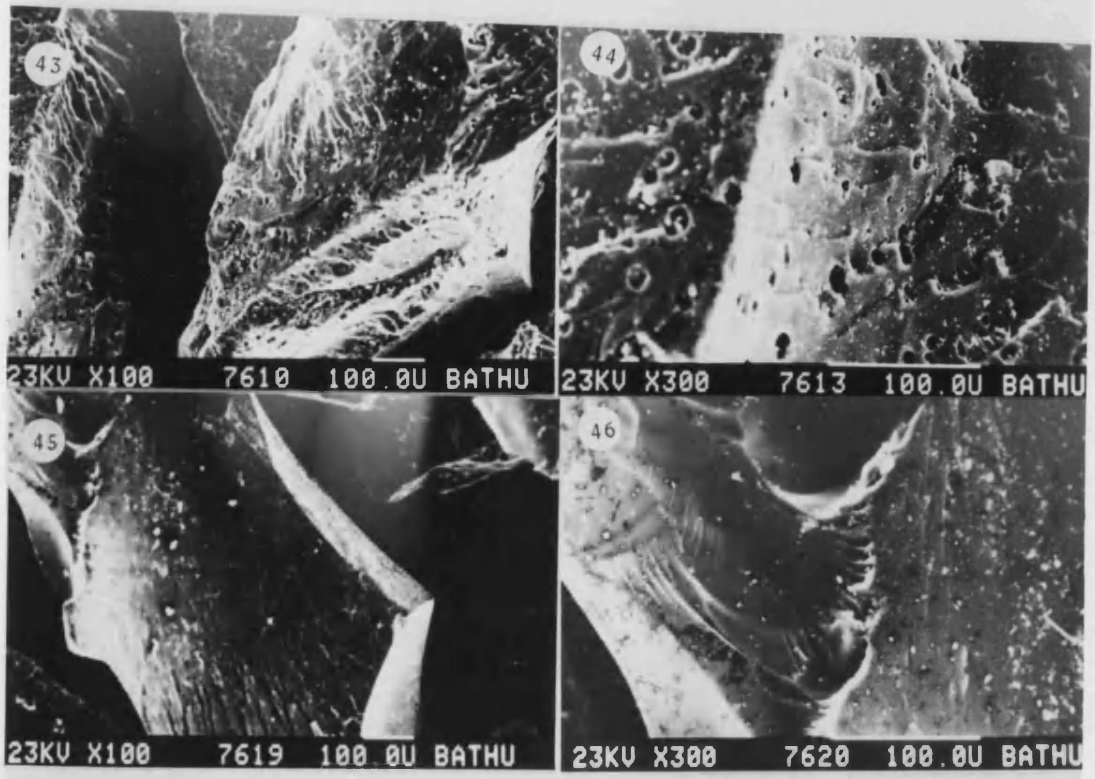


7.b DISTRIBUTION OF TDCP IN PA65 AND PT CARBONS
43-44) PT 45-46) PA65

P10

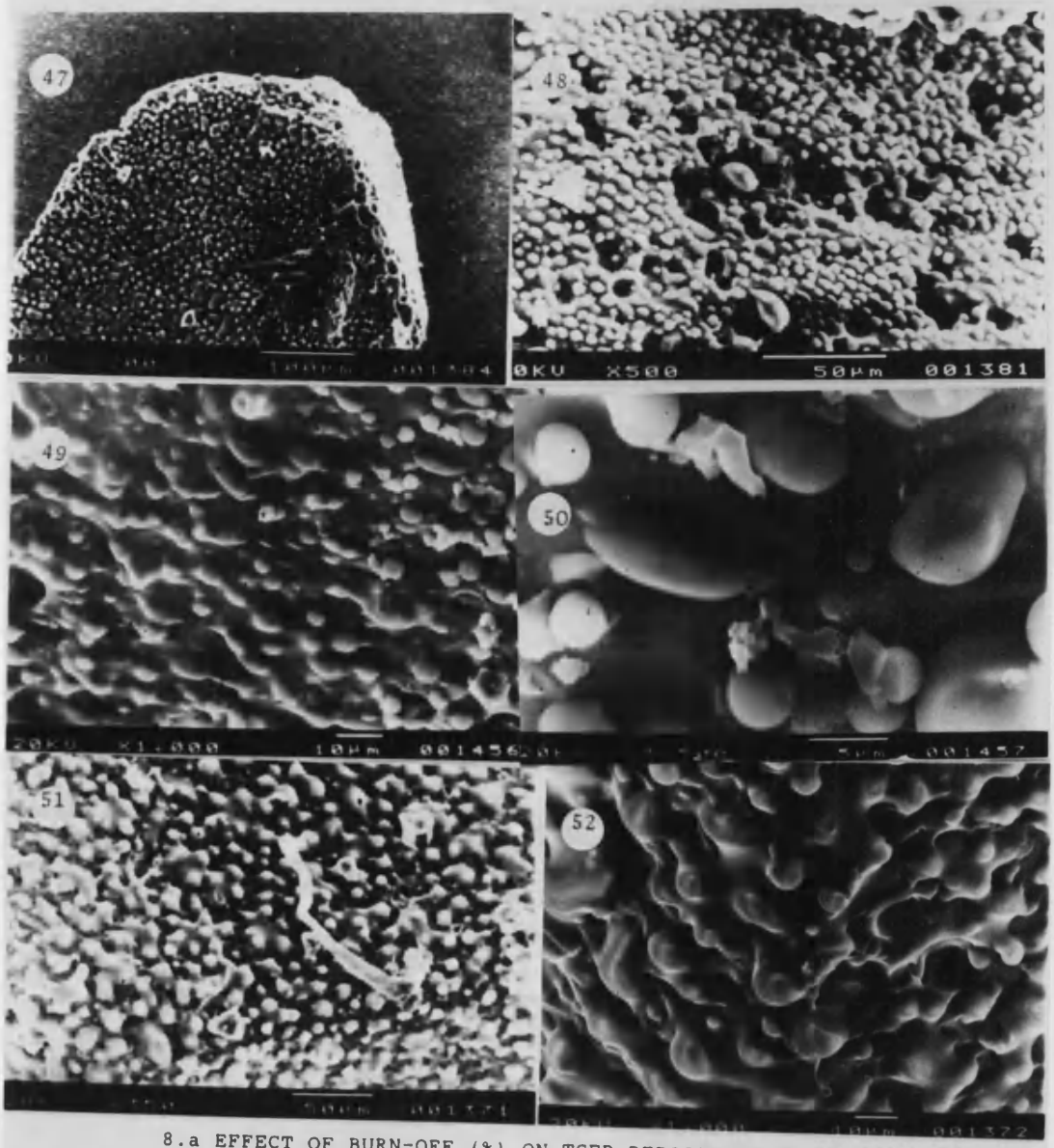


8.a EFFECT OF BURN-OFF (%) ON TCEP DEPOSITION ON PT CARBON SURFACE

47-50) 15%

8.b EFFECT OF BURN-OFF (%) ON TCEP DEPOSITION ON PT CARBON SURFACE

51-52) 30%

p11

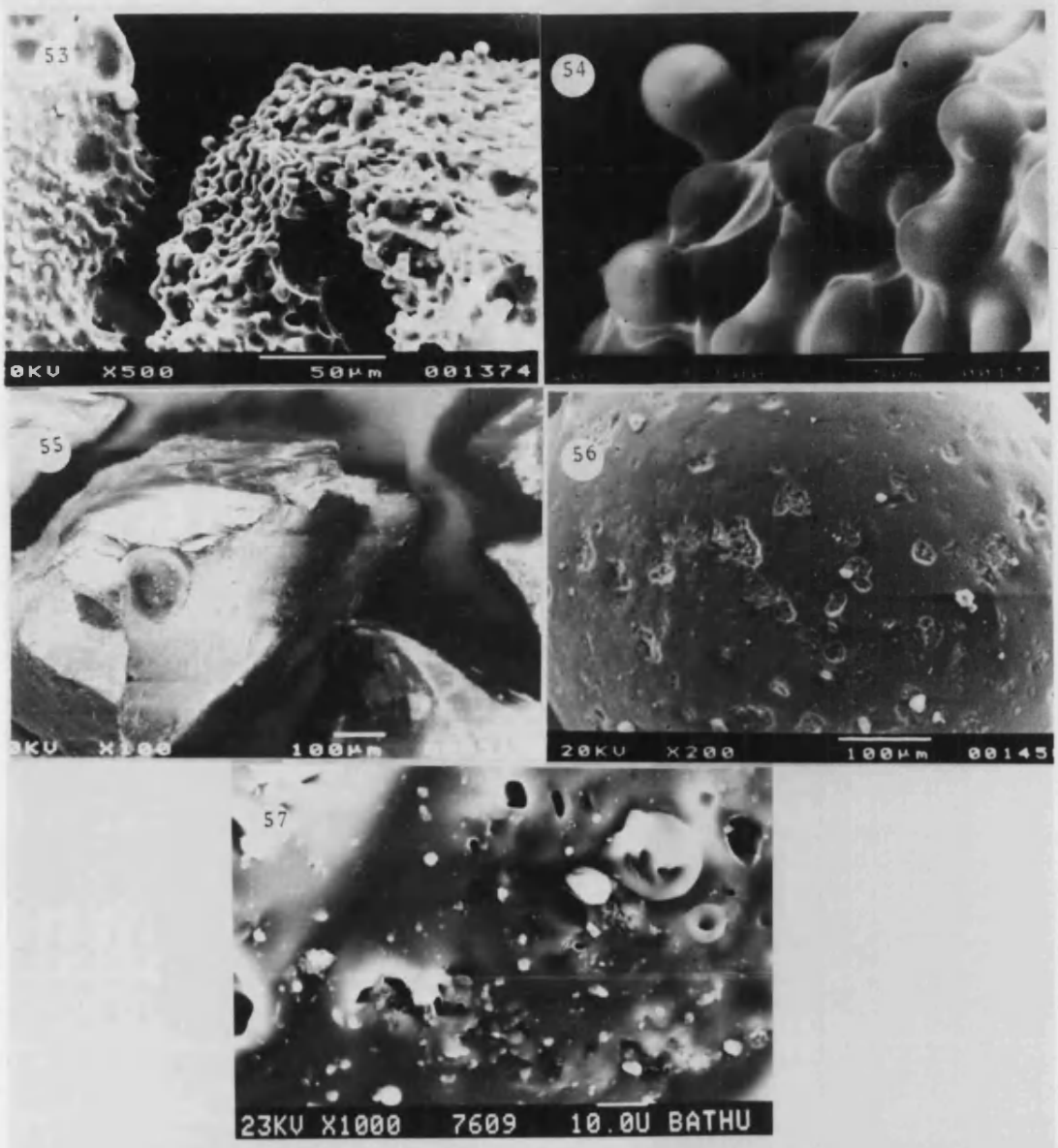


8.b EFFECT OF BURN-OFF (%) ON TCEP DEPOSITION ON PT CARBON SURFACE

53-54) 50%

9 SURFACE MORPHOLOGY OF THE BORONATED NOVOLAK RESIN AND CARBON

55) RESIN (180/24) 56-57) CARBON (180/24)

p12

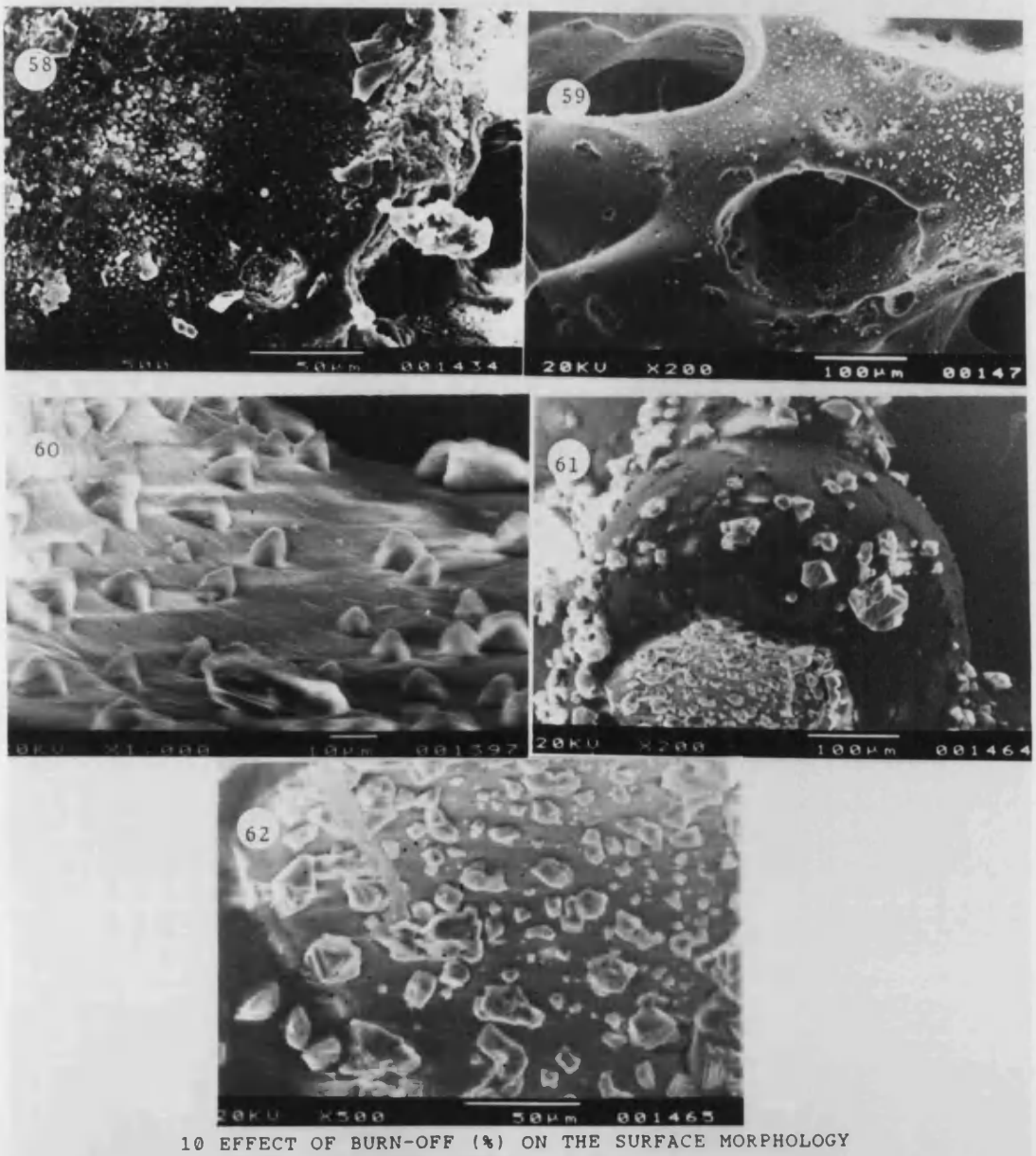


10 EFFECT OF BURN-OFF (%) ON THE SURFACE MORPHOLOGY OF THE BORONATED NOVOLAK CARBON

58) 15% 59) 30% 60) 50% 61-62) 70%

p13

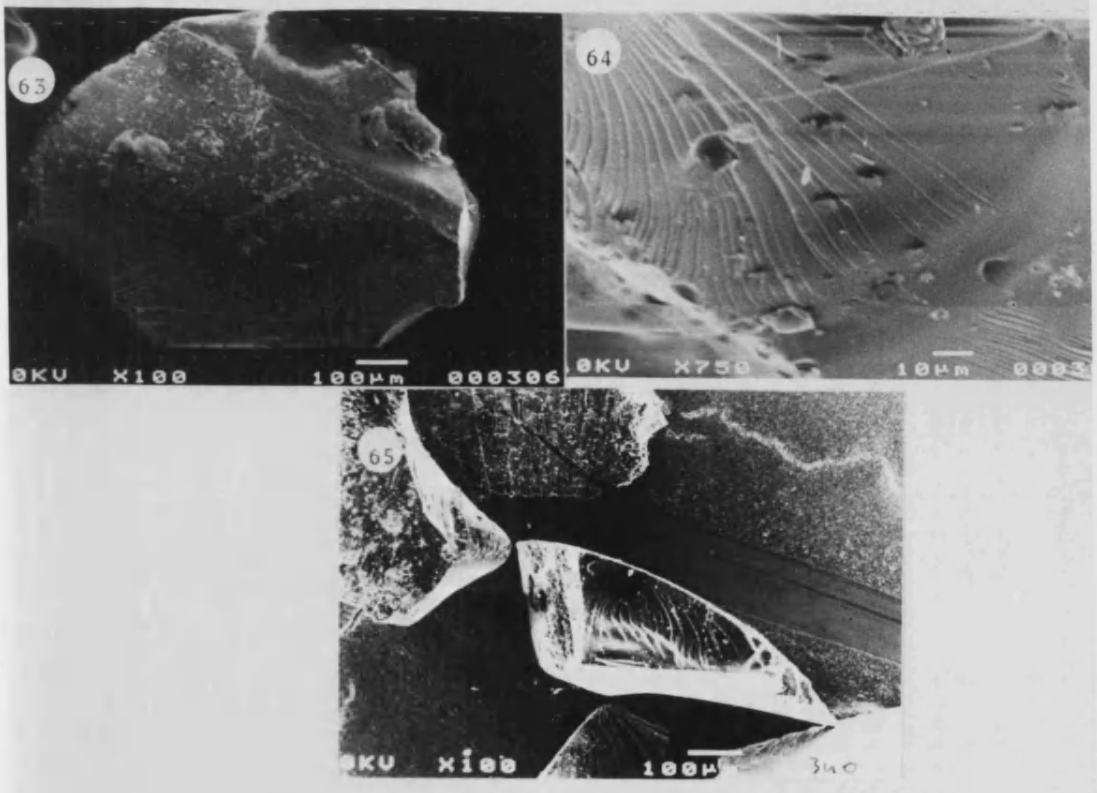


11 SURFACE MORPHOLOGY OF THE SILICON MODIFIED NOVOLAK RESIN AND ITS CARBON

63-64) RESIN (180/24) 65) CARBON (BC 970)

p14

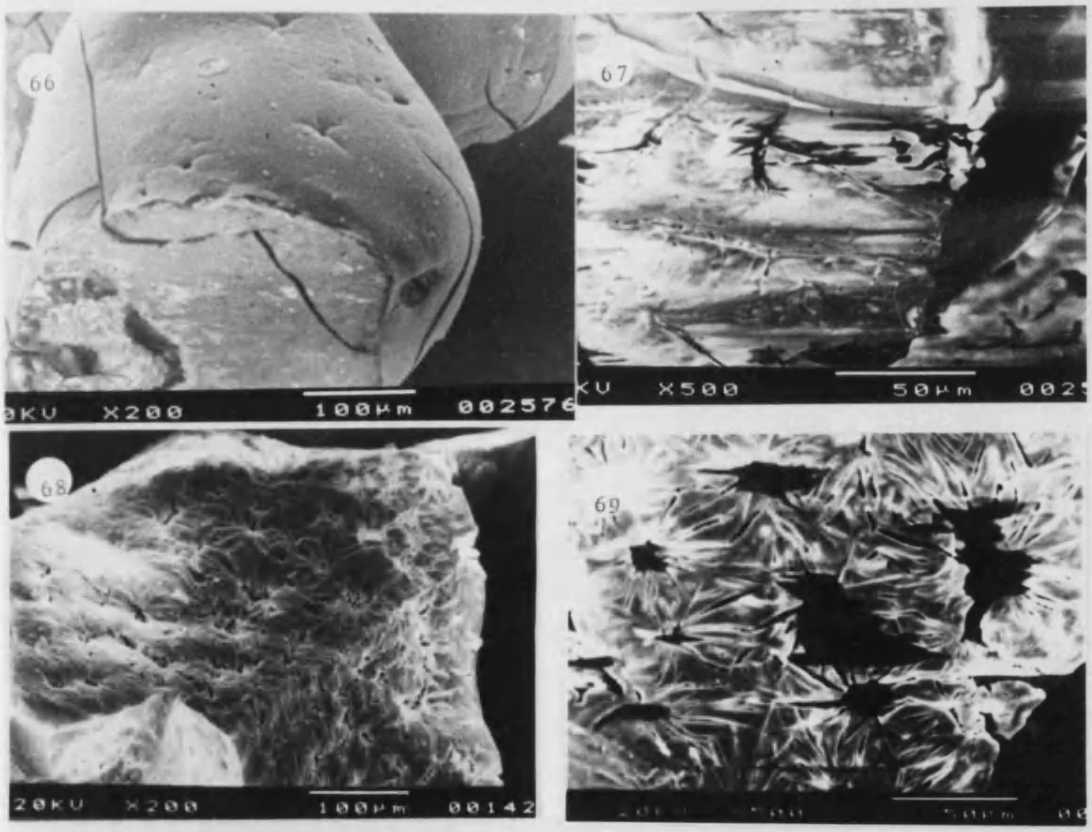


12 EFFECT OF BURN-OFF (%) ON THE SURFACE MORPHOLOGY OF THE SILICON MODIFIED CARBON

66) 15% 67) 30% 68-69) 40%

## 7.2 Adsorption Studies

### 7.2.1 Introduction

In addition to supplying information on surface areas of solids, adsorption isotherms, i.e. the amount of gas adsorbed on a solid, at a fixed temperature, as a function of gas pressure, and theories developed to explain and characterise them, have provided further structural information. Adsorption isotherms have been classified into five types viz. the Brunauer, Demming, Demming and Teller, BDDT, classification (185), Appendix 2. Developments of the adsorption theories have lead to adoption of the following slit width nomenclature when describing porous materials: macropores, >50nm; mesopores, 2-50nm and micropores, <2nm, respectively. In effect macropores and mesopores have been shown to exhibit adsorption potentials approximately equal to that exhibited by normal (plane) surfaces. Thus these pores are referred to as admission and diffusion pores, respectively. Most of the adsorption and any gas/adsorbent reactions are reported to occur mainly in micropores. The micropore range has been further sub-divided into ultra-micropores and super-micropores of slit width 0.53-0.8nm and 0.8-2nm, respectively. Dubinin (186) reports that most of the adsorption occurs in the micropore range (>90%) with ultra-microporous adsorption dominating.

### 7.2.2 A Brief Review on the Development of the Adsorption Theory

The Langmuirian theory of adsorption, 1918 (187-188) assumes that 1) adsorption occurs on localised sites; 2) all sites are of equal energy; and 3) adsorption is limited to a monolayer. Physical adsorption however, involves formation of multiple molecular layers. The Langmuir approach was thus modified to account for multilayer adsorption by Brunauer, Emmett and Teller (189), the BET equation (equation 1). In addition to the monolayer the BET approach takes into account adsorption of second and subsequent layers as being equivalent to the condensation of the bulk gas to a liquid. The BET equation allows calculation of monolayer capacities and surface areas provided the size of the adsorbate molecule is known. For an infinite number of layers, the BET equation is:

$$\frac{P}{n(P_o-P)} = \frac{1}{n_m C} + \frac{C-1}{n_m C}\frac{P}{P_o} \quad \text{.....1}$$

where $P_o$ is the saturated vapour pressure of the adsorptive, n is the amount of gas adsorbed in g/g of adsorbent at an equilibrium pressure, P, $n_m$ is the monolayer capacity per gram of adsorbent, i.e. the amount of adsorptive required to cover the surface with a molecular monolayer and C is the BET constant, i.e.

$$C = \exp[(q-L_v)/RT]$$

where q is the heat of adsorption of the first layer and $L_v$ is the heat of adsorption of second and subsequent layers and is equal to the latent heat of vapourisation of the adsorptive.

A plot of $P/n(P_o-P)$ vs $P/P_o$ should yield a straight line of slope, S, equal to $(C-1/n_mC)$ and intercept, i, of $(1/n_mC)$. Solving simultaneous equations gives: $n_m = 1/(S+i)$ and $C = (S/i)+1$. The total surface area, TSA or specific surface area, $A_s(m^2/g)$, of the adsorbent can thus be computed using equation 2 and $n_m$ derived above.

$$A_s = (n_m/M).a_m.N_A \times 10^{-18} \quad \ldots\ldots\ldots\ldots\ldots\ldots 2$$

where $a_m$ is the cross-sectional area of the adsorptive molecule, $nm^2$, M is the molecular weight of the adsorbate and $N_A$ is Avogadro's number.

Although the BET approach is widely used anomalous results are obtained when applied to microporous adsorbents. Unrealistically high surface areas have been reported for microporous carbons, e.g. saran char was reported to have $A_s = 3000m^2/g$. However the calculated surface area of an extended graphite layer plane counting both sides is only $2628m^2/g$ (190). This erroneous result is due to the fact that adsorption in micropores does not occur by successive build-up of molecular layers as implied by the BET theory. Micropores have been associated with an adsorption potential, A, defined as the isothermal work done by the adsorption forces on transferring a molecule from a gaseous phase to a particular point above the surface, emanating from the pore walls (191-192). In ultra-micropores, an enhanced adsorption potentfal is predicted due to overlap of the force fields from opposite pore walls. The enhanced adsorption potential in

micropores thus induces an adsorption process described as primary or micropore filling rather than surface coverage (193). Thus when reporting surface areas, the term specific surface area should be replaced by 'monolayer equivalent area'. The adsorbate in the micropores was shown to have a density ($\rho_1$) approximately equal to that of the bulk liquid adsorptive. When converted to a liquid volume (= $n/\rho_1$), by use of the density of the liquid adsorptive, it may be taken as equal to the micropore volume.

By development of the Polanyi-Potential theory (191-192), Dubinin and Radushkevich (189) were able to describe more accurately the adsorption of gases by microporous carbons and thus calculate the micropore volume, $V_o$, from the derived DR equation, equation 3.

$$V = V_o \exp -(A/E)^2 \quad \text{.....3}$$

where V is the amount adsorbed at a relative pressure ($P/P_o$), $V_o$ is the micropore volume, E is an energy constant (i.e. a function of the adsorbent-adsorptive system), A [= RT $\ln(P_o/P)$], is the adsorption potential; where R is the gas constant and T is the absolute temperature. Dubinin (189) showed that the energy constant, E, was related to the characteristic energy, $E_o$, (which was related to the the microporous structure of the adsorbent), and a scaling factor or affinity coefficient $\beta$. The latter is determined by comparing the isotherms of a given adsorptive with that of a standard adsorptive, e.g. benzene, for which $\beta$=1. The scaling factor allows the characteristic curves for different adsorptives on the same adsorbent to be superimposed. The assumption that adsorption is confined to

micropores is more acceptable at a lower relative pressure, i.e the DR equation is applicable in the relative pressure range, $P/P_o$ <0.1, although for some adsorbents a linear relationship may be obtained over a wider range. The linear form of the DR equation is:

$$\log V = \log V_o - D \log^2(P_o/P) \quad \ldots\ldots\ldots\ldots 4$$

where D is the DR isotherm constant [= $-(RT/E)^2$]. Thus plots of log V versus $\log^2(P_o/P)$, should yield a straight line of intercept on the ordinate equal to $V_o$ and a slope equal to D. The latter provides an indication of the microporous structure of the adsorbent, i.e the mean micropore diameter. A low value of D is associated with a steep rise of the adsorption isotherm at low relative pressures due to the presence of microporosity.

Deviations from linearity give rise to uncertain $V_o$ values but do provide structural information. Marsh and Rand classified three types of deviations from the DR equation (194-195), see also Appendix 2:

Type A (also shown by a reduction of the DR constant, D): Two linear sections with a downward deviation at low relative pressures. Such a deviation has been associated with activated diffusion (196-197) due to presence of ultra-micropores, or micropores having constricted entrance diameters, or entrances blocked by deposited volatiles or overhanging peripheral long chain carbon radical groupings attached to edge carbon atoms.
Type B: The DR plot is curved over the whole pressure range and

is characteristic of highly activated carbons with burn-off levels >30%.

Type C: The DR plot exhibits a linear section at low relative pressure and a positive deviation at high relative pressure. The latter deviation is postulated to represent the occurrence of capillary condensation in mesopores.

Further methods are available to provide more accurate information for materials prone to the above deviations, including the Dubinin-Astakhov, DA equation (198), the $\alpha_s$-plot and t-plot (199), nonane-preadsorption and isotherm substraction methods (200). Since it was deemed unnecessary to utilise these methods in the present work, they are not discussed further. Ample literature is available explaining the various methods (201-205).

### 7.2.3 Results and Discussion

Calibration of the apparatus was performed using reference materials: 1) Volumetric; helium gas being non-adsorbed was used for the determination of the 'dead volume', fig.7.1a.

2) Gravimetric spring balance; the spring constants were determined from the slope of extension vs weight graphs, fig.7.1b. The accuracy of the technique was tested using two Anthrasorb carbons of known surface area, fig.7.2. Application

of the BET equation, using a value of $0.162nm^2$ for the nitrogen cross-sectional area, $a_m$, gave an experimental total surface area, TSA, of $640\pm10m^2/g$ and $1035\pm15m^2/g$, respectively. The reported values were $612\text{-}640m^2/g$ and $1015\text{-}1040m^2/g$. Due to variation of $a_m$, Gregg and Sing (189) proposed an acceptable error range of $\pm20\%$ when using $0.162nm^2$ as $a_m$ for nitrogen.

3) Gravimetric microbalance; the apparatus was calibrated using Vulcan-3G, a non-porous graphitised carbon black often used as a standard reference material. The adsorption isotherm obtained using nitrogen at $77^oK$ is presented in fig.7.3. Application of the BET equation gave a TSA of $72.2\pm2.9m^2/g$ cf. reported value of $71.3\pm2.7m^2/g$.

The porosity of the adsorbent is known to effect the choice of the value for $a_m$ and the effective saturation vapour pressure $P_o$ of the adsorptive (204). For porous adsorbents, the $P_o$ value of the supercooled liquid has been recommended viz. 760Torr for nitrogen at $77^oK$. Nitrogen adsorption isotherms at $77^oK$ of the carbons are presented in Fig. 7.2-7.3, along with the reference materials. Activated diffusion effects of nitrogen at $77^oK$ were allowed for by using an equilibration time of 1.5-2h when obtaining adsorption points at low relative pressures, i.e. the BET range (197, 200).

The isotherms of the samples show that adsorption takes place in two stages. Micropore filling, when present, and monolayer adsorption occur at low relative pressures and are followed by

multilayer adsorption. In some cases capillary condensation occurred on the surface outside the micropore structure. Thus TPSX4 carbon, fig.7.2, shows a high adsorption at low relative pressures indicative of a considerable amount of microporosity. At higher relative pressure the isotherms exhibit a rounded knee which suggests presence of mesoporosity. The bulk of the adsorption in PA65 and PT carbons, fig.7.3, also occurs at low relative pressure, although the amount adsorbed is much less than on TPSX4 carbon, suggesting the presence of a reduced microporosity. It is difficult to classify these isotherms according to the BDDT classification since the experimental data do not extend to $P/P_o=1$. However the presence of a flat plateau in the BET range, fig.7.3, appears to indicate a type 1 (microporous) classification.

Fire retardant incorporation into PA65 dramatically decreases the amount of gas adsorbed, fig.7.3. This suggests that the additive decomposes during curing/carbonisation to form a surface coating which additionally penetrates and blocks off the microporosity. The pitch carbon, PP, gave an isotherm which was difficult to define, although the absence of microporosity is easy to discern, fig.7.3. The amount adsorbed is clearly much less than for the resin carbons. Adsorption on CTP and DP carbons was too small to be measured. It was thus concluded that these pitch carbons must possess lower surface areas than PP.

The BET plots for PP and resin carbons are linear over the relative pressure range from 0.005 to 0.12, although TPSX4 carbon

shows a linear range extending to 0.25, fig.7.4. The BET surface areas, i.e. monolayer equivalent areas, are presented in table 7.1. These surface areas are not corrected for the surface area of the ash in the carbons. However this is not expected to significantly affect the surface area value since the ash is present in small amounts. As implied by the adsorption isotherms, the BET surface areas of the resin carbons are greater than the pitch carbon. TPSX4 exhibits the highest TSA (=310$m^2/g$), table 7.1. The additive modified carbon PA65/TCEP exhibits the lowest TSA (=1.1$m^2/g$). Gregg and Sing (189) report that a high value for the BET constant C, a limited linear BET range, i.e. 0.05-0.1, and a high TSA are indicative of microporous carbons. This is observed for TPSX4 carbon, although the BET linear range is extended to 0.25. PA65 and PT carbons have lower surface areas and BET C values than TPSX4 carbon.

Typical DR plots for the carbons are presented in fig.7.5. PA65 and PT carbons give more-or-less linear plots. TPSX4 however shows a slight positive deviation at high relative pressures. The latter is linked to capillary condensation in mesopores. The presence of mesoporosity in TPSX4 is further indicated by the rounded knee of the adsorption isotherm, fig.7.2. The DR plots of PP and PA65/TCEP carbons exhibit a distinct upward deviation at high relative pressures indicating presence of well defined mesoporosity. The micropore volume, $V_o$, determined by extrapolation of the linear part of the DR plot to $\log^2(P_o/P)=0$ and the DR constant, D, obtained from the slope of the linear section, are presented in table 7.1. The micropore volume varies

in a similar manner to the surface area.

An increase in D corresponds to a decrease in the characteristic free energy, $E_o$, of the system which implies an increase in pore size (189). Thus PP and PA65/TCEP show a high D value, 0.17 and 0.07 respectively, compared to the resin carbons, D<0.024. This implies negligible levels of microporsity as confirmed by the very low micropore volumes, and presence of pores of mesopore/macropore dimensions. The TSA values for PP and PA65/TCEP carbons are low suggesting that large pores make only minor contribution to adsorption. For TPSX4 carbon, the low value of the DR constant and the high micropore volume, $V_o$, indicates a high level of microporosity, while the rounded knee of the adsorption isotherm implies presence of mesopores.

In summary, the adsorption isotherms, DR and BET plots yield the following information on the carbons:

TPSX4- an extensive pore size distribution is evident ranging from ultra-micropores (as implied by the steep rise in the adsorption isotherm at low relative pressures) to wider mesopores, shown by the rounded knee of the adsorption isotherm, high BET C value and positive deviation at high relative pressure of the DR plot. TPSX4 exhibits the highest TSA.

PA65 and PT- carbons show a reduced TSA and microporosity compared to TPSX4 but no mesoporosity.

PP and PA65/TCEP- carbons show no microporosity although mesoporosity is evident from the DR plots, and exhibit a very low TSA.

FIG.7.1 Determination of adsorption apparatus parameters: a) Volumetric; the 'dead volume' using helium gas as adsorbate at 77°K, b) Gravimetric; the spring constants

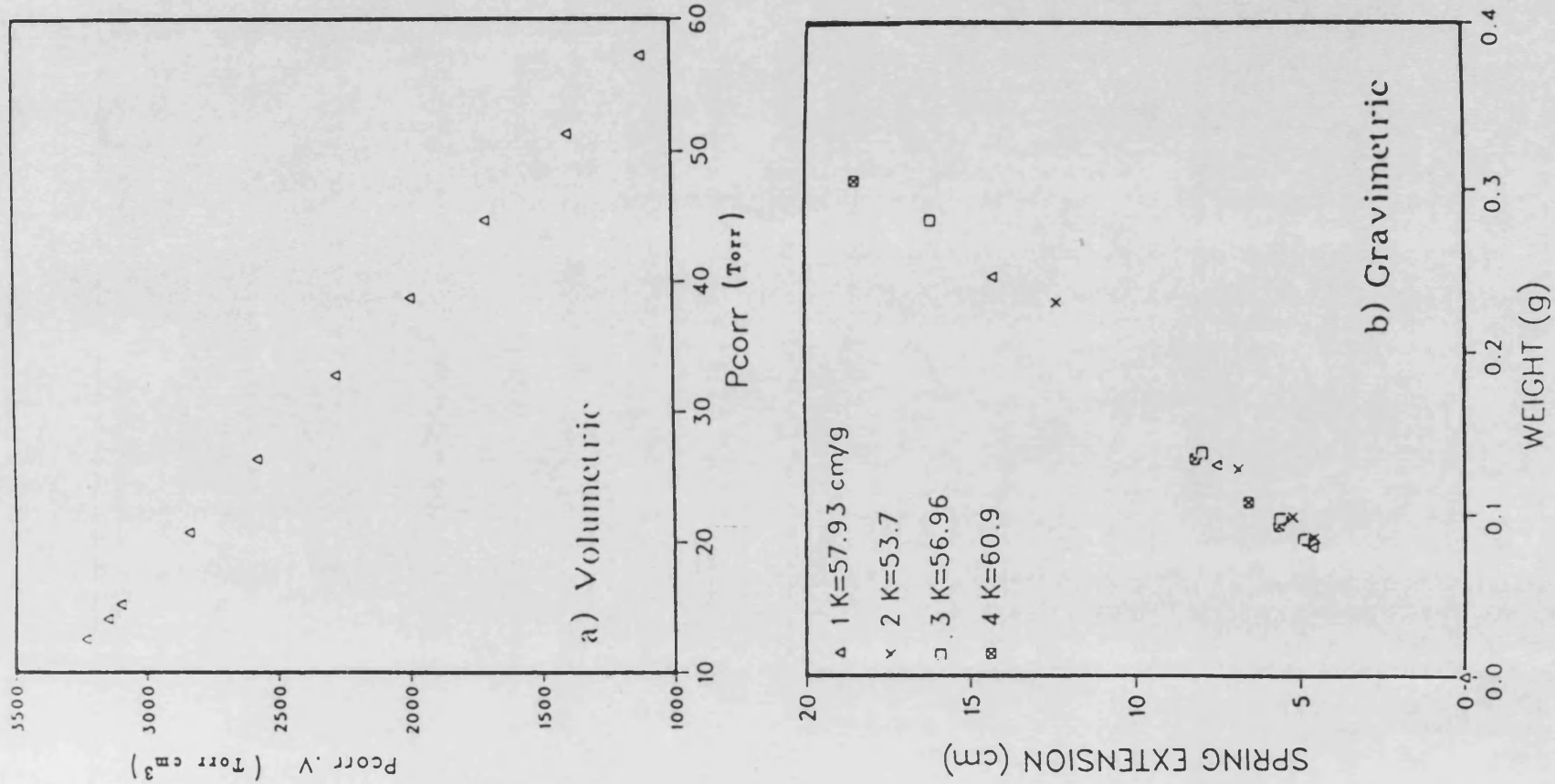

FIG.7.2 Nitrogen adsorption isotherms of Anthrasorb and TPSX4 carbons (77°K)

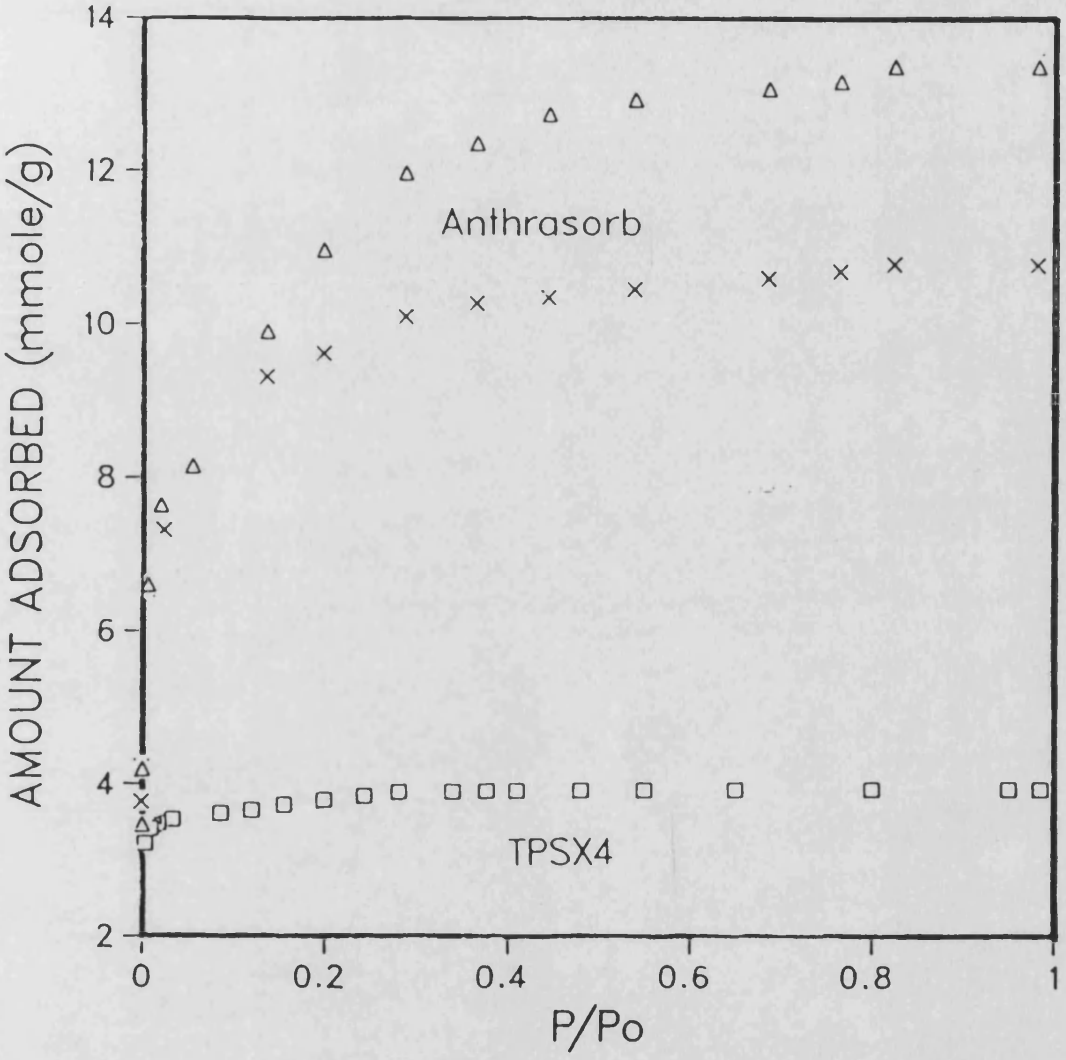

FIG.7.3 Nitrogen adsorption isotherms at 77K of the low surface area carbons

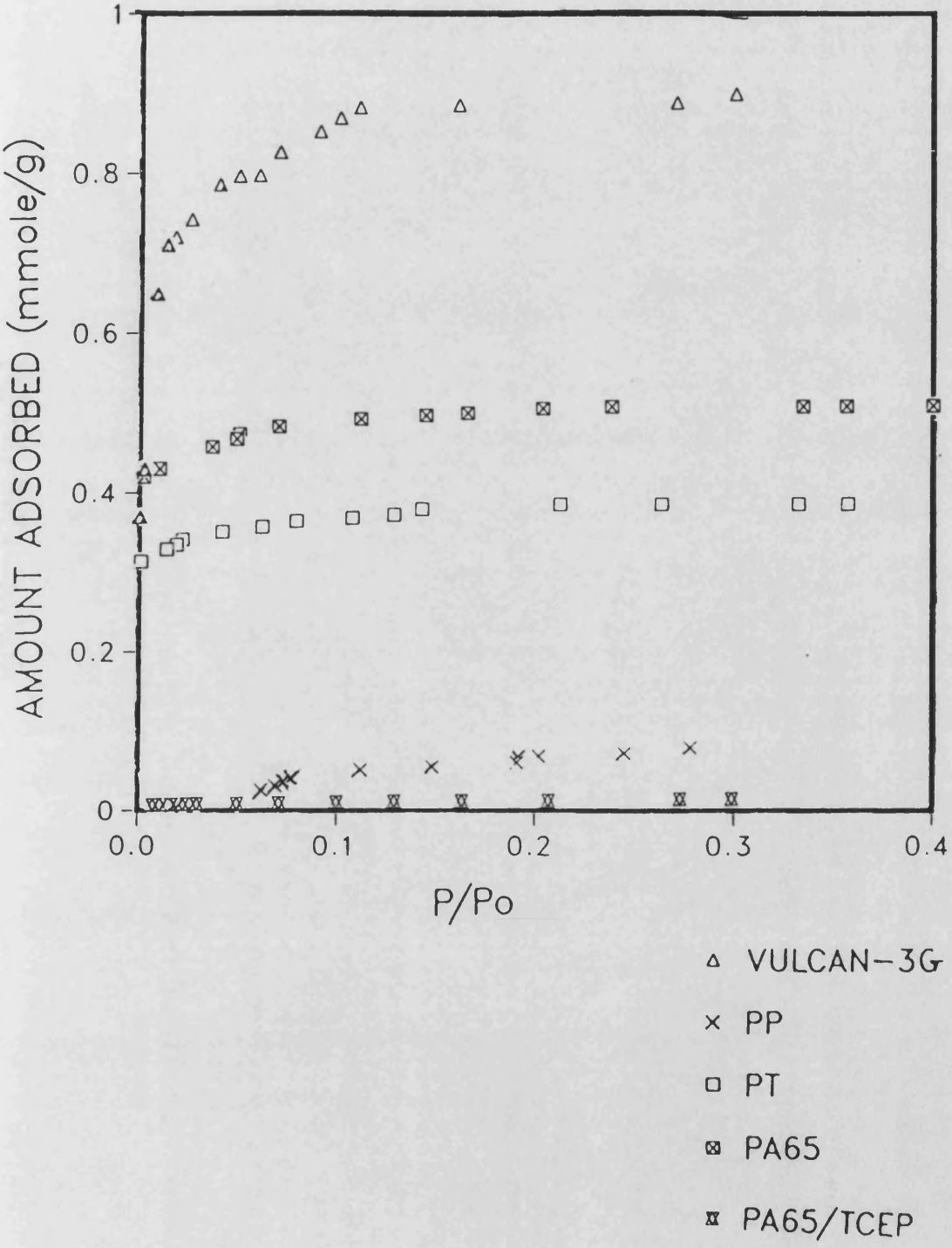

FIG.7.4 The BET plots for resin and pitch carbons using data from nitrogen adsorption isotherms at 77K

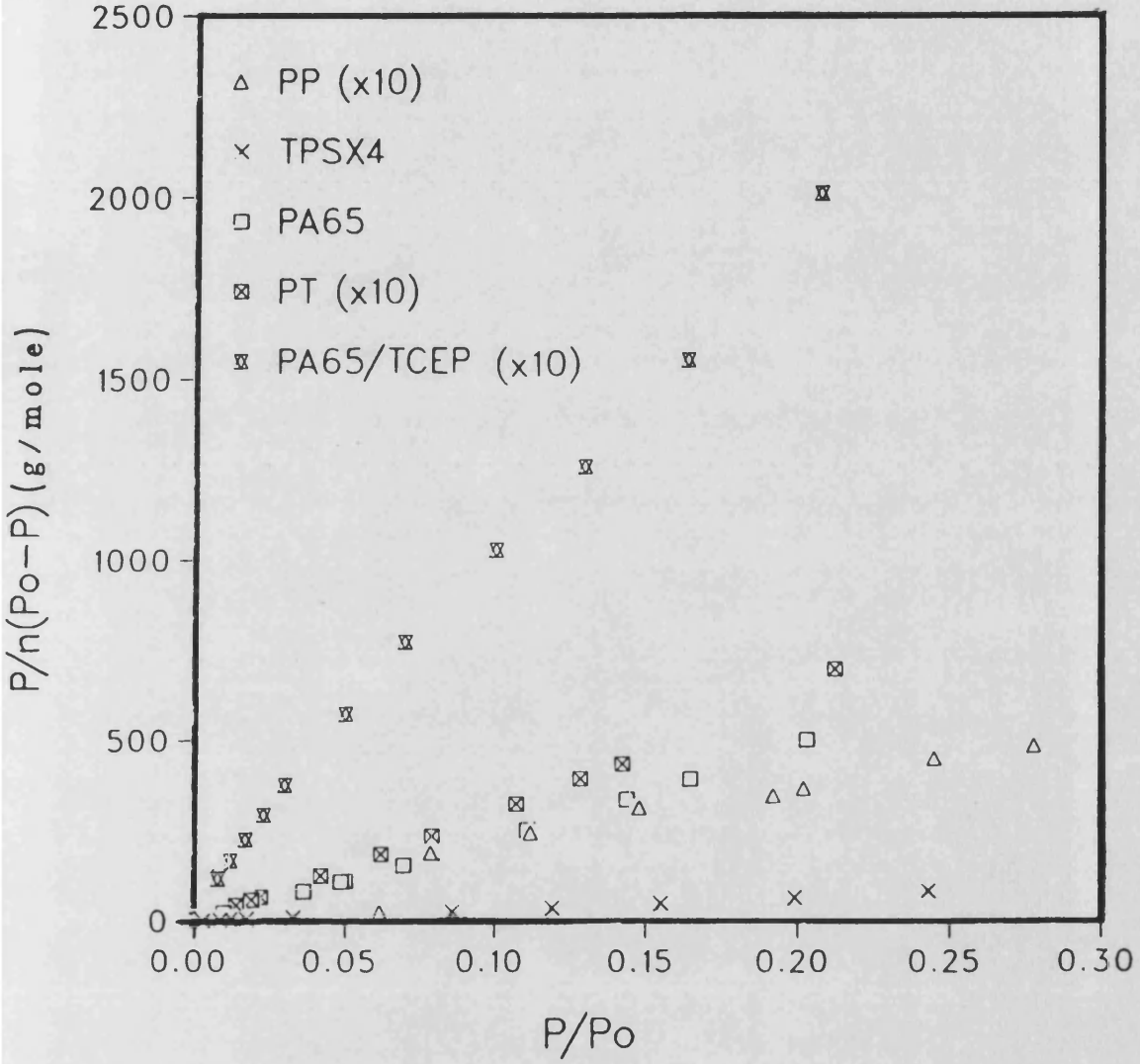

FIG.7.5 Adsorption isotherms of nitrogen at 77K plotted in DR co-ordinates for the resin and pitch carbons

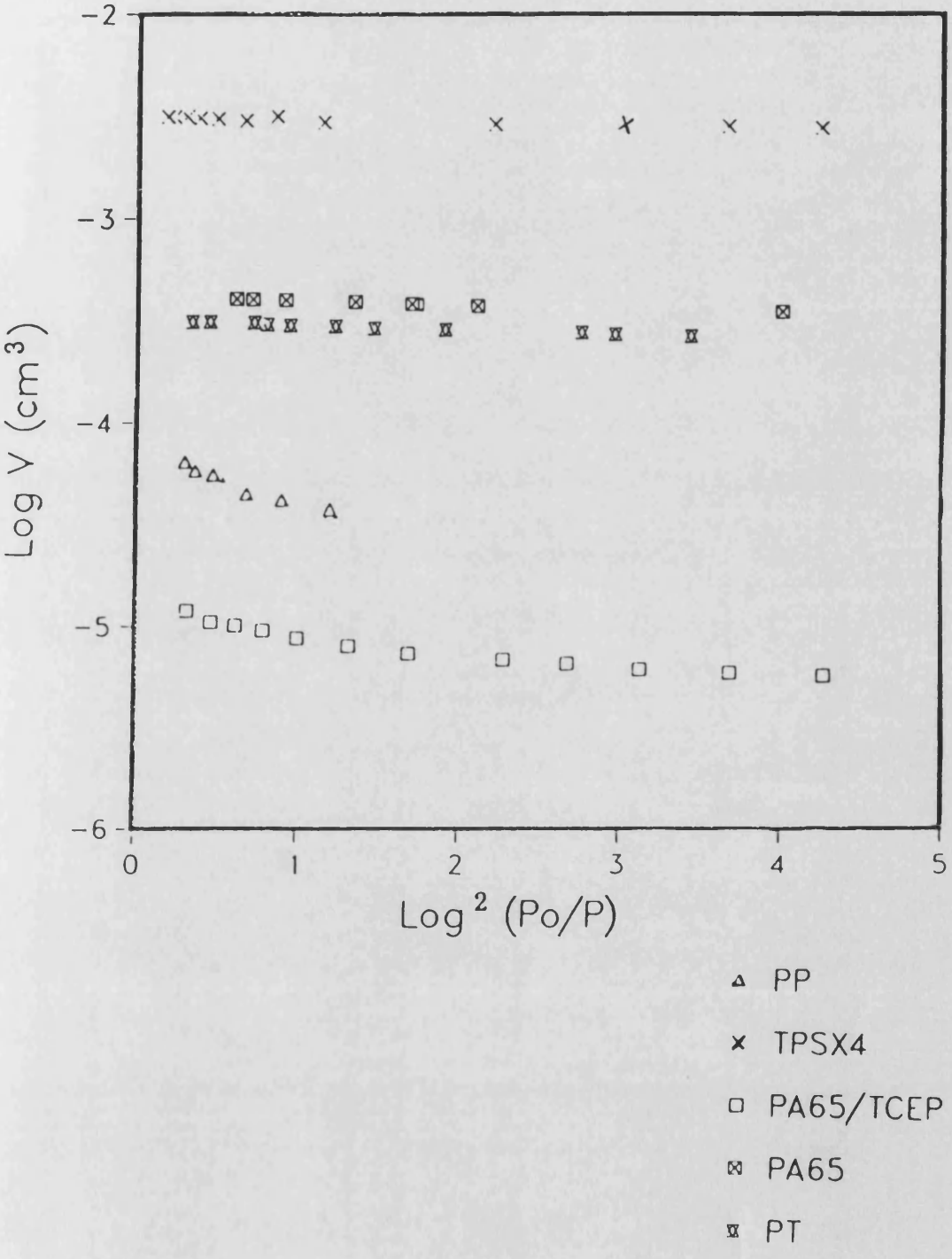

## 7.3 Mercury Porosimetry: Results and Discussion

### 7.3.1 Introduction

The technique of mercury intrusion under pressure to determine pore size distribution was first proposed by Washburn (201) and the technique is well documented (207-209). A brief summary of the theory is presented below. The surface tension (capillary depression) which opposes the entry of mercury into pores is given by ($-2\ \pi\ r\ \sigma\ \cos\ \theta$). This resistance may be overcome by applying an external pressure which will be a function of the pore size, i.e. $\pi\ r^2\ P$. At equilibrium, these forces are equal viz.

$$-2\ \pi\ r\ \sigma\ \cos\ \theta = \pi\ r^2\ P$$

Hence $$Pr = 2\ \sigma\ \cos\ \theta$$

and $$r = 2\ \sigma\ \cos\ \theta/P \quad \ldots\ldots\ldots\ldots 1$$

where $r$ = pore radius (nm), $\sigma$ = surface tension of the mercury (dynes/cm), $\theta$ = the wetting angle and $P$ = absolute applied pressure ($kg/cm^2$). By assuming that all pores are cylindrical an average value of the wetting angle $\theta$ (= $141.3^{o}$) and surface tension $\sigma$ (= 480dyne/cm) equation 1 can be simplified to yield equation 2.

$$r = 75000/P \quad \ldots\ldots\ldots\ldots 2$$

At a pressure P, the volume of mercury entering pores of a particular size is given by $V = (\pi\ r^2\ h/x)$, where h is the level of mercury compressed and x is the sample weight (g). Thus graphs of cumulative pore volume against pore diameter can be obtained. By extrapolation to the y-axis of these graphs, the macropore

volume, i.e. D>50nm, and total pore volumes were obtained. An estimate of the mesopore volume, i.e. assuming D is between 10-50nm (see above for further information on the adopted slit width nomenclature), was obtained by difference of the total and macropore volumes, table 7.1. The technique is unable to determine the micropore volume due to the distorting effect at high pressure, i.e. fracturing and in some cases compressing of the pore walls. Thus mercury porosimetry is not an accurate technique for measuring surface area. The lower limit for resolution of pores has been recommended as >10nm (189).

In determining mercury density table 7.2, the following conditions were assumed (207); 1) interparticle voids must be completely filled with mercury, and 2) all intraparticle voids (interstitial space) must be free of mercury. Interparticle voids are reported to be completely filled below one atmosphere and above this pressure, the mercury penetrates the pores. This assumes that all pores whose entrances are open to the exterior surface of the particles are smaller than the size which mercury can penetrate at one atmosphere, i.e. $D < 10^5$nm. Hence the values reported are apparent densities since the above assumption cannot be verified (208-209).

### 7.3.2 Results and Discussion

Mercury porosimetry curves for pitch carbons are presented in fig.7.6. The higher macroporosity of PP is consistent with loss of a greater amount of volatiles compared to both CTP and DP carbons. The relationship between volatile evolution and macropore structure for the resin carbons is further verified by the data of Fig. 7.7-7.8 and table 7.1. Thus TPSX4, cured using the schedule 150/1.5 involved loss of a large volume of volatiles, giving rise to a porous foam-type structure as shown by its high total mercury pore volume. Similar arguments can be applied to PA65 resin and carbon. A low amount of volatiles were released upon curing PA65 resin, which was aided by solvent evaporation, and this has resulted in a reduced pore volume in both the resin and carbon. The form of the graphs for all the materials, apart from PR77, shows a pore size distribution which extends beyond the limit of resolution . This suggests the presence of further smaller pores, i.e. mesopores and possibly micropores.

The additive modified PA65/TCEP carbon shows a reduced macroporosity compared to the unmodified PA65 carbon and a very low total mercury pore volume, indicating a blocking off of pores by deposition of a surface coating of the additive. However, the increasing slope of the graph, fig.7.8, implies generation of further smaller pores compared to the unmodified PA65 carbon. The pitch carbons show a higher total mercury pore volume indicative of a pronounced macroporosity compared to the resins and the resin

carbons, apart from TPSX4. Since pitch pyrolysis proceeds via an intermediate liquid phase, termed the carbonaceous mesophase, the macroporosity observed in the pitch carbon probably arises during secondary pyrolysis, i.e. loss of volatiles (~10%) entrapped in the matrix of the solidified pitch coke.

TABLE 7.1 Nitrogen surface areas and pore volumes of the carbons

| Carbon | TSA | Constants | | PORE VOLUMES (ml/g) | | | |
|---|---|---|---|---|---|---|---|
| | ($m^2/g$) | BET C | DR D | Micropore | Mesopore | Macropore | Total (mercury) |
| TPSX4 | 310 | 500 | 0.012 | 0.14 | 0.04 | 0.10 | 0.139 |
| PA65 | 44 | 130 | 0.019 | 0.02 | 0.00* | 0.01 | 0.015 |
| PA65/TCEP | 1 | 221 | 0.073 | 0.00 | 0.00 | 0.00 | 0.005 |
| PT | 36 | 150 | 0.023 | 0.01 | - | - | - |
| PR77 | - | - | - | - | 0.00 | 0.01 | 0.010 |
| PR77i | - | - | - | - | 0.00 | 0.02 | 0.021 |
| CTP | - | - | - | - | 0.00 | 0.01 | 0.018 |
| DP | - | - | - | - | 0.01 | 0.02 | 0.028 |
| PP | 4 | 50 | 0.170 | 0.00 | 0.01 | 0.03 | 0.037 |

* 0.00 means a pore volume of less than 0.005 ml/g

TABLE 7.2 Apparent mercury densities for the resin and pitch carbons (determined at a pressure of $10^{-3}$ Torr)

| Carbon Type | Mercury Density ($g/cm^3$) |
|---|---|
| CTP | 1.4718 |
| DP | 1.7635 |
| PP | 1.7598 |
| PR77 | 1.4032 |
| PR77i | 1.3832 |
| TPSX4 | 1.4510 |
| PA65. | 1.4952 |
| PT | 1.4922 |

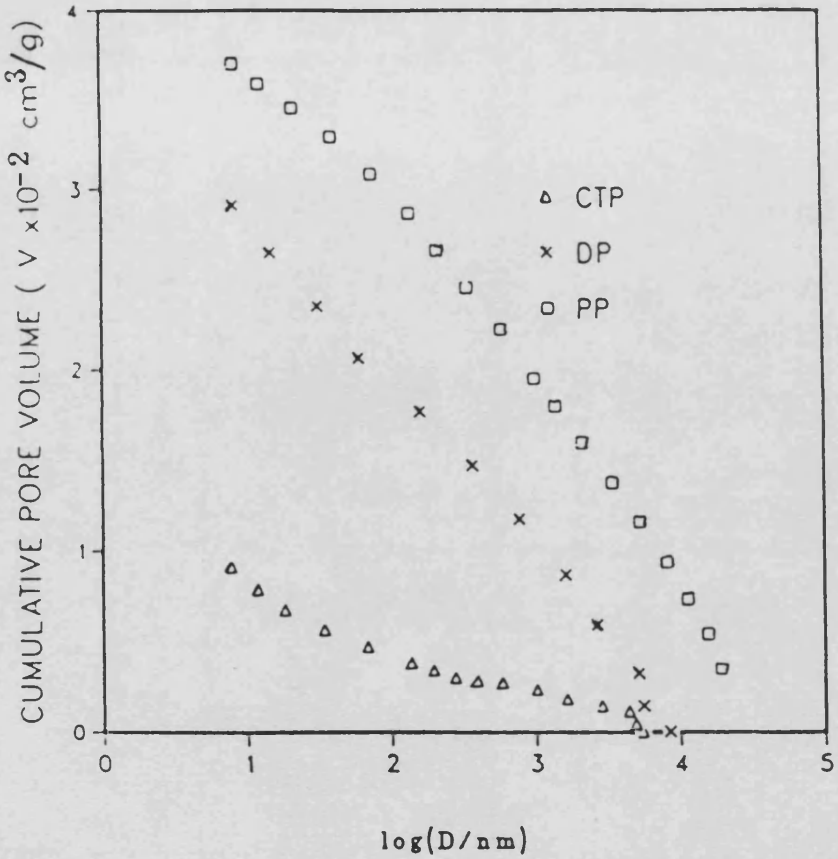


FIG.7.6 Mercury porosimetry results for the pitch carbons

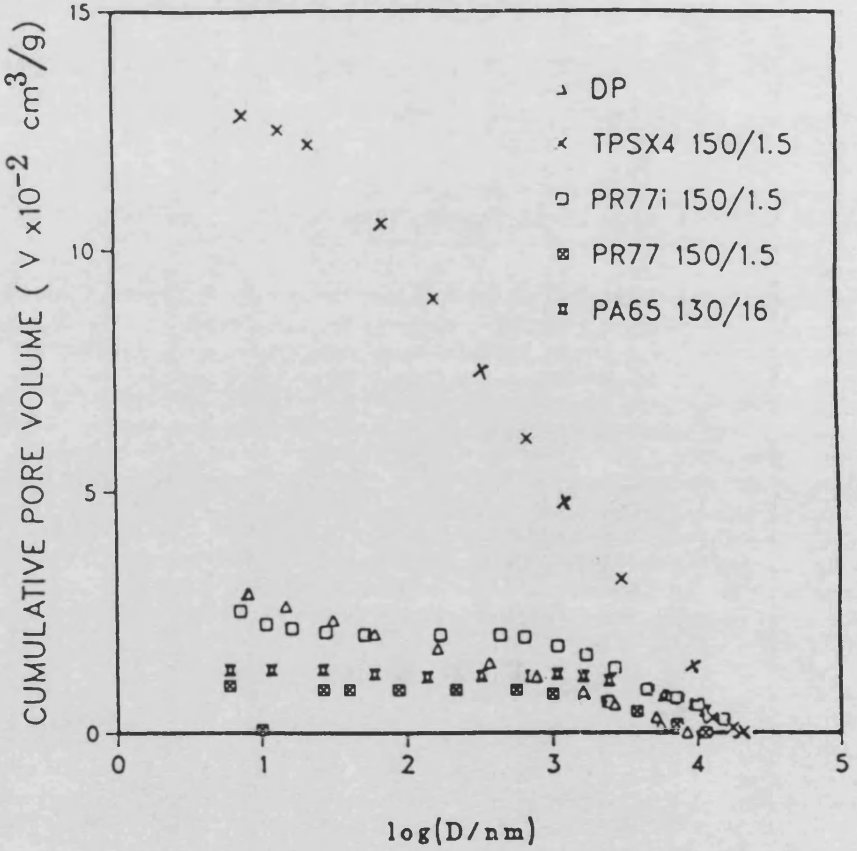


FIG.7.7 Mercury porosimetry results for the resin carbons; results for DP carbon included for comparison

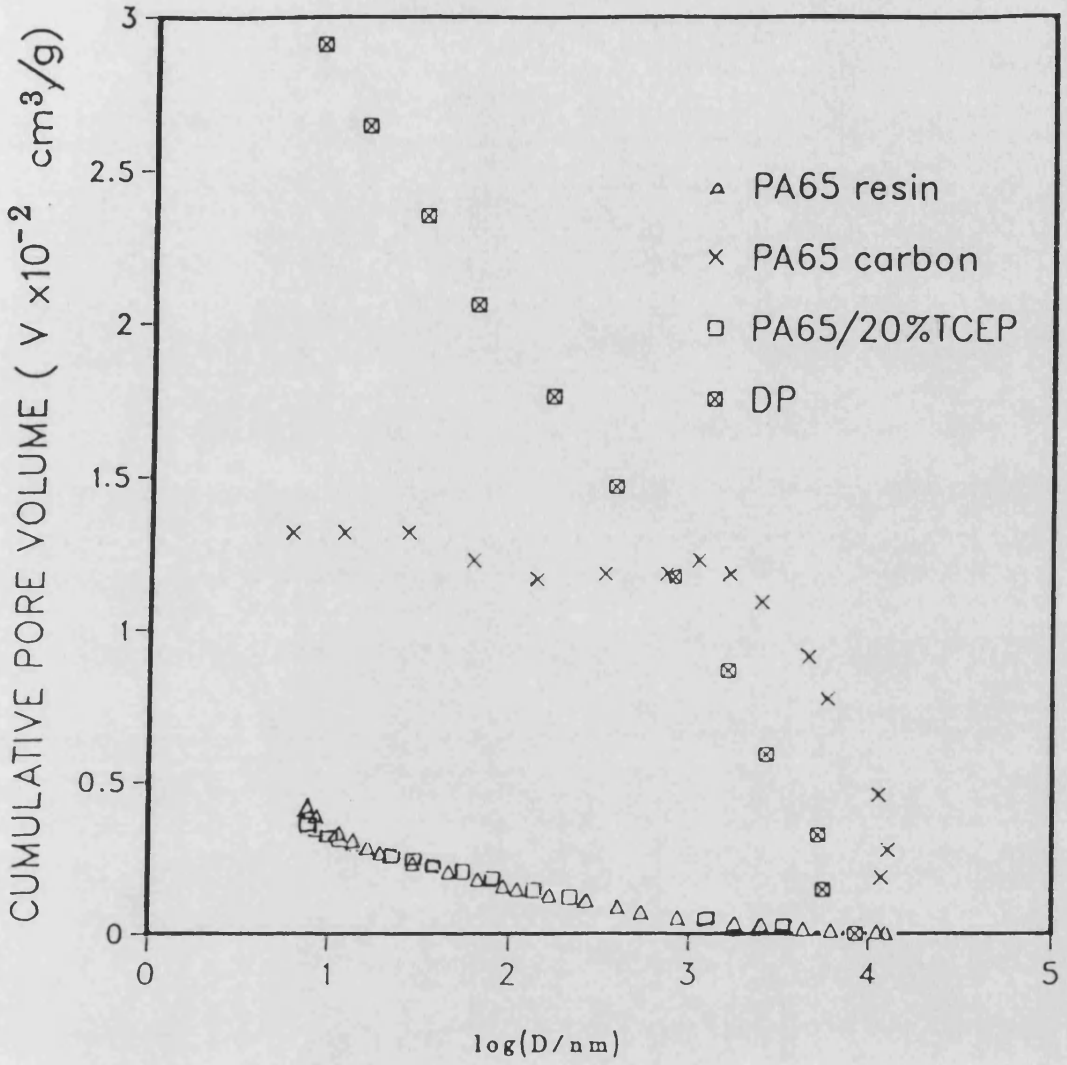


FIG.7.8 Mercury porosimetry results for PA65 resin and carbon compared to PA65/20-TCEP and DP carbons

## 7.4 Quantitative Image Analysis, (QIA)

### 7.4.1 Introduction

The computerised quantitative image analysis, QIA, system is capable of assessing a diverse range of measurements including length, breadth, perimeter and diameter of pores. The system is also capable of plotting histograms showing pore size distribution, frequency of pores of different area, length and shape factors. Thus in order to avoid excessive detail it was decided to limit the results to the following parameters:

1) Percentage Area fraction, $A_f\%$, or total percentage porosity. This was computed using the relationship,

$$[A_f\% = (\text{total pore area/field area} \times N)\ 100]$$

where N is the number of fields investigated.

2) Equivalent pore diameter, $D_e$; the size of a pore may be defined as the diameter of the circle with the same area of the pore; $D_e$ (um) = $(4 \times \text{pore area}/\pi)^{0.5}$

3) Pore shape; this was assessed by an aspect ratio (= l/b) where l is the maximum chord length and b is the maximum pore width perpendicular to the length.

4) Area fraction distribution; these were histograms showing the distribution of the area fraction with equivalent pore diameter.

### 7.4.2 Results and Discussion

The results presented in table 7.3 allow classification of the resin carbons into approximately three categories, with pitch carbon exhibiting further distinct characteristics. Thus considering area fraction, $A_f\%$, or porosity, the following classifications are apparent: class A, $A_f\%$ <1%: PA65 and PT; class B, $A_f\%$ 1-6.4%: DDM, saligenin, FRD2244, FRD2298, PR771 and PR77; class C, $A_f\%$ >40%: TPSX4 and class D, $A_f\%$ 15-24.5%: CTP, DP and PP. Similarly, class A and B materials showed mean diameters, $D_e$, in the range 2.7-7.7um, class C 15.2um and class D 3.5-5.0um. The above grouping of materials is consistent with the amount of volatile gas evolution, as indicated by the weight losses during curing and carbonisation. Thus class B was associated with a low loss of volatiles during carbonisation and a high carbon yield, apart from PR77 and PR771. Class A involved a high curing weight loss (>20wt%) which however, was aided by evaporation of the solvent, and a low carbonisation loss. Conversely, pyrolysis of TPSX4 and the pitches involves loss of large oligomeric fragments which greatly break-up the structure, leading to large pore dimensions.

The above classification of the materials is further verified by examination of the histograms showing distribution of the area fraction in relation to the pore diameter. PP shows a wider pore size distribution compared to CTP and DP, fig.7.9. The class A materials PA65 and PT show a pore size distribution which is below

10um apart from the single anomalous peak at 20um for PA65 carbon, fig.7.10. The class C materials show pore diameters ranging from sub micron voids to voids of diameter greater than 150um. Although the mean pore diameter of TPSX4 carbon is cited as 15.2um, the main contribution to porosity appears to be from pores in the range 80-100um, fig.7.10. This is due to the fact that the area contribution by the latter pore size range is greater, although their frequency of occurrence is lower, compared to the average sized pores.

The mean aspect ratio measurements, i.e. (l/b), of the pitch and resin carbon pores showed a value of <2. This low value suggests that the pore shape is globular, or bubble-like (since l/b=1 is a circle), as expected for pores generated by evolution of volatiles. Higher aspect ratios, maximum of 10 being obtained for PP, may be linked to fissures, or cracks, and interconnected pores.

The porosity developed in the resin during curing is shown to be retained in the carbon, fig.7.11, table 7.4. The 150/1.5 cure schedule involved a fast heating rate, $4^{o}C$/min, and gives rise to a resin of high porosity and large pore dimensions. Upon carbonisation, the pore dimensions are, more-or-less, retained in the carbon. Similar trends are obtained for the slow cured resin and carbon. This is consistent with the results reported by Donnett (210), for natural cellulose materials, namely, that the initial texture of the material was largely preserved during carbonisation, i.e. pores in the carbon were merely relics of

the original cells. The slight reduction in pore diameter of the carbon is linked to the shrinkage effect (due to mass loss of volatiles during pyrolysis) which can be as high as 25% (47). The data of fig.7.11 and table 7.4 further show the effect of heating rate on the resin . The fast heating rate clearly results in a foam-type structure of high porosity compared to the low heating rate. As reported previously in Chap.4, the slow cure schedule (180/24), allows uniform, unrestricted escape of volatiles before the resin structure becomes rigidified. Conversely, the faster cure (150/1.5) involves a rapid volatile loss and onset of rigidification before the bulk of the resin is fully cured. Thus volatiles tend to accumulate and escape only when build-up of pressure is sufficient to rupture the enclosing surface cured resin.

The effect of high heat treatment temperature, HTT, on the oxidation resistance of the carbons was discussed in Chap.6. The enhanced oxidation resistance was linked to various factors including a reduction in accessible surface area due to conversion of open micropores to closed micropores. Since image analysis has a lower limit of resolution extending to only 0.95um, information on the effects of HTT on micropore dimensions is unavailable, The results, fig.7.12, clearly show that the macroporosity is unaffected by the heat treatment, i.e. similar pore size distribution histograms were obtained for each of the heat treatments.

The data showing the effect of additive incorporation on surface morphology is presented in table 7.5 and Fig. 7.13-7.14. Addition of organophosphorus compounds to the co-polymer in all cases increased the porosity, pore dimensions and pore size distribution compared to the unadultered co-polymer. Similar results were obtained for MT59 which is a boron modified ortho-novolak of similar molecular weight distribution to the highly porous TPSX4. It is suggested that the phosphate (or borate) species penetrate the resin network, by reaction with phenolic hydroxyl groups to form ester links, and during carbonisation undergo polymerisation to form a glassy oxide film. In the higher temperature range of carbonisation, a part of the latter film is removed thus accounting for the enhanced pore size distribution. Furthermore, the greater volume of gaseous volatiles which are evolved, including those from decomposition of the fire retardant, will also cause pores to be generated.

Similar results have been reported for addition of phosphate (and borate) species to charcoals by Freeman (211-212). Indeed the latter species were added with the sole intention of promoting mesopore development. The formed glassy oxide film was reported to be substantially removed following activation, thus leaving behind a rigid mesoporous structure superimposed on the initial microporosity. This may explain the reduced oxidation resistance observed for PT carbon modified by the organophosphorus additives TIOP and TNOP. However PT modified by TCEP, TBP and TDCP and the MT59 carbon, although exhibiting an increased porosity and wide pore size distribution, nevertheless show a high oxidation

resistance. This is consistent with a retention of the additive coating. The data of table 7.5 further verifies that the pore texture established in the resin is retained in the carbon.

TABLE 7.3a Pore dimensions of resin carbons and pitch carbons measured by Quantitative Image Analysis

| Carbon Type | | Area Fraction ($A_f$%) | Equivalent Diameter $D_e$ (um) | Aspect Ratio |
|---|---|---|---|---|
| $DDM_a$ | maximum | - | 64.40 | 1.8 |
| | minimum | - | 4.50 | |
| | mean | 1.10 | 7.70 | |
| std deviation of mean* | | 0.00 | 0.12 | |
| total number of results | | 680 | | |
| $Saligenin_a$ | maximum | - | 102 | 1.1 |
| | minimum | - | 0.95 | |
| | mean | $1.10_4$ | 2.80 | |
| std deviation of mean | | $<10^{-4}$ | 0.01 | |
| total number of results | | 851 | | |
| $FRD2244_a$ | maximum | - | 29.70 | 1.2 |
| | minimum | - | 0.95 | |
| | mean | $1.95_4$ | 2.68 | |
| std deviation of mean | | $<10^{-4}$ | 0.10 | |
| total number of results | | 1431 | | |
| $FRD2298_a$ | maximum | - | 29.00 | 1.2 |
| | minimum | - | 0.95 | |
| | mean | 1.97 | 3.31 | |
| std deviation of mean | | 0.60 | 0.14 | |
| total number of results | | 707 | | |
| $PR771_b$ | maximum | - | 142 | 1.3 |
| | minimum | - | 0.95 | |
| | mean | 3.60 | 3.90 | |
| std deviation of mean | | 0.21 | 0.21 | |
| total number of results | | 483 | | |
| $PR77_b$ | maximum | - | 104 | 1.3 |
| | minimum | - | 0.95 | |
| | mean | 6.4 | 3.20 | |
| std deviation of mean | | 0.32 | 0.28 | |
| total number of results | | 760 | | |
| $TPSX4_b$ | maximum | - | 160 | 1.4 |
| | minimum | - | 0.95 | |
| | mean | 44.40 | 15.20 | |
| std deviation of mean | | 0.90 | 2.50 | |
| total number of results | | 799 | | |

* std (= standard)

a, b; resin cure schedules 110/16 and 150/1.5, respectively

TABLE 7.3b Pore dimensions of resin carbons and pitch carbons measured by Quantitative Image Analysis
(resin cure schedule: 130/16)

| Carbon Type | | Area Fraction ($A_f$%) | Equivalent Diameter (um) | Aspect Ratio |
|---|---|---|---|---|
| PA65 | maximum | - | 20.40 | 1.1 |
| | minimum | - | 0.95 | |
| | mean | $0.13_4$ | 2.70 | |
| std deviation of mean* | | $<10^{-4}$ | 0.03 | |
| total number of results | | 60 | | |
| PT | maximum | - | 7.52 | 1.1 |
| | minimum | - | 0.95 | |
| | mean | $0.70_4$ | 3.00 | |
| std deviation of mean | | $<10^{-4}$ | 0.65 | |
| total number of results | | 343 | | |
| DP | maximum | - | 132 | 1.5 |
| | minimum | - | 0.95 | |
| | mean | 24.50 | 5.00 | |
| std deviation of mean | | 0.06 | 0.10 | |
| total number of results | | 1025 | | |
| CTP | maximum | - | 158 | 1.5 |
| | minimum | - | 0.95 | |
| | mean | 15.20 | 3.50 | |
| std deviation of mean | | 0.01 | 0.05 | |
| total number of results | | 5809 | | |
| PP | maximum | - | 102 | 1.8 |
| | minimum | - | 0.95 | |
| | mean | 23.70 | 4.80 | |
| std deviation of mean | | 0.01 | | |
| total number of results | | 3014 | | |

* std (= standard)

TABLE 7.4 Effect of cure schedule on pore dimensions of TPSX4 resin compared to TPSX4 carbon

| | Area Fraction ($A_f$%) | Equivalent Diameter (um) |
|---|---|---|
| a) RESIN (150/1.5) | | |
| maximum | - | 160 |
| minimum | - | 0.95 |
| mean | 44.40 | 15.20 |
| std deviation of mean* | 0.92 | 2.50 |
| total number of results | 799 | |
| a) RESIN (180/24) | | |
| maximum | - | 110 |
| minimum | - | 0.95 |
| mean | 17.20 | 9.0 |
| std deviation of mean | 0.10 | 0.89 |
| total number of results | 680 | |
| b) CARBON (150/1.5) | | |
| maximum | - | 208 |
| minimum | - | 0.95 |
| mean | 44.70 | 17.32 |
| std deviation of mean | 0.10 | 0.65 |
| total number of results | 810 | |
| b) CARBON (180/24) | | |
| maximum | - | 124 |
| minimum | - | 0.95 |
| mean | 20.28 | 9.80 |
| std deviation of mean | 0.10 | 0.89 |
| total number of results | 676 | |

* std (= standard)

TABLE 7.5 Effect of fire retardant addition (20wt%) on the pore dimensions of the resin carbons (cure schedule:130/16)

| Material | Area Fraction ($A_f$%) | Equivalent Diameter (um) |
|---|---|---|
| PT (carbon) maximum | - | 7.52 |
| minimum | - | 0.95 |
| mean | 0.70 | 3.00 |
| std deviation of mean* | $<10^{-4}$ | 0.65 |
| total number of results | 343 | |
| PT/TCEP (resin) | | |
| maximum | - | 43.68 |
| minimum | - | 0.95 |
| mean | 5.20 | 5.62 |
| std deviation of mean | 0.01 | 0.18 |
| total number of results | 1167 | |
| PT/TCEP (carbon) | | |
| maximum | - | 38.50 |
| minimum | - | 0.95 |
| mean | 7.70 | 0.12 |
| std deviation of mean | 0.01 | $<10^{-4}$ |
| total number of results | 1504 | |
| PT/TDCP (carbon) | | |
| maximum | - | 59.00 |
| minimum | - | 0.95 |
| mean | 2.42 | 6.40 |
| std deviation of mean | 0.01 | 0.30 |
| total number of results | 1602 | |
| PT/TIOP (carbon) | | |
| maximum | - | 82.00 |
| minimum | - | 0.95 |
| mean | 5.00 | 3.50 |
| std deviation of mean | 0.03 | 0.15 |
| total number of results | 1388 | |
| MT59 (resin) | | |
| maximum | - | 91.90 |
| minimum | - | 0.95 |
| mean | 11.74 | 12.69 |
| std deviation of mean | 0.01 | 1.09 |
| total number of results | 1140 | |
| MT59 (carbon) | | |
| maximum | - | 249 |
| minimum | - | 0.95 |
| mean | 16.74 | 8.30 |
| std deviation of mean | 0.22 | 0.53 |
| total number of results | 1187 | |
| Z6018 (carbon) | | |
| maximum | - | 6.24 |
| minimum | - | 0.95 |
| mean | 0.38 | 1.30 |
| std deviation of mean | $<10^{-4}$ | 0.03 |
| total number of results | 461 | |

* std (= standard)

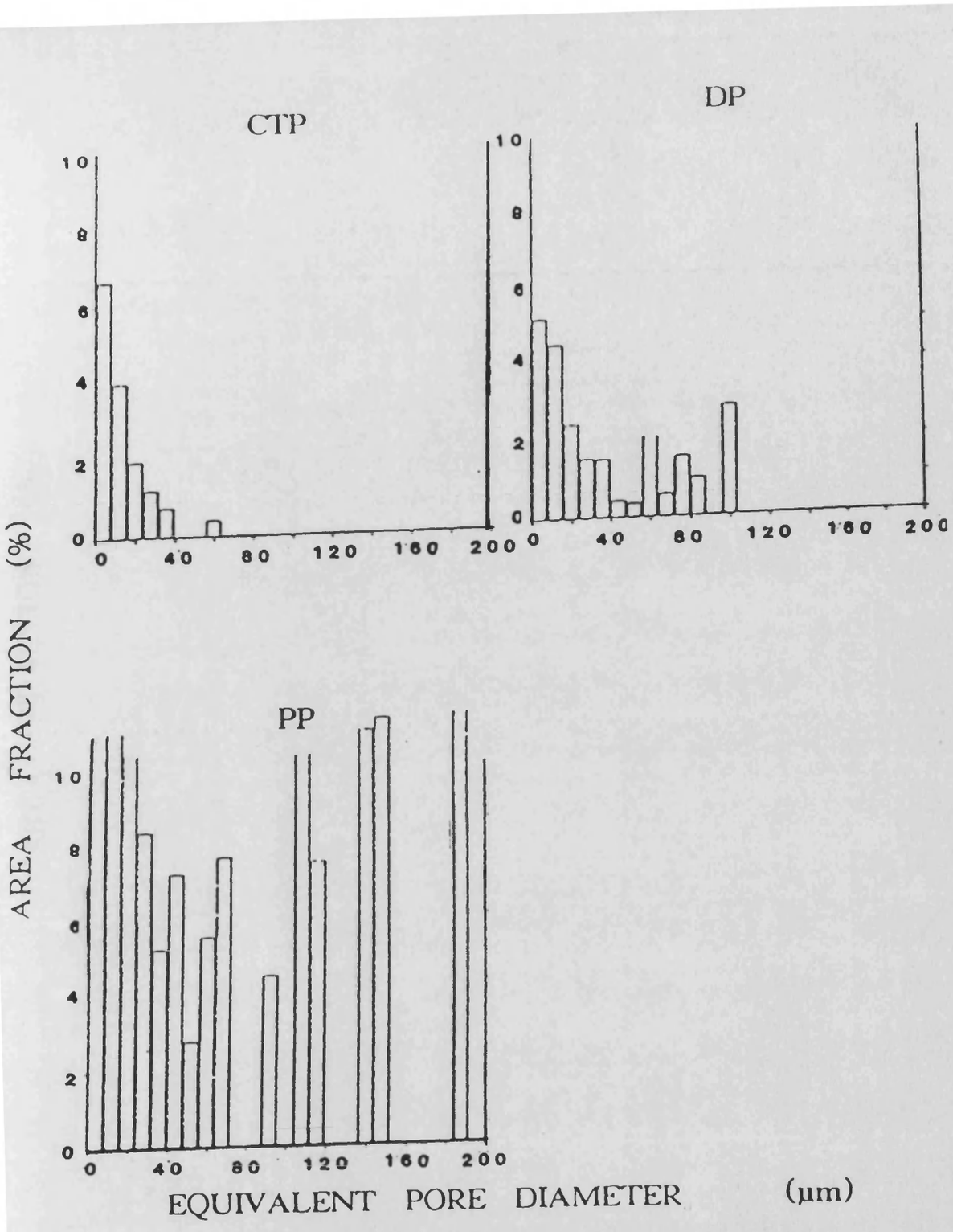


FIG.7.9 QIA data showing macropore size distribution of the pitch carbons

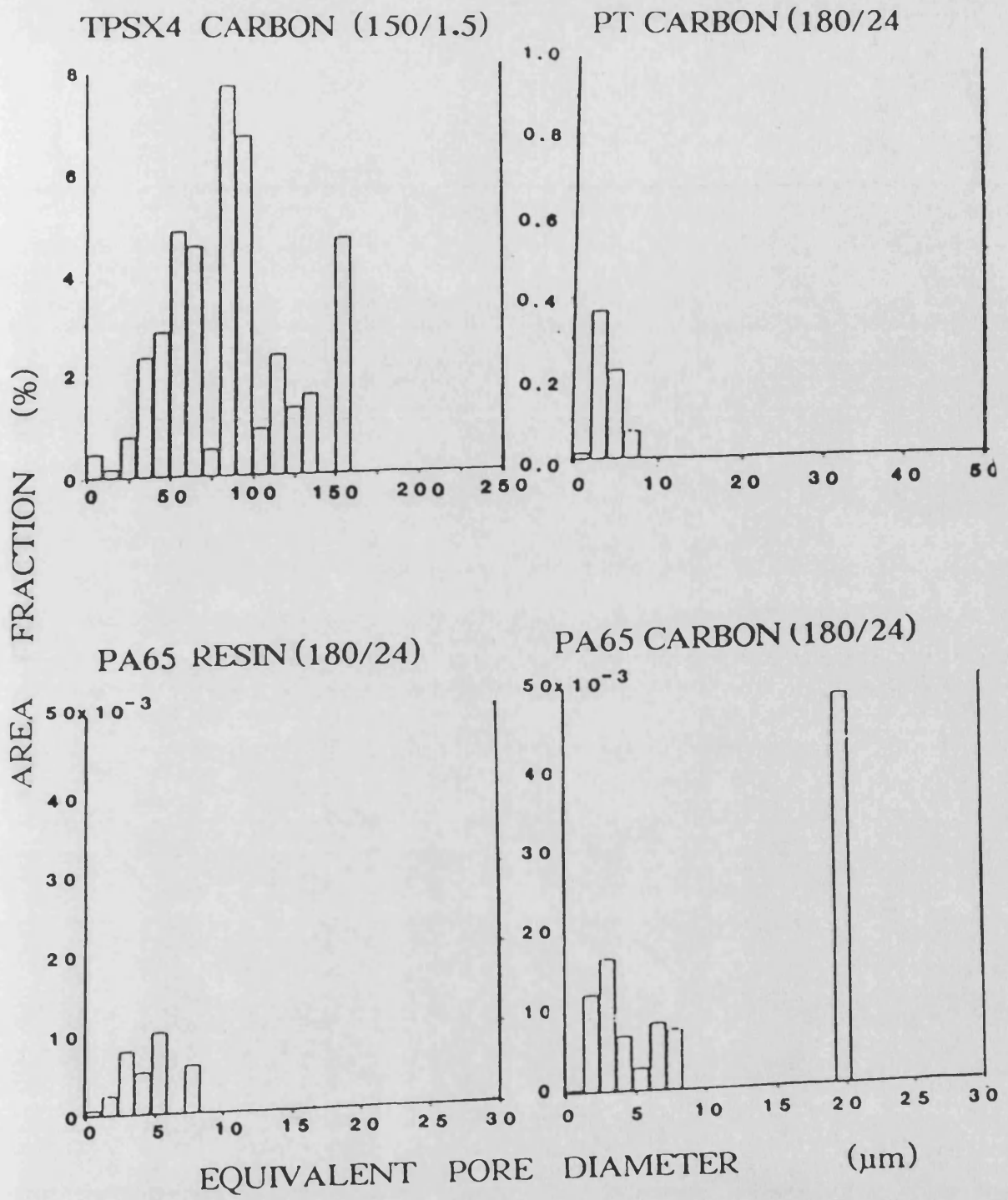


FIG.7.10 QIA data showing macropore size distribution of the resins and the resin carbons

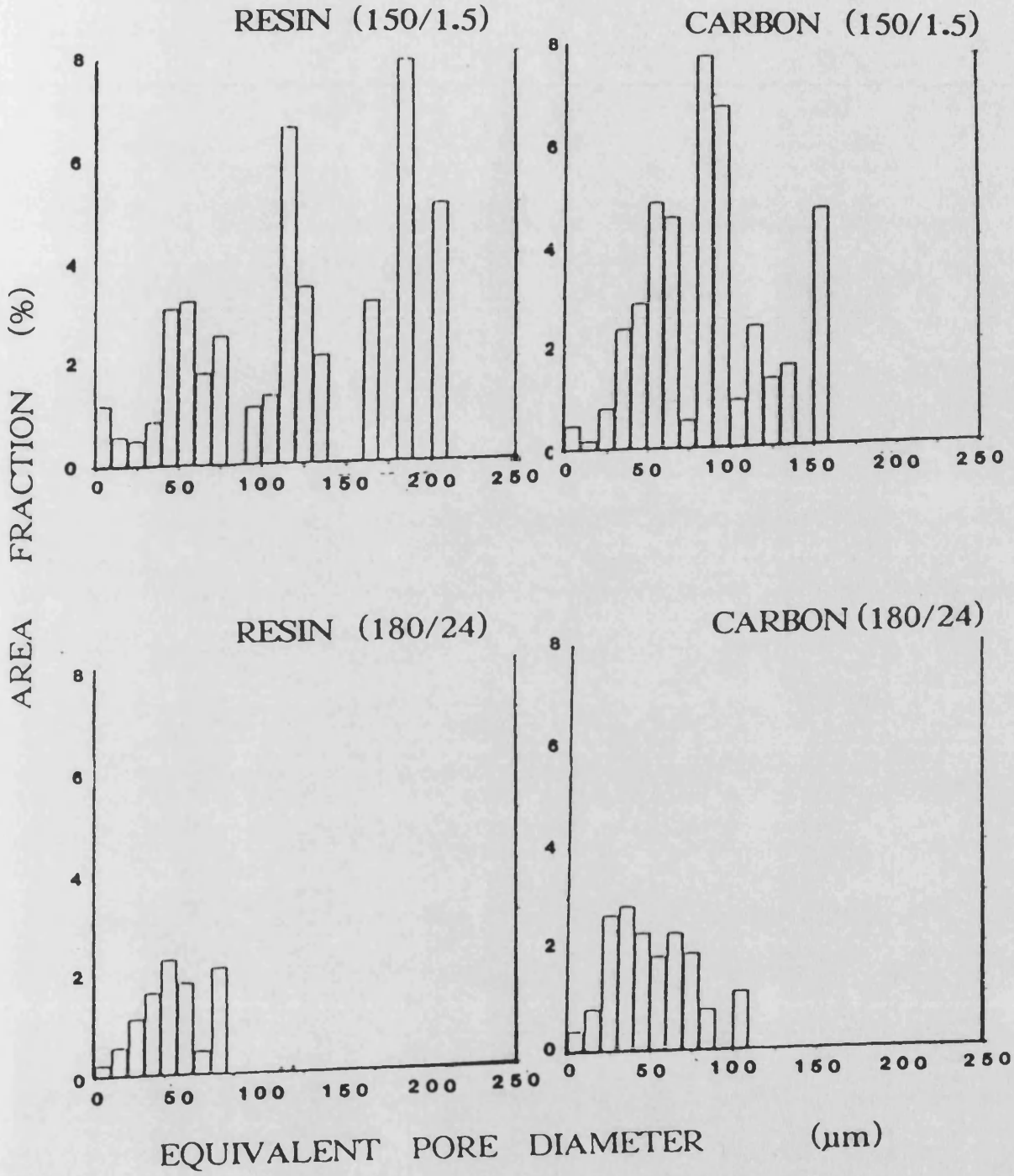


FIG.7.11 QIA data showing the effect of cure schedule on macropore size distribution of TPSX4 resin and carbon

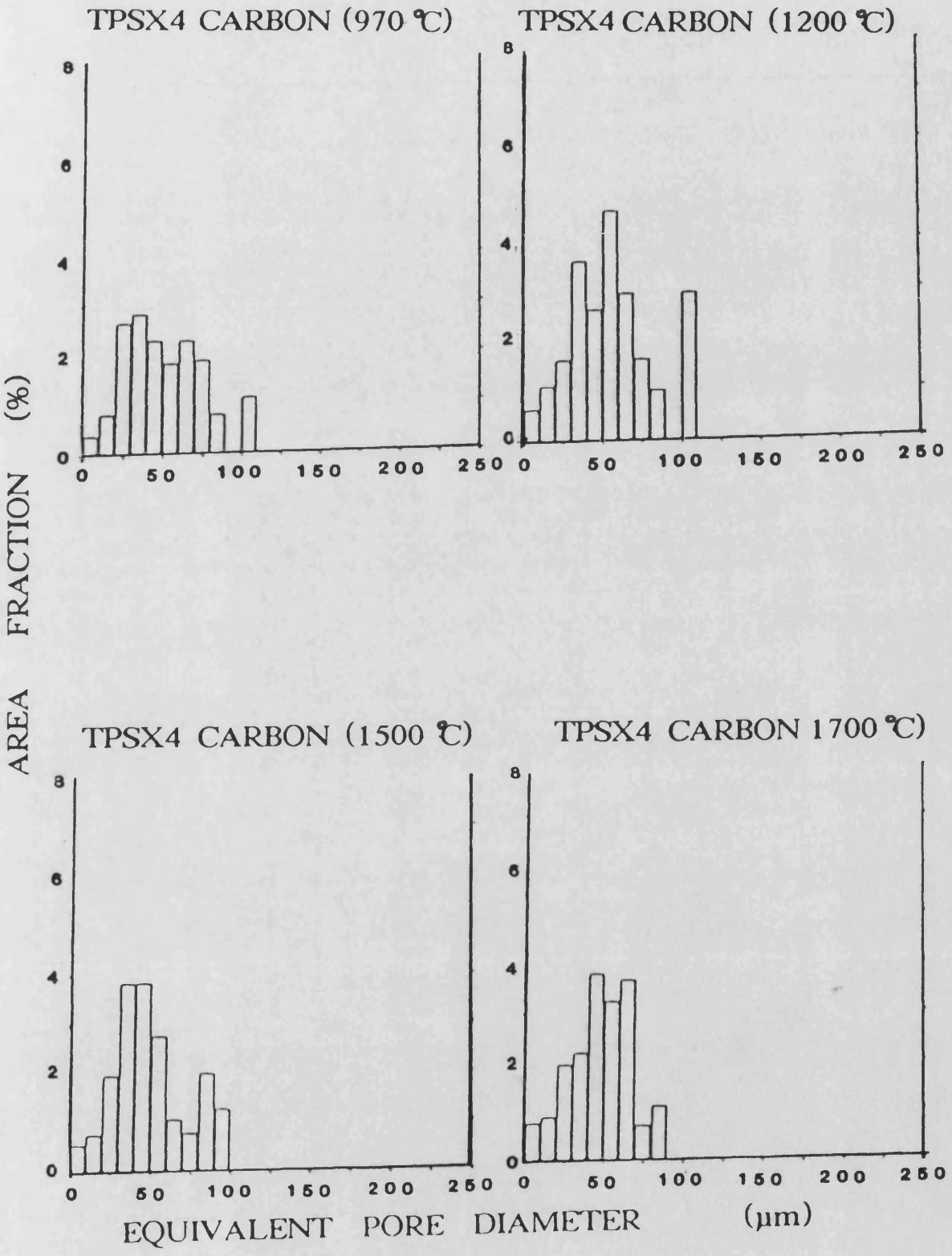


FIG.7.12 QIA data showing the effect of heat treatment temperature on macropore size distribution of TPSX4 carbon

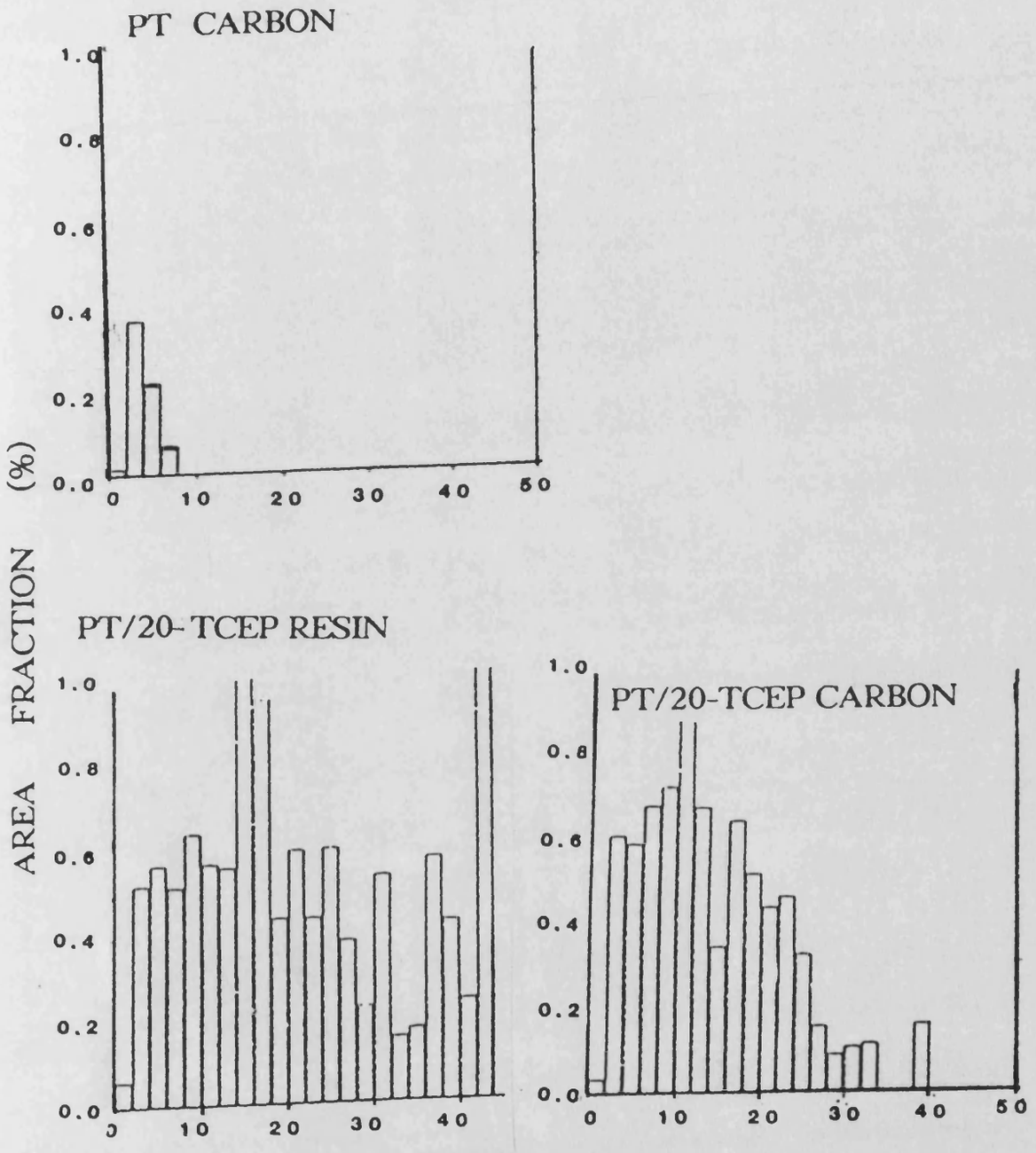


FIG.7.13 QIA data showing macropore size distribution of PT/TCEP modified resin and carbon compared to PT carbon (180/24)

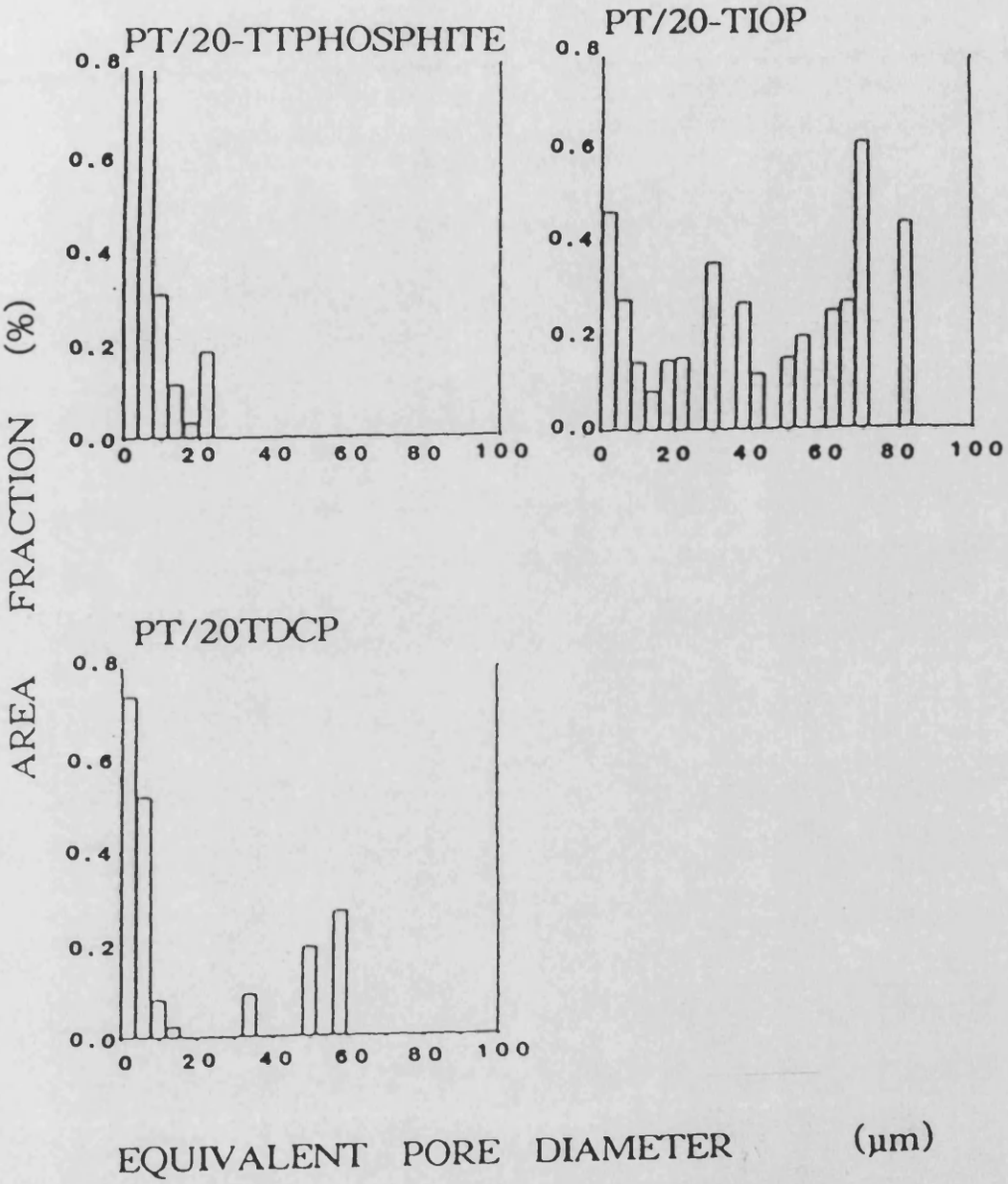


FIG.7.14 QIA data showing macropore size distribution of the additive modified PT carbon

## 7.5 Overall Summary of Chapter 7

The various techniques used to investigate the surface morphology of the carbons generally gave complementary results. The adsorption isotherms and the corresponding BET and/or DR plots allow classification of the carbons into three groups viz. 1) microporous and mesoporous with a high specific surface area-TPSX4 2) reduced microporosity and TSA- PA65 and PT and 3) negligible microporosity, very low TSA and evidence of mesoporosity- PP and PA65/TCEP

The remaining techniques supplied information on the bulk structure of the materials, i.e. the macroporosity, although mercury intrusion afforded limited results on mesoporosity. The extensive pore size distribution observed for TPSX4 carbon is clearly evident from the various techniques. Image analysis and SEM prints show that the porous structure established in the resin is maintained in the carbon. The results obtained from the techniques, i.e. including percentage porosity, total mercury pore volume and pore size distribution show the following descending order of total porosity, for the carbons:

TPSX4 > pitches > remaining resin carbons

The surface morphology of the pitch carbons was found to be mainly macroporous with negligible microporosity as shown by the low TSA.

Interesting results are obtained for the additive modified systems, i.e. PT/TCEP, PA65/TCEP and MT59. Mercury intrusion, SEM and QIA data show a clear enhancement of porosity and pore size distribution compared to the unmodified co-polymer. However, the adsorption isotherms, for PA65/TCEP carbon, gave a reduced TSA and the DR plot showed an upward deviation at high relative pressure, which is indicative of mesoporosity, and a negligible micropore volume. The low TSA implies that the mesopores (and macropores) do not make a major contribution to the adsorption but merely function as feeder pore systems for diffusion of the adsorptive. The low micropore volume suggests that despite generation of mesopores and macropores, the micropores, which were present in the unmodified PT carbon, are blocked off by the additive decomposition products and oxide coating.

# CHAPTER 8 GENERAL DISCUSSION

In the preceeding chapters the results were followed by an appropriate discussion. Thus the effect of curing schedule, carbonisation and oxidation resistance of the resins and pitches were presented in Chap. 4. In Chap. 5 the effect of additive modification is outlined, while Chap. 6 presents data on the effect of high temperature heat treatment, isothermal oxidation studies, energy dispersive analysis of x-rays and elemental analyses. Textural characterisation of the resins and resin and pitch carbons was presented in Chap. 7. An overall discussion of the results, with correlation of the data, where appropriate, is presented in this chapter.

For carbon oxidation to proceed, the bond between the carbon atom and the reactant gas must be stronger than the C-C bond. Thus the reactivity of the carbon is assumed to vary with the number and density of active carbon free sites, collectively referred to as the active surface area, ASA (173, 213 ). These sites consist of dangling carbon atoms (singly bonded), edge carbon atoms (doubly bonded) basal carbon atoms (trigonally bonded), mineral matter, heteroelements and structural defects such as porosity and cracks. Carbon oxidation involves the following elementary reactions:

1) $C + O_2 \longrightarrow CO_2$ 2) $2C + O_2 \longrightarrow 2CO$

3) $2CO + 2O_2 \longrightarrow 2CO2$ 4) $CO_2 + C \longrightarrow 2CO$

These reactions proceed via intermediate carbon-oxygen, C(O),

complexes. At low temperature $CO_2$ formation is dominant and occurs at catalytically active sites (214) while at high temperature CO is formed at the carbon edges.

Walker (215 showed that reactivity of carbon was due to: 1) high concentration of reactive sites i.e. carbon atoms located at edges of crystallites within the char. Thus carbon atoms common to 2 or 3 rings are non-reactive whereas peripheral (or edge) carbon atoms common to only one ring are reactive. 2) high accessibility of reactant gases to the active sites and 3) high catalytic activity and/or dispersion of the inherent inorganic impurities.

The active carbon free sites are distributed throughout the carbon structure due to lattice imperfections or dislocations. These sites provide unpaired electrons for effecting chemisorption of reactant gas constituents to form surface complexes. Study of carbon active sites are not well understood, although, Coulson (216) reports three different electronic configurations for atoms located at edges of graphitic planes: 1) valence orbital occupied by one electron, 2) partial triple bond by deformation of the structure and pairing of the electrons, and 3) sigma electron pairs (reversion from $sp^3$ to $sp^2$ hybridisation)

Preferential attack at edges of basal planes or at discontinuities in basal planes during graphite oxidation was shown by Hennig (173). The latter increased the basal plane

area (by crystal cleavage) and showed that oxidation of graphite was same as the uncleaved crystal, i.e. the concentration of edge carbon sites was unaffected by crystal cleavage and hence the amount of oxygen complex adsorbed remained constant.

The superior oxidation resistance of pitch carbons compared to resin carbons has thus been linked to possession of a more ordered, graphitic structure of low accessible surface area compared to the amorphous, non-graphitic, high surface area of resin carbons. Upon pyrolysis the similar shape of the TG thermograms of the fully cured resin, i.e. model compound, novolak, resole or resole/novolak co-polymer, implied similar chemical behaviour, i.e. the route and extent of pyrolysis of the resin is solely dependent on the thermal stability of the dihydroxydiphenylmethane unit. Differences in oxidation resistance observed between the resin carbons therefore must be linked to physical differences in the acquired carbon structure, i.e. the extent of porosity, pore size distribution and surface area. However, the presence of linear carbon radicals, the percentage of edge carbon atoms, heteroelements, presence of surface functional groups and metallic impurities are expected to have an important bearing on controlling the oxidation of the bulk material (177, 216-219).

Although studies on the effects of cure schedule on the oxidation resistance of the resin carbons failed to provide a clear relationship, it was deduced that an extended high temperature cure schedule was a prerequisite to obtaining complete

resin cure. Furthermore, it was postulated that a low rate of curing allows a uniform loss of volatiles before the onset of structural rigidification. In contrast, the short, high temperature cure involved a rapid heating rate and generation of a large volume of volatiles over a short time interval. The latter volatiles, entrapped by the surface cured resin, only escaped by the build-up of pressure, thereby leaving behind large bubble-like pores and fissures. Failure to remove the bulk of the volatiles during curing i.e. unreacted monomers, water of condensation, ammonia from HMTA decomposition, and oligomeric species, entrapped in the matrix of the cured resin would require their removal from a solid state during pyrolysis and hence a further distortion of the carbon structure.

The SEM prints, plate P1, prints 1-4 clearly show the highly disordered and porous structure of TPSX4 resin when the latter was cured using the fast cure schedule 150/1.5, compared to the slower cure 180/24. Further evidence is provided by image analysis which shows the high percentage porosity and larger pore dimensions of TPSX4 resin cured by the 150/1.5 schedule compared to the 180/24 schedule, table 7.4. The results for these and other schedules show that the surface morphology of the resin is retained in the carbon. Solvent evaporation is expected to aid removal of the volatiles thus giving a less porous structure as shown by SEM prints, 15-16 and pore size distribution fig.7.7, for PR77 and PR77i. Consequently the carbon formed from the solvent containing PR77 resin carbon exhibits a higher oxidation resistance compared to the non-solvent containing PR77i.

A combination of the above factors, viz. low volume of decomposition products, presence of solvent and use of an extended cure schedule, may explain the high oxidation resistance observed for the resole and the co-polymer PT, fig.7.7 and SEM plates P4-P5, prints 15-26. The various experimental results show a marked difference in surface morphology between the resin carbons. The percentage porosity, pore size distribution and specific surface area of PA65 and PT carbons are lower than, for example, TPSX4 carbon. A high surface area provides a greater number of reactive sites e.g. edge carbon atoms, which enable rapid oxidation. The latter fact is supported by the shape of the oxidation thermograms e.g. fig. 4.3. The characteristic shape is largely controlled by the carbon surface area and porosity. Thus with onset of carbon oxidation two important factors are postulated to occur; 1) enlarging of the open pores initially present and 2) opening up of closed pores (43). Thus as the total number of pores is increased, as well as their average diameter, the specific surface area (and specific pore volume), also increases. This initial carbon oxidation, or induction period, is followed by a region of rapid carbon oxidation.

High temperature heat treatment, HTT, is known to affect the carbon in several ways including a reduction in accessible surface area as open pores are sealed off. The latter was reported to occur above 1500°C (169) and was accompanied by removal of heteroelements and catalytic impurities, and the breakage of inter-chain links and hence a release of strain energy as a stabilised carbon structure is established. These factors may

explain the enhanced oxidation resistance observed for the carbons heated to 1700°C compared to the lower temperature heat treatments, fig.s 6.1-3.

The relationship between a reduction in porosity and enhanced oxidation resistance is however, not apparent for the additive modified carbons. Addition of the fire retardant was shown to promote porosity, i.e. generation of mesopores (as shown by the positive deviation at high relative pressure of the DR plot for PA65/TCEP, fig.7.5) and macropores, (see image analysis data fig.7.12-7.13). Addition of fire retardants still gives rise to a carbon of increased oxidation resistance, fig.5.12. Similarly, the pitch carbons exhibit a high oxidation resistance despite the high percentage porosity and extended pore size distribution, table 7.3, fig.7.9, compared to many of the resin carbons. Image analysis showed that HTT, which is reported to seal off mainly microporosity, had a negligible effect on the pore structure assessed by the technique, i.e macropores, fig.7.12. Despite the high percentage porosity, the pitch carbons exhibit a very low surface area compared to the resin carbons, implying that the mesoporosity and macroporosity makes only a minor contribution to the adsorption. The additive modified carbon, PA65/TCEP similarly exhibited a reduced surface area, $1.1m^2/g$, despite the more developed macropore structure, compared to PA65, $45m^2/g$.

Since oxidation is a surface phenomenon prevalent at points of disorder or active sites, the bulk sum of which constitutes the

active surface area, ASA, the oxidation resistance is expected to increase with decrease of TSA, i.e. assuming ASA < TSA. For graphite oxidation Graham (213) reported ASA to be 1.25% of the total BET surface area. TSA acted as a useful index of reactivity for the additive modified carbon PA65/TCEP, i.e. a low TSA exhibited a corresponding high oxidation resistance. However, DP and PT carbons did not conform to the above rule, i.e. PT exhibits a high TSA and a high $T_{0.5}$ compared to DP carbon. This anomaly may be due to the following properties of PT carbon:

1) possession of a low concentration of active sites, i.e. most of the TSA of PT carbon is unreactive,
2) presence of very active sites which are unavailable due to formation of stable carbon-oxygen complexes, and
3) presence of sites of low reactivity which have difficulty in forming the carbon-oxygen intermediate.

Since high TSA is usually associated with the presence of microporosity, the reduced TSA observed for PA65/TCEP implies that the glassy oxide barrier must percolate the polymeric network and block off the pores, i.e. micropores and possibly smaller mesopores. Entry of the fire retardant into the resin network and its retention in the carbon, following pyrolysis, is clearly shown by the EDAX micrographs and histograms which were obtained from samples previously polished and sectioned. In addition to the surface barrier effect (which hinders the diffusion of the reactant gas to the carbon), provided by the additive, the enhanced oxidation resistance observed for the modified carbon will also be aided by the ability of the additive to function as a heat sink, during the various stages of decomposition leading to

oxide formation. The improvement in oxidation resistance of the additive modified carbons compared to the pitch carbon is shown by the high carbon yield following non-isothermal oxidation at 1000°C, table 5.3. Further evidence is provided by isothermal oxidation studies which show very low rates of burn-off and high carbon residues despite prolonged high temperature exposure in air, fig.6.4c and table 6.2.

In a recent investigation Freeman (211-212) reported that mesopore development induced by phosphate impregnants involved formation of an oxide film in the carbon network which was easily removed following gasification. Removal of the oxide film was reported to be responsible for generation of a mesoporous structure superimposed on the microporosity. The present research however shows that the oxide film arising from several phosphate impregnants e.g. TCEP, TBP and TDCP was not removed, and indeed, was retained, despite high levels of carbon oxidation (>50%). Conclusive evidence for this is provided by both SEM and EDAX micrographs and histograms. The latter showed that the glassy layer coating increased in thickness with increasing severity of oxidation, see also table 6.4. Similarly, elemental analysis showed that as percentage burn-off increased, the level of carbon, as expected, decreased but the level of the additive element (obtained from the mass balance) increased, table 6.5. The high concentration of fire retardant element detected at various points along the particle, see EDAX micrographs 1-4, Chap.6:3 and SEM plates P10-P12, prints 47-62, Chap.7.1, is consistent with a globular, although continuous, surface coating

morphology when describing additive distribution. Although no data are available describing the distribution of the organophosphorus additives which failed significantly to improve the oxidation resistance of the carbon, i.e. TIOP, TNOP, and TTPhosphate, it may be postulated that the latter additives were removed from the carbon network during the early stages of oxidation.

Readily charged particles, distinct from the bulk carbon, were detected for the boron-containing and silicon-containing carbons. They probably represent remnants of the additive-based oxide coating which separates from the carbon following a degree of oxidation. This spalling is probably due to differences in the coefficient of thermal expansion between the oxide layer and the resin carbon. Differences of thermal expansion, widely reported for silicon based fire retardants and resin carbon, results in generation of cracks in the oxide film, plate P14, print 66. The latter allows the reactant gas to permeate the underlying carbon structure leading to rapid carbon oxidation. Thus plate P14 clearly shows that even after 15% oxidation distinct silica particles become evident and after 30% oxidation only silica particles were detected. Conversely the organophosphorus additive TCEP shows a thick oxide layer apparently adhering to the carbon particle even after 50% oxidation implying similar coefficients of thermal expansion for the two materials. The high oxidation resistance and carbon residue following prolonged isothermal heating in air of MT59 carbon indicates formation of a more impervious oxide coating. Thus charged particles (probably $B_2O_3$)

only become evident following 70% carbon oxidation, plate P12. As the thickness of the oxide film increases there is a greater tendency for generation of cracks and fissures in the oxide coating. The latter are probably responsible for continual loss of carbon, despite the presence of a thick oxide coating, in the later stages of oxidation.

Despite the similarly low TSA and a more ordered graphitic structure of the pitch carbon, the additive modified resin carbons exhibit a superior oxidation resistance. This indicates that the physical barrier to diffusion of the reactant gas, provided by the oxide film, has a greater bearing on controlling the oxidation resistance than the actual carbon structure. Thus fig.6.2 portraying the effect of HTT on PA65/TCEP, shows that after the initial improvement in $T_{0.5}$ (presumably due to formation of a more impermeable oxide coating) further increase of HTT, which is expected to stabilise the carbon structure, as manifested by the increased oxidation resistance of the unmodified resin and pitch carbons, fig.6.1, does not significantly affect the oxidation curves of the additive modified carbon.

The present research has shown that the oxidation of the granular pitch carbon is rapid and leaves negligible residue. Conversely, oxidation of granular resin carbons, e.g. stabilised co-polymer PT, additive modified PT and PA65 and various heat treated, at 1700°C, resin carbons, is slower with a significant carbon residue. The amount of carbon residue is important since magnesia briquettes used in the furnace linings

are subjected to cyclic heating, during removal of the formed steel or during furnace charging. The presence of the carbon residue in the briquette allows many heating cycles to be performed before it becomes necessary to repair the wear areas (220-228).

# CHAPTER 9 CONCLUSION AND SUGGESTIONS FOR FURTHER WORK

Initial studies using model compounds, novolaks and a resole showed that the resole gave a carbon in high yield and of oxidation resistance approaching that of the pitch carbon. Furthermore, the oxidation resistance of the resole, PA65, could be improved by co-polymerisation with the high molecular weight novolak, TPSX4, forming the co-polymer PA65-90/10-TPSX4, or PT. Synthesis of the highly stable resole carbon, prepared using the cure schedule 180/24 was not as reproducibile as the co-polymer PT. Furthermore, although the 180/24 cure schedule gave a carbon of high oxidation resistance for both the resole and the co-polymer PT, the 130/16 schedule consistently resulted in a more stable PT carbon compared to PA65. Further superiority of the PT carbon is shown by the higher oxidation resistance of the PT/additive modified carbon compared to the analogous PA65/additive carbon. Although no decisive conclusion was drawn from studies of the effect of cure schedule on the resins TPSX4, saligenin and the co-polymer PT, the results showed that an extended high temperature cure schedule was necessary for obtaining a carbon of optimum $T_{0.5}$. Combined experimental results showed that the surface morphology established in the resin was retained in the carbon.

Image analysis, mercury porosimetry and electron microscopy showed a well developed pore size distribution for the pitch carbons and TPSX4 resin and carbon, compared to the remaining

resin carbons. The adsorption data obtained for TPSX4 carbon showed a high total (or BET) surface area and the upward deviation at high relative pressure of the DR plot and mercury porosimetry data showed the presence of mesoporosity. The pitch carbons had a low TSA suggesting that the observed mesopores and macropores functioned only as a feeder pore system for transport of the reactant gas and made only a minor contribution to the overall adsorption. PA65 and PT carbons showed a reduced TSA and pore size distribution compared to TPSX4 carbon and consequently a higher $T_{0.5}$.

High temperature heat treatment is known to decrease TSA, which is consistent, in part, with the observed increase of $T_{0.5}$ of the various resin and pitch carbons. However TSA data available in the present research failed to show a quantitative relationship with reactivity for all the carbons studied. Such a relationship may exist with ASA which has been reported to provide a good index for reactivity of graphite oxidation (227)

Addition of several types of fire retardants to resins gave resin carbons of remarkably high oxidation resistance. The various experimental results showed that the mode of inhibition by the additive involved formation of an intumescent coating which restricted the diffusion of the reactant gas to the underlying carbon substrate. Although additive modification resulted in generation of macroporosity, adsorption studies showed that the latter did not contribute greatly to the surface area. Indeed the surface area was reduced by blocking off the microporosity by

decomposition products of the additive. Presence of cracks and crazes, which arose due to differences in the coefficient of thermal expansion between the oxide layer and the carbon resulted in rapid carbon oxidation, as observed for the silicon resin carbon, Z6018.

The following suggestions are made for further clarifying and possibly quantifying the various aspects of the present research:

1) investigation on the effect of the rate of heating on the extent of resin curing and on the resin surface morphology,
2) mode of additive decomposition and nature of its interaction with the resin and the carbon, i.e. during curing, carbonisation and oxidation,
3) Quantitative assessment of the thickness and distribution of the additive coating after various degrees of oxidation,
4) determination of adsorption isotherms for the remaining resin and additive modified resin carbons and establishment of a relationship, if any, between ASA and $T_{0.5}$.
5) manufacture of the actual composite MgO or $Al_2O_3$/carbon binder/graphite, incorporating 5-25% resin binder.

The work described in this thesis show that phenolic resin carbons, e.g. TPSX4, carbonised at a lower temperature viz. 970-1500°C, exhibit a lower oxidation resistance than the corresponding pitch carbon. However, the study clearly shows

that after the higher heat treatment viz. 1700°C, which is the expected service temperature for the carbon containing composite, the resin carbons, including unmodified TPSX4 and PT, exhibit a superior oxidation resistance compared to the pitch carbon.

The results also show that modification of the resin by addition of fire retardants gives rise to a carbon, after pyrolysis at 970°C, of high oxidation resistance. The various analytical techniques indicate that the mode of carbon combustion inhibition, by the phosphate or borate additives, involves formation of an intumescent oxide film or coating which physically retards the diffusion of the oxygen to the carbon substrate. The high oxidation resistance of pitch carbons has been attributed to the possession of an ordered graphitic structure. However, the carbon structure is not expected to have an important bearing when the rate controlling mechanism for carbon oxidation is due to diffusion of the reactant gas to the substrate through the intumescent coating or barrier. Thus fire retardant addition to pitches will not necessarily give a carbon exhibiting higher oxidation resistance than the corresponding additive modified resin carbon. Additive modification of the phenolic resin is preferable since the resin, and its carbon, exhibit further superior properties compared to the pitch, as outlined in Chap.2, the literature survey.

## APPENDIX

Standard thermogravimetric conditions for oxidation were obtained by testing of various parameters, viz. heating rate, H.R., particle size, P.S., air flow rate, Air and initial sample weight. The final condition chosen was based on various factors, e.g. ease of sample preparation (i.e. larger sample particles were easier to prepare thus avoiding dangers from dust), recommended working condition and reproducibility of the data. Appendix A2 presents some information for gas adsorption studies.

A1.1 Effect of heating rate ( C/min) on the oxidation of PP carbon; P.S. 850–500um Air 5ml/min initial weight 10mg

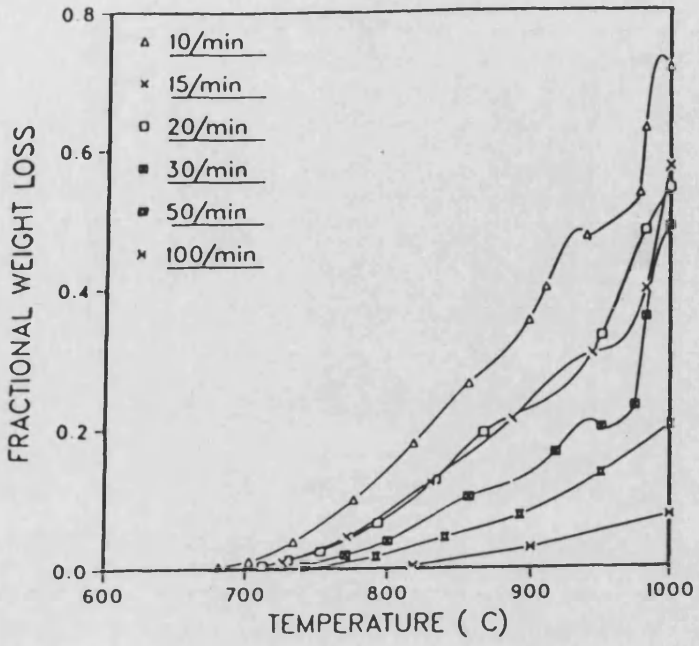


A1.2 Effect of air flow rate (ml/min) on the oxidation of PP carbon; P.S. 850–500um H.R. 15 C/min initial weight 10mg

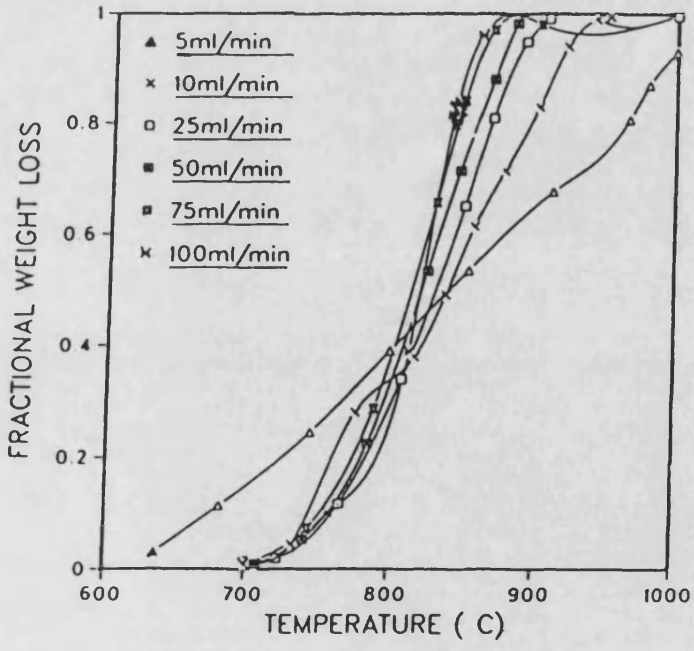

A1.3 Effect of particle size (um) on the oxidation of PP carbon; H.R. 15 C/min Air 50ml/min initial weight 10mg

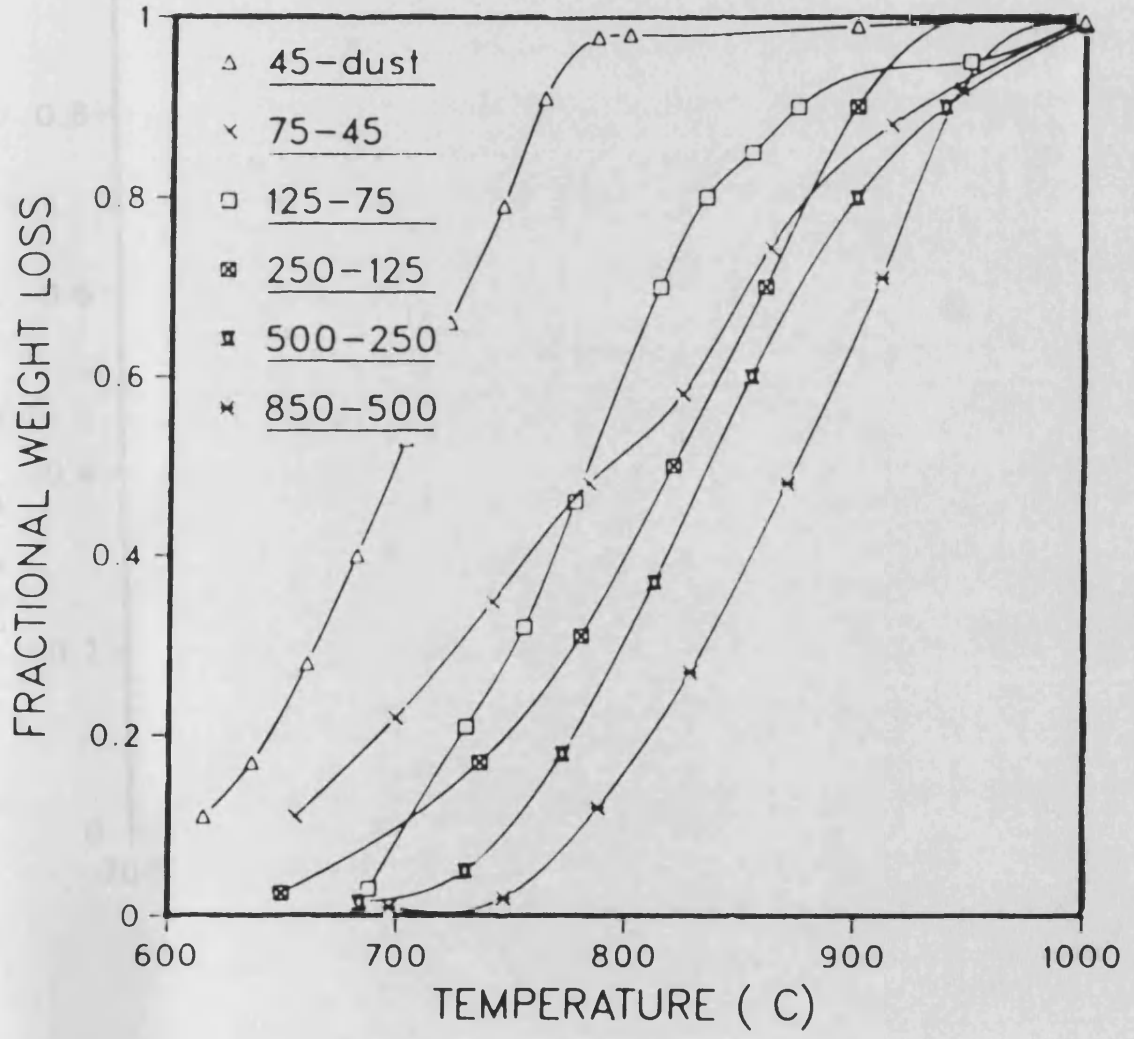

A1.4 Effect of initial weight (mg) on the oxidation of PP carbon; P.S. 850–500um, Air 50ml/min, H.R. 15 C/min

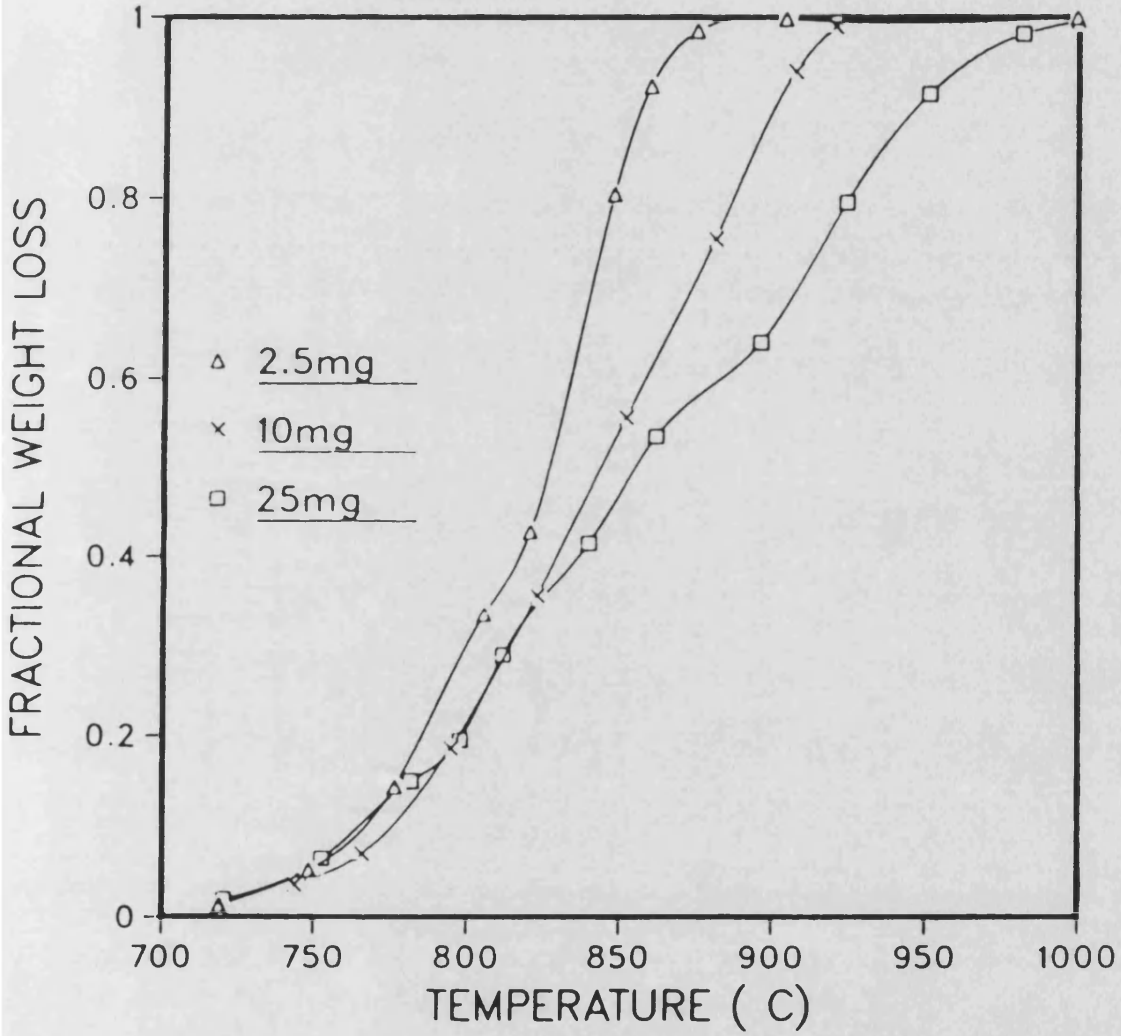

A1.5 Effect of heating rate on the oxidation of TPSX4 carbon; P.S. 850–500um, Air 5ml/min, initial weight 10mg resin cure schedule 150/1.5

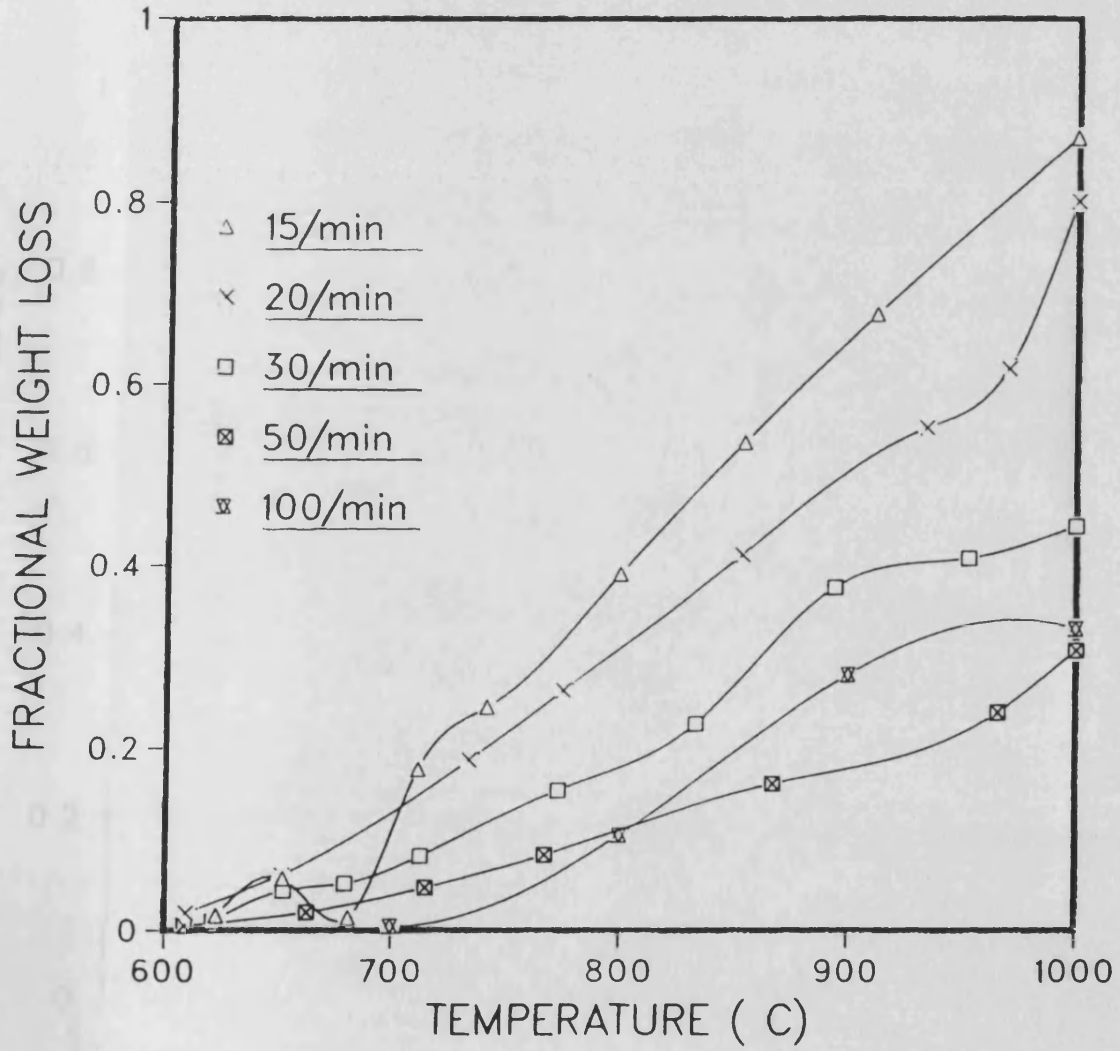

A1.6 Effect of air flow rate (ml/min) on the oxidation of TPSX4 carbon; H.R. 20 C/min P.S. 850–500um initial weight 10mg resin cure schedule 150/1.5

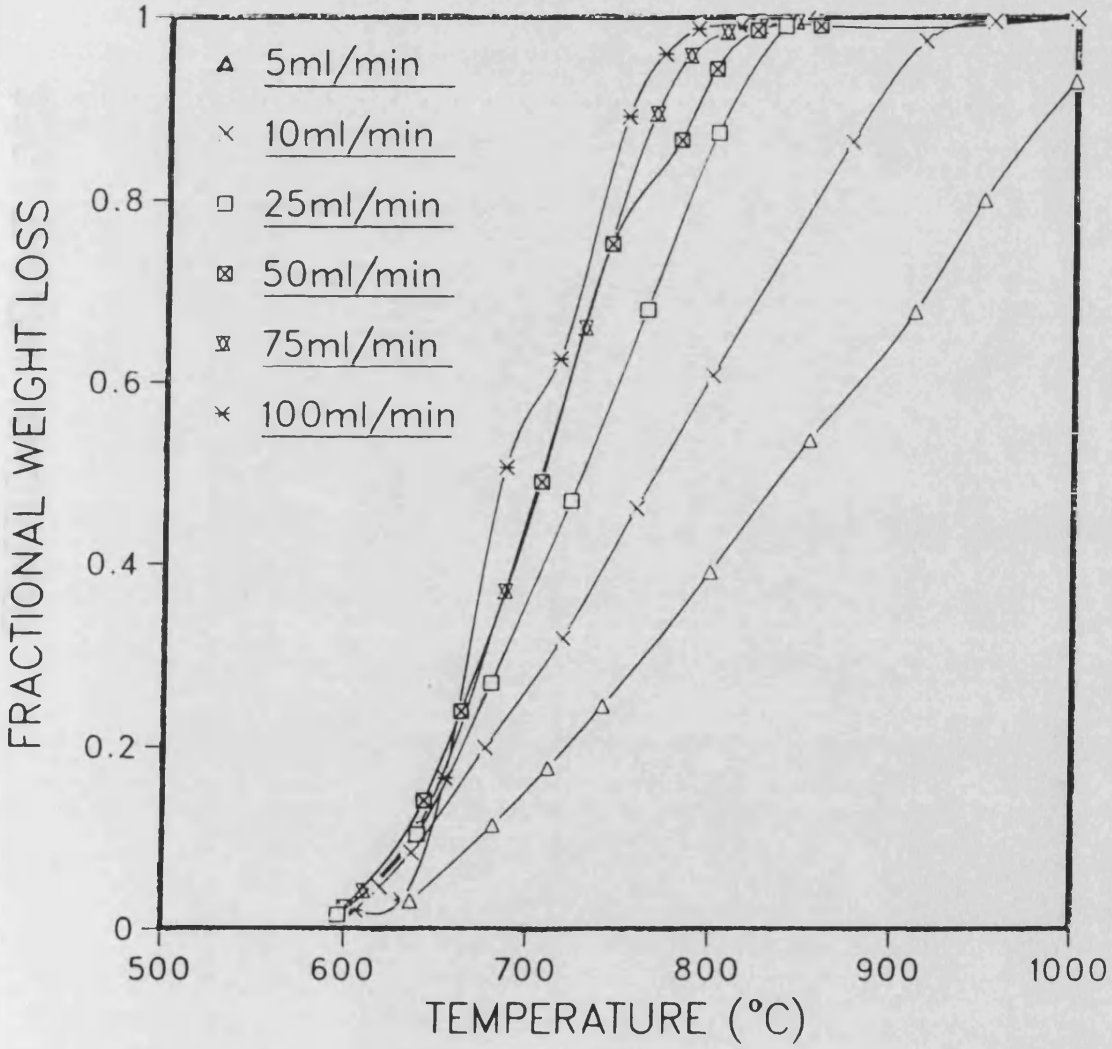

A1.7 Effect of particle size (um) on the oxidation of TPSX4 carbon; H.R. 10 C/min Air 50ml/min initial weight 10mg resin cure schedule 150/1.5

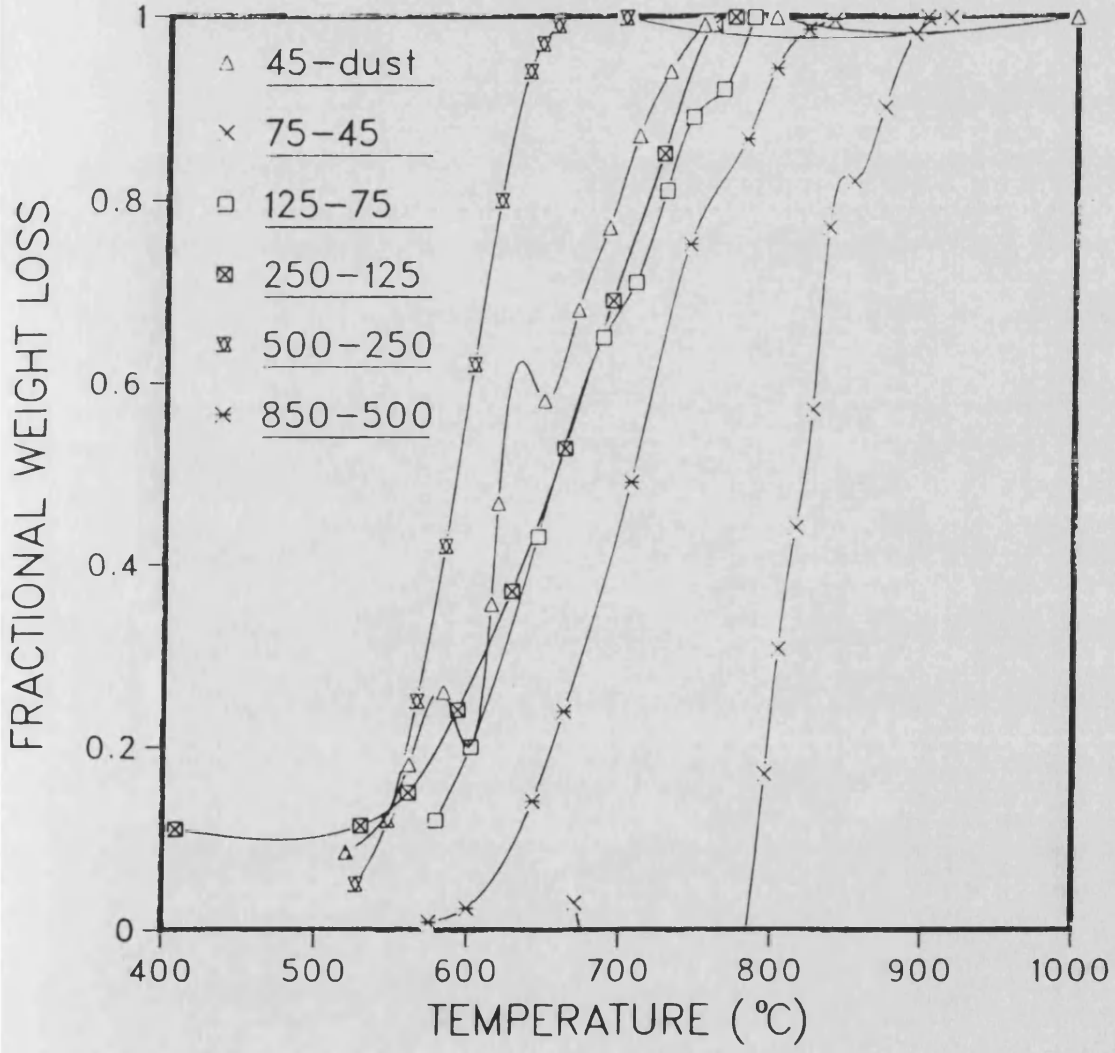

A2.2 The BDDT classification of adsorption isotherms

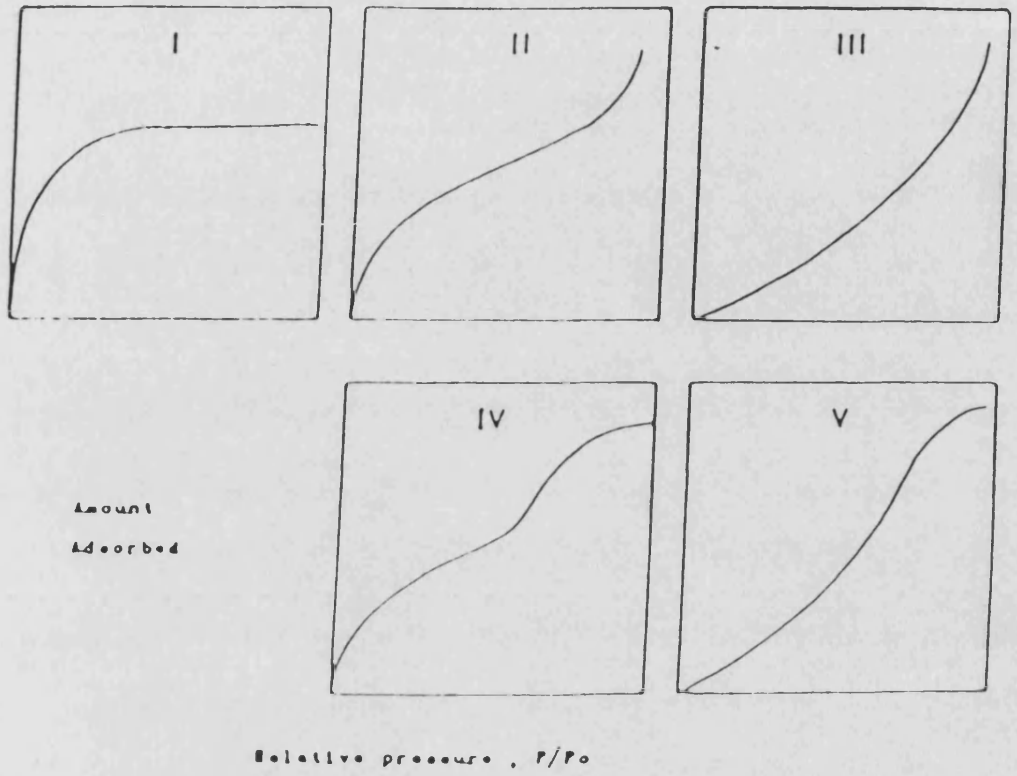


A2.1 Calibration of the baratron pressure readings for the volumetric nitrogen gas adsorption technique

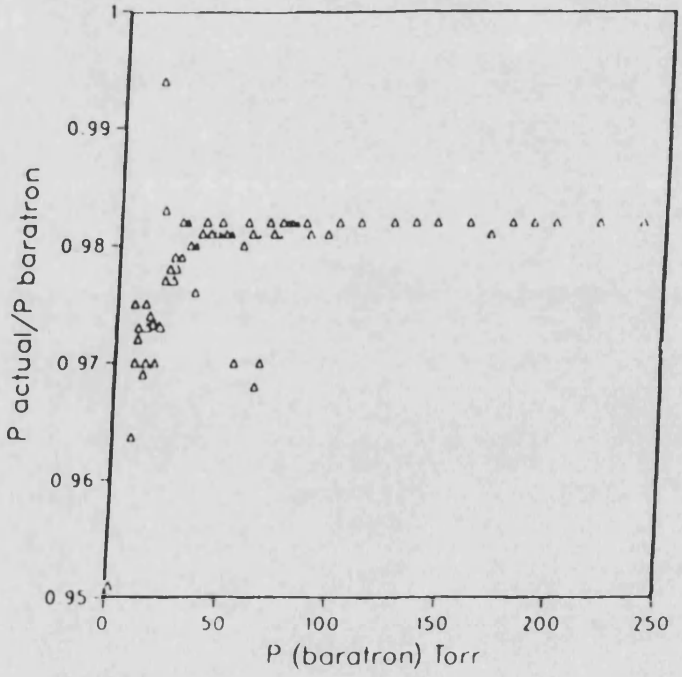

A2.3 The Marsh and Rand classification of deviations from linear DR plots

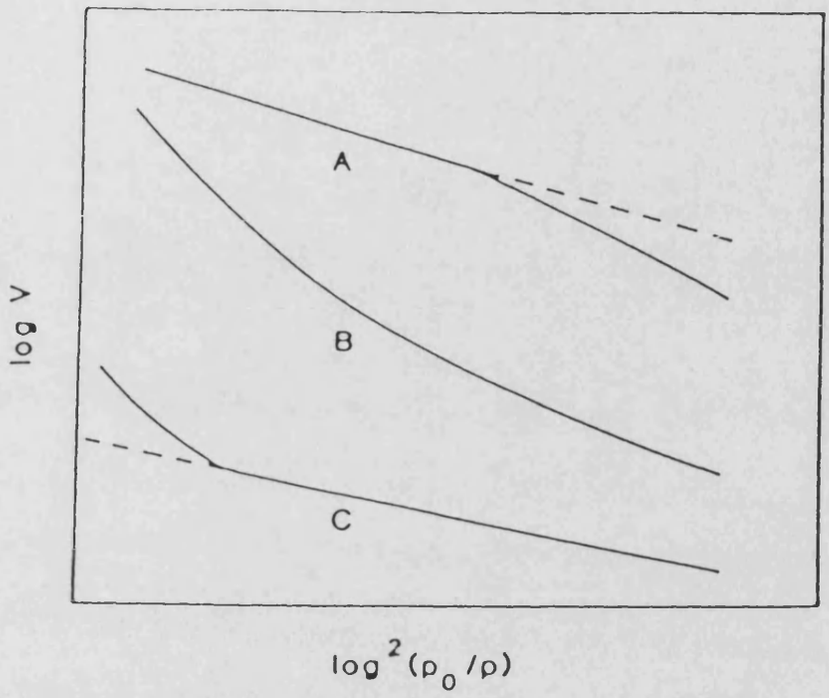


A2.4 Corrections to pressure readings due to thermal transpiration on the microbalance

| Pressure Reading (Torr) | % Error in Pressure Reading |
|---|---|
| | $N_2$ |
| 0.001 | 28.3 |
| 0.01 | 3.1 |
| 0.02 | 1.0 |
| 0.05 | 0.2 |

## REFERENCES


1 Brown, A.; Refractories J.; 58 (2) 7 (1983)

2 Cooper, C.F.; Refractories; 55 (6) 11 (1980)

3 Cooper, C.F.; Chemistry and Industry; No.18 678 (1982)

4 Fitchett, A.M. and Wiltshire, B.; Brit. ceram. Trans. J.; 83 58 (1984)

5 Ochiai, T; Itoi, H., Ando, K. and Oikawa, K.; Sprechsaal 10 755 (1979)

6 Rand, B. and McEnaney, B.; Brit. Ceram. Trans. J.; 84 157 (1985)

7 Lemon, P.H.R.B.; Brit. Ceram. Trans. J.; 84 53 (1985)

8 Gardziella, A.; Proc. 4th Int. Carbon Conf., Baden-Baden; 30th June (1986) p.787

9 Knop, A. and Scheib, W.; "Chemistry and Applications of Phenolic Resins"; Springer-Verlag (1979)

10 McEnaney, B. and Rand, B.; Brit. Ceram. Trans. J.; 84 193 (1985)

11 Bayer, A.; Ber. deut. Chem. Ges.; 25 280 (1872)

12 Baekland, L.H.; Ind. Eng. Chem. 1 409 (1909)

13 Fitzer, E.; Angew, Chemie; 19 375 (1980)

14 De Jong, J.I. and De Jong, J.; Rec. Trav. Chim.; 72 497 (1953)

15 Zsavitsas, A.A.; Am. Chem. Soc. Div. Org. Coatings and Plastic Preprints; 26 93 (1966)

16 Freeman, J.H. and Lewis, C.W.; J. Am. Chem. Soc.; 76 2080 (1954)

REFERENCES (cont.)

17 Kornblum, N., Smiley, R.A. and Blackwood, R.K.; ibid 77 726 (1959)

18 Megson, N.J.L.; "Phenolic Resin Chemistry", London, Butterworth (1958)

19 Ishida, S. and Nakamoto, I.; Polymer Preprints ACS 24 No.2 167 (Aug. 1983)

20 Mackey, J.H., Tiede, M.L., Sojka, S.A. and Wolfe, R.A.; Polymer Preprints ACS 24 No.2 (Aug. 1983) p.179

21 Lum, R.M., Wilkins, C.W., Lyons, A.M. and Jones, R.P.; Polymer Preprints ACS 24 No.2 (Aug. 1983) p.186

22 Shulmann, G.P. and Lochte, H.W.; J. Appl. Polym. Sci. 10 619 (1966)

23 Conley, R.T.; " Developement of Applied Spectroscopy", Plenum Press, New York; 4 377 (1965)

24 Woodbrey, J.C., Higgenbottom, H.P. and Culbertson, H.M.; J. Polym. Sci. 3 1079 1965)

25 Pasch, H., Goetzky, P., Grundemann, E. and Raubach, H.; ACTA Polymerica; 32 14 (1981)

26 Yamashita, Y. and Ouchi, K.; J. Fuel Soc. Jap.; 53 1064 (1974)

27 Toyoda, S.; Rep. Resources Res. Inst. Jap.; No.74 (1959)

28 Kobayashi, K, Sugawara, S., Toyoda, S. and Honda, H.; Carbon; 6 359 (1968)

29 Jackson, W.M. and Conley, R.T.; J. Appl. Polym. Sci.; 8 2163 (1964)

30 Conley, R.T. and Bieron, J.; J. Appl. Polym. Sci.; 7 103 (1963)

REFERENCES (cont.)

31 Conley, R.T. and Bieron, J.; J. Appl. Polym. Sci.; 7 171 (1963)

32 Conley, R.T.; J. Appl. Polym. Sci.; 9 1117 (1965)

33 Lochte, H.W., Straus, E.L. and Conley, R.T.; J. Appl. Polym. Sci.; 9 2799 (1965)

34 Bellemy, L.J.; "The Infrared Spectra of Complex Molecules" 2nd ed., Wiley, New york, (1958)

35 Cook, C.D., Khun, D.A. and Fianu, P.; J. Am. Chem. Soc.; 78 2002 (1956)

36 Kharasch, M.S. and Jooshi, B.S.; J.Org. Chem.; 22 1439 (1957)

37 Heron, G.F.; Conf. on High Temperature Resistance and Thermal Degradation of Polymers, Monograph 13, Plastics and Polymers Group, Soc. of Chemical Ind. London; p.475 (1961)

38 Ouchi, K. and Honda, H.; Fuel; 38 429 (1959)

39 Madorsky, S. and Straus, S.; WADC Techn. Report; p.59 (June 1959)

40 Beecher, N. and Rosenweig, R.E.; ARS Journal; p.532 (Aug. 1932)

41 Wilkins, C.W.; Labortories New Jersey, U.S.A., Applications of Pyrolysis-Mass-Spectrometry to the Study of Carbon Phenolic Composites

42 Johnson, R.J. Jr. and Biefield, R.M.; Polymer Preprints ACS 24 No.2 p.189 (Aug. 1983)

43 Chang, H.W. and Rhee, S.K.; Carbon; 16 17 (1978)

44 Fitzer, E.; Angew Chemie, Int. Ed. Engl., heft 5/1980,

REFERENCES (cont.)

45 Franklin, R.E.; Proc. Roy. Soc.; A209 196 (1951)

46 Franklin, R.E.; ACTA Cryst.; 3 107 (1950)

47 Jenkins, G.M. and Kawamura, K.; "Polymeric Carbons", Cambridge Univ. Press, Cambridge, (1976)

48 Bennett, S.C. and Johnson, D.J.; Proc. 5th London Int. Carbon and Graphite Conf.; 1 377 (1978)

49 Dickakian, G.B.; 15th Biennial Conf. on Carbon, Extended Abstracts and Program, Philadelphia, p.137 (1981)

50 Lewis, R.T.; Extended Absr., 12th Bienn. Conf. on Carbon Pittsburgh, Penn. Am. Carbon Soc.; p.215 (1975)

51 McNeil, D. and Wood, L.J.; Conf. on Ind. Carbon and Graphite; p.162 (1957)

52 Barr, J.B. and Lewis, I.C.; 15th Bienn. Conf. on Carbon, Extended Absr. Philadelphia, p.162 (1981)

53 Bartle, K.D., Collins, G., Stadelhofer, J.W. and Zander, M.J.; Chem. Tech. Biotech.; 29 531 (1979)

54 Karr, C. Jr.; "Analytical Methods for Coal and Coal Products", vol.2 Academic Press, New York, (1978)

55 Greinke, R.A. and O'Connor, L.H.; Anal. Chem.; 52 1877 (1980)

56 Dickenson, E.J.; J. Soc. Chem. Ind.; 64 121 (1945)

57 Fisher, P., Stadelhofer, J.W. and Zander, M.; Fuel; 57 345 (1978)

58 Ladner, W.R. and Snape, C.E.; Fuel; 57 658 (1978)

59 Marsh, H. and Walker, P.L. Jr.; Chem. and Phys. of Carbon 15 230 (1979)

REFERENCES (cont.)

60 Fitzer, E., Mueller, K. and Schaeffer, W.;
Chem. and Phys. of Carbon; 7 237 (1971)

61 DOW Chem. Co., U.S. Pat. 2,270,199

62 Carbon Electrodes, Germany, Aluminium Ind., FIAT Final
Report 986 4 (HMSO, London)

63 Brooks, J.D. and Taylor, G.H.; Chem. and Phys. of Carbon;
4 243 (1968)

64 Dubois, J., Agache, C. and White , J.L.; Metallography;
17 223 (1979)

65 Buechler, N., Ng, C.B., Weinberg, V.C. and White, J.C.;
Carbon '80, 3rd Int. Carbon Conf. Deutschem, Keramiochem
Gessellschaft p.346 (1980)

66 Otani, S.; Carbon; 5 219 (1967)

67 Marsh, H. and Smith, J.; "Characterisation of Coal and
Coal Derivatives; (C. Karr, ed. ) Acad. Press, New York,
p.371 (1978)

68 Marsh, H., Foster, J.M., Hermon, G. and Iley, M.;
Fuel; 52 234 (1973)

69 Brooks, J.D. and Taylor, G.H.; Carbon; 3 185 (1965)

70 Mering, J. and Maire, J.; J. Chim. Phys.; 57 803 (1960)

71 Fishbach, D.B.; Chem. and Phys. Carbon; 7 1 (1971)

72 Pacault, A.; Chem. and Phys. Carbon; 7 107 (1971)

73 Noda, T. and Tanaka, M.; Kogyo Kagaku Zasshi;
65 1329 (1962)

74 Noda, T. and Kato, H.; Carbon; 3 289 (1965)

REFERENCES (cont.)

75 Marsh, H. and Warburton, A.P.; J. Appl. Chem.; 20 133 (1970)

76 Oya, A. and Marsh, H.; J. Mat. Sci.; 17 309 (1982)

77 Gay-Lussac, J.L.; Ann. Chim. Phys.; 18 (2) 211 (1821)

78 National Commission of Fire Prevention and Control, Report Entitled "America Burning, 1973"

79 Marvel, C.S.; Soc. Plast. Eng. J.; 20 220 (1964)

80 Cassidy, P.E. and Fawcett, N.C.; J. Macromol. Sci. Rev. Macromol. Chem.; C17 209 (1979)

81 Criscione, J.M.; ML-TDR-64-173 (1964)

82 Nicholas, F., Prantis, C. and Dickenson, M.; ASD-TDR-62-205, Contract AF33 (616)-8175 (1962)

83 Roller, D.; WA DC-TR-59-415 (1955)

84 Galli, J.R.; WA DC-TR-58-493 ASTIA 20913 (1963)

85 Mellors, G.W.; Electrochem. Soc. J.; 180C 110 (1974)

86 Chandrasekhariah, M.S.; "Volatiles of Refractories", BNL-7454 New York, (1963)

87 Fitzer, E.; F. Benesousky, Hochschmetiscade Metalle 3. Planseeseminar, Reutte (1958), Springer-Verlag

88 Sazonova, M. and Appen, A.A.; Zh. Frikl. Khim.' 37 7 (1964)

89 Fitzer, E., Herbst, H. and Schlichting, J.; Carbon; p.401 (1982)

90 Harris, J.A., Keating, E.J. and Goynes, W.R.; J. Appl. Polym. Sci.; 25 2195 (1980)

REFERENCES (cont.)

91 Bashir, M.K.; in 'A Study of the Effects of Chain Transfer Agents in Bulk Photoinitiated (Meth)Acrylate Systems', MSc thesis, Queen's University of Belfast, 1984

92 Hastie, J.W.; J. Res. Natl. Bur. Stand. Sect. A77a No. 0,733 (1973)

93 Stuetz, P.; "Symposium on Flammability Characteristics of Polyeric Materials", Univ. of Utah, (June, 1971)

94 Fenimore, C.P. and Martin, F.J.; Combustion Flame; 10 135 (1966)

95 Fenimore, C.P.; "Flame Retardant Polymeric Materials", ed.s Lewin, M., Atlas, S.M. and Pearce, E.M.; Plenum Press New York; 1 371 (1975)

96 Turie, E.A. (ed.); "Thermal Characteristics of Polymeric Materials", Acad. Press, New York, (1981)

97 Fenimore, C.P. and Martin, F.J.; Flammability of Polymers, Combustion and Flame; 10 (3) 295 (1966)

98 Milby, R.V.; Plastics Technology, McGraw-Hill, N.Y. (1973)

99 Schmidt, D.L.; "Ablative Plastics", (ed.s D'Alelio, G.F. and Parker, J.A.), Marcel-Dekker, N.Y. p.1 (1971)

100 D'Alelio, G.F.; "Ablative Plastics" Marcel-Dekker, New York, p.85 (1971)

101 Rhys, J.A.; Chem. Ind. (London); p.187 (1969)

102 Kuryla, W.C. and Papa, A.J.; "Flame Retardancy of Polymeric Materials", Marcel-Dekker, N.Y., vol.1 (1973)

103 Economy, J., Frechette, F.J and Wohrer, L.C.; Ger. Pat. 1,948,412 (April 1970)

REFERENCES (cont.)

104 Quarles, R.W. and Baumann, J.A.; Union Carbide, U.S. Pat. 3,298,973 (1967)

105 Brit. Pat. 1,091,238 to Compagnie de Saint-Gobain (1967)

106 Lyons, J.W.;"The Chemistry and Uses of Fire Retardants", Wiley, Interscience, New York, p.23 (1970)

107 McKee, D.W.; Chemistry and Physics of Carbon, (ed. Walker, P.L., Jr and Thrower, P.A.) Marcel Dekker, New York, vol.16 (1981)

108 McKee, D.W.; Carbon; 24 737 (1986)

109 Jawed, I and Nagle, D.C.; Materials res. Bull.; 21 1391 (1986)

110 Soule, E.C., Burnett, L.S. and Wagner, G.M.; U.S. Pat. 3,038,822 (1962)

111 Smith, H.A.; U.S. Pat. 3,320,213 (1967)

112 Brit. Pat. 969,095; to Monsanto Co. (1964)

113 Hull, M.E. and Simpson, E.W.; French Pat. 1,364,821 (1964)

114 Shimizu, S.; Jap. Pat. 13,073 (1965)

115 Elmer, C. and Mestdagh, J.J.; U.S. Pat. 3,352,746 (1967)

116 Norde-Aviatione Soc. Nat. Constructions Aeron. DE-AS 1,816,241 (1968)

117 Soc. Francaise Albert, Fr. addn. 88,149 9to Fr. Pat. 1,389,825 (1966)

118 Hoxie, L.E.; U.S. Pat. 3, 377, 317 (1968)

119 Erickson, A.N. and Erickson, P.N.; U.S. Pat. 3,256,216 (1966)

REFERENCES (cont.)

120 Wright, H.R. and Zentfmann, H.; Chem. Ind. London 101,244 (1952)

121 Dannels, B.F. and Shepard, A.F.; Inorganic Esters of Novolaks; J. Polym. Sci. A-1 6 2051 (1968)

122 Monsanto Co., Phos-chek P/30, Phosphorus based Fire Retardant Tech. Bull. I-270 Inorg. Chem. Division.

123 Vandersall, H.L.; Paper presented at Polymer Conf. Series on Flammability Characteristics of Polymeric Materials, Univ. of Utah

124 Little, R.W.; Flame Proofing Textile Fabrics, Am. Chem. Soc., Monograph Series, No. 104, Reinhold N.Y. (1947)

125 Lyons, J.W.; J. Fire and Flam.; 1 302 (1970)

126 Kindler, A.E.; 17th Carbon Conf. p.407 (1985)

127 Johnson, N.J. and Nickerson, J.D.; U.S. Pat. 2,868,672 (1959)

128 Conley, R.T. and Chow, L.L.; Rep. Org. Coatings Plast. Chem.; 27 133 (1967)

129 Hanton, D.; Fr. Pat. 1,588.803 (1968)

130 Cherubim, M.; Kunstoff Rundschau; 13,235 (1966)

131 Gen. Electric. Co., U.S. Pat. 2,258,218 (1941)

132 Dannels, B.F. and Shepard. A.F.; U.S. Pat. 2,258,218 (1968)

133 Sunshine, N.B.; "Flame Retardancy of Polymeric Materials" , vol.4 p.201

134 Williams, J.M. and Impressica, R.J.; J. Spacecraft; 12 (3) 151 (1975)

REFERENCES (cont.)

135 DOW Corning Corp. DE-PS 937,555 (1956)

136 Noll, W.; Chemie und Tech. Silicone, Verlag Chemie Weinheim (1968)

137 Walker, A.G.; Brit. Plastics; (7) 42 128 (1969)

138 Green, H.A.; U.S. Pat. 3,262,894 (1964)

139 FMC Corp., Belgian Pat. 699,508 (1967)

140 Hecker, K.C.; Rubber World, (3) 59 159 (1968)

141 Pitts, J.J. and Scott, P.H.; J. Cell. Plast.; (1) 6 35 (1970)

142 Sebenik, A.; Vizovisek, I. and Lapanje, S.; Europ. Polym. J.; 10 273 (1974)

143 Westwood, A.R. and Kay, R.; Europ. Polym. J.; 11 25 (1975)

144 Doyle, C.D.; 'Techniques and Methods of Polymer Evaluation' (ed.s Slade, D.E. and Jenkins, L.T.) Arnold-Dekker, vol.1,

145 Friedman, H.L.; J. Polym. Sci.; B7 41 (1969)

146 van Krevelen, D.W.; Polymer; 16 615 (1975)

147 McEnaney, B. and Weedon, C.J.; 'Proceedings 3rd Conf. on Carbon and Graphite', Soc. Chem. Ind. (London); p.207 (1971)

148 Walls, J.R. and Strickland-Constable, R.E.; Carbon; 1 333 (1964)

149 Sobolov, I. and Woychesin, F.A.; J. Fire Flam/Fire Retardant Chem.; 1 13 (1974)

150 Linares-Solano, A.; Lopez-Gonzalez, J.D.; Martinez-Martinez, J.M. and Rodriguez-Reinoso, F.; Ads. Sci. Techn.; 1 123 (1984)

151 Walker, P.L. Jr.; Rusinko, F. Jr. and Austin, L.G. Adv. in Catalysis, X1 134 (1959)

REFERENCES (cont.)


152 Szekely, J.; Evans, J.W. and Sohn, H.V.; 'Gas-Solid Reactions' Academic Press, New York (1976)

153 Oszgen, O.S. and Rand, B.; Br. Ceram. Trans. J.; 84 70 (1985)

154 Martinez-Martinez, J.M.; Rodriguez-Reinoso, F; Molina Sabio, M. and McEnaney, B.; Carbon; 24 (3) 255 (1986)

155 Learmonth, G.S. and Osborn, P.; J. Appl. Polym. Sci.; 12 1815 (1968)

156 Winslow, F.H.; 1st Conf. Ind. Carbon; p.190 (1957)

157 Gilbert, J.B. and Kipling, S.J.; Fuel; 41 493 (1962)

158 Heintz, E.A. and Parker, W.E.; Carbon; 4 473 (1966)

159 Rakaszawski, J.F. and Parker, W.E.; Carbon; 2 53 (1964)

160 Jackson, B. and Patridge, T.J.; Trans. J. Brit. Ceram. Soc.; 72 139 (1973)

161 Ninin, V.K. and Shner, S.V.; USSR Pat.; 200-149 (1967)

162 Chimizu, S.; Jap. Pat.; 13 073 (1965)

163 Kobayashi, K.; Abstracts 12th Conf. on Carbon; p.247 (1975)

164 Lowell, C.E.; J. Amer. Soc.; 50 142 (1967)

165 Davis, B.D.; Elvis, E. and Morgan, R.E. Jr.; Ger. Pat.; 1-960-201 (June 1970)

166 Taniuchi, A. and Koide, M.; Jap. Pat.; 70-11-432 (Apr 1970)

167 Tokuda, T.; Ito, T. and Yamaguchi, T.; Naturforschung; 26A 2058 (1971)

168 Kipling, J.J. and McEnaney, B.; Carbon; 13 515 (1975)

169 Masters, K.J. and McEnaney, B.; Carbon; 22 (6) 595 (1984)

170 Thomas, J.M. and Walker, P.L.; Carbon; 2 434 (1965)

171 Gallagher, J.T. and Harker, H.; Carbon; 2 163 (1964)

REFERENCES (cont.)

172 Walker, P.L. Jr.; Shelef, M. and Anderson, R.A.; Chemistry and Physics of Carbon; 4 287 (1968)

173 Hennig, G.R.; Proc. 2nd Conf. on Carbon, Pergamon Press, New York; 1 143 (1962)

174 Renton, J.J.; 'Coal Structure'; (ed. Meyers, R.A.) Academic Press, New York, (1982)

175 Wallouch, R.W.; 'Process and Composition for the Manufacture of Oxidation Resistant Graphite Articles', U.S. Pat; 3-706-596

176 Tingly, G.L.; 'Extended Abstract , 12th Biennial Conf. on Carbon', p.181 (1975)

177 Lewis, J.B.; in 'Modern Aspects of Graphite Technology', (ed. Blackman, L.C.F.), Academic Press, London, P.129 (1970)

178 Lewis, J.B.; 2nd Conf. on Ind. Carbon and Graphite, Soc. of Chem. Ind., London; (1965)

179 Huttinger, K.J. and Krauss, W.; Fuel; 61 291 (1982)

180 Otto, K. and Shelef, M.; Ext. Absr. Prog. Biennial Conf. on Carbon; 13 50 (1977)

181 Fisher, P.M. and Szirmae, A.; Proc. 14th Biennial. Conf. on Carbon; p.151 (1979)

182 Otto, K.; Bartosiewicz, L. and Shelef, M.; Fuel; 58 85 (1979)

183 McKee, D.W.; Spiro, C.L.; Kosky, P.G. and Lamby, E.J.; Proc. Int. Symp. FUNCAT COGAS, Amsterdam, P.219 (1982)

184 Luthra, K.L.; Carbon; 26 (2) 217 (1988)

185 Brunauer, S.; Demming, L.S.; Demming, W.E. and Teller, E.; J. Amer. Chem. Soc.; 62 1723 (1940)

186 Dubinin, M.M.; J. Colloid Interface Sci.; 46 351 (1974)

REFERENCES (cont.)

187 Langmuir, I.; J. Amer. Chem. Soc.; 38 2221 (1916)

188 Langmuir, I.; J. Amer. Chem. Soc.; 40 1361 (1918)

189 Gregg, S.J. and Sing, K.S.W.; in 'Adsorption, Surface Area and Porosity', 2nd edition, Academic Press, New York, (1982)

190 Marsh, H. and Lamond, T.G.; Carbon; 1 293 (1963)

191 Polanyi, M.; Verh Deutsch. Phys. Ges.; 16 1012 (1914)

192 Polanyi, M.; Trans. Faraday Soc.; 28 316 (1932)

193 Dubinin, M.M.; in 'Characterisation of Porous Solids', (eds. Gregg, S.J.; Sing, K.S.W. and Stoeckli, H.F.), Soc. Chem. Ind. (1979)

194 Marsh, H. and Rand, B.; J. Colloid Interface Sci.; 33 101 (1970)

195 Marsh, H. and Rand, B.; in 'Proc. 3rd Conf. on Ind. Carbon and Graphite', London Soc. of Chem. Ind.; p.172 (1970)

196 Toda, Y.; Hatami, M.; Toyoda, S.; Yashida, Y. and Honda, H.; Carbon; 8 565 (1970)

197 Masters, K.J. and McEnaney, B.; J. Colloid Interface Sci,; 95 340 (1983)

198 Dubinin, M.M. and Astakhov, V.A.; Izv, Akad Nauk, SSSR, SER Khim; 5 11 (1971)

199 Lippens, B.C. and de Boer, J.H.; J. Catalysis; 4 319 (1965)

200 Ali, S.; in 'A Study of Microporous and Non-microporous Adsorption in Activated Carbons', MSc thesis, Univ. of Bath, (1984)

201 Everett, D.H. and Prowl, J.C.; J. Chem. Soc. Faraday Trans. .; 1 619 (1976)

REFERENCES (cont.)

202 Stoeckli, H.F.; Helv. Chim. Acta; 57 2195 (1974)

203 McEnaney, B.; Carbon; 25 (1) 69 (1987)

204 Harris, M.R. and Sing, K.S.W.; Chem. Ind.; 18 757 (1967)

205 Dubinin, M.M.; in 'Industrial Carbon and Graphite', Soc. of Chem. Ind., London; p.219 (1958)

206 Washburn, E.W.; Proc. Nat. acad. Sci.; 7 115 (1921)

207 Gan, H.; Nandi, S.P. and Walker, P.L., Jr.; Fuel; 51 272 (1972)

208 Orr, C., Jr.; Powder Technol.; 3 117 (1969)

209 Svata, M.; Powder Technol.; 5 345 (1971)

210 Donnet, J.B.; 17th Biennial Conf. on Carbon, Lexington, Kentucky; p.26 (1985)

211 Freeman, J.J.; Gimblett, F.G.R.; Roberts, R.A. and Sing, K.S.W.; Carbon; 26 (1) 7 (1988)

212 Freeman, J.J. and Gimblett, F.G.R.; Carbon; 25 565 (1987)

213 Graham, D.; J. Phys. Chem.; 61 1310 (1957)

214 Laurendau, N.M.; Pro. Energy Combust. Sci.; 4 221 (1978)

215 Walker, P.L., Jr.; Fuel; 60 801 (1981)

216 Coulson, C.A.; Pro. 4th Conf. on Carbon, Pergamon Press, New York, p.215 (1960)

217 Blackwood, J.D.; Culls, B.D. and McCarthey, D.J.; Aust. J. Chem.; 20 1561 (1967)

218 Laine, N.R.; Vastola, F.J. and Walker, P.L., Jr.; J. Phys. Chem.; 67 2030 (1963)

219 Laine, N.R.; Vastola, F.J. and Walker, P.L., Jr.; Proc. 5th Carbon Conf. Pergamon Press, New York; p.211 (1963)

REFERENCES (cont.)

220 Watanabe, A. and Takeuchi, Y.; Applications of MgO-C bricks to Converter Linings, Taikabutsu; 1 40-48 (1981)

221 Komo, T. and Tabata, A.; Taikabutsu; 32 (3) 163-169 (1980)

222 Barthel, H. and Kaltner, E.; 'The Effect of Carbon in C-containing Magnesia bricks on the wear in BOF', preprint of 1st Int. Conf. on Refr., Tokyo; p.91 (1983)

223 Nameish, W.; Taikabutsu; 32 583 (1980)

224 Ohishi, T.; Taikabutsu; 34 (6) 318 (1982)

225 Barthel, H.; Buchebener, G. and Kaltner, E.; 27th Int. Coll. on Refr. for Steel-making Converters; Aachen pp 33-64 (1984)

226 Darroudi, T; Hughes, R.H. and Landy, R.A.; 1st Int. Conf. Refr., Jap.; p.105 (Nov. 1983)

227 Brezny, B.; 'Magnesia brick containing Metallic Magnesium', Steel-making Proceedings, Pittsburgh; 65 60-65 (1982)

228 Watanabe, A.; Takahashi, H.; Matsuki, T. and Takahashi, M.; Preprints 1st Int. Conf. Refr., Tokyo; pp125-134 (1983)